Optimal Design and Operation of Energy Polygeneration Systems

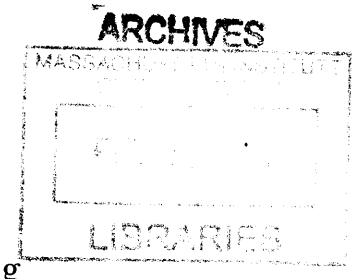

by

Yang Chen

Submitted to the Department of Chemical Engineering
in partial fulfillment of the requirements for the degree of

Doctor of Philosophy in Chemical Engineering

at the

MASSACHUSETTS INSTITUTE OF TECHNOLOGY

February 2013

Author .....
Department of Chemical Engineering
October 25, 2012

Certified by .....
Paul I. Barton
Lammot du Pont Professor of Chemical Engineering
Thesis Supervisor

Certified by .....
Thomas A. Adams II
Assistant Professor of Chemical Engineering
Thesis Supervisor

Accepted by .....
Patrick S. Doyle
Professor of Chemical Engineering
Chairman, Committee for Graduate Students

Optimal Design and Operation of Energy Polygeneration Systems

by

Yang Chen

Submitted to the Department of Chemical Engineering
on October 25, 2012, in partial fulfillment of the
requirements for the degree of
Doctor of Philosophy in Chemical Engineering

Abstract

Polygeneration is a concept where multiple energy products are generated in a single plant by tightly integrating multiple processes into one system. Compared to conventional single-product systems, polygeneration systems have many economic advantages, such as potentially high profitability and high viability when exposed to market fluctuations.

The optimal design of an energy polygeneration system that converts coal and biomass to electricity, liquid fuels (naphtha and diesel) and chemical products (methanol) with carbon dioxide (CO_2) capture under different economic scenarios is investigated. In this system, syngas is produced by gasification of coal and/or biomass; purified by a cleaning process to remove particles, mercury, sulfur and CO_2; and then split to different downstream sections such as the gas turbine, FT process and the methanol process. In this thesis, the optimal design with the highest net present value (NPV) is determined by optimizing equipment capacities, stream flow rates and stream split fractions.

The case study results for static polygeneration systems reveal that the optimal design of polygeneration systems is strongly influenced by economic conditions such as feedstock prices, product prices, and potential emissions penalties for CO_2. Over the range of economic scenarios considered, it can be optimal to produce a mixture of electricity, liquid fuels, and methanol; only one each; or mixtures in-between. The optimal biomass/coal feed ratio significantly increases when the carbon tax increases or the biomass price decreases. An economic analysis of the optimal static polygeneration designs yielded a slightly higher NPV than comparable single-product plants.

The flexible operation is then considered for the energy polygeneration system. In real applications, product prices can fluctuate significantly seasonally or even daily. The profitability of the polygeneration system can potentially be increased if some operational flexibility is introduced, such as adjusting the product mix in response to changing market prices. The major challenge of this flexible design is the determination of the optimal trade-off between flexibility and capital cost because higher flexibility typically implies both higher product revenues and larger equipment sizes.

A two-stage optimization formulation for is used for the optimal design and operation of flexible energy polygeneration systems, which simultaneously optimizes design decision variables (e.g., equipment sizes) and operational decision variables (e.g., production rate schedules) in several different market scenarios to achieve the best expected economic performance. Case study results for flexible polygeneration systems show that for most of market scenarios, flexible polygeneration systems achieved higher expected NPVs than static polygeneration systems. Furthermore, even higher expected NPVs could be obtained with increases in flexibility.

The flexible polygeneration optimization problem is a potentially large-scale nonconvex mixed-integer nonlinear program (MINLP) and cannot be solved to global optimality by state-of-the-art global optimization solvers, such as BARON, within a reasonable time. The nonconvex generalized Benders decomposition (NGBD) method can exploit the special structure of this mathematical programming problem and enable faster solution. In this method, the nonconvex MINLP is relaxed into a convex lower bounding problem which can be further reformulated into a relaxed master problem according to the principles of projection, dualization and relaxation. The relaxed master problem yields an nondecreasing sequence of lower bounds for the original problem. And an nonincreasing sequence of upper bounds is obtained by solving primal problems, which are generated by fixing the integer variables in the original problem. A global optimal objective is obtained when the lower and upper bounds coincide. The decomposition algorithm guarantees to find an ϵ-optimal solution in a finite number of iterations.

In this thesis, several enhanced decomposition methods with improved relaxed master problems are developed, including enhanced NGBD with primal dual information (NGBD-D), piecewise convex relaxation (NGBD-PCR) and lift-and-project cuts (NGBD-LAP). In NGBD-D, additional dual information is introduced into the relaxed master problem by solving the relaxed dual of primal problem. The so-obtained primal dual cuts can significantly improve the convergence rate of the algorithm. In NGBD-PCR, the piecewise McCormick relaxation technique is integrated into the NGBD algorithm to reduce the gap between the original problem and its convex relaxation. The domains of variables in bilinear functions can be uniformly partitioned before solution or dynamically partitioned in the algorithm by using the intermediate solution information. In NGBD-LAP, lift-and-project cuts are employed for solving the piecewise lower bounding problem. In all three enhanced decomposition algorithms, there is a trade-off between tighter relaxations and more solution times for subproblems.

The computational advantages of the enhanced decomposition methods are demonstrated via case studies on the flexible polygeneration problems. The computational results show that, while NGBD can solve problems that are intractable for a state-of-the-art global optimization solver (BARON), the enhanced NGBD algorithms help to reduce the solution time by up to an order of magnitude compared to NGBD. And enhanced NGBD algorithms solved the large-scale nonconvex MINLPs to ϵ-optimality in practical times (e.g., a problem with 70 binary variables and 44136 continuous variables was solved within 19 hours).

Thesis Supervisor: Paul I. Barton
Title: Lammot du Pont Professor of Chemical Engineering

Thesis Supervisor: Thomas A. Adams II
Title: Assistant Professor of Chemical Engineering

Acknowledgments

I would like to begin my acknowledgments by thanking my thesis advisors Prof. Paul I. Barton and Prof. Thomas A. Adams II. They provided me excellent suggestions and detailed advisories for my research, both in mathematical and engineering aspects. I appreciate that they helped me a lot overcome the obstacles, while gave me abundant freedom to develop my own ideas.

I would like to thank my thesis committee members: Prof. John G. Brisson, Prof. Ahmed F. Ghoniem and Prof. William H. Green. They are very enthusiastic to my research project and provided many useful suggestions to improve my modeling methodologies. My sincerely thanks to them for providing me broader insight to energy systems design from areas other than process systems engineering.

I would express my gratitude to BP-MIT Advanced Conversion Project and Martin Fellowship for Sustainability for funding my PhD research.

I would appreciate the BP-MIT Conversion Project team for their essential collaboration work. Randall Field, Huan Hsu and Robert Brasington, who are current or former research staffs at MIT Energy Initiative, constructed an Aspen Plus simulation model for the polygeneration process, which provided technical parameters in my optimization model. Some former student working for different tasks of the conversion project gave me significant help for the model construction. Dr. Rory Monaghan (mechanical engineering) provided detailed parameters for biomass gasification. Dr. Barbara Botros (mechanical engineering) estimated the efficiency of low-temperature steam turbines. Sarah Bashadi (technology and policy) evaluated the economic performance of Selexol process. My gratitude will also expressed to engineers at BP, especially George Huff, Martin Sellers and Bruce Briggs, for their suggestions on the process flowsheet, modeling method and technical and economic parameters.

My research was greatly benefited from the help of members in Process Systems Engineering Laboratory (PSEL). I closely collaborated with Prof. Xiang Li for the NGBD algorithm development. Part of this thesis, e.g., Chapter 5 and 6, shows

results of the collaboration work. Xiang is also a very good personal friend of mine, and we discussed a lot for many areas outside of current research. Dr. Kai Hoeffner coordinated the Task 6A team in BP-MIT Conversion Project, and compiled all reports and presentations to BP for Kamil and me. Ajay Selot helped me a lot for algorithm development and C++ programming. Joseph Scott provided me great help for preparation of thesis proposal and committee meetings. Matthew Stuber and Achim Wechsung helped to solve many problems encountered with computer and program issues.

I sincerely thank Viet Phan and Adam Newby at Aspen Systems. They helped me solve multiple computing and operating problems of the cluster Banquo, not only benefiting my research but also facilitating research of other PSEL members.

I would like to greatly appreciate my family and my friends. My parents gave me a lot of insight and help for my life. They also took care of me well when I wrote my thesis. My friends at Boston are a essential part of my life, especially for some of very good friends at MIT who provided me countless help. It is impossible for me to express the gratitude to them in a few sentences, therefore I thank all friends who helped me in my life.

Contents

List of Figures

List of Tables

Chapter 1

Introduction

1.1 Energy Polygeneration Processes

1.1.1 Clean Coal Conversion Processes

Energy and the environment are two crucial issues for the world's sustainable development. The global energy demand is expected to grow by one-third from 2010 to 2035 due to the increase of population and the economic growth [37]. Fossil fuels, with advantages of low cost, large scale and high stability, will still contribute over 80% of total energy supply in the next several decades [108].

At present the global economy is heavily dependent on the supply of crude oil, which is limited and potentially unstable. Proven oil reserves are projected to be depleted in about 46 years globally and in fewer than 20 years in most countries [2], based on the current production rates with no additional oil discoveries. In addition, the geographical concentration of oil reserves is a great disadvantage for the energy security of oil-importing countries. By contrast, coal is an abundant and relatively cheap fuel, whose price is typically $1-2 per million Btu, compared to $6-12 per million Btu for natural gas and oil [20]. Coal resources are also widely distributed around the world, including some large energy consuming countries such as United States, China and India [2, 20]. Hence coal will be an alternative to crude oil in the new century, used for power generation, synthetic liquid fuels and chemicals. The Energy

Information Administration (EIA) projects that coal will account for about 20% of primary energy usage in the United States up to the year 2035 [52].

However, a significant problem that may obstruct wide utillization of coal is air pollution from coal conversion processes. Coal-fired plants generate large amounts of particulates, sulphur oxides and nitrogen oxides. Coal is also the largest contributor to global carbon dioxide (CO_2) emissions for energy use (41%) [20]. More concerns about global warming, which is partially caused by increasing CO_2 levels in the atmosphere, have led to efforts to reduce CO_2 emissions all over the world. CO_2 capture and sequestration technologies must be applied to coal conversion processes in the future greenhouse gas constrained world [54]. And, coal conversion processes with higher efficiency should be utilized to achieve lower CO_2 emissions for the same amount of energy produced.

Several coal-based conversion processes with high energy efficiency and low CO_2 emissions, such as Integrated Gasification Combined Cycle (IGCC) and Coal-to-Liquids (CTL) processes with carbon capture and sequestration (CCS), are being developed at present [108, 182, 173, 174, 8], serving as potential supplements for current oil-based processes.

Figure 1-1 shows the flowsheet of a typical IGCC process with CCS [182]. In the IGCC process, coal is converted to synthesis gas (or syngas), which primarily contains carbon monoxide (CO), hydrogen (H_2), CO_2 and water, by gasification. High-temperature oxygen-blown entrained-flow gasifiers are selected to achieve high conversion of coal and low methane content in the syngas. Coal can be slurry-fed (with water) or dry-fed (with nitrogen or CO_2) depending on the gasification technology. An air separation unit (ASU) is installed to produce pure oxygen for gasification. After gasification, syngas is cooled and passes through the scrubber to remove particulate, ammonia and chlorine species. Then syngas is sent to a water gas shift (WGS) reactor converting CO and water to CO_2 and H_2. The sulfur species (which is primarily hydrogen sulfide (H_2S)) and CO_2 in the syngas are removed in the absorption unit, in which chemical solvents (amine) or physical solvents (Selexol, Rectisol, Purisol, etc.) are used. Physical solvents are currently more economically affordable for large-

scale CO_2 capture. In recent years, several advanced separation processes, including adsorption and membrane technologies, have been developed for highly efficient CO_2 removal, which can be possibly incorporated into the IGCC process in the future. The clean H_2-rich syngas with very low sulfur content and low CO_2 content is sent to the power generation unit (the gas turbine or fuel cell) to produce electricity. The captured H_2S is converted to elemental sulfur in the sulfur recovery unit (e.g., the Claus process), and the captured CO_2 is compressed and sent to some geological storage sites. All high-quality heat generated in the process is recovered in steam cycles and used for additional electricity generation by steam turbines. Note that it is optional to install the CO_2 capture units (including WGS reactors and the acid gas absorption unit) in the IGCC process, depending on the economics and policy. For example, the IGCC plant without CCS is suggested to be built first, and when carbon capture becomes profitable, CO_2 capture units can be then installed.

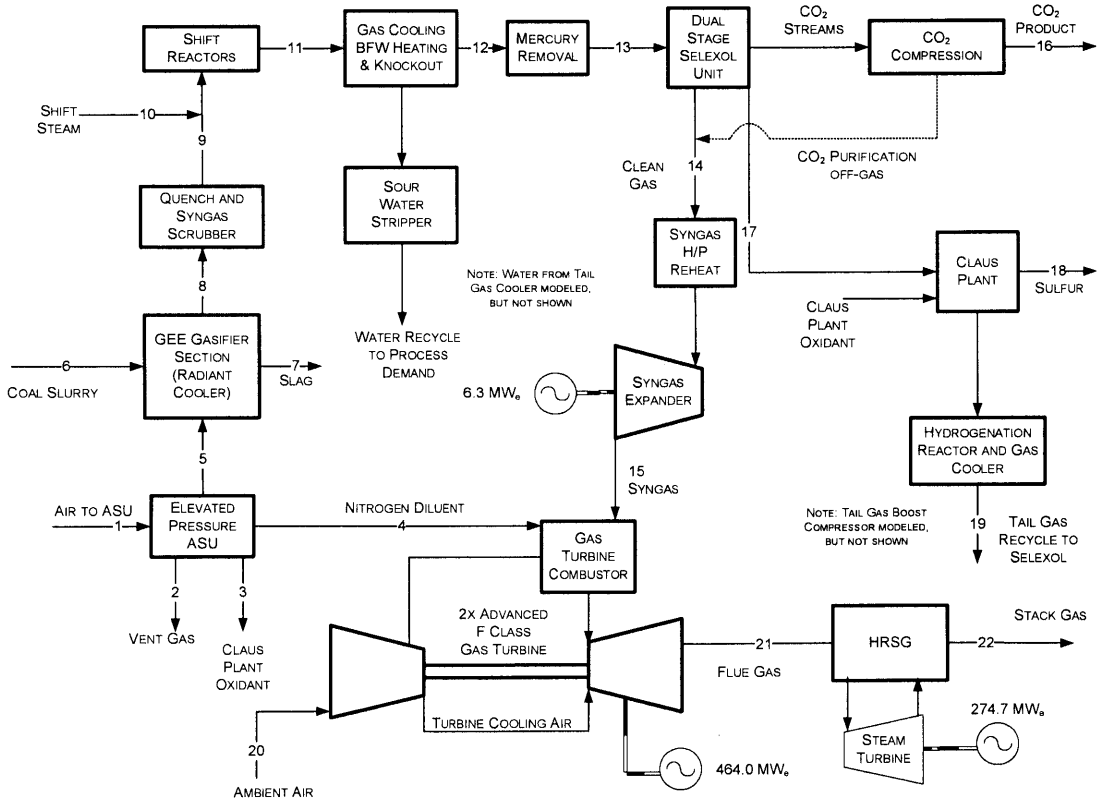

Figure 1-1: The flowsheet of an example IGCC process with CCS. [182]

The IGCC power plant achieves high energy conversion efficiency (up to 45%

(HHV) for the plant without CCS), which is much higher than most of currently operated pulverized coal (PC) fired power plants (33-37%, HHV) [108]. The environmental benefit of the IGCC process is also significant. In the IGCC process, most of the air pollutants, including particulates, mercury, sulfur and nitrogen species, can be removed before combustion at relatively high concentrations. On the other hand, these pollutants have to be removed from much more diluted flue gas in PC plants. Therefore, pollutant control will be a easier task for IGCC plants compared to conventional PC plants [108]. A similar situation is encountered for the control of CO_2 emissions. The implementation of pre-combustion carbon capture in IGCC plants will correspond to 5-8% of energy efficiency loss, while post-combustion carbon capture in PC plants will cause about 12% of energy efficiency loss [182].

The CTL process contains some similar unit operations as those in the IGCC process, including gasification, air separation, WGS reaction, acid gas removal, sulfur recovery and electricity generation. Figure 1-2 shows the flowsheet of a typical CTL process [174]. Coal is first converted to raw syngas by gasification, and syngas is then cleaned and upgraded by scrubber, WGS reactors and acid gas absorption units (e.g., Selexol or Rectisol units). The clean syngas that is ideal for liquid fuels and chemicals production should possess a H_2/CO mole ratio equal to 2, be free of sulfur species, and have low concentrations of all other species, especially CO_2 and water. In order to protect the catalyst for liquids production, very low sulfur content in the syngas is required. The clean syngas can be synthesized to liquid products by two different pathways: the methanol process and the Fischer-Tropsch (FT) process. In the methanol process, clean syngas is converted to methanol by the methanol synthesis reaction, followed by a separation unit removing unreacted syngas, water and higher alcohols from the methanol product. Unreacted syngas is recycled back to the reactor or sent to the gas turbine to produce electricity. The methanol product can be directly sold to the market or further upgraded to other products, such as dimethyl ether (DME), gasoline (by the MTG process) or olefines (by the MTO process). In the FT process, clean syngas is converted to hydrocarbons with a wide range of carbon numbers by the FT synthesis reaction. The composition of the FT product is highly

dependent on the catalyst and operating conditions (e.g., temperature and pressure). A complicated separation system is required to obtain qualified products. Typically, five different streams are produced from the separation system: light ends (including unreacted syngas and hydrocarbons with small carbon numbers), naphtha, diesel, wax and water. Naphtha and diesel can be directly sold or further upgraded. Wax is usually converted to naphtha and diesel by catalytic cracking or hydrocracking. Light ends are sent to the gas turbine to produce electricity, or converted back to syngas by steam reforming or partial oxidization for the FT reaction.

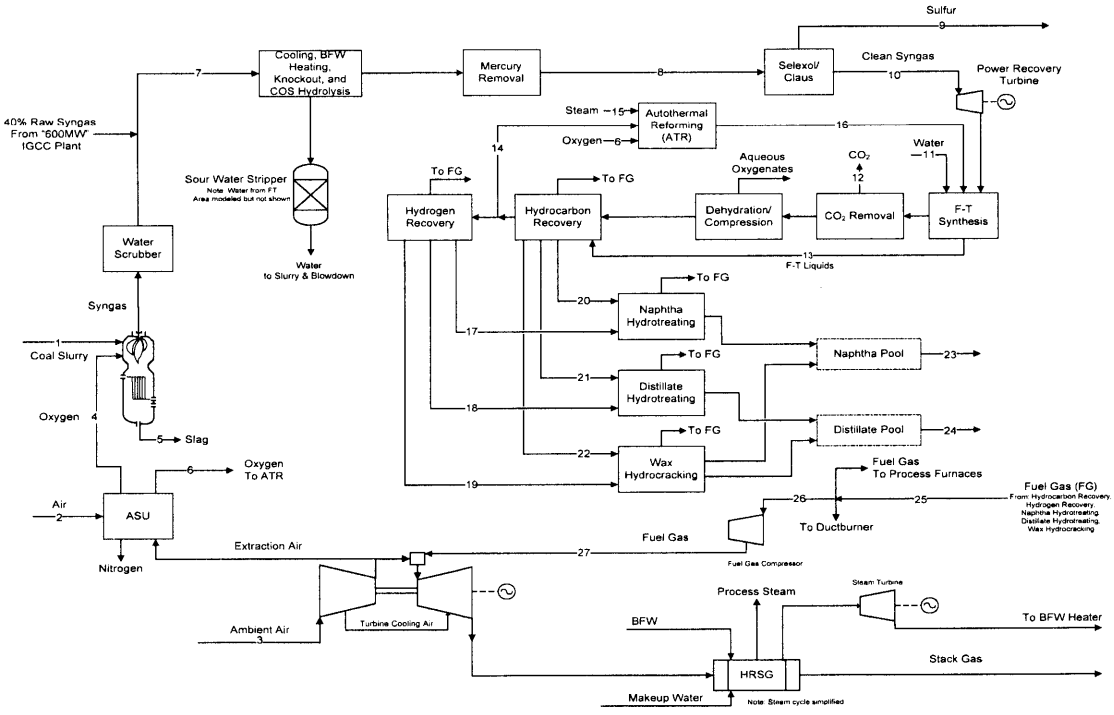

Figure 1-2: The flowsheet of an example CTL process. [174]

The liquid fuels produced by the CTL process are considered as alternatives to current petroleum-derived fuels, especially for those oil-importing countries. The FT products have nearly no sulfur and very low content of aromatics, which can be sold as high-quality fuels or blended with high-sulfur fuels. The economic performance of the CTL process has been studied, and it is indicated that the CTL plant will be profitable if the crude oil price stays above $37 per barrel [173]. The CTL process with CCS will not generate more CO_2 emissions than the oil refinery process. It is

estimated that CTL-derived diesel will result in 5-12% less life cycle CO_2 emissions than the average petroleum-derived diesel [167]. At present, several small-scale CTL demonstration plants are being built worldwide.

1.1.2 Biomass Conversion Processes

Biomass is a promising energy source with its abundant reserves and renewable supplies, low air pollution and very low lifecycle CO_2 emissions [81]. The EIA predicts that biomass will lead to the growth of renewable electricity generation and biofuel will lead to the growth of the liquid fuel supply in the next 25 years [52].

Biomass-derived transportation fuels are produced via several approaches, including fermentation, gasification and pyrolysis. At present, fermentation is the only commercialized biofuel production technology. Compared to the other two ways, fermentation has advantages of lower capital cost and flexible operation. However, feedstocks for the fermentation approach are quite limited so far, e.g., only grains and sugar can be used as feedstock based on the current technology. Development of grain-based biofuel will eventually threaten global food supply. In contrast to fermentation, the gasification approach is able to utilize a wide range of non-grain biomass feedstocks, including wood, grass and crop residues. Combined with the FT process, the gasification approach produces liquid fuels (naphtha and diesel) that can be directly used by vehicles and is compatible with the current infrastructure. Biomass-to-liquids (BTL) processes (via gasification) are therefore of increasing interest to the energy industry.

The BTL process has a similar structure to the CTL process, and both of them include the gasifier, scrubber, sulfur removal unit, FT system, gas turbine and steam turbine. Since biomass is a carbon neutral feedstock, CO_2 sequestration is not needed for the BTL process. The air-blown circulating fluidized bed (CFB) gasifier, which is operated at relatively low temperature and low pressure, is usually selected for biomass gasification. CFB gasifiers suffer from incomplete conversion of feedstock and formation of certain amounts of hydrocarbons. Larger hydrocarbons generated in the CFB gasifier, including BTX (benzene, toluene and xylene) and tars, must be

removed before the FT process. Several methods are available for tar removal, e.g., thermal cracking, catalytic cracking and scrubbing. A typical BTL process flowsheet with three tar removal alternatives is shown in Figure 1-3 [82]. In order to achieve higher conversions, oxygen-blown entrained-flow gasifiers are also considered for the BTL process, with some additional feedstock pre-treatment steps such as drying and torrefaction before gasification.

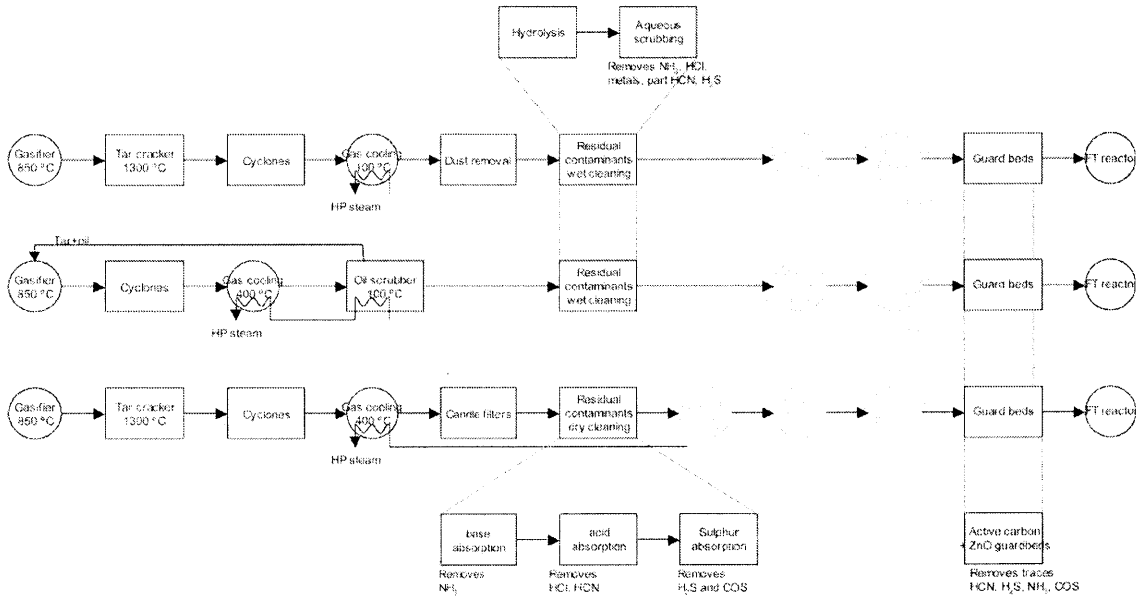

Figure 1-3: The flowsheet of an example BTL process with three tar removal alternatives. [82]

1.1.3 Energy Polygeneration Processes

The aforementioned coal and biomass conversion processes have advantages of high energy efficiency, low toxic pollutants and low CO_2 emissions. However, several problems are encountered before these processes become applicable. One major drawback of IGCC, CTL and BTL is the high capital cost per unit of product. For example, the capital cost for an IGCC plant with CCS can be as high as \$2390/kW based on an estimation in 2007 [182]. With the increase of construction material prices and more understanding of technical difficulties, the estimated capital cost for IGCC and CTL will be even higher in the future. Another drawback of these processes is that

a fixed production rate must be maintained due to rigorous operational requirements for the gasifier. These single-product processes cannot easily adapt to the fluctuation of product market prices, especially liquid fuels prices, and their profitability cannot be guaranteed under all economic conditions. The availability of feedstocks for the BTL process might also be a problem. Biomass is usually harvested in certain seasons, while the gasifier requires continuous operation during the whole year. The BTL plant will suffer from either shortages of feedstock during some times or high feedstock storage costs. High capital costs, uncertainties in the product market and the feedstock supply result in high investment risks for potential application of these single-product processes.

Energy polygeneration could be a plausible way to address the above issues. Polygeneration, or cogeneration, is a concept in which multiple products are generated in a single plant from multiple feedstocks by tightly integrating multiple processes into one system. Polygeneration is attractive for the above advanced energy conversion processes. Note that IGCC, CTL and BTL processes share some common unit operations, including gasification, scrubbing, acid gas removal and power generation. It is possible to design an energy polygeneration process by integrating IGCC, CTL and BTL processes together, which uses coal and biomass as feedstocks and co-produces electricity, liquid fuels, chemicals, hydrogen and heat in one plant.

Compared to single-product energy processes, energy polygeneration processes have many economical and environmental advantages. With polygeneration, the capital cost and production cost per unit of product will be possibly reduced since some equipment included in the IGCC, CTL and BTL can be shared in one process [183, 118, 119]. For example, in a polygeneration plant co-producing DME and electricity, the production cost of DME will be \$6-6.5/GJ, which is comparable with conventional fuel prices [118, 51]. Moreover, in a polygeneration process, economic risks can be reduced by diversification of product portfolios, and potentially higher profits can be achieved compared to the single-product plants by optimization of the portfolios. Higher energy efficiency may also be attained in polygeneration processes due to the tight heat integration of the system [118], e.g., heat generated in exother-

mic reactors in the FT or methanol synthesis process can be recovered by steam generation systems for additional power production.

Polygeneration is a promising process that facilitates the usage of biomass. In polygeneration processes, biomass and coal can be co-gasified in high-temperature entrained-flow gasifiers with high conversions, and the biomass pre-treatment becomes unnecessary. A stable supply of biomass is not required in polygeneration because coal can be used as feedstock for gasifiers when biomass is unavailable. Liquid fuels produced by co-gasification of biomass and coal with CCS will lead to much lower life cycle CO_2 emissions than petroleum-based fuels. Biomass and coal polygeneration processes with CCS will even have negative process CO_2 emissions, which can be sold as carbon credits or compensate for CO_2 emissions from other processes.

Design and operation of energy polygeneration processes is a challenging task, in which knowledge and information in different disciplines such as chemical engineering, mechanical engineering, thermal engineering, biochemical engineering and electrical engineering are needed. Because of the high system complexity, engineering experience and experimental methods, which are frequently used for traditional process design, are not enough for the design of polygeneration processes. Hence, advanced simulation and optimization technologies need to be developed and applied to the optimal design and operation of energy polygeneration systems. Mathematical programming is an effective method for this purpose. By formulating design and operational problems as typical optimization problems, such as nonlinear programming (NLP) problems or mixed-integer nonlinear programming (MINLP) problems, the mass and energy integration of the whole process is systematically studied, and all design and operational variables are optimized to achieve best economic performance or lowest pollutant emissions. Global optimization algorithms can be applied in order to ensure global optimal solutions for these problems.

In this thesis, a polygeneration system co-producing electricity, liquid fuels (naphtha and diesel) and chemicals (methanol) from coal and biomass as feedstock is investigated. The detailed process is described in Chapter 2. The optimal design and operation of (static) polygeneration systems under different economic and policy sce-

narios is studied. Optimal product portfolios are obtained under different product price scenarios. The influence of different carbon tax policies on the optimal production strategy, such as the implementation of CCS or biomass usage, is also explored. The case study results are presented in Chapter 3.

1.1.4 Flexible Energy Polygeneration Processes

Conventional energy and industrial processes attempt to maintain operations at their maximum capacities during the whole operational period, which are called static processes. Static processes are relatively easy to operate and control, and most of equipment are most efficient when operated at their design capacity. However, static processes may not be economically optimal. In reality, market prices and demands fluctuate frequently. For example, prices of liquid fuels (i.e., gasoline and diesel) vary seasonally; power prices fluctuate during the course of the day due to the difficulty of storage, and both are affected by unpredictable human behavior. Static plants may suffer from high inventory levels or lack of stock under some unpredictable market conditions, resulting in significant profit loss. More significant problems are encountered for static power plants, such as coal-fired power plants, nuclear power plants and even IGCC power plants (due to the inflexible operation of the gasifier). Power prices and demands at peak times can be several times higher than those at off-peak times, and power demands can be extremely high under some bad weather conditions such as high temperatures. High dependence on static power plants will lead to serious power shortages at some peak times and significant energy wastage in off-peak times.

The concept of a flexible polygeneration process, which allows variable product mixes during the project lifetime according to market prices and demands, is therefore proposed. A flexible polygeneration plant alters the production rates of individual products in response to changing market conditions by oversizing equipment. In other words, the flexible plant focuses on power generation during peak times when the power price and demand is high, and is switched to liquids production during off-peak times when the power price and demand drop significantly. Liquids can be stored

for a short time and then sold to the market. The flexible polygeneration process redirects production from unstorable energy (electricity) to storable energy (liquid fuels) during off-peak times, and significantly increases the total feedstock utilization. In order to obtain higher profits and prevent high product inventory, the production pattern of flexible polygeneration plants also changes monthly or seasonally according to market conditions. Flexible polygeneration processes try to focus on producing the most profitable product at different times under the capacity constraints, hence they can adapt the product mix to market fluctuations and have the potential to achieve better economic performance than static processes.

However, the overall profitability of flexible polygeneration processes cannot be easily justified. Greater operational flexibility allows larger production rates for the most profitable product in the corresponding time period, and increases the total product revenue. Meanwhile, greater operational flexibility requires larger equipment sizes and increases the capital investment. Inappropriate oversizing of equipment may cause significant "capacity wastage" and reduction in returns on capital. The major challenge in the design of flexible polygeneration systems is determination of the optimal trade-off between operational flexibility and capital cost. It means that the long-term design problem and the short-term operational problems must be solved simultaneously, while they are often considered to be separate problems in most of current system design studies [50].

The joint design and operational problem can be addressed by advanced mathematical programming technologies. A stochastic/multiperiod optimization formulation, which simultaneously optimizes design decision variables and operational decision variables to obtain the maximum overall or expected net profit over the whole project lifetime, is a suitable modeling framework for this problem. It is expected to be a large-scale optimization problem with high computational complexity, and cutting-edge modeling methods and global optimization algorithms need to be developed to solve it efficiently. In this thesis, the optimal product portfolios, equipment capacity usages and CO_2 emissions of flexible energy polygeneration systems under different market conditions are studied. The detailed case study results are discussed

in Chapter 4.

1.1.5 Literature Review

Much progress has been made on the design and operation of coal/biomass-based polygeneration systems using simulation technologies. Mantripragada and Rubin [123] developed a comprehensive techno-economic assessment model of a CTL plant and a polygeneration plant co-producing liquid fuels and power that is capable of incorporating CCS, and investigated its capability of mitigating CO_2 emissions compared to conventional coal-fired power plants. Wang et al. [179] simulated a co-production system including a FT synthesis reactor and a gas turbine in Aspen Plus and GS software, in which over 50% energy conversion efficiency and only 6-7 years of payback time were achieved. Hamelinck et al. [82] analyzed the technical and economic performance of a biomass conversion system that produced liquid fuels and electricity in Aspen Plus, in which the influence of device parameters on investment costs, FT efficiency, electricity efficiency, and resulting FT diesel costs were evaluated. Starfelt et al. [162] evaluated the performance of a polygeneration system that integrated a lignocellulosic wood-to-ethanol process and an existing combined heat and power (CHP) plant, and showed that the integrated polygeneration system reached a total efficiency of 50% and the total biomass consumption was reduced by 13.9% when producing the same amounts of products as in the single-product systems. Yu et al. [187] investigated the performance of polygeneration processes converting coal to liquid fuels and electricity with CCS, in which the thermal efficiency and CO_2 emissions were studied. Li et al. [109] proposed a polygeneration system utilizing natural gas and biomass as feedstocks and co-producing methanol and electricity, in which feedstock input was reduced by at least 9% compared to individual systems with the same output illustrated by Aspen Plus simulation results. Lin et al. [116] performed a techno-economic analysis for coal-based polygeneration systems co-producing methanol and electricity with and without CO_2 recovery, and showed that the polygeneration technology could effectively reduce the cost penalty for CO_2 recovery. Adams and Barton [9, 10] studied polygeneration systems converting coal and natural gas to electricity, methanol,

gasoline and diesel, and compared different natural gas reforming strategies for the best energy efficiency and profitability. Ng and Sadhukhan [140, 141] analyzed energy efficiency and production costs for bio-oil integrated gasification and methanol synthesis (BOIG-MeOH) systems and bio-oil integrated gasification and Fischer-Tropsch (BOIG-FT) systems. Gassner et al. [64, 63, 62] built a thermo-economic model for the polygeneration process that co-produces synthetic natural gas (SNG), electricity and heat from waste biomass, and studied the most profitable system configurations under different energy price scenarios and scales. Li et al. [115] performed an exergoeconomic analysis for a dual-gas (syngas from coal gasification and coke oven gas) sourced polygeneration process co-producing methanol, DME and dimethyl carbonate (DMC), and studied the exergy loss and the production cost in the process. Some other studies for coal- and/or biomass-based polygeneration systems can be found in Refs [149, 99, 186, 86, 61, 185, 142]. These studies provide potential feasible polygeneration system designs for real applications and demonstrate that polygeneration processes exhibit better economic performance and lower CO_2 emissions than conventional energy production processes. However, no systematic optimization for process design and operation variables was done in these studies.

Optimal design and operation of coal/biomass-based polygeneration systems based on mathematical programming has been investigated in several papers. Liu et al. [118] constructed a mixed-integer linear programming (MILP) model in GAMS for a coal polygeneration system co-producing methanol and power, in which the net present value (NPV) was maximized by optimizing different combinations of feedstocks and technologies. This demonstrated that polygeneration processes with fixed electricity and methanol yields have advantages over methanol synthesis processes in a vast range of methanol/power price ratios. Following this work, Liu et al. [119, 121, 120] developed a series of MINLP models in GAMS for coal-based polygeneration systems co-producing methanol and power, in which combinations of technologies together with design and operational variables were optimized to obtain the best annual profit or NPV. Compared to the original work [118], more process details were added into the model in [119], a multi-objective optimization approach was applied in [121] and

process uncertainties were considered in [120]. Baliban et al. [27, 28, 29, 30] studied a hybrid coal, biomass and natural gas to liquids (CBGTL) process that produced transportation fuels (gasoline, diesel and kerosene). A MINLP model was formulated for the optimal process synthesis with simultaneous heat, power and water integration. Optimal designs under different feedstocks, plant capacities and process superstructures were investigated. The case study results showed that the break-even oil prices for liquid fuels production were \$61.36/bbl for the small capacity, \$60.45/bbl for the medium capacity, and \$55.43/bbl for the large capacity. So far, systematic studies of optimal design and operation of polygeneration systems under different market and policy scenarios have not been made.

The concept of flexible designs has been studied for some power generation systems. For example, Yunt et al. [189] developed a two-stage optimization formulation for the optimal design of a fuel cell system for varying power demands. This formulation incorporates a design stage and an operational stage, optimizing the design decision variables (such as equipment sizes) and the operational decision variables (such as temperatures and flow rates) for all potential power demands simultaneously. The authors pointed out that an optimal design based on a nominal power demand would perform poorly or even become infeasible for some peak power demands, and they also demonstrated that a flexible design determined by the two-stage formulation achieved higher fuel energy densities than other designs.

Flexible polygeneration systems have been studied in several papers. Meerman et al. [132, 130, 131] investigated technical possibilities and performances of a flexible polygeneration system, called integrated gasification polygeneration (IG-PG), by Aspen Plus simulations. This polygeneration system uses oil residues, coal and biomass as feedstocks, and co-produces H_2, electricity, FT-liquids, methanol and urea. The flexible system produced electricity during peak hours, while was switched to chemical productions during off-peak hours. The authors studied the influence of feedstock on the performance of the system, including CO_2 emissions and energy efficiency. The possible ranges for equipment load under flexible operations were also studied, e.g., the operation of the FT section was restricted to 60-100% load to prevent that the

gas turbine load is below 40%. No optimization on the system design and operation was done in these works. Liu et al. [121] studied the optimal design of a coal polygeneration system co-producing power and methanol with multiple operation periods. In this study, the feedstock and product prices were assumed to increase from period to period due to inflation. The optimal design and operation schedule in three periods (with several years in one period) were determined by a two-stage formulation. However, seasonal variations of market prices and daily fluctuations of power prices, which are critical in flexible polygeneration systems, were not considered in this study.

Design and operational optimization work has also been done in some other energy conversion systems. Liszka and Ziebik [117] developed a design optimization model for a metal production system consisting of a Corex unit (one of technologies for cokeless hot metal production), a combined cycle power plant and an ASU, and optimized the NPVs for different price scenarios in the coal, iron and electricity markets. Karuppiah et al. [98] minimized the energy requirement of a corn-based bioethanol plant through the use of heat integration and mathematical programming techniques, and the results showed that the steam consumption required could be reduced by more than 40% compared to the initial basic design. Martin and Grossmann [127, 128, 129] investigated the optimal design of several biofuel production processes, including a FT-diesel production process using switchgrass via gasification [127], a bioethanol production process using switchgrass via hydrolysis [128] and a biodiesel production process using waste cooking oil and algae oil via catalytic reactions [129]. In these studies, the optimal technology alternatives and operational conditions were obtained by solving MINLP models. The results indicated that low production costs and low energy and water consumptions could be achieved in these processes. Much work has also been done on optimal design and operation of CHP systems, co-producing electricity, heat and chilled water, to achieve minimum annual costs, energy costs or CO_2 emissions [21, 15, 44, 42, 155, 144, 83, 180, 146, 50].

1.2 Stochastic/Multiperiod Optimization Problems

1.2.1 Problem Formulation & Applications

Stochastic/multiperiod optimization problems are often formulated using the following two-stage framework [35, 93]:

$$
\begin{aligned}
\max_{\mathbf{y}} \; & f^{(1)}(\mathbf{y}) + \sum_{h=1}^{s} \mathrm{Occu}_h M_h(\mathbf{y}, \mathrm{Par}_h) \\
\text{s.t.} \; & \mathbf{g}^{(1)}(\mathbf{y}) \leq \mathbf{0} \\
& \mathbf{h}^{(1)}(\mathbf{y}) = \mathbf{0} \\
& M_h(\mathbf{y}, \mathrm{Par}_h) \equiv \left.\begin{aligned} \max_{\mathbf{x}_h} \; & f^{(2)}(\mathbf{y}, \mathbf{x}_h, \mathrm{Par}_h) \\ \text{s.t.} \; & \mathbf{g}^{(2)}(\mathbf{y}, \mathbf{x}_h, \mathrm{Par}_h) \leq \mathbf{0} \\ & \mathbf{h}^{(2)}(\mathbf{y}, \mathbf{x}_h, \mathrm{Par}_h) = \mathbf{0} \\ & \mathbf{x}_h \in \mathbf{X}_h \end{aligned}\right\} \forall h \in N_h \\
& \mathbf{y} \in \mathbf{Y}
\end{aligned}
\tag{1.1}
$$

where $\mathbf{y}$ are design decision variables, $\mathbf{x}_h$ are operational decision variables in scenario h; $\mathbf{Y}$ are bounds on the design decision variables, $\mathbf{X}_h$ are bounds on the operational decision variables in scenario h; $\mathbf{g}^{(1)}$ and $\mathbf{h}^{(1)}$ are design inequality and equality constraints, respectively, such as equipment cost calculations; $\mathbf{g}^{(2)}$ and $\mathbf{h}^{(2)}$ are operational inequality and equality constraints, respectively, such as mass and energy balances, reactor feedstock specifications and emission regulations; $f^{(1)}$ is the part of the objective function that is only dependent on design decision variables, e.g, a function of capital costs; $f^{(2)}$ is the part of the objective function that is dependent on both design and operational variables, e.g., a function related to product revenues, feedstock costs and operational costs; Occu_h is the probability or fraction of occurrence of scenario h over the plant lifetime; Par_h are the economic parameters in scenario h; $N_h \equiv \{1, \ldots, s\}$ is the set of scenarios over the plant lifetime. M_h is the optimal solution of the h^{th} second-stage (or operational-stage) program. The size of the whole

problem depends on the number of scenarios s. When s is large, the problem can be a large-scale MINLP problem even if the second-stage problem M_h is small.

The program (1.1) can be simplified to an equivalent single-level program, as shown in Eq (1.2):

$$\begin{aligned}
\max_{\mathbf{y},\mathbf{x}_1,\ldots,\mathbf{x}_s} \quad & f^{(1)}(\mathbf{y}) + \sum_{h=1}^{s} \mathrm{Occu}_h f^{(2)}(\mathbf{y}, \mathbf{x}_h, \mathrm{Par}_h) \\
\text{s.t.} \quad & \mathbf{g}^{(1)}(\mathbf{y}) \leq \mathbf{0} \\
& \mathbf{h}^{(1)}(\mathbf{y}) = \mathbf{0} \\
& \left.\begin{aligned} & \mathbf{g}^{(2)}(\mathbf{y}, \mathbf{x}_h, \mathrm{Par}_h) \leq \mathbf{0} \\ & \mathbf{h}^{(2)}(\mathbf{y}, \mathbf{x}_h, \mathrm{Par}_h) = \mathbf{0} \\ & \mathbf{x}_h \in \mathbf{X}_h \end{aligned}\right\} \forall h \in N_h \\
& \mathbf{y} \in \mathbf{Y}.
\end{aligned} \tag{1.2}$$

Program (1.2) is much easier to solve than program (1.1) in practice, and thus is widely used for stochastic/multiperiod problems. However, the solution sets of (1.1) and (1.2) are only guaranteed to be identical for their global optimal solutions [189]. Hence, a global optimization solver must be applied to problem (1.2) in order to obtain the global solution of the two-stage program (1.1).

Stochastic and multiperiod programming problems have the same two-stage structure. However, there are several subtle differences between the two problems. In multiperiod programs, all scenarios will occur during the plant lifetime with a known frequency of occurrence and the overall profit during the plant lifetime is optimized. In stochastic programs, the scenarios are random events and only one with estimated probability of occurrence will occur during the plant lifetime. The stochastic program is intended to optimize the expected value of the profit whose actual value is unknown before the plant begins to operate.

Stochastic/multiperiod pooling problems are a class of optimization problems, in which the only nonlinear functions are bilinear functions. They are widely used for optimization of chemical systems when blending and separation processes are

involved and stream compositions need to be tracked in the whole system. Stochastic/multiperiod pooling problems are potentially large-scale nonconvex MINLP problems, where the nonconvexity originates from the bilinear functions.

Besides flexible energy polygeneration optimization problems, two-stage stochastic/multiperiod programming formulations are also applied to a wide range of other engineering design and optimization problems. For example, the two-stage multiperiod formulation is used for the design and planing of power generation systems [189, 122], petroleum production and supply systems [138, 175, 139], utility systems [87, 88, 6, 159], water supply systems [165], supply chain networks [38, 46, 184, 94], batch manufacturing facilities [125, 177, 26, 137, 176], production and distribution of multiproduct systems [89] and oil spill response [192]; and the two-stage stochastic formulation is extensively applied to optimization problems with the presence of uncertainty, such as oil & gas production [161, 110, 72, 91, 103, 166], refinery planning [148, 104, 105, 18, 107], power generation [73, 172, 90, 143, 43, 40], heat integration [147, 65], water management [85, 22, 17, 71, 96], coal polygeneration [120], reactor design [126], real-time optimization (RTO) [191] and supply chain networks [156, 80, 75, 78, 92, 79, 16, 45].

1.2.2 Global Optimization Algorithms & Literature Review

Global optimization algorithms guarantee the global optimal solutions for nonconvex MINLP problems. For simplicity, the following discussion is only based on the minimization problems, and it could be easily modified for the maximization problems. In global optimization algorithms, a sequence of lower and upper bounds on the optimal objective value is generated. At each iteration, the lower bound is obtained by solving a relaxation of the original problem, and the upper bound is obtained by solving a restriction of the original problem. The lower and upper bounds will converge to the global optimal solution (within the specified tolerance) after a finite number of iterations. Several global optimization algorithms have been developed so far, including branch-and-bound, outer approximation (OA), generalized Benders decomposition (GBD) and Lagrangian decomposition [113, 76].

In branch-and-bound algorithms, the domain of the problem is partitioned at each iteration. The lower bounds are generated by solving relaxations (typically convex relaxations) of the problem on each of the subdomains, and the upper bounds are generated by solving restrictions or obtaining local optima or feasible solutions of the problem on each of the subdomains. A large number of subdomains may be fathomed by comparing the upper and lower bounds. For example, when the local optima or feasible solutions of the problem are used for upper bounds, subdomains whose lower bounds are higher than or equal to the lowest upper bound can be fathomed. The branch-and-reduce algorithm is a typical branch-and-bound algorithm, which applies range reduction techniques [152, 154, 169, 168, 170]. The αBB algorithm is another type of branch-and-bound algorithm for general twice-differentiable functions [19, 14, 12, 13]. The computational times of branch-and-bound algorithms might increase exponentially with the problem size in the worst case. Therefore it will be quite challenging for branch-and-bound algorithms to handle large-scale MINLP problems, including stochastic/multiperiod optimization problems.

In OA algorithms, the original problem is reformulated to a master problem by projection and outer linearization, which potentially contains a large number of constraints. The relaxed master problem is then generated by selecting a finite subset of the constraints in the master problem, and its solution provides a lower bound on the optimal objective. A restriction of the original problem, called the primal problem, is solved to give an upper bound on the optimal objective. By iteratively solving primal problems and relaxed master problems, a sequence of nonincreasing upper bounds and nondecreasing lower bounds are generated. The global optimal solution is obtained when the upper bound and lower bound coincide. Note that although the primal problem may possibly be decomposed into subproblems with smaller sizes, the relaxed master problem still needs to solved in the space of all variables. The development for OA algorithms can be found in Ref [57, 178, 59, 176]. The original OA is designed for problems with only convex nonlinear functions. Kesavan et al. [100, 101] developed a new OA algorithm that extends the application of OA to problems with nonconvex functions. OA cannot fully exploit the special structure of

two-stage stochastic/multiperiod problems (e.g., the size of the relaxed master problem depends on the number of scenarios) and it is usually not practical for problems with a large number of scenarios.

GBD is the extension of Benders decomposition (BD) [32] (which is also called the L-shaped method for stochastic linear programs [160, 34, 36]) to nonlinear problems, which was originally developed by Geoffrion [68]. In GBD algorithms, a master problem is generated by projection and dualization of the original problem, and it contains an infinite number of constraints. GBD algorithms have almost the same procedure as OA algorithms. Primal problems and relaxed master problems are solved for upper and lower bounds. The relaxed master problem in GBD only contains a subset of the variables, which are typically complicating variables (or first-stage variables in two-stage problems), and its size could be much smaller than that in OA. GBD is quite suitable for the two-stage stochastic/multiperiod programming problems since GBD can fully exploit the special mathematical structure of those problems. When applied to two-stage programs, primal problems in GBD are constructed by fixing the first-stage variables, which then naturally decomposed into a series of subproblems that only contain the variables of one scenario. The relaxed master problems only include first-stage variables, and their sizes are independent of the number of scenarios. Therefore, the computational time for GBD is expected to increase linearly with the number of scenarios. The original version of GBD can only solve problems with convex nonlinear functions. Recently, Li et al. [113, 114] developed a new version of the GBD algorithm, called nonconvex generalized Benders decomposition (NGBD), for problems with nonconvex functions. NGBD has been successfully applied to several large-scale stochastic programming problems, including the Haverly pooling problem, pump network configuration and natural gas production network design [110, 112, 113, 114].

Lagrangian decomposition is another important algorithm for MINLP problems [77, 134], which is also widely used for two-stage stochastic programs [151]. In Lagrangian decomposition algorithms, the original problem is reformulated by duplicating the first-stage variables and adding additional equality constraints (or linking con-

straints) to link these variables. The dual of this reformulated problem, or Lagrangian relaxation of the original problem, is generated by dualizing the linking constraints into the objective function. The Lagrangian relaxation can be naturally decomposed into a series of much smaller subproblems for each scenario. The Lagrangian decomposition is usually used in a branch-and-bound framework to guarantee convergence to a global optimal solution when applied to nonconvex MINLP problems [97, 102]. Note that within the branch-and-bound framework for the Lagrangian decomposition, branching needs to be performed in the full variable space whose size depends on the number of scenarios. Hence, Lagrangian decomposition may not practically solve problems with a large number of scenarios.

Compared to other global optimization algorithms, NGBD is the most suitable one for the flexible polygeneration optimization problems. In this thesis, NGBD is further developed to enhance its performance and applied to case studies of flexible polygeneration design and operation. Discussions will be found in Chapter 5, 6 and 7.

Chapter 2

Process Description of Energy Polygeneration Systems

2.1 Overview

In this thesis, a polygeneration system co-producing power, liquid fuels (naphtha and diesel) and chemicals (methanol) from coal and biomass as feedstock is investigated [48, 47]. A simplified process flowsheet of the polygeneration system is shown in Figure 2-1. Coal and biomass are first converted to synthesis gas (syngas) in the gasifier. Then, the sulfur species, CO_2, and other pollutants in the syngas are removed in the syngas cleaning and upgrading process. Finally, the syngas is split to different downstream energy product processes such as the Fischer-Tropsch synthesis process, the methanol synthesis process and the gas turbine. All usable heat generated in the process is recovered in the heat recovery steam generator (HRSG) for additional power generation using steam turbines.

The whole system comprises six subsystems: air separation unit (ASU) and gasifier, syngas cleaning and upgrading process, Fischer-Tropsch (FT) synthesis process, methanol (MeOH) synthesis process, gas turbine (GT), and heat recovery steam generator (HRSG) and steam turbine. The detailed process flowsheet is shown in Figure 2-2, where each subsystem is placed in the same position as in Figure 2-1. IGCC and CTL process designs in NETL reports [182, 173, 174] are selected as references for

the polygeneration system design.

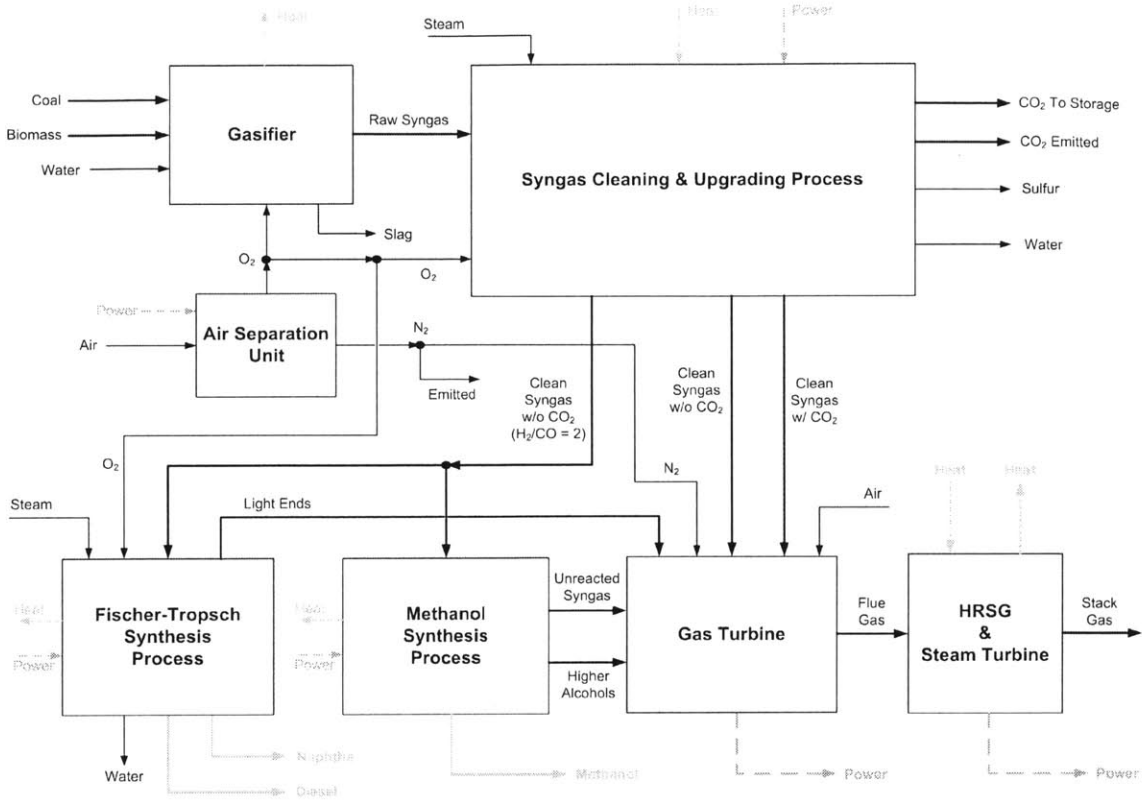

Figure 2-1: Simplified process flowsheet of the polygeneration system.

2.2 ASU and Gasifier

In the air separation unit, O_2 with over 95 mol % purity and a N_2 stream are produced by a cryogenic distillation process. Most of the O_2 is compressed and fed into the gasifier, and the rest is sent to the Claus plant in the syngas cleaning process and the auto-thermal reforming reactor in the Fischer-Tropsch synthesis process. Part of the N_2 is used as diluent in the gas turbine combustor to prevent excessive temperatures in the gas turbine generator and to reduce nitrogen oxide emissions.

A slurry-feed, oxygen-blown, entrained-flow gasifier is selected, where the coal (and biomass) and water are fed. High temperature, high pressure syngas is produced. Based on the current designs of entrained-flow gasifiers, biomass cannot totally replace coal as the carbon source and the biomass/coal mass ratio cannot exceed an upper

limit. The raw syngas produced consists mostly of H_2 and CO with smaller amounts of water vapor and CO_2 and small amounts of H_2S, COS and other impurities. Coal ash is melted and flows out of the gasifier as slag, which can be used to produce building materials. Hot syngas from the gasifier passes a radiant cooler and a convective cooler to recover high temperature heat and middle temperature heat, and then is sent to the syngas cleaning process.

2.3 Syngas Cleaning and Upgrading Process

The syngas cleaning process removes impurities in the raw syngas (including particulates, chlorides, sulfides, mercury and CO_2) and adjusts the H_2 to CO mole ratio in the clean syngas to appropriate levels for downstream processes.

Raw syngas first passes a scrubber to remove particulates and chlorides, and then enters a COS hydrolysis reactor, where almost all COS is converted to CO_2 and H_2S by the following reaction:

$$COS + H_2O \rightleftharpoons CO_2 + H_2S \tag{2.1}$$

The syngas exiting the COS hydrolysis reactor is cooled and passes through a carbon bed to remove over 95% of mercury. Then, cool syngas enters a Selexol unit, where almost all H_2S is removed. The H_2S rich stream is sent to the Claus plant, where H_2S is converted to elemental sulfur, a product of the polygeneration process, via the following reaction:

$$H_2S + \frac{1}{2}O_2 \rightleftharpoons H_2O + S \tag{2.2}$$

The syngas exiting the Selexol unit is almost free of H_2S and other pollutants. The clean syngas is reheated and split into three branches: the left branch for production of syngas with H_2/CO mole ratio of 2 for Fischer-Tropsch synthesis and methanol synthesis processes, the middle branch for generation of H_2 rich gas for the gas turbine, and the right branch for electricity production with the gas turbine. In the polygeneration system design, the split fractions of syngas to these three branches

can be adjusted to change the production rates of power and liquids (naphtha, diesel and methanol) and decide whether carbon capture and sequestration (CCS) is implemented in the power generation section.

The left and middle branches have similar structure. Clean syngas first passes through three-stage water gas shift (WGS) reactors in series, which include two high-temperature reactors and one low-temperature reactor, to convert part of the CO by the following exothermic reaction:

$$CO + H_2O \rightleftharpoons CO_2 + H_2 \tag{2.3}$$

The heat generated can be recovered for power generation. The H_2/CO mole ratios in the syngas after the WGS reactors are different in the two branches. In the left branch, the H_2/CO mole ratio is strictly equal to 2; while in the middle branch, the H_2/CO mole ratio has flexible values much higher than 2. Syngas is then cooled and enters another Selexol unit to remove most of the CO_2. Part of the CO_2 from the Selexol unit is compressed and sequestered, and rest is emitted. In the left branch, syngas after the Selexol unit passes through a Zinc oxide (ZnO) bed to remove trace amount of remaining H_2S, and a small portion of the CO_2 lean syngas is sent to a pressure-swing adsorption (PSA) unit to separate H_2 for the Fischer-Tropsch process. Syngas is then reheated and sent to different downstream processes.

2.4 Fischer-Tropsch Synthesis Process

Sulfur-free syngas with a H_2:CO molar ratio of 2:1 from the left branch of the syngas cleaning and upgrading process passes through a turbine (or expander) to decrease the pressure and is fed to the Fischer-Tropsch (FT) synthesis reactor, where a cobalt-based catalyst is used and syngas is converted into linear paraffinic hydrocarbons with carbon numbers from 1 to 70 by the following reaction:

$$nCO + (2n + 1)H_2 \rightleftharpoons C_nH_{2n+2} + nH_2O \tag{2.4}$$

The FT reaction is highly exothermic; hence a large amount of steam can be produced for power generation. The products of FT synthesis are separated into several streams in the hydrocarbon separation unit: light ends (including unreacted syngas, C_1-C_4 hydrocarbons), naphtha (C_5-C_{10} hydrocarbons), diesel (C_{11}-C_{22} hydrocarbons), wax (above C_{22} hydrocarbons), and water. Naphtha and diesel are products of this polygeneration system, and can be further upgraded in existing refinery processes. Wax is sent to a hydrocracking reactor, converted to light hydrocarbons, naphtha and diesel, and recycled back to the hydrocarbon separation unit. Light ends gas is compressed after the separation unit. Part of the light ends are sent to the gas turbine, and the rest is sent to an autothermal reforming reactor, where light hydrocarbons are converted back to syngas by the following reactions:

$$CO + \frac{1}{2}O_2 \rightarrow CO_2 \tag{2.5}$$

$$H_2 + \frac{1}{2}O_2 \rightarrow H_2O \tag{2.6}$$

$$C_nH_{2n+2} + \frac{3n+1}{2}O_2 \rightarrow nCO_2 + (n+1)H_2O \tag{2.7}$$

$$C_nH_{2n+2} + nH_2O \rightleftharpoons nCO + (2n+1)H_2 \tag{2.8}$$

Part of the syngas produced by the reforming reactor is recycled to the FT synthesis reactor, and the rest is sent back to the syngas cleaning process to remove CO_2.

2.5 Methanol Synthesis Process

Sulfur free syngas with a H_2:CO molar ratio of 2:1 from the left branch of the syngas cleaning and upgrading process is fed to the methanol (MeOH) synthesis reactor, where a copper-based catalyst is used and syngas is converted into methanol by the following reaction:

$$CO + 2H_2 \rightleftharpoons CH_3OH \tag{2.9}$$

The MeOH reaction is highly exothermic; hence a large amount of steam can be produced for power generation. The products of the MeOH synthesis reactor are separated into several streams in the methanol separation unit: unreacted syngas, methanol with purity of 99.8% and higher alcohols that are byproducts of the methanol synthesis reaction. High purity methanol is one of the products of the polygeneration system. Part of the unreacted syngas and higher alcohols are sent to the gas turbine as fuel. The rest of the syngas is recycled to the methanol synthesis reactor.

2.6 Gas Turbine

Clean syngas from the middle and right branches of the syngas cleaning and upgrading process passes through several expanders to reduce the pressure to the maximum operating pressure of the gas turbine, generating some additional power. This is mixed with the tail gas of the PSA unit, light ends from FT synthesis, unreacted syngas and higher alcohols from MeOH synthesis, compressed air, nitrogen from the ASU, and steam to form the feedstock of the gas turbine combustor. High temperature and high pressure flue gas produced from the combustor drives the gas turbine to generate a large amount of power. The exhaust gas exiting the gas turbine with high temperature passes through the HRSG where additional heat is recovered for power generation. The flue gas exiting the HRSG is discharged through the plant stack.

2.7 HRSG and Steam Turbine

Heat generated in units such as the gasifier, WGS reactors, FT reactor, MeOH reactor, Claus plant and gas turbine is recovered in the heat recovery steam generator (HRSG). Part of the heat recovered is supplied to heat-consuming units such as the hydrocarbon separation unit and the methanol separation unit. The rest of the heat is used in the steam turbines to produce additional power.

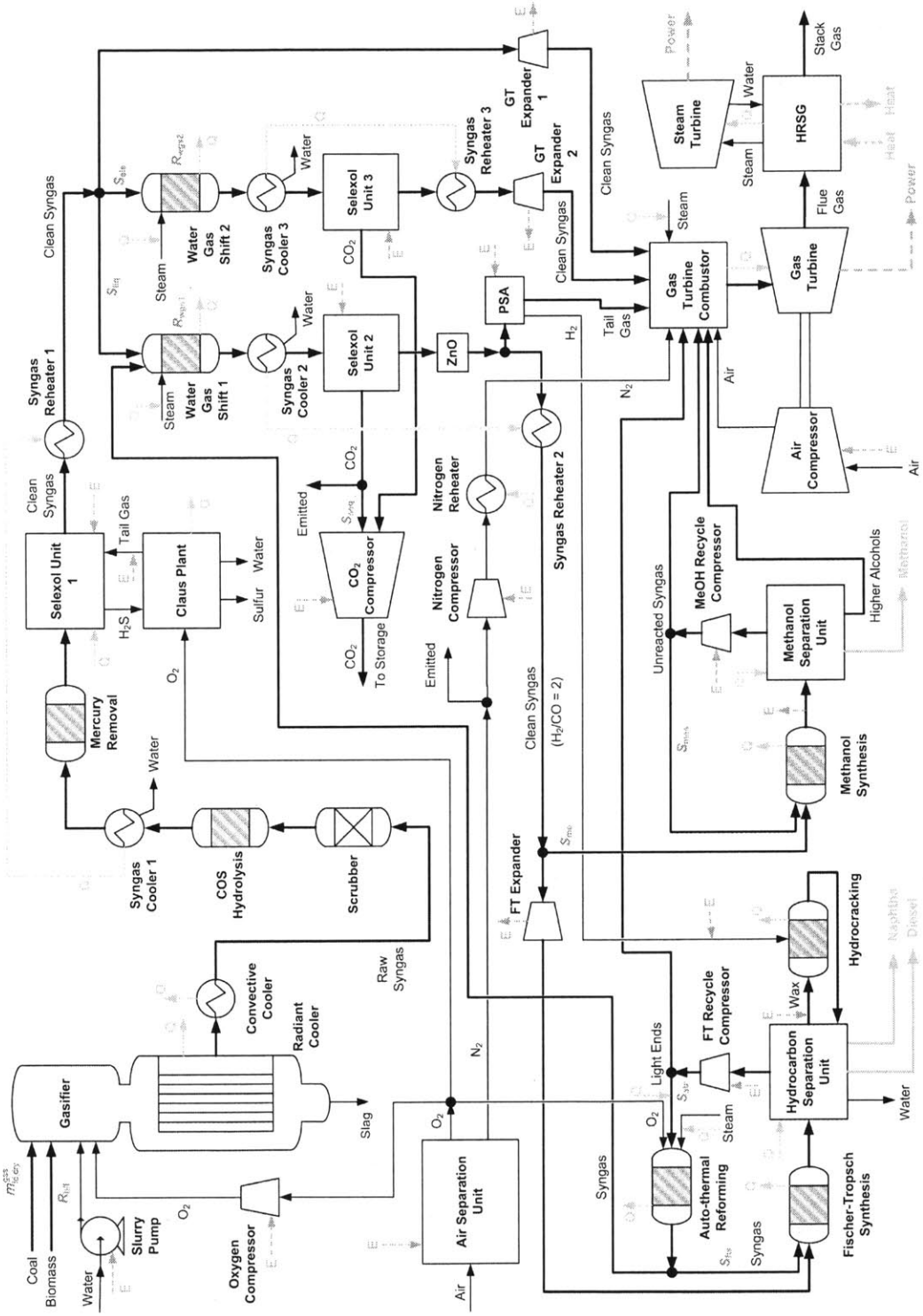

Figure 2-2: Detailed process flowsheet of the polygeneration system.

Chapter 3

Optimal Design and Operation of Static Energy Polygeneration Systems

3.1 Mathematical Model

3.1.1 Overview

This work focuses on the influence of different economic and policy conditions on the optimal design and operation of polygeneration systems [48]. The objective is to maximize the economic performance of the whole plant while satisfying all design and operational constraints. Material and energy balances describe the entire system. To both keep the problem tractable for current global optimization solvers and maintain the accuracy of the model, reduced models are used to represent all unit operations using parameters estimated from detailed Aspen Plus simulation models, the literature, or industrial experience.

The key decision variables are shown in Figure 2-2 and explained in Table 3.1. $m^{\text{gas}}_{\text{fd,dry}}$, which is limited by the gasifier capacity, determines both the feedstock consumption rates and production rates of the whole plant. $R_{\text{b/f}}$ determines the biomass usage level. S_{liq}, S_{ele} and S_{me} determine the flows of syngas to the different down-

stream processes and hence the production distribution. R_{wgs1} and R_{wgs2} determine the optimal CO conversions in the WGS reactors. High CO conversions in the WGS reactors (or deep shifts) achieve low CO_2 emissions, but result in high steam consumption which reduces the energy efficiency of the whole system. Hence the CO conversions need to be optimized based on the product prices and carbon emission tax. S_{seq} determines the CO_2 sequestration ratio, which represents a tradeoff: high CO_2 sequestration ratios imply low CO_2 emissions but high power consumptions. S_{atr} and S_{fts} determine the recycle ratios in the FT process, and S_{mes} determines the recycle ratio in the MeOH process.

Table 3.1: Key decision variables in the model

Decision Variables	**Description**
$m^{\text{gas}}_{\text{fd,dry}}$	Mass flow rate of the dry feedstock fed into the gasifier
$R_{\text{b/f}}$	Dry mass fraction of biomass in the gasifier feedstock
S_{liq}	Split fraction of the clean syngas to the liquid fuel production (or the left) branch in the syngas cleaning and upgrading process
S_{ele}	Split fraction of the clean syngas to the power generation with CCS (or the middle) branch in the syngas cleaning and updating process
R_{wgs1}	Conversion of CO in Water Gas Shift Reactor 1
R_{wgs2}	Conversion of CO in Water Gas Shift Reactor 2
S_{seq}	Split fraction of the CO_2 stream to sequestration
S_{me}	Split fraction of the clean syngas with H_2/CO mole ratio of 2 to the methanol synthesis process
S_{atr}	Split fraction of the light ends exiting the hydrocarbon separation unit to the autothermal reforming reactor
S_{fts}	Split fraction of the syngas exiting the autothermal reforming reactor to the Fischer-Tropsch synthesis reactor
S_{mes}	Split fraction of the unreacted syngas exiting the methanol separation unit to the methanol synthesis reactor

Most parameters in the reduced models of unit operations are estimated from an Aspen Plus simulation model of the polygeneration process [9]. In the Aspen Plus model, RStoic models (reactor models with specified conversions) and RPlug

models (rigorous plug flow reactor models with detailed kinetics) models are selected for reactors, RadFrac models (rigorous 2 or 3-phase distillation models) are used for distillation columns, and compressor/turbine models with isentropic efficiencies are employed for compressors and turbines.

The mathematical models in this study include the following sub-models: mass balances in each unit operation, energy balances, enthalpy calculations, capital cost calculations, production rates, CO_2 emission rates, and economic analyses. Detailed equations are listed in Appendix A. Assumptions and some key equations in each sub-model will be discussed here.

3.1.2 Mass Balance

Air Separation Unit

In the air separation unit, air is separated into O_2 and N_2 rich streams. Only three major species, N_2, O_2 and Ar, are included in mass balance calculations. The split fraction of O_2 in air to the O_2 rich stream is 0.94 [182, 9].

Gasifier

Gasification is the most important unit operation in the polygeneration process. Complex chemical kinetics models, transport models and thermodynamics models are required to represent the entire gasification process accurately. For the highest amount of accuracy, solving these models needs extremely high computational effort and hence they cannot be incorporated into the optimal design model.

In this model, the operating temperature and pressure are fixed as parameters. Six elements (C, H, O, N, S and Cl) in the feedstock are converted to eleven species (CO, H_2, CO_2, H_2O, CH_4, N_2, Ar, H_2S, COS, NH_3 and HCl) in the raw syngas. Conversions of all elements are assumed constant under such operating conditions, e.g., the conversion of C is 0.98 and conversions of all other elements are assumed to be 1 [182, 9].

In this study, Illinois #6 coal is used and straw is selected as the biomass. The

mass fractions of water in Illinois #6 coal and straw are 0.1112 and 0.082, repectively [182, 171]. Their dry mass compositions are listed in Table 3.2 [182, 171].

Table 3.2: Dry mass compositions of feedstocks

Mass Fractions of Elements	Illinois #6 Coal	Straw
C	0.7172	0.476
H	0.0506	0.058
O	0.0775	0.4012
N	0.0141	0.005
S	0.0282	0.0008
Cl	0.0033	0.001

The mole composition of raw syngas from the gasifier is assumed to be unchanged under a given feedstock portfolio. Hence the molar flow rates of all species in the raw syngas can be easily related to the molar flow rates of some key species. Due to the design limitations of current gasifiers, the mass fraction of biomass in the feedstock $R_{\mathrm{b/f}}$ cannot exceed an upper limit $R_{\mathrm{b/f,max}}$ (typically 30%) [167]. In this model, the molar compositions of raw syngas from pure coal and the coal/biomass mixture with the biomass mass fraction of 30% are obtained from the Aspen simulation results [9, 136]. The gasification of coal and biomass is assumed to take place independently, hence the molar composition of the raw syngas from the feedstock with any biomass mass fraction between 0 and 30% is a linear combination of the above two given molar compositions.

Scrubber

Species with high solubility in water (HCl and NH_3) are assumed to be totally removed in the scrubber, while the absorption of other species is neglected.

COS Hydrolysis Reactor

In industry, high COS conversion (typically over 99.5% [182]) can be achieved in the hydrolysis reactors. The COS is thus assumed to be totally converted in this model.

Selexol Units

In this model, the operating temperature and pressure are fixed as parameters for all Selexol units, though feedstock compositions may change in different designs. For simplicity, the H_2S or CO_2 split fraction is assumed to be constant in all cases. This is an adequate approximation when the feedstock compositions do not vary in a wide range, which is true for this study.

The Selexol unit for H_2S removal is assumed to only separate H_2S and CO_2 from the syngas, and absorption of N_2 and Ar are neglected. The split fraction of H_2S to the clean syngas is 6×10^{-6} [9]. The H_2S rich stream from the Selexol unit is assumed to have a fixed composition under a wide range of operating conditions. The mole fraction of H_2S in the H_2S rich stream is 0.48, and the remaining species is CO_2 [9].

Similarly, the Selexol unit for CO_2 removal is assumed to only separate CO_2 from the syngas, and absorption of N_2 and Ar are neglected. There is only trace amount of H_2S in the feedstock; hence the absorption of H_2S is also not considered. The split fraction of CO_2 to the clean syngas is 0.031 [9]. CO_2 stream produced is assumed to be pure CO_2.

Claus Plant

The conversion of H_2S in the Claus reaction is assumed to remain unchanged in all cases, which is 0.975 [182, 9], and O_2 is totally consumed.

Water Gas Shift Reactors

The product molar flow rates of the WGS reaction is constrained by the following nonlinear correlation:

$$F^{\text{wgs}}_{\text{pd,H}_2} F^{\text{wgs}}_{\text{pd,CO}_2} + A^{\text{wgs}} F^{\text{wgs}}_{\text{pd,CO}} F^{\text{wgs}}_{\text{pd,H}_2\text{O}} = 0 \tag{3.1}$$

where $F^{\text{wgs}}_{\text{pd,CO}}$, $F^{\text{wgs}}_{\text{pd,H}_2\text{O}}$, $F^{\text{wgs}}_{\text{pd,CO}_2}$ and $F^{\text{wgs}}_{\text{pd,H}_2}$ are molar flow rates of CO, H_2O, CO_2 and H_2 in the product stream of the three-stage WGS reactor respectively; A^{wgs} is equal to 42.77, which is a factor regressed from simulation results of the detailed WGS

reactor model [7]. The CO conversions (overall conversions of the three-stage WGS reactors) predicted by this model and the detailed model differ less than 5%.

The H_2/CO mole ratio in the product of WGS Reactor 1 is required to be 2, and there is no product requirement for WGS Reactor 2.

Pressure-swing Adsorption Unit

In the PSA, only H_2 is adsorbed by assumption, thus pure H_2 stream is produced. The H_2 recovery is constant in this model because the operating conditions of PSA are specified for all cases. The split fraction of H_2 to the H_2 stream is 0.9 [163].

Fischer-Tropsch Synthesis Reactor

In the FT reactor, over 100 species of hydrocarbons with carbon numbers from 1 to 70 are synthesized. It is too complicated to model the FT reaction by representing each hydrocarbon species individually. Instead, the following lumped model is employed:

$$CO + H_2 \rightleftharpoons \text{light products} + \text{naphtha} + \text{dieselwax} + \text{oxygenates} + H_2O \qquad (3.2)$$

Light products, which are hydrocarbons with carbon numbers between 1 and 4, are modeled as individual species including CH_4, C_2H_4, C_2H_6, C_3H_6, C_3H_8, C_4H_8 and C_4H_{10}. Naphtha, diesel and wax are lumped species. Each lumped species is simply represented by the middle species in that lump, e.g., C_6H_{14} and C_8H_{18} represent naphtha, $C_{16}H_{34}$ represents diesel, and $C_{33}H_{68}$ represents wax. CO_2 is assumed to be the only oxygenate product.

Due to the lack of detailed FT reactor kinetics, a fixed conversion and product distribution are estimated from the advice and industrial experience of BP engineers. The conversion of CO is 0.65, and the carbon selectivity of C_6H_{14}, C_8H_{18} and $C_{16}H_{34}$ are 0.08, 0.11 and 0.22, respectively. The detailed parameters are available in Appendix A.

There is a feedstock specification for the FT synthesis reactor: the CO_2 mole fraction in the feedstock cannot exceed an upper limit, typically 0.05, based on the

industrial experience of BP engineers.

Hydrocarbon Separation Unit

All species except C_6H_{14} are assumed to be sharply split in the hydrocarbon separation unit: all light ends including C_1-C_4 hydrocarbons, CO, H_2, N_2, Ar and CO_2 enter the light ends stream, all C_8H_{18} enters the naphtha stream, all $C_{16}H_{34}$ enters the diesel stream, all $C_{33}H_{68}$ enters the wax stream, and all H_2O enters the water stream. Most of the C_6H_{14} enters the naphtha stream while the remaining portion enters the light ends stream. A fixed split fraction of C_6H_{14} to the naphtha stream, which is 0.986, is assumed [9].

Hydrocracking Reactor

In real applications, thousands of species and millions of reactions are involved in the hydrocracking reaction, which is impossible to be accurately modeled based on current technology. In this model, the hydrocracking reaction is simply represented by:

$$\text{wax} + H_2 \rightarrow \text{naphtha} + \text{diesel} \tag{3.3}$$

Or

$$C_{33}H_{68} + xH_2 \rightarrow yC_8H_{18} + zC_{16}H_{34} \tag{3.4}$$

The conversion of wax is 0.3333. The values of y and z are 0.4344 and 1.8453, respectively. They are estimated based on industrial experience of BP engineers.

Auto-thermal Reforming Reactor

In the autothermal reforming (ATR) reactor, part of the CO, H_2 and hydrocarbons need to be oxidized to provide the heat for the endothermic steam reforming reactions. For simplicity, the ATR is modeled as two separate reactions in series: the combustion reactions (2.5) (2.7) happen first, then the steam reforming reactions (2.8) take place. The conversion of species in the combustion reaction, which is assumed to be equal for all species, is a decision variable. The conversions of species in the steam reforming

reactions are fixed, e.g., the conversion of CH_4 is 0.96 [190]. The detailed parameters are available in Appendix A.

Methanol Synthesis Reactor

In the methanol synthesis (MeOH) reactor, methanol (CH_3OH) and a small portion of higher alcohols are produced from syngas. The water gas shift reaction is neglected here due to the very low water content in the feedstock. Higher alcohols in this model are represented by ethanol (C_2H_5OH). Hence, two reactions take place in the MeOH reactor. The main reaction is:

$$CO + 2H_2 \rightleftharpoons CH_3OH \tag{3.5}$$

The side reaction is:

$$CO + 2H_2 \rightleftharpoons \frac{1}{2}C_2H_5OH + \frac{1}{2}H_2O \tag{3.6}$$

Due to the lack of detailed MeOH reactor models, the total conversion of CO in the two reactions is assumed to be fixed at 0.33 for simplicity [106]. The selectivity of CO to the main reaction is fixed to be 0.99, which is estimated from the industrial experience of BP engineers, because the operating temperature and pressure are fixed in this model.

The CO_2 mole fraction in the feedstock of MeOH reactor is constrained by an upper limit, which is typically 0.1, based on the industrial experience of BP engineers.

Methanol Separation Unit

All species except CH_3OH are assumed to be sharply split in the methanol separation unit: all light ends including CO, H_2, N_2, Ar, CO_2 and CH_4 enter the unreacted syngas stream, and all H_2O and C_2H_5OH enters the higher alcohols stream. Most of the CH_3OH enters the methanol stream while the remaining portion enters the unreacted syngas stream and the higher alcohols stream. Fixed split ratios of CH_3OH among above three streams are assumed: the split fractions of CH_3OH to the unreacted syngas stream and the methanol stream are 0.031 and 0.959 respectively [9].

Gas Turbine

In the gas turbine combustor, all combustible species are assumed to be totally consumed. Excess oxygen must be fed into the gas turbine combustor to ensure full combustion of the fuel. The excess ratio of O_2 is specified as 0.647, which is the typical value in real applications [182, 9].

The sulfur emission regulation is applied here. The ratio of the sulfur mass flow rate in the flue gas to the sulfur mass flow rate in the feedstock of the entire process cannot exceed 0.001 [182].

Gas Coolers and Heaters

In the gas coolers without water output and gas heaters, which are single input and single output unit operations, the mass balance is trivial.

In the gas coolers with water output, the mole fraction of water in the output stream is assumed to be fixed as 0.032 because the operating temperature and pressure are specified [9].

Other Unit Operations

The mass balances for compressors, turbines, mixers and splitters are available in Appendix A.

3.1.3 Energy Balance

All streams are assumed to be ideal mixtures; hence their enthalpy can be calculated as the weighted sum of the enthalpies of pure species.

Only heat generated above 220°C, which can be utilized in the steam turbine, is included in the energy balance calculation for the HRSG. Gas coolers with water output have exit temperatures much lower than 220°C, hence their heat is only used to preheat the streams before gas heaters and is not considered for power generation.

All reactors except the gas turbine combustor are operated under isothermal conditions. The gas turbine combustor is assumed to be an adiabatic reactor, and its

product temperature cannot exceed 1200°C [182, 9].

The heat and power consumptions of the separation units are assumed to be proportional to the total molar flow rate of the feedstock stream or the product stream. Their heat or power consumption coefficients are estimated from the Aspen Plus model [9], and are available in Appendix A.

Similarly, the power consumption rates in compressors and power generation rates in turbines except the gas turbine and steam turbines are assumed to be proportional to the total molar flow rate of their input streams. The total molar flow rates of their input streams in the base case and their power consumption or generation rates in the correspond base case are estimated from the Aspen Plus model [9], and are available in Appendix A.

In the gas turbine reduced model, the isentropic efficiency and the mechanical efficiency are assumed to be 0.899 and 0.985, respectively [182]. The power generated in the steam turbines is divided into two parts: power generated from high quality heat and low quality heat, whose energy conversion efficiencies are different. High quality heat only includes the heat generated at relatively high temperatures, such as the heat from the gasifier radiant cooler, the gasifier convective cooler and the gas turbine flue gas cooler. Low quality heat comprises all other heat generated in the process with temperatures above 220°C, such as the heat from water gas shift reactors, the Fischer-Tropsch synthesis reactor and the methanol synthesis reactor. Power conversion efficiencies from the high quality heat and low quality heat in the steam turbine are 0.4407 and 0.1542, respectively, based on rigorous steam cycle simulations within Aspen Plus [9, 39].

3.1.4 Enthalpy Calculation

The molar enthalpy of each species is expressed as the polynomial function of temperature, which is available in Appendix A.

3.1.5 Production Rates and Feedstock Consumption Rates

The feedstock requirement and production rate in this polygeneration plant are assumed to be much smaller than the market supply and demand, respectively. Hence, feedstock consumption rates and production rates are not constrained here, and the market prices will not be influenced by this plant. The detailed feedstock consumption rates and production rates are provided in Appendix A.

3.1.6 Capital Costs

Capital costs of equipment are calculated by the following power law scaling up relationship:

$$C^l = C^l_{\mathrm{b}} \left(\frac{F^l}{F^l_{\mathrm{b}}} \right)^{\mathrm{sf}^l} \tag{3.7}$$

where C^l is the capital cost of equipment l, F^l is the total mass (or molar) flow rate of the input streams of equipment l. F^l_{b} is the total mass (or molar) flow rate of the input streams of equipment l in the base case, C^l_{b} is the capital cost of equipment l in the corresponding base case, and sf^l is the sizing factor of equipment l, which are all specified parameters estimated from [182, 173, 174, 106, 31, 163, 158, 9] and are available in Appendix A.

The upper bound on the total dry mass flow rate of the gasifier feedstock is set to be 1042 tonne/hr or 7.815 Mt/yr (Mt = million tonnes) [9].

3.1.7 Economic Analysis

The total annual cost is:

$$\mathrm{Cost} = \mathrm{Cost}_{\mathrm{fed}} + \mathrm{Cost}^{\mathrm{car}}_{\mathrm{tax}} + \mathrm{Cost}^{\mathrm{car}}_{\mathrm{ccs}} + \mathrm{Cost}_{\mathrm{ope}} \tag{3.8}$$

where Cost is the total annual cost, $\mathrm{Cost}_{\mathrm{fed}}$ is the cost of purchasing the feedstock, $\mathrm{Cost}^{\mathrm{car}}_{\mathrm{tax}}$ is the carbon emissions tax, $\mathrm{Cost}^{\mathrm{car}}_{\mathrm{ccs}}$ is the cost of carbon sequestration and $\mathrm{Cost}_{\mathrm{ope}}$ is the operational cost.

The carbon tax is given by:

$$\text{Cost}_{\text{tax}}^{\text{car}} = P_{\text{tax}}^{\text{car}} \, \text{Emis}_{\text{net}} \tag{3.9}$$

where Emis_{net} is the annual net CO_2 emissions; $P_{\text{tax}}^{\text{car}}$ is the carbon tax per tonne of CO_2 emitted, which is a specified parameter. CO_2 emissions are calculated by:

$$\text{Emis}_{\text{gro}} = \text{MW}_{\text{CO}_2} \left[F_{\text{fl,CO}_2}^{\text{sg}} + (1 - S_{\text{seq}}) \, F_{\text{car}}^{\text{se2}} \right] t_{\text{op}} \tag{3.10}$$

$$\text{Emis}_{\text{net}} = \text{Emis}_{\text{gro}} - \frac{\text{MW}_{\text{CO}_2}}{\text{MW}_{\text{C}}} (1 - w_{\text{bio,H}_2\text{O}}) \, w_{\text{bio,C}} \, m_{\text{bio}}^{\text{gas}} \, t_{\text{op}} \tag{3.11}$$

where Emis_{gro} is the annual gross CO_2 emissions. If the carbon tax policy also taxes the carbon in the liquid fuels (since they will ultimately be burned in their final use), the annual net CO_2 emissions are given by:

$$\begin{aligned} \text{Emis}_{\text{net}} = &\text{Emis}_{\text{gro}} - \frac{\text{MW}_{\text{CO}_2}}{\text{MW}_{\text{C}}} (1 - w_{\text{bio,H}_2\text{O}}) \, w_{\text{bio,C}} \, m_{\text{bio}}^{\text{gas}} \, t_{\text{op}} \\ &+ \text{MW}_{\text{CO}_2} \left(6F_{\text{nap,C}_6\text{H}_{14}}^{\text{hs}} + 8F_{\text{nap,C}_8\text{H}_{18}}^{\text{hs}} + 16F_{\text{dis}}^{\text{hs}} \right) t_{\text{op}} \end{aligned} \tag{3.12}$$

where $F_{\text{fl,CO}_2}^{\text{sg}}$ is the molar flow rate of CO_2 in the gas turbine flue gas, $F_{\text{car}}^{\text{se2}}$ is the molar flow rate of CO_2 stream exiting Selexol Unit 2, $F_{\text{nap,C}_6\text{H}_{14}}^{\text{hs}}$ and $F_{\text{nap,C}_8\text{H}_{18}}^{\text{hs}}$ are the molar flow rates of C_6H_{14} and C_8H_{18} in the naphtha stream exiting the hydrocarbon separation unit respectively, $F_{\text{dis}}^{\text{hs}}$ is the molar flow rate of diesel stream exiting the hydrocarbon separation unit, $m_{\text{bio}}^{\text{gas}}$ is the mass flow rate of biomass fed into the gasifier, and S_{seq} is the split fraction of CO_2 stream to sequestration. $w_{\text{bio,H}_2\text{O}}$ is the mass fraction of water in the wet biomass, and $w_{\text{bio,C}}$ is the mass fraction of C in the dry biomass, which are available in Table 3.2. t_{op} is the annual operation time, which is 7500 hr/yr in this study [173, 174].

The detailed economic analyses are available in Appendix A. The market prices and carbon tax will be discussed later. The cost of carbon sequestration is \$10/tonne CO_2 based on the industrial experience of BP engineers.

The net present value (NPV), which is the objective function of this model, is

given by:

$$\text{NPV} = -\text{Cap} + \text{Pro}_{\text{net}} \frac{1}{r}\left(1 - \frac{1}{(1+r)^{t_{\text{lf}}}}\right) + \frac{R_{\text{tax}}\,\text{Cap}}{t_{\text{dp}}} \frac{1}{r}\left(1 - \frac{1}{(1+r)^{t_{\text{dp}}}}\right) \quad (3.13)$$

where Cap is the capital investment of the plant, Pro_{net} is the annual net profit. R_{tax} is the tax rate (including both federal and state taxes), r is the annual discount rate, t_{lf} is the life time of the project, and t_{dp} is the depreciation time of the project, which are specified parameters. In this study, $R_{\text{tax}} = 40\%$ [173, 174], $r = 0.12$ [173, 174], $t_{\text{lf}} = 30$ yr [173, 174], and $t_{\text{dp}} = 10$ yr [158].

3.1.8 Model Summary

The objective is to maximize the NPV subject to design and operational constraints including mass and energy balances, production and feedstock consumption rates, capital costs relationships, and the economic analyses. The decision variables include the molar (or mass) flow rates of streams, split fractions, heat (and power) consumption (and generation) rates, equipment capital costs, etc. The model is formulated in GAMS 22.8 [41]. It is a nonconvex NLP model, including 659 variables and 652 constraints. Of the constraints, there are 6 inequality constraints and 646 equality constraints, of which 119 are nonlinear. The nonconvexity in the model mainly originates from bilinear terms in mass balances and power law capital costs relationships. The model is solved to global optimality by BARON 8.1 [153, 154] with SNOPT [70] as the local NLP solver and CPLEX [1] as the LP solver. A cluster with 32 Intel 2.8 GHz processes was used to study many cases in parallel. The CPU times of case studies varied between 180 s to 10800 s.

3.2 Case Study Results

In this part, the optimal design of a coal/biomass polygeneration system co-producing electricity, naphtha, diesel and methanol will be discussed and compared using different product prices and carbon taxes. In each case study, two economic parameters

will be varied, and all other parameters will remain the same. All market prices and NPVs are expressed in 2007 dollars. All projects are assumed to operate between the years of 2015 and 2045; hence the market prices are the projected prices for 2030, which is assumed to be the average price during the above operating period.

3.2.1 Detailed Results of Two Sample Case Studies

In this section, the detailed optimization results of two sample case studies are presented. Case 1 only includes power generation, while Case 2 focuses on the liquid fuels (naphtha and diesel) and methanol production. The economic parameters used in the two case studies are listed in Table 3.3.

Table 3.3: Economic parameters in Case 1 and Case 2

Parameters	**Case 1**	**Case 2**	**Unit**
Coal Price	40	40	\$/tonne
Biomass Price	60	60	\$/tonne
Water Price	0.75	0.75	\$/tonne
Power Price	135	60	\$/MWh
Naphtha Price	600	1350	\$/tonne
Diesel Price	630	1417.5	\$/tonne
Methanol Price	270	607.5	\$/tonne
Sulfur Price	100	100	\$/tonne
CCS Cost	10	10	\$/tonne CO_2
Carbon Tax	20	20	\$/tonne CO_2

The feedstock consumption rates and production rates in two cases are shown in Table 3.4.

The optimal results of key decision variables in two cases are listed in Table 3.5.

From Table 3.5, it can be seen that all syngas enters the right (power generation without CCS) branch in the syngas cleaning and updating process in Case 1, while all syngas enters the left (liquid production) branch in the syngas cleaning and updating process and most of the clean syngas with H_2/CO mole ratio of 2 enters the methanol synthesis process in Case 2. Since power generation with CCS is not implemented,

Table 3.4: Feedstock consumption rates and production rates in Case 1 and Case 2

	Case 1		Case 2	
	tonne/hr	Mt/yr	tonne/hr	Mt/yr
Feedstock				
Coal	1172.367	8.793	1172.367	8.793
Biomass	0	0	0	0
Water	360.466	2.703	196.54	1.474
Product				
Power	3944.218*	29.582**	90.26*	0.677**
Naphtha	0	0	14.833	0.111
Diesel	0	0	39.049	0.293
Methanol	0	0	712.421	5.343
Sulfur	29.384	0.22	29.384	0.22
CO_2 sequestrated	0	0	1427.717	10.708

* : the unit is MW (MW = mega watt).
** : the unit is TWh (TWh = tera watt hour).

CO conversion in WGS Reactor 2 is not used in both cases.

The optimal product distributions of the two cases are shown in Table 3.6. The product distribution is expressed as the output fraction of each product, which is calculated by the following equation:

$$\text{Fraction of product } i = \frac{\text{Energy content in product } i}{\text{Total energy content}} \tag{3.14}$$

where energy contents in the liquid fuels and methanol are represented by their lower heating values (LHVs), and energy content in the power is the net power exported to the grid rather than the gross power. The total energy content can be expressed as:

$$\begin{aligned}\text{Total energy content} = {} & \text{Net power generation} + \text{Naphtha LHV} + \text{Diesel LHV} \\ & + \text{Methanol LHV}\end{aligned} \tag{3.15}$$

and the fraction of liquid fuels is the sum of the fractions of naphtha and diesel.

Table 3.5: Optimal results of key decision variables in Case 1 and Case 2 *

Decision Variables	Case 1	Case 2	Unit
$m_{\text{fd,dry}}^{\text{gas}}$	1042	1042	tonne/hr
$R_{\text{b/f}}$	0	0	
S_{liq}	0	1	
S_{ele}	0	0	
R_{wgs1}	n/a	0.394	
R_{wgs2}	n/a	n/a	
S_{seq}	n/a	1	
S_{me}	n/a	0.78	
S_{atr}	n/a	1	
S_{fts}	n/a	0	
S_{mes}	n/a	0.975	

* : some results are not applicable (n/a) because the corresponding unit operations are absent in the optimal design.

Table 3.6: Optimal product distributions in Case 1 and Case 2

Product Distribution (%)	Case 1	Case 2
Power	100	1.71
Naphtha	0	3.73
Diesel	0	9.67
Liquid Fuels	0	13.40
Methanol	0	84.89

The net present values in Case 1 and Case 2 are \$10.561 billion and \$10.878 billion, respectively, and the annual CO_2 emissions in Case 1 and Case 2 are 20.128 Mt/yr and 0.828 Mt/yr, respectively.

3.2.2 Power Price vs. Naphtha Price

In this section, the trade-off between power generation and liquids (naphtha, diesel and methanol) production will be discussed. For simplicity, diesel and methanol prices are assumed to be proportional to the naphtha price. The power price is varied

from \$30/MWh to \$165/MWh, and the naphtha price is varied from \$300/tonne to \$1650/tonne. They are assumed to be independent of each other. The economic parameters are listed in Table 3.7.

Table 3.7: Economic parameters in case studies under different power prices and naphtha prices

Parameter	**Value**	**Unit**
Coal Price	40	\$/tonne
Biomass Price	60	\$/tonne
Water Price	0.75	\$/tonne
Power Price	Varied	\$/MWh
Naphtha Price	Varied	\$/tonne
Diesel Price	1.05 × Naphtha Price	\$/tonne
Methanol Price	0.45 × Naphtha Price	\$/tonne
Sulfur Price	100	\$/tonne
CCS Cost	10	\$/tonne CO_2
Carbon Tax	20	\$/tonne CO_2

The optimal product distributions under different power and naphtha prices are shown in Figure 3-1. The product distributions in Case 1 and Case 2 are also marked in Figure 3-1.

From Figure 3-1, it is obvious that power generation is favored at higher power price and lower naphtha price and liquids production is favored at higher naphtha price and lower power price. There is a net output of electricity in every case even when the liquid production dominates the polygeneration process because the combustion of the FT and MeOH off gases plus the heat recovered from the HRSG produces more power than needed in the plant for compressing and pumping. The optimal product portfolio changes in a non-smooth way, which implies that the optimal design will always be either a pure power plant or a liquid plant with small amount of net power output in our case studies. Co-production of power and liquid in comparable fractions is only optimal under some high power prices and high naphtha prices. The major reason is that it will lead to a much higher capital investment to co-build the power generation and liquid production facilities on comparable scales,

and it always reduces the net profit when the product prices are not high enough. The boundary line between power generation and liquid production regions is near the line of the following price relationship: naphtha price ($/tonne) = 10 × power price ($/MWh). Hence, the decision of producing power or liquid strongly depends on the ratio of naphtha price to power price. If this ratio is above 10, liquids, which can be liquid fuels, methanol or their mix, are preferred products for the higher NPV, and power is generated mostly for internal use with small amounts of output. If this ratio is below 10, power is the preferred product, and the polygeneration plant is reduced to an IGCC plant without any liquids production. Co-production between liquid fuels (naphtha and diesel) and methanol will be discussed later.

The net present values under different power and naphtha prices (shown in Figure 3-2) also clearly shows the non-smooth transition between different optimal product portfolios. In the power generation region (left part), the NPVs are not influenced by the naphtha prices because no liquids are produced there. The opposite holds in the liquid production region.

The annual CO_2 emissions are shown in Figure 3-3 (based on the dry feedstock consumption rate of 7.815 Mt/yr). High CO_2 emissions in the power generation region imply that carbon capture and sequestration (CCS) is not profitable to implement in IGCC under the given market prices and carbon emission policy. In the liquid production region, CO_2 is captured in all price scenarios to produce the syngas satisfying the feedstock specifications of the Fischer-Tropsch or methanol reactor, but CO_2 is only sequestered for power prices lower than $100/MWh. At higher power prices, it becomes economical to pay the carbon tax and forgo CCS to reduce the power consumption in the CO_2 compressor, increasing the output power to the grid.

3.2.3 Naphtha Price vs. Methanol Price

In this section, the trade-off between liquid fuels (naphtha and diesel) production and methanol production will be discussed. The diesel price is assumed to be proportional to the naphtha price, which is assumed to be independent of the methanol price. The naphtha price is varied from $300/tonne to $1650/tonne, and the methanol price is

varied from \$160/tonne to \$700/tonne. The power price is set to be low at \$40/MWh, which is a typical off-peak price, to minimize the influence of power generation. The economic parameters are listed in Table 3.8.

Table 3.8: Economic parameters in case studies under different naphtha prices and methanol prices

Parameter	Value	Unit
Coal Price	40	\$/tonne
Biomass Price	60	\$/tonne
Water Price	0.75	\$/tonne
Power Price	40	\$/MWh
Naphtha Price	Varied	\$/tonne
Diesel Price	1.05 × Naphtha Price	\$/tonne
Methanol Price	Varied	\$/tonne
Sulfur Price	100	\$/tonne
CCS Cost	10	\$/tonne CO_2
Carbon Tax	20	\$/tonne CO_2

The optimal product distributions under different naphtha prices and methanol prices are shown in Figure 3-4. In all price scenarios, power is generated by combustion of off- gas from liquid fuels or methanol production and most of it is consumed in the process. It is clear that the liquid fuels (naphtha + diesel) are favorable products under the high naphtha prices and low methanol prices, and methanol production is favored under high methanol prices and low naphtha prices. The transition between different optimal product portfolios here is also non-smooth: the optimal polygeneration design is either a liquid fuel plant or a methanol plant in most price scenarios. The boundary line between the region favoring liquid fuels and the region favoring methanol is close to the straight line with the following relationship: naphtha price (\$/tonne) = 2.6 × methanol price (\$/tonne). Hence, the production choice between liquid fuels and methanol is strongly dependent on the ratio of naphtha price to methanol price. Liquid fuel production is more favorable than the methanol production if this ratio is well above than 2.6, and it becomes less favorable than methanol production if this ratio drops much lower than 2.6. It is only profitable to co-build

the Fischer-Tropsch synthesis system and the methanol synthesis system in one plant and co-produce liquid fuels and methanol in comparable fractions in several cases when the naphtha price and methanol price are both high and near the boundary line. High capital investment is the major factor that prohibits the co-production of liquid fuels and methanol under low liquid fuel and methanol prices. However, this obstacle is overcome under high product prices. Co-production of different liquid products is not only a way to increase the total profit but also a strategy to reduce significantly the risk caused by fluctuations in liquid product market prices.

The optimal net present values are shown in Figure 3-5, which also implies the non-smooth transition between the liquid fuels production region and the methanol production region. In each region, the optimal NPVs are not influenced by the price of the other product.

The CO_2 emissions under different price scenarios are shown in Figure 3-6 (based on the dry feedstock consumption rate of 7.815 Mt/yr). CCS is economic under the moderate carbon tax and low power price; hence CO_2 emissions are quite low in all cases. Almost all of the CO_2 emitted comes from the gas turbine flue gas, which is the combustion product of the light ends in the Fischer-Tropsch process or unreacted syngas in the methanol synthesis process.

3.2.4 Biomass Price vs. Carbon Tax

In this section, carbon taxes and biomass prices that promote biomass usage and reduce CO_2 emissions in the power generation are investigated. A high power price (a typical peak-time price) and relatively low liquid fuels and methanol prices are selected to create a scenario in which pure power generation is optimal. Biomass prices are varied from \$10/tonne to \$100/tonne, and carbon taxes are varied from \$0/tonne CO_2 to \$135/tonne CO_2. The economic parameters are listed in Table 3.9.

The optimal results show that electricity corresponds to 100% of total energy output in all scenarios.

The gross CO_2 emission and net CO_2 emission are shown in Figure 3-7 and 3-8. The gross CO_2 emission is the total amount of CO_2 emitted by the polygeneration

Table 3.9: Economic parameters in case studies under different biomass prices and carbon taxes

Parameter	Value	Unit
Coal Price	40	\$/tonne
Biomass Price	Varied	\$/tonne
Water Price	0.75	\$/tonne
Power Price	120	\$/MWh
Naphtha Price	600	\$/tonne
Diesel Price	630	\$/tonne
Methanol Price	270	\$/tonne
Sulfur Price	100	\$/tonne
CCS Cost	10	\$/tonne CO_2
Carbon Tax	Varied	\$/tonne CO_2

process. The net CO_2 emission is the amount of CO_2 emitted only generated by coal, which equals gross CO_2 emission minus the CO_2 originating from biomass. This assumes that biomass will be credited as a "net-zero emissions" fuel, as recent policy debates have supported. The optimal CO_2 emissions, which reflect the optimal CO_2 reduction strategies, are highly dependent on the carbon tax rate. At low carbon taxes (\$30/tonne CO_2 or lower), carbon capture and sequestration (CCS) equipment is not installed and all de-sulfured syngas is directly sent to the gas turbine, which results in high CO_2 emissions. When carbon taxes are higher than \$30/tonne CO_2, CO_2 emissions significantly drop because all de-sulfured syngas enters the power generation from the CCS branch. CO_2 emissions are reduced by increasing the CO conversion of the water gas shift reactor at the expense of losing more high-temperature steam used for steam turbines. Gross CO_2 emissions cannot drop to zero due to the limit of the CO_2 removal efficiency in the Selexol unit. Further reduction of CO_2 emissions can be achieved by blending some biomass into the feedstock. This is confirmed by the optimal results. At extremely high carbon tax, net CO_2 emissions become zero due to the biomass usage although the corresponding gross CO_2 emissions are still non-zero.

The optimal biomass/feedstock ratios under different biomass prices and carbon

taxes are shown in Figure 3-9. Biomass will only be used in the power generation under very high carbon taxes, such as carbon taxes higher than \$75/tonne CO_2. Biomass usage is also strongly dependent on the biomass price. At the same carbon tax, more biomass is preferred under lower biomass prices. Since biomass produces less syngas than coal for the same mass input rate, biomass is not profitable without high carbon taxes even when the biomass price is quite low. However, using biomass in the feedstock ($R_{b/f} > 0$) is a cheap way to realize deep reduction of CO_2 emissions, which is even cheaper than deep shifts in WGS Reactor 2 (high values for R_{wgs2}) for the purpose of generating CO_2 for pre-combustion capture. When the CO conversion in WGS Reactor 2 reached 90%, it was more profitable to use biomass than to try a higher CO conversion in WGS Reactor 2. In this study, credits from negative CO_2 emissions are not considered and the objective of biomass usage is just to bring the CO_2 emissions to zero. More biomass may be incentivized if the carbon policy were to allow the sale of surplus carbon credits.

Comparing Figures 3-8 and 3-9, one concludes that the carbon tax is the most important driving force to decrease the CO_2 emissions and increase the biomass content in the feedstock. With the increase of carbon tax, CCS will first be implemented to achieve substantial reduction of CO_2 emissions. When CO_2 emissions are low, CCS plus biomass is an effective way to further reduce net CO_2 emissions to zero.

The optimal net present values are shown in Figure 3-10. The cost of reducing CO_2 emissions significantly decreases the NPV. A given project will generally lose nearly half its NPV if the carbon tax increases from \$0/tonne CO2 to \$75/tonne CO_2. However, when the carbon tax is high enough, the NPV only slightly drops with further increases of carbon tax because CCS is already implemented and CO_2 emissions are very low. In this study, the power price is set high enough to ensure positive NPV under all price scenarios. In real cases, allowances may be needed for CCS and biomass usage when the power price is low.

The influence of biomass prices and carbon taxes on CO_2 emissions and biomass usage is similar in liquid fuels and methanol production. Compared to power generation, CCS will be implemented under lower carbon taxes (\$20/tonne CO_2) in liquids

production, and less biomass will be used in the feedstock since the CO_2 emissions from liquids production are much lower than from power production.

3.2.5 Carbon Tax without Fuel vs. Carbon Tax with Fuel

The CO_2 emissions charged for carbon taxes in the previous sections only include the CO_2 emitted by the process. However, the liquid fuels (naphtha and diesel) produced will lead to additional CO_2 emissions in downstream processes such as transportation and heating, which may also be subject to carbon taxes under different policies. In this section, two different carbon tax cases are compared: carbon tax only for process CO_2 emissions and carbon tax for total CO_2 emissions (process CO_2 emissions plus downstream CO_2 emissions from liquid fuels). Methanol produced in the polygeneration plant will be used as a chemical which will not emit additional CO_2 in downstream processes; hence it will not be subject to carbon taxes in either case. Carbon taxes are set to be varied from \$0/tonne CO_2 to \$50/tonne CO_2. The economic parameters are listed in Table 3.10.

Table 3.10: Economic parameters in case studies under different carbon tax policies

Parameter	Value	Unit
Coal Price	40	\$/tonne
Biomass Price	60	\$/tonne
Water Price	0.75	\$/tonne
Power Price	70	\$/MWh
Naphtha Price	1000	\$/tonne
Diesel Price	1050	\$/tonne
Methanol Price	400	\$/tonne
Sulfur Price	100	\$/tonne
CCS Cost	10	\$/tonne CO_2
Carbon Tax	Varied	\$/tonne CO_2

The optimal production distributions under two different carbon tax cases are shown in Figures 3-11 and 3-12. The production strategies are highly dependent on the carbon tax case. For these market conditions, liquid fuels are favored under all

of the carbon taxes when only process CO_2 emission is charged for carbon taxes. If downstream CO_2 emissions are also included in the carbon tax, the favorable products will switch from liquid fuels to methanol with increasing carbon tax. The transition point is between \$20/tonne CO_2 and \$30/tonne CO_2. Hence, the optimal product portfolio can be very different under middle or high carbon tax if a different carbon tax policy is implemented, even when all the market prices are the same.

The optimal net present values are shown in Figure 3-13. Varying the carbon tax policy from charging process CO_2 emissions to total CO_2 emissions causes a considerable loss of net present value. However, the new product portfolio has greatly mitigated such profit loss.

The process CO_2 emissions and total CO_2 emissions are shown in Figures 3-14 and 3-15. Although process CO_2 emissions from the two product portfolios are nearly the same, their total CO_2 emissions differ much under middle and high carbon taxes. The polygeneration strategy under the new carbon tax policy achieves much lower total CO_2 emission by replacing liquid fuels production with methanol production. However, this does not imply that other technologies (such as refining) would produce less liquid fuels.

3.2.6 Polygeneration System vs. Single-product System

In this section, the profitability of a polygeneration plant and different single-product plants (power plant with CCS, power plant w/o CCS, liquid fuels plant and methanol plant) are compared. Product distributions can be varied in the polygeneration plant and must be fixed in single-product plants. In power plants, liquid fuels and methanol production rates are both zero. In liquid fuels plants or methanol plants, only the minimum amount of electricity is exported to the grid. In this study, the power price is fixed to be \$75/MWh. The naphtha price is varied here, and diesel and methanol prices are assumed to be proportional to the naphtha price. The economic parameters are listed in Table 3.11.

Under different price scenarios, different optimal designs are obtained for polygeneration systems, but the designs for each single-product system are almost the same.

Table 3.11: Economic parameters in case studies comparing the polygeneration and single-product systems

Parameter	Value	Unit
Coal Price	40	\$/tonne
Biomass Price	60	\$/tonne
Water Price	0.75	\$/tonne
Power Price	75	\$/MWh
Naphtha Price	Varied	\$/tonne
Diesel Price	1.05 × Naphtha Price	\$/tonne
Methanol Price	0.45 × Naphtha Price	\$/tonne
Sulfur Price	100	\$/tonne
CCS Cost	10	\$/tonne CO_2
Carbon Tax	20	\$/tonne CO_2

The optimal product distributions for the polygeneration system are shown in Figure 3-16.

The net present values of the polygeneration plant with the optimal design and all single-product plants are shown in Figure 3-17. The polygeneration plant never has lower NPVs than a single-product plant in all price scenarios. Under some price scenarios, the NPVs of the polygeneration plant can be much higher than some kinds of single-product plants. This fact demonstrates the advantage of polygeneration system in the economic performance. The NPVs of the polygeneration plant, liquid fuels plant and methanol plant are more clearly shown in Figure 3-18, in which the differences between NPVs of each plant and NPVs of the liquid fuels plant are presented. However, it is also indicated that the optimal design of a static polygeneration system is always close to or equal to a single-product system, hence the economical benefit of static polygeneration is not significant.

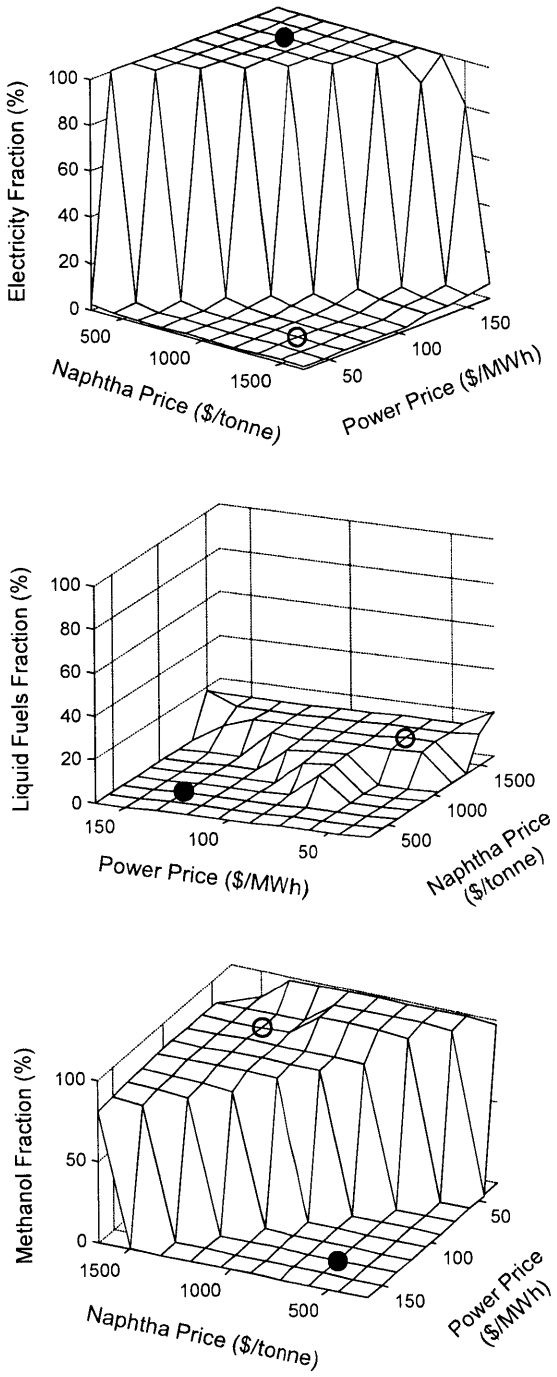

Figure 3-1: Product distributions in case studies under different power prices and naphtha prices. (The axes are rotated to provide a favorable view.) [Grey circle : Case 1, White circle : Case 2.]

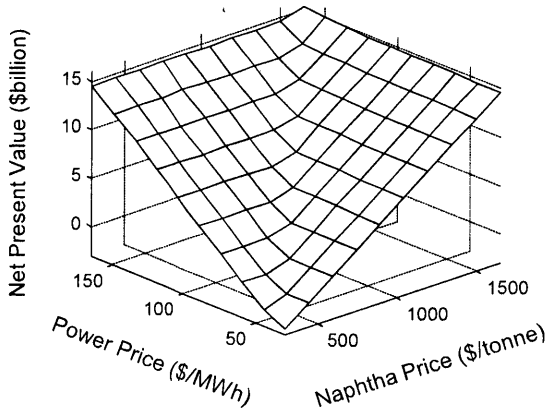

Figure 3-2: Net present values in case studies under different power prices and naphtha prices.

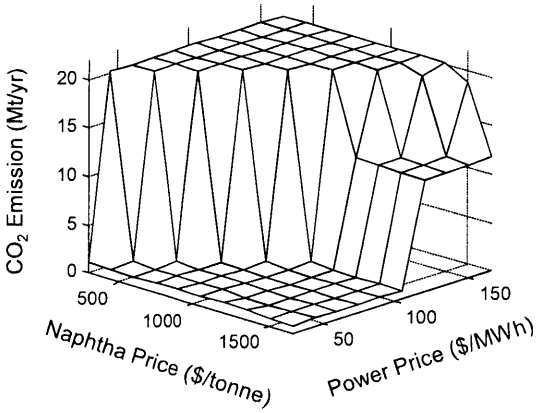

Figure 3-3: Annual CO_2 emission in case studies under different power prices and naphtha prices.

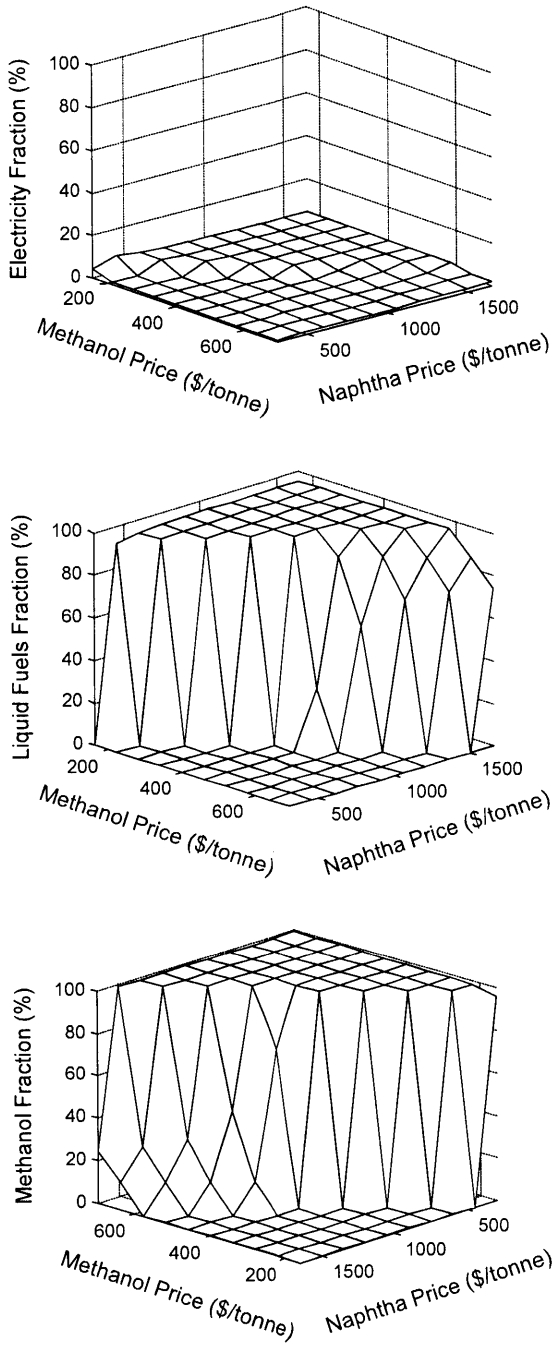

Figure 3-4: Product distributions in case studies under different naphtha prices and methanol prices. (The axes are rotated to provide a favorable view.)

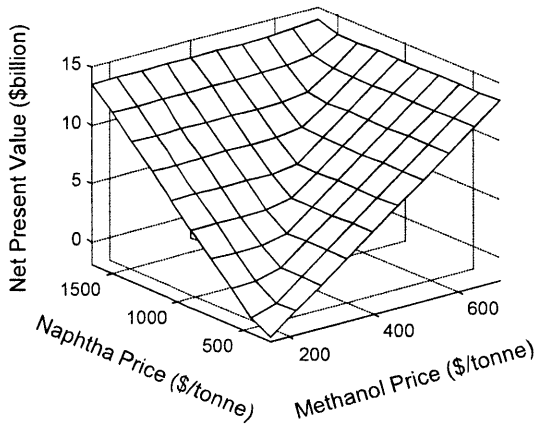

Figure 3-5: Net present values in case studies under different naphtha prices and methanol prices.

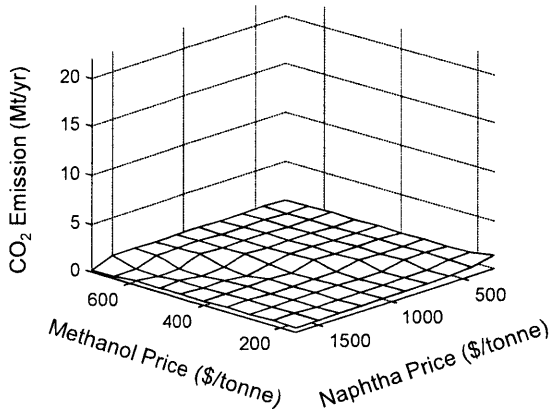

Figure 3-6: Annual CO_2 emission in case studies under different naphtha prices and methanol prices.

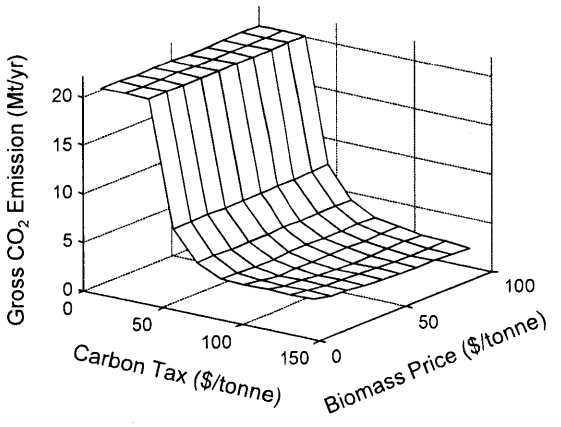

Figure 3-7: Annual gross CO_2 emission in case studies under different biomass prices and carbon taxes.

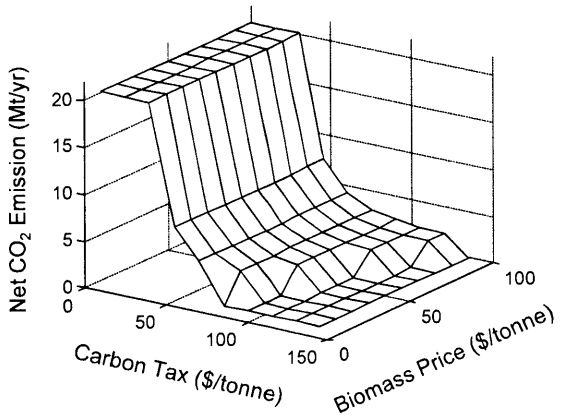

Figure 3-8: Annual net CO_2 emission in case studies under different biomass prices and carbon taxes.

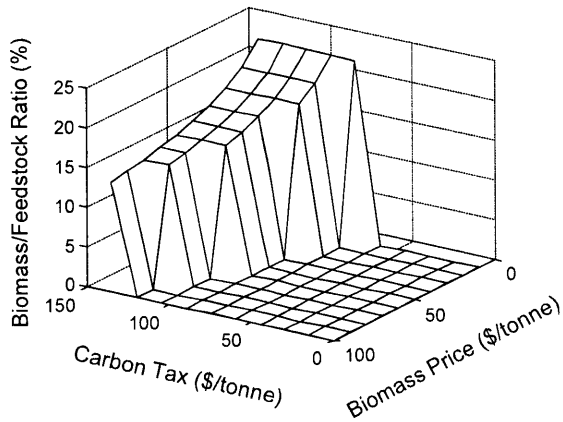

Figure 3-9: Biomass usage in case studies under different biomass prices and carbon taxes.

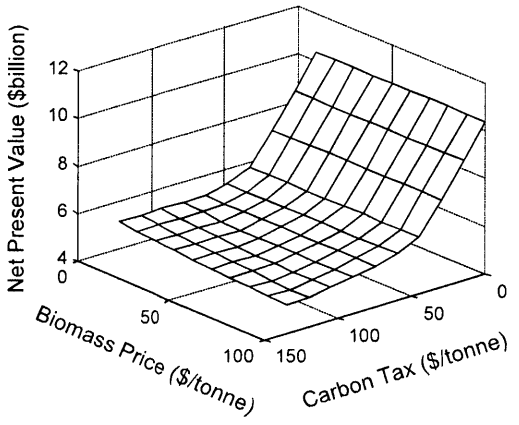

Figure 3-10: Net present values in case studies under different biomass prices and carbon taxes.

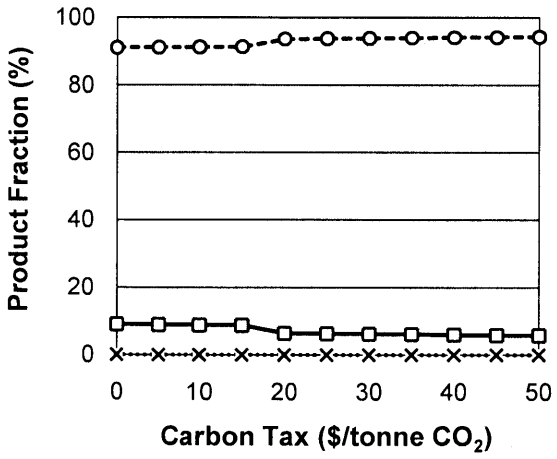

Figure 3-11: Product distributions in case studies under carbon taxes for process CO_2 emissions. [—□— : electricity, --- ○--- : liquid fuels, ·····×····· : methanol]

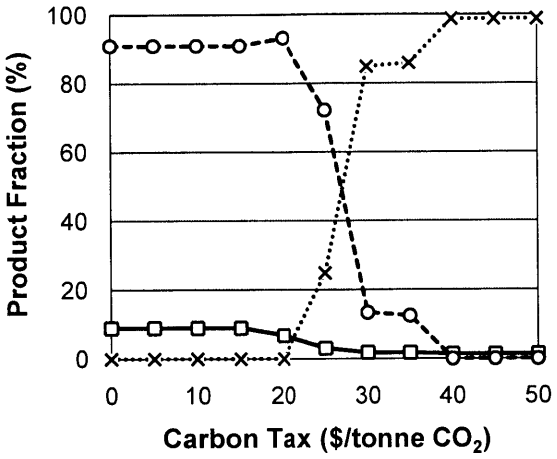

Figure 3-12: Product distributions in case studies under carbon taxes for total CO_2 emissions. [—□— : electricity, --- ○--- : liquid fuels, ····×···· : methanol]

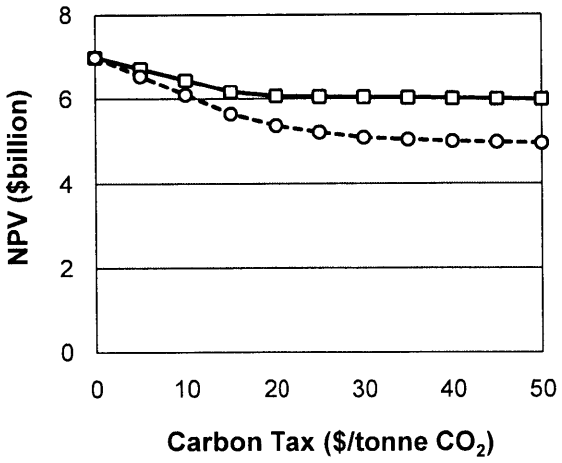

Figure 3-13: Net present values in case studies under two carbon tax cases. [—□— : carbon tax w/o fuel, --- ○---- : carbon tax w/ fuel]

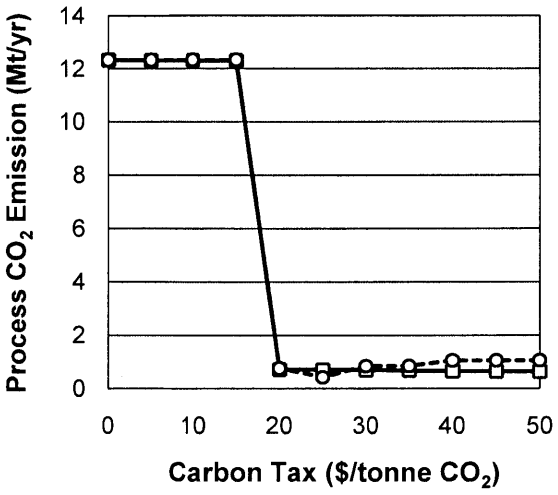

Figure 3-14: Annual process CO_2 emissions in case studies under two carbon tax cases. [—□— : carbon tax w/o fuel, --- ○ --- : carbon tax w/ fuel]

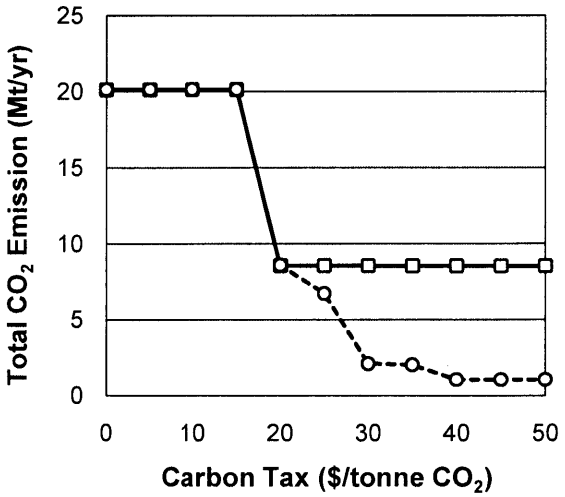

Figure 3-15: Annual total CO_2 emissions in case studies under two carbon tax cases. [—□— : carbon tax w/o fuel, --- ○---- : carbon tax w/ fuel]

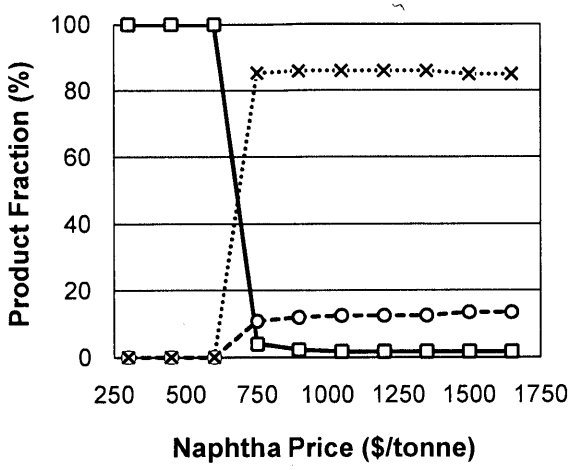

Figure 3-16: Product distributions in the polygeneration systems with the optimal designs. [—□— : electricity, --- ○ --- : liquid fuels, ····· × ····· : methanol]

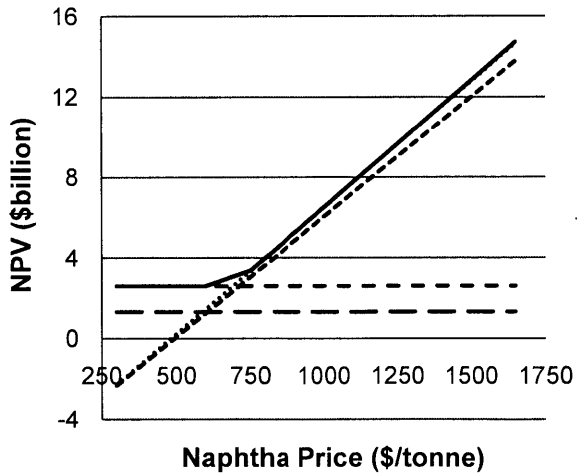

Figure 3-17: Net present values of the polygeneration systems and different single-product systems. [——— : polygeneration plant, — — : power plant w/ CCS, - - - : power plant w/o CCS, ------ : liquid fuels plant, ····· : methanol plant]

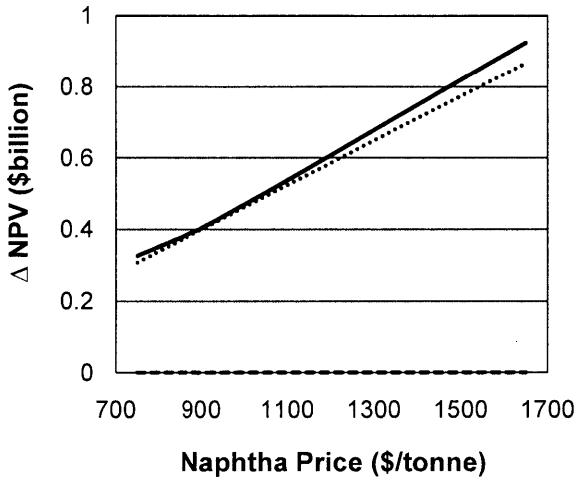

Figure 3-18: Net present values of the polygeneration systems and several single-product systems (enlarged view). [——— : polygeneration plant, ------ : liquid fuels plant, ····· : methanol plant]

Chapter 4

Optimal Design and Operation of Flexible Energy Polygeneration Systems

4.1 Mathematical Model

4.1.1 Overview

The two-stage formulation (as shown in Eq (1.1) and (1.2)) is applied in this study [47]. The market prices of all products are assumed to vary daily and seasonally. A collection of scenarios, which will occur with a certain frequency over the plant lifetime, are assumed to represent these price fluctuations. Product prices are fixed within each scenario, but can change between scenarios. The objective of this formulation is to maximize the overall economic performance of the plant while satisfying all design constraints and operating constraints in all scenarios. The key design decision variables are equipment capacities, and the key operational decision variables are listed in Table 4.1 and shown in Figure 2-2, which are similar to those in the static polygeneration model in Chapter 3. The values of operational decision variables vary between different scenarios.

For simplicity, the feedstock (including coal and biomass) compositions are as-

Table 4.1: Key operational decision variables in the model

Operational Variables	Description
$m_{\text{fd,dry}}^{\text{gas}}$	Mass flow rate of the dry feedstock fed into the gasifier
$R_{\text{b/f}}$	Dry mass fraction of biomass in the gasifier feedstock
S_{liq}	Split fraction of the clean syngas to the liquid fuel production (or the left) branch in the syngas cleaning and upgrading process
S_{ele}	Split fraction of the clean syngas to the power generation with CCS (or the middle) branch in the syngas cleaning and updating process
R_{wgs1}	Conversion of CO in Water Gas Shift Reactor 1
R_{wgs2}	Conversion of CO in Water Gas Shift Reactor 2
S_{seq}	Split fraction of the CO_2 stream to sequestration
S_{me}	Split fraction of the clean syngas with H_2/CO mole ratio of 2 to the methanol synthesis process
S_{atr}	Split fraction of the light ends exiting the hydrocarbon separation unit to the autothermal reforming reactor
S_{fts}	Split fraction of the syngas exiting the autothermal reforming reactor to the Fischer-Tropsch synthesis reactor
S_{mes}	Split fraction of the unreacted syngas exiting the methanol separation unit to the methanol synthesis reactor

sumed to be fixed in all scenarios. Operations are considered to be at steady state at all times, and the transition times between different operational conditions are neglected in this model. A constant conversion or efficiency is assumed for all equipment during the whole project life time, which is considered as the best case analysis. In real applications, the performance of equipment may drop when operated below its design capacity. Introducing those equipment performance correlations (which are typically highly nonlinear equations) into the operational constraints will be a topic of future work after more advanced optimization algorithms are developed.

The mathematical model here is similar to the static polygeneration model in Chapter 3, and details are provided in Appendix B. Some key differences will be discussed here.

4.1.2 Capital Costs

The capital costs are calculated by the following power law scale-up relationship:

$$C^l = C^l_{\mathrm{b}} \left(\frac{\bar{F}^l}{\bar{F}^l_{\mathrm{b}}} \right)^{\mathrm{sf}^l} \tag{4.1}$$

where C^l is the capital cost of equipment l, and $\bar{F}^l$ is the mass (or molar) capacity of equipment l, which are the design decision variables in this model. Eq (4.1) is the only constraint on design decision variables. $\bar{F}^l_{\mathrm{b}}$ is the mass (or molar) capacity of equipment l in the base case (which is equal to F^l_{b} in Chapter 3), C^l_{b} is the capital cost of equipment l in the corresponding base case, and sf^l is the sizing factor of equipment l, which are the same specified parameters as in Chapter 3, based on other studies [182, 173, 174, 106, 31, 163, 158, 9]. They are available in Appendix B.

The mass (or molar) capacity of equipment l is calculated by

$$F^l_h \leq \bar{F}^l \ , \quad \forall h \in N_h \tag{4.2}$$

and

$$F^l_h \geq \mathrm{Ca}_{\min} \, \bar{F}^l \ , \quad \forall h \in N_h \tag{4.3}$$

where F^l_h is the total mass (or molar) flow rate of the input stream of equipment l in scenario h. $\mathrm{Ca}_{\min}$ is the lower limit of the flow-rate/capacity ratio, which is a specified parameter representing the operational flexibility. Eq (4.2) represents the constraint that the input flow rates in all scenarios cannot exceed the equipment capacity, while Eq (4.3) represents the constraint that the input flow rates also cannot drop below a minimum fraction of the equipment capacity in order to maintain stable, continuous operation. The flow rate F^l_h is forced to be 0 when equipment l is not built ($\bar{F}^l = 0$).

The upper bound of the dry mass capacity of the gasifier is set to be 1042 tonne/hr or 7.815 Mt/yr on the basis of industrial experience of BP engineers [9].

4.1.3 Economic Analysis

The total annual variable cost is

$$\text{Cost} = \text{Cost}_{\text{fed}} + \text{Cost}_{\text{tax}}^{\text{car}} + \text{Cost}_{\text{ccs}}^{\text{car}} + \text{Cost}_{\text{ope}} \tag{4.4}$$

where Cost is the total annual variable cost, Cost_{fed} is the purchase cost of the feedstock, $\text{Cost}_{\text{tax}}^{\text{car}}$ is the carbon emissions tax, $\text{Cost}_{\text{ccs}}^{\text{car}}$ is the cost of carbon sequestration, and Cost_{ope} is the operational cost, including the cost of labor and utilities.

The feedstock cost is given by

$$\text{Cost}_{\text{fed}} = \sum_{h} \text{Occu}_h \left(\sum_{q} P_q^{\text{f}} \, m_{q,h}^{\text{f}} \right) t_{\text{op}} \ , \quad \forall q \in \text{Feed}, \ \forall h \in N_h \tag{4.5}$$

where $m_{q,h}^{\text{f}}$ is the consumption rate of feedstock q in scenario h. P_q^{f} is the average market price of feedstock q, and t_{op} is the annual operating time, which are specified parameters. Feed is the set of feedstocks. t_{op} is equal to 7500 hr/yr in this study [173, 174].

The carbon tax is given by

$$\text{Cost}_{\text{tax}}^{\text{car}} = P_{\text{tax}}^{\text{car}} \, \text{Emis}_{\text{net}} \tag{4.6}$$

where Emis_{net} is the annual net CO_2 emissions; $P_{\text{tax}}^{\text{car}}$ is the carbon tax per tonne of CO_2 emitted, which is a specified parameter. CO_2 emissions are calculated by

$$\text{Emis}_{\text{gro}} = \text{MW}_{\text{CO}_2} \sum_{h} \text{Occu}_h \left[F_{\text{fl,CO}_2,h}^{\text{sg}} + (1 - S_{\text{seq},h}) \, F_{\text{car},h}^{\text{se2}} \right] t_{\text{op}} \ , \quad \forall h \in N_h \tag{4.7}$$

$$\text{Emis}_{\text{net}} = \text{Emis}_{\text{gro}} - \frac{\text{MW}_{\text{CO}_2}}{\text{MW}_{\text{C}}} \left(1 - w_{\text{bio,H}_2\text{O}}\right) w_{\text{bio,C}} \sum_{h} \text{Occu}_h \, m_{\text{bio},h}^{\text{gas}} \, t_{\text{op}} \ , \quad \forall h \in N_h \tag{4.8}$$

where Emis_{gro} is the annual gross CO_2 emissions, $F_{\text{fl,CO}_2,h}^{\text{sg}}$ is the molar flow rate of CO_2 exiting the gas turbine flue gas in scenario h, $F_{\text{car},h}^{\text{se2}}$ is the molar flow rate of the CO_2 stream exiting Selexol Unit 2 in scenario h, $m_{\text{bio},h}^{\text{gas}}$ is the mass flow rate of biomass

fed into the gasifier in scenario h, and $S_{\text{seq},h}$ is the split fraction of CO_2 stream to sequestration in scenario h (see Figure 2-2); $w_{\text{bio,H}_2\text{O}}$ is the mass fraction of water in the wet biomass, and $w_{\text{bio,C}}$ is the mass fraction of C in the dry biomass, which are available in Chapter 3. Note that with this carbon policy, CO_2 emissions are reduced by the amount of carbon in the biomass, since it is a carbon neutral energy source. In this work, we also consider cases in which the carbon emissions policy taxes the carbon in the liquid fuels in addition to the CO_2 emissions from the plant itself. In this case, the annual net CO_2 emissions are given by

$$\begin{aligned}\text{Emis}_{\text{net}} =& \text{Emis}_{\text{gro}} - \frac{\text{MW}_{\text{CO}_2}}{\text{MW}_{\text{C}}}\left(1 - w_{\text{bio,H}_2\text{O}}\right) w_{\text{bio,C}} \sum_h \text{Occu}_h \; m^{\text{gas}}_{\text{bio},h} \; t_{\text{op}} \\ &+ \text{MW}_{\text{CO}_2} \sum_h \text{Occu}_h \left(6F^{\text{hs}}_{\text{nap,C}_6\text{H}_{14},h} + 8F^{\text{hs}}_{\text{nap,C}_8\text{H}_{18},h} + 16F^{\text{hs}}_{\text{dis},h}\right) t_{\text{op}} \;, \quad \forall h \in N_h\end{aligned} \tag{4.9}$$

where $F^{\text{hs}}_{\text{nap,C}_6\text{H}_{14},h}$ and $F^{\text{hs}}_{\text{nap,C}_8\text{H}_{18},h}$ are the molar flow rates of C_6H_{14} and C_8H_{18} in the naphtha stream exiting the hydrocarbon separation unit in scenario h, respectively, and $F^{\text{hs}}_{\text{dis},h}$ is the molar flow rate of the diesel stream exiting the hydrocarbon separation unit in scenario h.

The revenue is given by

$$\text{Reve} = \sum_h \text{Occu}_h \left(\sum_q P^{\text{p}}_{q,h} \; m^{\text{p}}_{q,h}\right) t_{\text{op}} \;, \quad \forall q \in \text{Prod}, \; \forall h \in N_h \tag{4.10}$$

where $m^{\text{p}}_{q,h}$ is the production rate of product q in scenario h. $P^{\text{p}}_{q,h}$ is the market price of product q in scenario h, which are specified parameters. Prod is the set of products.

The detailed economic analyses are available in the Appendix B. The tax rate (including both federal and state taxes) is 40% [173, 174], and the cost of carbon sequestration is \$10/tonne CO_2 based on the Encyclopedia of Energy [84] and the advice and industrial experience of BP engineers.

The net present value (NPV), which is the objective function of this model, is

denoted by

$$\text{NPV} = -\text{Cap} + \text{Pro}_{\text{net}} \frac{1}{r}\left(1 - \frac{1}{(1+r)^{t_{\text{lf}}}}\right) + \frac{R_{\text{tax}}\text{Cap}}{t_{\text{dp}}} \frac{1}{r}\left(1 - \frac{1}{(1+r)^{t_{\text{dp}}}}\right) \quad (4.11)$$

where Cap is the capital investment of the plant (which is the fixed cost), Pro_{net} is the annual net profit. R_{tax} is the tax rate (including both federal and state taxes), r is the annual discount rate, t_{lf} is the life time of the project, and t_{dp} is the depreciation time of the project, which are specified parameters. In this study, $r = 0.12$ [173, 174], $t_{\text{lf}} = 30$ yr [173, 174], and $t_{\text{dp}} = 10$ yr [158].

In order to be better fit to the two-stage framework in Eq (1.1), the objective function is rewritten as

$$\text{NPV} = \text{Cap}\left[-1 + \frac{R_{\text{tax}}}{t_{\text{dp}}} \frac{1}{r}\left(1 - \frac{1}{(1+r)^{t_{\text{dp}}}}\right)\right] + \sum_h \text{Occu}_h \, \text{Pro}_{\text{net},h} \frac{1}{r}\left(1 - \frac{1}{(1+r)^{t_{\text{lf}}}}\right) \quad (4.12)$$

where $\text{Pro}_{\text{net},h}$ is the net profit in scenario h.

4.1.4 Model Summary

The objective is to maximize the NPV subject to design and operational constraints including mass and energy balances in all scenarios, enthalpy calculations, production and feedstock consumption rates, capital cost relationships, and economic analyses. The decision variables include the operational decision variables such as molar (or mass) flow rates of streams, split fractions, heat/power consumption (or generation) rates in all scenarios, and design decision variables such as equipment capacities. The model is formulated in GAMS 22.8 [41]. It is a large-scale nonconvex NLP model, including 4988 variables and 5237 constraints. Of the variables, there are 55 design decision variables and 4933 operational decision variables. Of the constraints, there are 376 inequality constraints and 4861 equality constraints, of which 742 are nonlinear. The nonconvexity in the model mainly originates from bilinear terms in mass balances and power law capital cost relationships. The model was solved using BARON 8.1 [169] with SNOPT [70] as the NLP solver and CPLEX [1] as the LP

solver. A cluster with 32 Intel 2.8 GHz processors was used to study many cases in parallel, where each case was solved on a single CPU. The CPU times for solving individual case studies varied between 24 hr to 96 hr.

4.2 Case Study Results

4.2.1 Case Study Problems

In this part, the optimal product portfolios and net present values of both flexible and static plants are studied for different economic cases, including different oil prices and carbon taxes. The average prices of all products during the plant lifetime are assumed to correlate to the oil price (in different degrees). The CO_2 emissions are also investigated for all economic cases, especially for different carbon taxes.

In this study, eight scenarios are considered, which are the peak time and off-peak time in four seasons, respectively. The peak time is defined to be 7 am − 11 pm on working days, and the off-peak time is the rest of the time in the year, including 11 pm − 7 am on weekdays, and the whole day on weekends and holidays. The fractions of occurrence of all scenarios over the life time of the plant are shown in Table 4.2.

Table 4.2: Fractions of occurrence of all scenarios

Scenario	Occurrence
Spring Peak	12.01 %
Spring Off-peak	13.21 %
Summer Peak	11.82 %
Summer Off-peak	13.39 %
Fall Peak	11.32 %
Fall Off-peak	13.61 %
Winter Peak	11.19 %
Winter Off-peak	13.46 %

All product prices vary seasonally, and the power price also differs greatly between peak and off-peak. In this study, the degree of fluctuation of all product prices in different scenarios are represented by scale factors for prices in these scenarios. The

scale factors for product prices are defined as

$$\mathrm{ScF}_{q,h} = \frac{P^{\mathrm{p}}_{q,h}}{P^{\mathrm{p}}_{q}} , \quad \forall h \in N_h \tag{4.13}$$

where $\mathrm{ScF}_{q,h}$ is the scale factor for the price of product q in scenario h, $P^{\mathrm{p}}_{q,h}$ is the price of product q in scenario h, and P^{p}_{q} is the average price of product q during the whole plant life time. The scale factors for the power price, the naphtha price, the diesel price and the methanol price are estimated from historical market data [3, 5, 4], and their values are shown in Figure 4-1. In each case study, the product prices in all scenarios are obtained by multiplying the price scale factors by the average product price selected for that market case study.

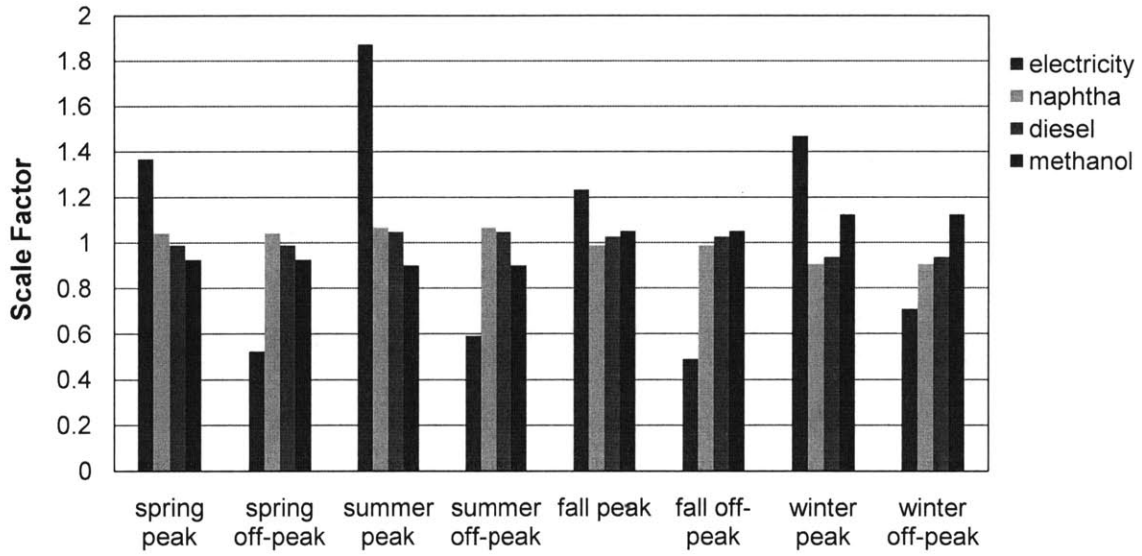

Figure 4-1: Scale factors for product prices in different scenarios.

The plant is assumed to operate for 30 years beginning in 2016. The average feedstock prices and product prices during the plant lifetime are assumed to be equal to those predicted for the year 2030. The average prices (except those of water and sulfur) are assumed to correlate to the oil price, and their values for the high, middle and low oil price are listed in Table 4.3. These average prices are estimated by multiplying estimated average 2007 wholesale prices from historical data [3, 5, 4] by growth factors (i.e., the ratios of projected product prices in 2030 to those in 2007)

predicted by EIA Energy Outlook [53]. The values of carbon taxes for the high, middle and low carbon tax are listed in Table 4.4.

Table 4.3: The average prices for different oil prices

Price	Low Oil Price	Middle Oil Price	High Oil Price	
Coal	36.6	39.5	41.4	\$/tonne
Biomass	54.9	59.2	62.1	\$/tonne
Water	0.8	0.8	0.8	\$/tonne
Power	67.3	98.9	125.8	\$/MWh
Naphtha	530.7	1012.8	1427.1	\$/tonne
Diesel	562.2	1035.5	1485.1	\$/tonne
Methanol	263.1	449.8	586.3	\$/tonne
Sulfur	100.0	100.0	100.0	\$/tonne

Table 4.4: The values of different carbon taxes (\$/tonne of CO_2)

Price	Low Carbon Tax	Middle Carbon Tax	High Carbon Tax
Carbon Tax	10	20	50

For each oil price and carbon tax case study, three different designs for polygeneration systems are compared: the static design with fixed operation at all times or 0% operational flexibility (Ca_{min} = 100%), the "realistic" flexible design with 50% operational flexibility (in which equipment capacity usage varies between 50% and 100%, or Ca_{min} = 50%) and the ideal flexible design with 100% operational flexibility (in which equipment capacity usage varies between 0 and 100%, or Ca_{min} = 0%). In total, 27 combinations are considered (all possible combinations of oil prices, carbon taxes and operational flexibility).

4.2.2 Optimization Results of a Sample Case Study

The detailed results of the polygeneration system design with 0%, 50% and 100% operational flexibility for the middle oil price and the middle carbon tax case are

presented in this section. The optimal values of key decision variables (as shown in Table 4.1) in all scenarios are listed in Table 4.5.

The feedstock consumption rates and production rates of the three different designs for all scenarios are listed in Table 4.6 and 4.7. For simplicity, only the operation in the year 2030 (with multiple scenarios), which is the average year in the lifetime of the plant, is studied. The optimal operation is assumed to be repeated in all years during the plant lifetime. Hence, the annual feedstock consumption rates and production rates remain the same from year to year.

Tables 4.5 and 4.6 show that production rates in the flexible polygeneration systems are adjusted in different scenarios by varying values of key decision variables (including split fractions and WGS conversions), and their variations are limited by the operational flexibility.

The product distribution is expressed as the output fraction of each product, which is calculated by the following equation:

$$\text{Fraction of product } i = \frac{\text{Energy content in product } i}{\text{Total energy content}} \tag{4.14}$$

where energy contents in the liquid fuels and methanol are represented by their lower heating values (LHVs), and energy content in the power is the net power exported to the grid rather than the gross power. The fraction of liquid fuels is the sum of the fractions of naphtha and diesel. The total energy content can be expressed as

$$\begin{aligned}\text{Total energy content} = {} & \text{Net power generation} + \text{Naphtha LHV} + \text{Diesel LHV} \\ & + \text{Methanol LHV}\end{aligned} \tag{4.15}$$

The optimal product distributions will be discussed in the following sections. The annual optimal product distributions, the annual CO_2 emissions and the annual net profit remain the same from year to year.

4.2.3 Operations in Flexible Polygeneration Systems

Optimal product distributions for all 50% and 100% operational flexibility cases are shown in Figures 4-2 and 4-3, respectively. In general, product distributions are influenced the most by the product market prices. The difference of product distributions between peak and off-peak in each season is significant in most cases. In our studies, the power price is assumed to fluctuate drastically between peak and off-peak, while the liquids (naphtha, diesel and methanol) prices are assumed to vary considerably less by comparison from season to season. At peak times, power prices are usually higher than liquids prices; hence power generation dominates the polygeneration process. At off-peak times, power prices drop below the liquids prices, and liquids become the favorable products. On the contrary, the differences in product distributions between different seasons are small in most cases, implying that the seasonal fluctuations of all product prices are not significant enough to influence the production plans.

The oil price, to which the average product prices are correlated, and the carbon tax are important influences on the product distributions. In our studies, the methanol price is higher than liquid fuels (naphtha and diesel) prices for the low oil price, and lower than the liquid fuels prices for the high oil price. Hence, it is favorable to co-produce power and methanol for the low oil price, while power and liquid fuels for the high oil price. The production plan for the middle oil price, where the methanol price and the liquid fuels prices are very close to each other, is more complex and depends on the operational flexibility, as shown in Figure 4-2 (B) (E) (H) and Figure 4-3 (B) (E) (H). The influence of the carbon tax on the production is not as significant as the oil price. However, for the high carbon tax, power is not a favorable product because either the carbon tax must be paid, or, carbon capture and sequestration (CCS) must be implemented. Both are costly and the result is less profitable than liquids production. Note that this carbon policy does not tax the carbon in the liquid fuels.

The product distributions here are quite different from those for the static poly-

generation systems (as shown in Chapter 3), where co-production of power and liquids (naphtha, diesel and/or methanol) in comparable amounts is rarely optimal due to the high capital cost of the co-installation of power generation and liquids production equipment. In the flexible polygeneration systems, however, this high capital cost can be justified by the extra profit obtained from the optimal production plans in different scenarios. For example, the extra profit of power generation at peak times, when power prices are much higher than their average prices, is higher than the additional capital cost of the co-installed gas turbine and steam turbines in most cases. Similarly, the extra profit of liquids productions at off-peak times not only recovers the capital cost of the Fischer-Tropsch (FT) system or methanol (MeOH) system but also improves the net present value (NPV) of the whole plant. Co-production of liquid fuels and methanol is still rarely optimal in flexible polygeneration designs because the liquid prices in all scenarios are not far from their average prices and not enough extra profit can be gained from such co-production to recover the extremely high capital cost of the co-installation of a FT system and a MeOH system.

Like the product distributions, the equipment load also varies in different scenarios. It is represented by the equipment capacity usage, which is defined as

$$U^l_{\text{cap},h} = \frac{F^l_{\text{in},h}}{\bar{F}^l} \times 100\% \,, \quad \forall h \in N_h \tag{4.16}$$

where $U^l_{\text{cap},h}$ is the percentage usage of the capacity of equipment l in scenario h, $F^l_{\text{in},h}$ is the total molar (or mass) flow rate of the input stream of equipment l in scenario h, and $\bar{F}^l$ is the molar (or mass) capacity of equipment l.

The equipment capacity usages for the middle carbon tax and 50% operational flexibility case and the middle carbon tax and 100% operational flexibility case are shown in Figures 4-4 and 4-5, respectively. From Figures 4-2 and 4-4, all equipment (except compressors and equipment that are not built) are operated between the half and full capacity in all scenarios for 50% operational flexibility, resulting in a limited variation in product distributions. From Figures 4-3 and 4-5, some equipment are allowed to be fully operated in some scenarios and totally shut down in other

scenarios for 100% operational flexibility, leading to totally different production plans in different scenarios. For example, for the low oil price, the polygeneration plant with 100% operational flexibility operates optimally as a pure power plant during the peak times and a methanol plant with a small amount of power output during the off-peak times (as shown in Figure 4-5 (A)). In real applications, the gas turbine can start up or shut down quickly without much difficulty, while the equipment in the chemical processes usually needs to be operated above a minimum capacity (typically 50% of the full capacity) at all times since its start-up is difficult and lengthy. Hence, the polygeneration plant with 50% operational flexibility can be potentially realized in industry, while the plant with 100% operational flexibility is currently only an ideal construct. However, the results for 100% operational flexibility provide the maximum potential economic benefit from all flexible designs and operations considered. The operational flexibility can potentially be increased by the development of advanced control and operational technologies in the future. From Figures 4-4 and 4-5, it can be seen that the fluctuation of the capacity usage of the steam turbine (and its steam generation system) is much smaller than other equipment because the amount of steam generated by the power generation process is not very different from that by the liquid production process. This result mitigates the operational difficulties in the potential real application of flexible polygeneration plants.

CO_2 emissions for the middle oil price and 50% operational flexibility case and the middle oil price and 100% operational flexibility case are shown in Figures 4-6 and 4-7, respectively (based on the dry feedstock consumption rate of 1042 tonne/hr). In most cases, the process CO_2 emissions at peak times are higher than those at off-peak times. There are two reasons: first, power generation (without CCS) is usually favored at peak times, emitting essentially all carbon from the feedstock into the atmosphere, while at off-peak times a large portion of the carbon enters the liquid fuels or methanol; second, the CCS for the CO_2 produced in the liquids production process is turned off at peak times (with high power prices) to produce more power to export to the grid and it is turned on at off-peak times (with low power prices) to pay less carbon tax. However, total CO_2 emissions, which are equal to process CO_2

emissions plus the downstream CO_2 emissions from the liquid fuels may be the same between peak times and off-peak times in some cases (such as for the low carbon tax, the middle oil price and 50% operational flexibility case, as shown in Figure 4-6 (A)). With an increase in the carbon tax, CO_2 emissions are significantly decreased because it becomes more economical to implement CCS instead of paying the carbon tax or to switch from power generation without CCS to liquids production.

4.2.4 Comparison of Static Designs and Flexible Designs

The annual product distributions for all 0%, 50% and 100% operational flexibility cases are shown in Figure 4-8. In static polygeneration designs, the fraction of one product is much higher than other products in most cases, as discussed in Chapter 3. In flexible polygeneration designs, the product distributions become much more uniform, implying that one product cannot dominate the portfolio in all scenarios in most cases. The influence of the oil price and the carbon tax on the product distributions is similar for all three designs.

The annual CO_2 emissions for all 0%, 50% and 100% operational flexibility cases are shown in Figure 4-9 (based on the dry feedstock consumption rate of 7.815 Mt/yr). Flexible polygeneration systems produce higher or lower CO_2 emissions than static ones, depending on the product distributions. If the fraction of liquid fuels or methanol increases in the product portfolio, CO_2 emissions will be reduced; if the fraction of power increases and no CCS is implemented, CO_2 emissions will increase. CO_2 emissions in all three designs are significantly reduced with an increase in the carbon tax.

The economic performance of polygeneration systems for all 0%, 50% and 100% operational flexibility cases are compared in Figures 4-10 – 4-13. The total capital investments for the three kinds of polygeneration systems in all cases are shown in Figure 4-10, their annual net profits are shown in Figure 4-11, and their net present values are shown in Figure 4-12. Higher capital investments are needed for flexible plants than the corresponding static plants because all equipment must be oversized to realize operational flexibility. However, flexible systems also achieve higher annual

net profits than static systems through their more flexible production strategies. Considering these two factors, flexible systems obtain better overall economic benefits, such as higher net present values (NPV) as shown in Figure 4-12. A higher NPV can be achieved if more operational flexibility is realized. The percentage increases of the NPV in flexible polygeneration systems compared to those in static ones are shown in Figure 4-13. For the low oil price and the middle carbon tax case, the flexible plant with 100% operational flexibility can yield as high as 63% more NPV than the static plant. Hence, the more expensive, high flexibility plants provide greater returns. However, at these very large scales, the initial capital investment required may be prohibitive, such that a less-flexible (and less profitable) design may be desirable.

Higher NPVs are realized for polygeneration plants with different operational flexibilities for higher oil prices or lower carbon taxes. For higher oil prices and higher carbon taxes, the gains in the NPV achieved by increasing the flexibility is less significant, since the NPVs of all polygeneration plants are very high for the high oil price cases (as shown in Figure 4-12 (C)). For the high carbon tax case, liquids production is preferred to power production for all operational flexibilities, resulting in smaller variations of production plans among different scenarios (as shown in Figure 4-8 (C)).

Table 4.5: Optimal values of key decision variables in the sample case study *

Decision Variables		Operational Flexibility		
		0%	50%	100%
$m_{\text{fd,dry}}^{\text{gas}}$ *				
	All Seasons, Peak & Off-peak	1042	1042	1042
$R_{\text{b/f}}$				
	All Seasons, Peak & Off-peak	0	0	0
S_{liq}				
	Spring, Summer & Fall, Peak	1	0.481	0
	Winter Peak	1	0.483	0
	All Seasons, Off-peak	1	0.991	1
S_{ele}				
	All Seasons, Peak & Off-peak	0	0	0
R_{wgs1}				
	Spring, Summer & Fall, Peak	0.398	0.381	n/a **
	Winter Peak	0.398	0.387	n/a
	All Seasons, Off-peak	0.398	0.415	0.415
R_{wgs2}				
	All Seasons, Peak & Off-peak	n/a	n/a	n/a
S_{seq}				
	Spring & Fall, Peak	1	1	n/a
	Summer & Winter, Peak	1	0	n/a
	All Seasons, Off-peak	1	1	1
S_{me}				
	All Seasons, Peak	0.822	0	n/a
	All Seasons, Off-Peak	0.822	0	1
S_{atr}				
	Spring, Summer & Fall, Peak	1	0.358	n/a
	Winter Peak	1	0.348	n/a
	All Seasons, Off-peak	1	0.257	n/a
S_{fts}				
	Spring, Summer & Fall, Peak	0	0	n/a
	Winter Peak	0	0.170	n/a
	All Seasons, Off-peak	0	1	n/a
S_{mes}				
	All Seasons, Peak	0.957	n/a	n/a
	All Seasons, Off-Peak	0.957	n/a	0.971

* : All decision variables are unitless except $m_{\text{fd,dry}}^{\text{gas}}$, which is tonne/hr.
** : Some results are not applicable (n/a) because the corresponding equipment are absent in the optimal design.

Table 4.6: Feedstock consumption rates and production rates for the sample case study in all scenarios *

		Operational Flexibility		
		0%	50%	100%
Feedstock				
Coal				
	All Seasons, Peak & Off-peak	1172	1172	1172
Biomass				
	All Seasons, Peak & Off-peak	0	0	0
Water				
	Spring, Summer & Fall, Peak	350	617	197
	Winter Peak	350	619	197
	All Seasons, Off-peak	350	517	412
Product				
Power *				
	Spring & Fall, Peak	208	2676	3944
	Summer & Winter, Peak	208	2728	3944
	All Seasons, Off-peak	208	1312	71
Naphtha				
	All Seasons, Peak	12	34	0 **
	All Seasons, Off-Peak	12	68	0 **
Diesel				
	All Seasons, Peak	31	90	0 **
	All Seasons, Off-Peak	31	178	0 **
Methanol				
	All Seasons, Peak	713	0 **	0
	All, Seasons, Off-Peak	713	0 **	831
Sulfur				
	All Season, Peak & Off-peak	29	29	29
CO_2 Sequestered				
	Spring & Fall, Peak	1424	695	0
	Summer & Winter, Peak	1424	0	0
	All Seasons, Off-peak	1424	1390	1403

* : The unit of all quantities is tonne/hr, except power, which is MW.
** : Some production rates are zero because the corresponding equipment are absent in the optimal design.

Table 4.7: Annual feedstock consumption rates and production rates for the sample case study *

	0% Flexibility	50% Flexibility	100% Flexibility
Feedstock			
Coal	8.79	8.79	8.79
Biomass	0	0	0
Water	2.62	4.23	2.34
Product			
Power *	1.56	14.67	13.99
Naphtha	0.09	0.39	0 **
Diesel	0.23	1.03	0 **
Methanol	5.35	0 **	3.35
Sulfur	0.22	0.22	0.22
CO_2 sequestered	10.68	6.81	5.64

* : The unit of all quantities is Mt/yr, except power which is TWh/yr.
** : Some production rates are zero because the corresponding equipment are absent in the optimal design.

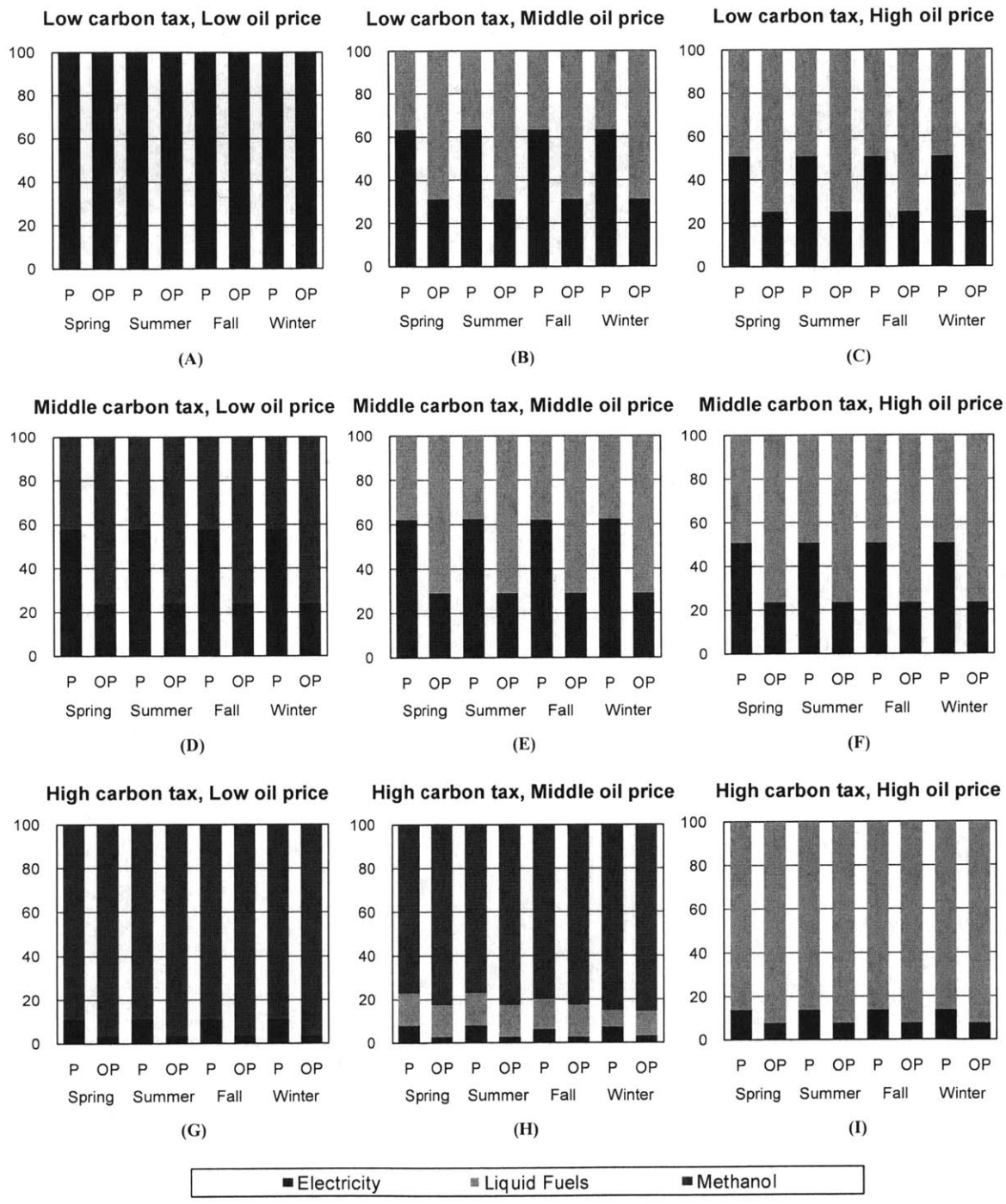

Figure 4-2: Product distributions for the 50% operational flexibility case (%). [P = peak, OP = off-peak.]

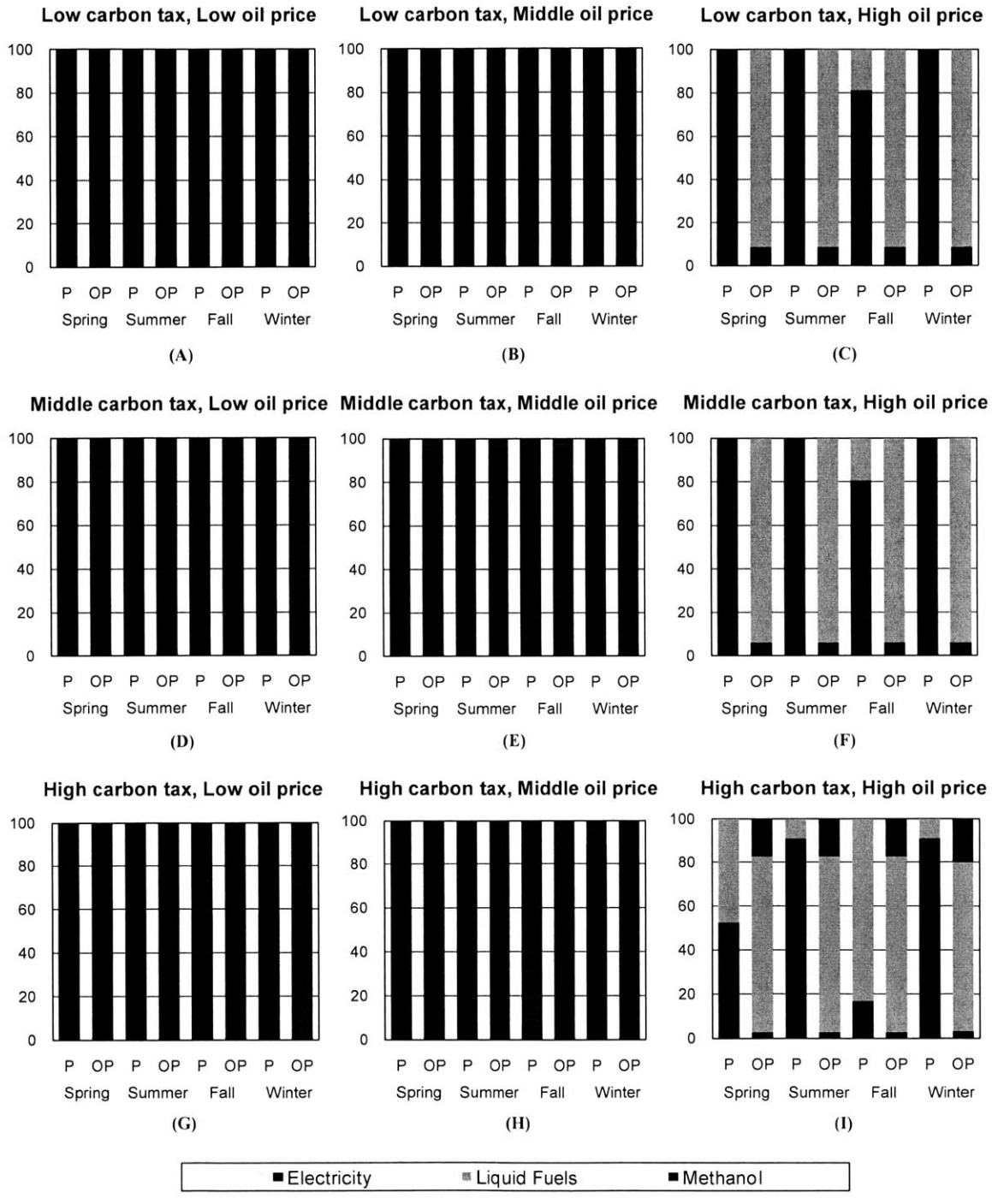

Figure 4-3: Product distributions for the 100% operational flexibility case (%). [P = peak, OP = off-peak.]

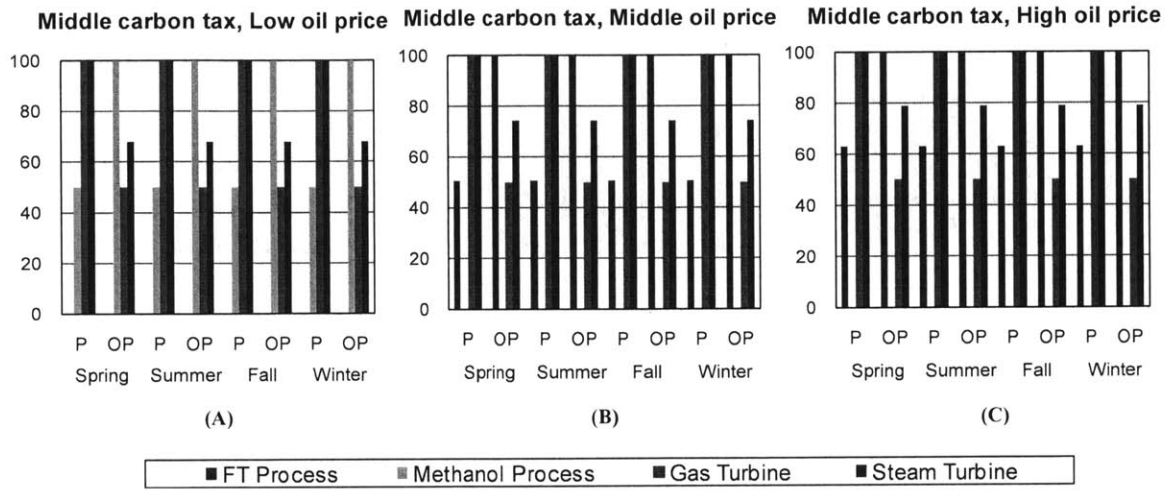

Figure 4-4: Equipment capacity usages for the middle carbon tax and 50% operational flexibility case (%). [P = peak, OP = off-peak.]

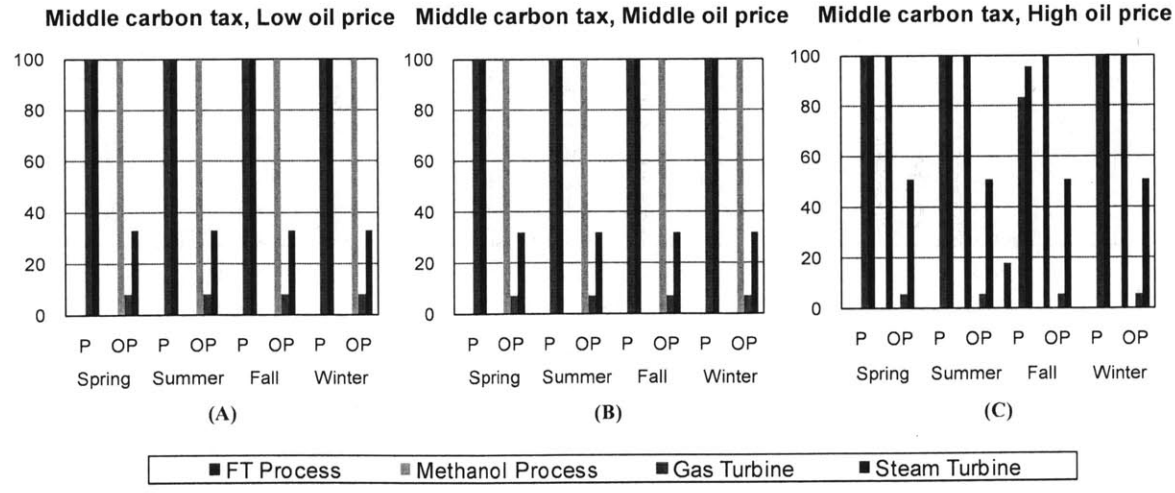

Figure 4-5: Equipment capacity usages for the middle carbon tax and 100% operational flexibility case (%). [P = peak, OP = off-peak.]

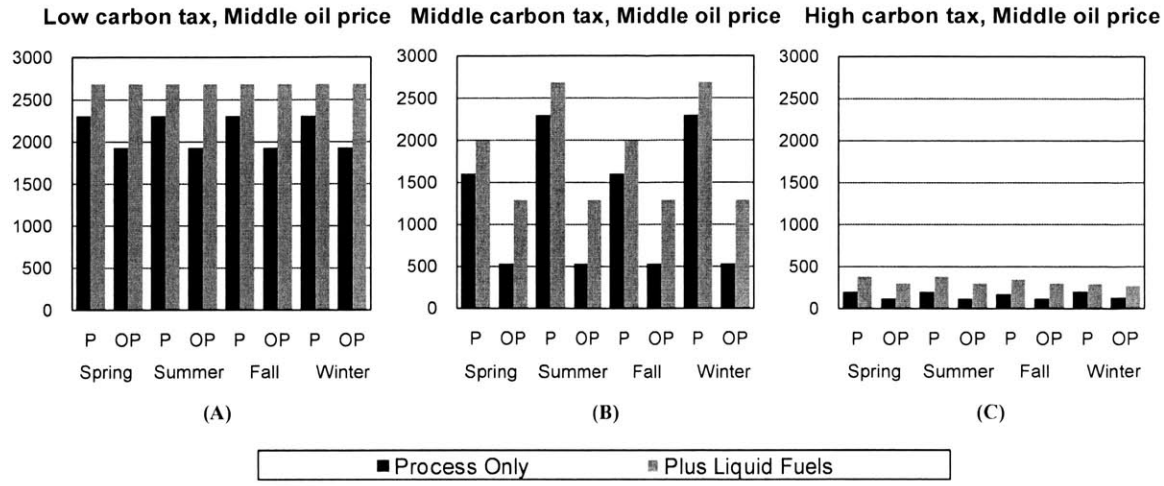

Figure 4-6: CO_2 emission rates for the middle oil price and 50% operational flexibility case (tonne/hr). [P = peak, OP = off-peak; Process Only = carbon taxes only apply to CO_2 emissions in the process, Plus Liquid Fuels = carbon taxes apply to both the CO_2 emissions from the process, and to the carbon in the fuels which will eventually be combusted.]

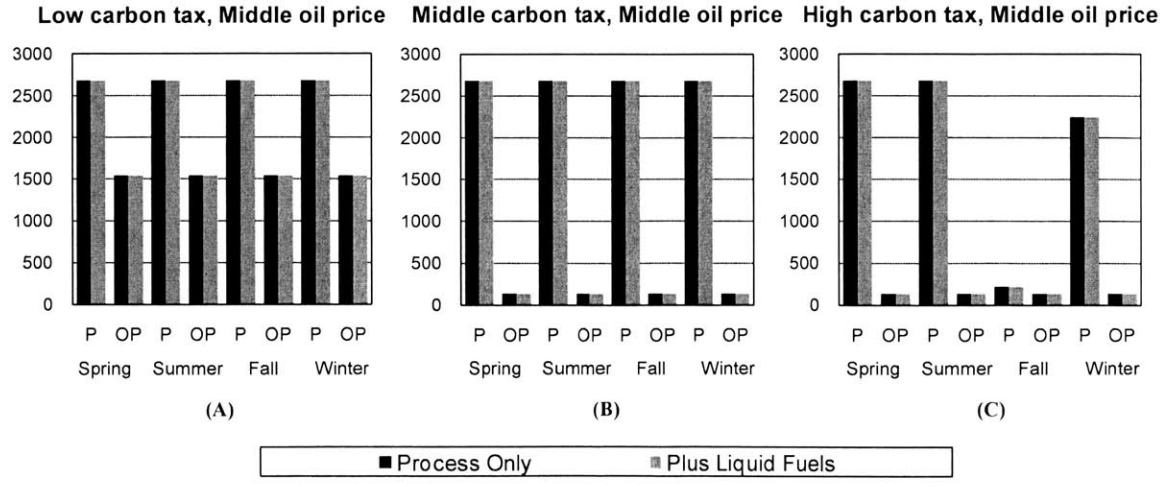

Figure 4-7: CO_2 emission rates for the middle oil price and 100% operational flexibility case (tonne/hr). [P = peak, OP = off-peak; Process Only = carbon taxes only apply to CO_2 emissions in the process, Plus Liquid Fuels = carbon taxes apply to both the CO_2 emissions from the process, and to the carbon in the fuels which will eventually be combusted.]

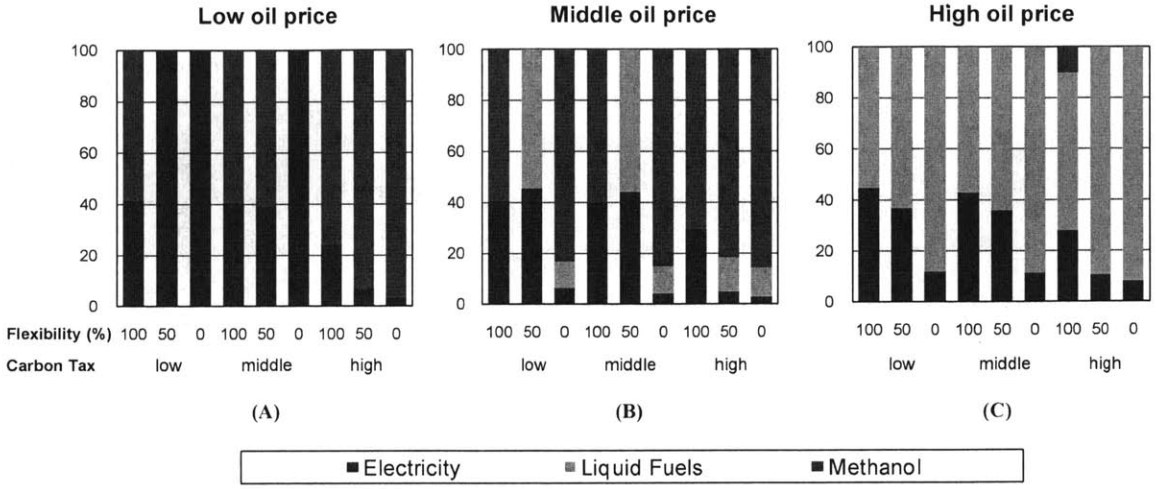

Figure 4-8: Annual product distributions for three different operational flexibilities (%).

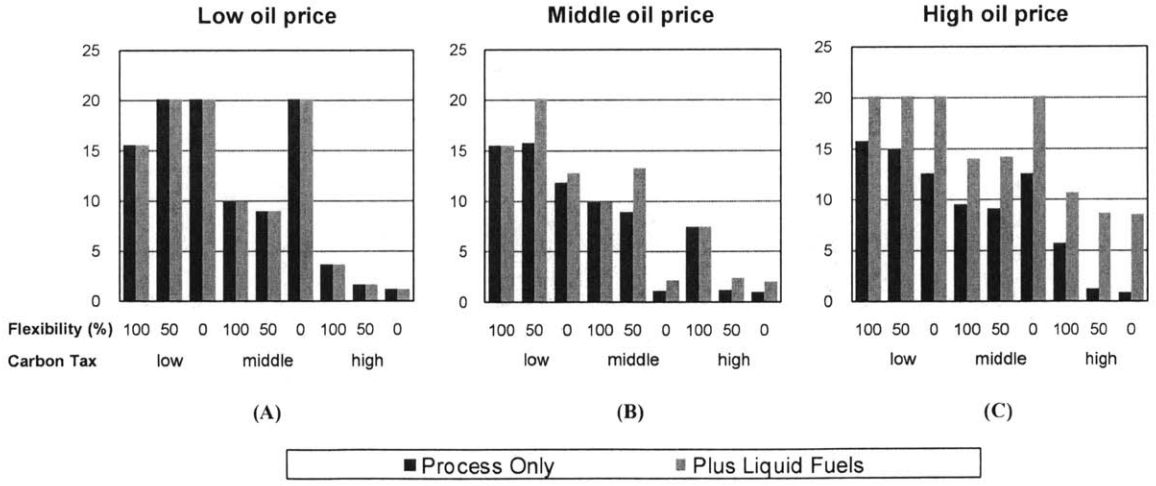

Figure 4-9: Annual CO_2 emissions for three different operational flexibilities (Mt/yr). [Process Only = carbon taxes only apply to CO_2 emissions in the process, Plus Liquid Fuels = carbon taxes apply to both the CO_2 emissions from the process, and to the carbon in the fuels which will eventually be combusted.]

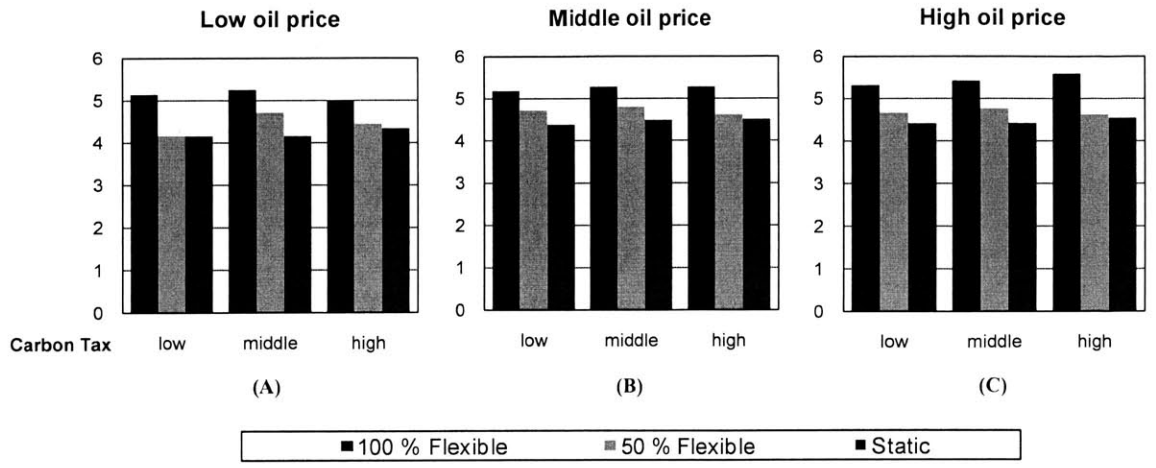

Figure 4-10: Capital investments in all cases ($billion).

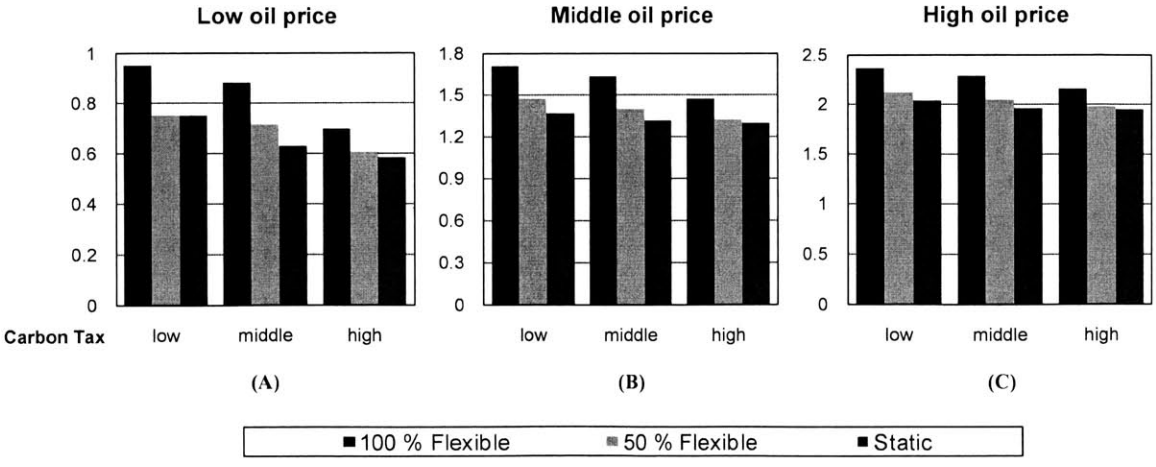

Figure 4-11: Annual net profits in all cases ($billion/yr).

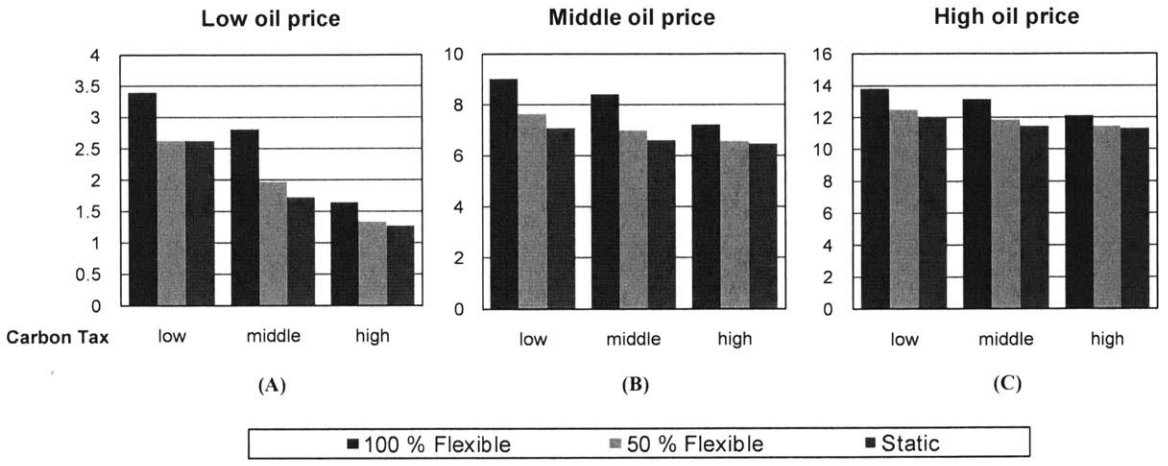

Figure 4-12: Net present values in all cases ($billion).

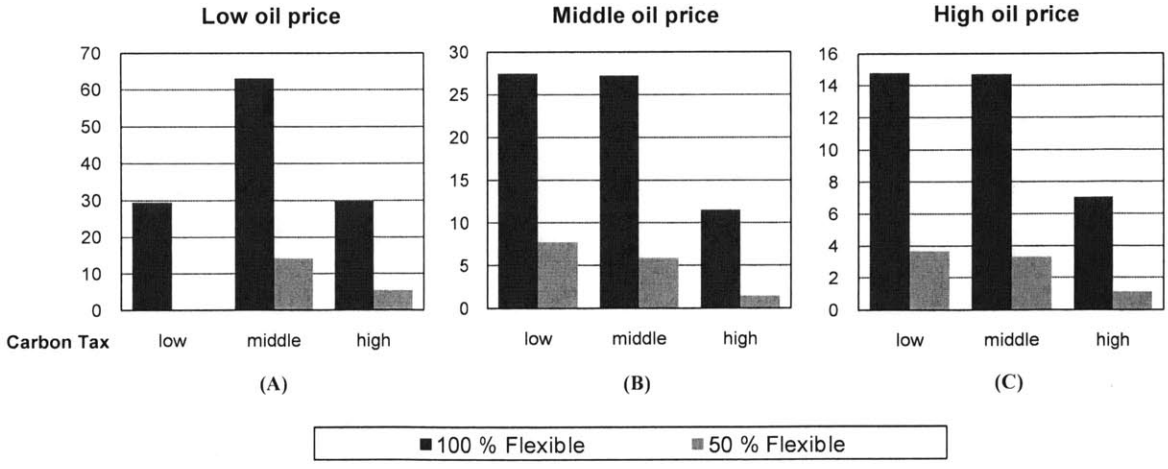

Figure 4-13: Increase of NPV in flexible polygeneration systems compared to the corresponding static polygeneration systems (%).

Chapter 5

Nonconvex Generalized Benders Decomposition Algorithm

5.1 Motivation

The optimal design and operation of flexible polygeneration systems, which is formulated as a multi-period optimization problem (as shown in Chapter 4), is a potentially large-scale nonconvex mixed-integer nonlinear programming (MINLP) problem with high computational burden. In Chapter 4, the state-of-the-art global optimization solver, BARON, was employed to obtain the global optimum for the polygeneration optimization problem. However, BARON required a considerable amount of CPU time to solve the problem, and the solution time increases exponentially with the number of scenarios. Therefore, more efficient algorithms need to be developed to solve this multi-period optimization problem for larger numbers of scenarios.

A decomposition algorithm recently developed for the stochastic pooling problem [110, 112, 113, 114] is attractive for this large-scale multi-period optimization problem because it can fully exploit the decomposable structure of the problem. By applying the decomposition algorithm, the solution time of the multi-period optimization problem is expected to increase linearly with the number of scenarios, and the global optimization of large-scale flexible polygeneration design problems can be achieved in reasonable times.

5.2 Overview

The decomposition method is an extension of Benders decomposition [32] and is developed based on the framework of concepts presented by Geoffrion for the design of large-scale mathematical programming techniques [68, 66, 67]. This framework includes two groups of concepts: problem manipulations and solution strategies. Problem manipulations, including convexification, projection, and dualization, are devices for restating a given problem in an alternative form more amenable to solution. The result is often what is referred to as a master problem. Solution strategies, including relaxation and restriction, reduce the master problem to a related sequence of simpler subproblems.

In this thesis, the stochastic/multiperiod pooling problem with the following form is studied:

$$
\begin{aligned}
\min_{\substack{y,x_1,\ldots,x_s,\\ q_1,\ldots,q_s,u_1,\ldots,u_s}} \quad & c_1^{\mathrm{T}} y + \sum_{h=1}^{s} \left(c_{2,h}^{\mathrm{T}} x_h + c_{3,h}^{\mathrm{T}} q_h + c_{4,h}^{\mathrm{T}} u_h \right) \\
\text{s.t.} \quad & u_{h,l,t} = x_{h,l} q_{h,t}, \quad \forall (l,t) \in \Omega, \ \forall h \in \{1,\ldots,s\}, \\
& A_{1,h} y + A_{2,h} x_h + A_{3,h} q_h + A_{4,h} u_h \leq b_h, \quad \forall h \in \{1,\ldots,s\}, \\
& (x_h, q_h, u_h) \in \Pi_h, \ \forall h \in \{1,\ldots,s\}, \quad y \in Y,
\end{aligned}
\tag{P}
$$

where

$$
\begin{aligned}
\Pi_h = \{ (x_h, q_h, u_h) \in \mathbb{R}^{n_x} \times \mathbb{R}^{n_q} \times \mathbb{R}^{n_u} : \tilde{A}_{2,h} x_h + \tilde{A}_{3,h} q_h + \tilde{A}_{4,h} u_h \leq \tilde{b}_h, \\
x_h^{\mathrm{L}} \leq x_h \leq x_h^{\mathrm{U}}, \ q_h^{\mathrm{L}} \leq q_h \leq q_h^{\mathrm{U}} \},
\end{aligned}
$$

$$
Y = \{ y \in \{0,1\}^{n_y} : By \leq a \}.
$$

The index $h \in \{1,\ldots,s\}$ indicates the different scenarios for uncertainty realizations or time periods; y represents complicating variables, which are binary variables in this study; x_h, q_h and u_h are non-complicating variables in scenario h, which are continuous. The set Π_h is a nonempty, compact and convex polyhedron. Note that the classical pooling problem formulations, including p-, q- and pq-formulations [168],

can all be written in the form of Problem (P).

Remark 1. Problem (P) has finite optimal objective values or is infeasible because the set Π_h is compact.

In the decomposition method, Problem (P) is reformulated into a lower bounding problem by convexification and underestimation of the bilinear functions. The lower bounding problem is potentially a large-scale MILP, which can be transformed into an equivalent master problem by the principle of projection and dualization [68].

The master problem contains an infinite number of constraints and is usually difficult to solve directly. Instead it is solved through solving a sequence of **Primal Bounding Problems (PBP)**, **Feasibility Problems (FP)**, and **Relaxed Master Problems (RMP)**, which are much easier to solve.

The **Primal Bounding Problem** is constructed by restricting the integer variables to specific values in the lower bounding problem, whose solution yields a valid upper bound on the optimal objective value of the lower bounding problem (and hence the master problem). When the primal bounding problem is infeasible for an integer realization, a corresponding **Feasibility Problem** is solved, which yields valid information for the algorithm to proceed. Both the primal bounding problems and the feasibility problems are potentially large-scale LPs, but they can be further decomposed into LP subproblems for each scenario with much smaller sizes.

The **Relaxed Master Problem** is constructed by relaxing the master problem with a finite subset of the constraints (or cuts). Canonical integer cuts are also added into the problem so that no integer realizations will be visited twice by the algorithm. The solution of the relaxed master problem yields a valid lower bound on the optimal objective value of the master problem augmented with the integer cuts. The relaxed master problem is a MILP whose size is independent of the number of scenarios.

On the other hand, a restriction of Problem (P), which is called the **Primal Problem (PP)**, is constructed by restricting the integer variables to specific values in Problem (P), whose optimal objective value yields an upper bound of that of Problem (P). The primal problem is potentially a large-scale nonconvex NLP, but it can be further decomposed into NLP subproblems for each scenario with much

smaller sizes.

The details of the aforementioned subproblems are given in the next section.

5.3 Subproblems in the Decomposition Method

5.3.1 Primal Bounding Problem

The primal bounding problem (PBP) is generated by fixing the integer variables in the lower bounding problem to $y^{(k)}$, which is the integer realization at the k^{th} iteration. Problem (PBP) can be naturally decomposed into subproblems (PBP_h) for the s scenarios:

$$\begin{aligned} \text{obj}_{\text{PBP}_h}\left(y^{(k)}\right) = \min_{x_h, q_h, u_h} \; & c_{2,h}^{\text{T}} x_h + c_{3,h}^{\text{T}} q_h + c_{4,h}^{\text{T}} u_h \\ \text{s.t.} \; & A_{1,h} y^{(k)} + A_{2,h} x_h + A_{3,h} q_h + A_{4,h} u_h \leq b_h, \\ & (x_h, q_h, u_h) \in \hat{\Pi}_h, \end{aligned} \tag{PBP_h}$$

where

$$\begin{aligned} \hat{\Pi}_h = \{(x_h, q_h, u_h) \in \Pi_h : \; & u_{h,l,t} \geq x_{h,l}^{\text{L}} q_{h,t} + x_{h,l} q_{h,t}^{\text{L}} - x_{h,l}^{\text{L}} q_{h,t}^{\text{L}}, \\ & u_{h,l,t} \geq x_{h,l}^{\text{U}} q_{h,t} + x_{h,l} q_{h,t}^{\text{U}} - x_{h,l}^{\text{U}} q_{h,t}^{\text{U}}, \\ & u_{h,l,t} \leq x_{h,l}^{\text{U}} q_{h,t} + x_{h,l} q_{h,t}^{\text{L}} - x_{h,l}^{\text{U}} q_{h,t}^{\text{L}}, \\ & u_{h,l,t} \leq x_{h,l}^{\text{L}} q_{h,t} + x_{h,l} q_{h,t}^{\text{U}} - x_{h,l}^{\text{L}} q_{h,t}^{\text{U}}, \\ & \forall (l,t) \in \Omega \; \}. \end{aligned}$$

$\text{obj}_{\text{PBP}_h}\left(y^{(k)}\right)$ is the optimal objective value of Problem (PBP_h) for $y = y^{(k)}$, $h = 1, \ldots, s$. The objectives of Problem (PBP) and (PBP_h) satisfy the following relationship:

$$\text{obj}_{\text{PBP}}\left(y^{(k)}\right) = c_1^{\text{T}} y^{(k)} + \sum_{h=1}^{s} \text{obj}_{\text{PBP}_h}\left(y^{(k)}\right). \tag{5.1}$$

where $\text{obj}_{\text{PBP}}\left(y^{(k)}\right)$ is the optimal objective value of Problem (PBP) for $y = y^{(k)}$.

5.3.2 Feasibility Problem

If Problem (PBP) is infeasible, the corresponding feasibility problem (FP) is solved. Problem (FP) can be naturally decomposed into subproblems (FP_h) for the s scenarios:

$$\begin{aligned} \min_{x_h, q_h, u_h, z_h} \ & \sum_{i=1}^{m} z_{h,i} \\ \text{s.t.} \ & A_{1,h} y^{(k)} + A_{2,h} x_h + A_{3,h} q_h + A_{4,h} u_h - b_h \leq z_h, \\ & (x_h, q_h, u_h) \in \hat{\Pi}_h, \ z_h = (z_{h,1}, \ldots, z_{h,m}) \in Z, \end{aligned} \tag{FP_h}$$

where $Z = \{z \in \mathbb{R}^m : z \geq 0\}$, and each nonnegative variable $z_{h,i}$ measures the violation of the corresponding constraint, $h = 1, \ldots, s$.

5.3.3 Relaxed Master Problem

After solving the primal bounding subproblems or feasibility subproblems for k integer realizations, a relaxed master problem (RMP^k) is solved to generate a new integer realization:

$$\begin{aligned} \min_{y, \eta} \ & \eta \\ \text{s.t.} \ & \eta \geq \alpha^{(j)} y + \beta^{(j)}, \quad \forall j \in T^k, \\ & \gamma^{(i)} y + \theta^{(i)} \leq 0, \quad \forall i \in S^k, \\ & \sum_{l \in \{l : y_l^{(t)} = 1\}} y_l - \sum_{l \in \{l : y_l^{(t)} = 0\}} y_l \leq |\{l : y^{(t)} = 1\}| - 1, \quad \forall t \in T^k \cup S^k, \\ & y \in Y, \ \eta \in \mathbb{R}, \end{aligned} \tag{RMP^k}$$

where

$$\begin{aligned}
\alpha^{(j)} =& c_1^{\mathrm{T}} + \sum_{h=1}^{s} \left(\lambda_h^{(j)}\right)^{\mathrm{T}} A_{1,h}, \\
\beta^{(j)} =& \sum_{h=1}^{s} \left[c_{2,h}^{\mathrm{T}} x_h^{(j)} + c_{3,h}^{\mathrm{T}} q_h^{(j)} + c_{4,h}^{\mathrm{T}} u_h^{(j)}\right] + \\
& \sum_{h=1}^{s} \left[\left(\lambda_h^{(j)}\right)^{\mathrm{T}} \left(A_{2,h} x_h^{(j)} + A_{3,h} q_h^{(j)} + A_{4,h} u_h^{(j)} - b_h\right)\right], \\
\gamma^{(i)} =& \sum_{h=1}^{s} \left(\mu_h^{(i)}\right)^{\mathrm{T}} A_{1,h}, \\
\theta^{(i)} =& \sum_{h=1}^{s} \left[\left(\mu_h^{(i)}\right)^{\mathrm{T}} \left(A_{2,h} x_h^{(i)} + A_{3,h} q_h^{(i)} + A_{4,h} u_h^{(i)} - b_h\right)\right],
\end{aligned}$$

and the index sets are

$$\begin{aligned}
T^k &= \{j \in \{1, \ldots, k\} : \text{Problem PBP } \left(y^{(j)}\right) \text{ is feasible}\}, \\
S^k &= \{i \in \{1, \ldots, k\} : \text{Problem PBP } \left(y^{(i)}\right) \text{ is infeasible}\}.
\end{aligned}$$

$\lambda_h^{(j)}$ denotes the Lagrange multipliers of Problem (PBP_h) when $y = y^{(j)}$ ($\forall j \in T^k$), and $\mu_h^{(i)}$ denotes the Lagrange multipliers of Problem (FP_h) when $y = y^{(i)}$ ($\forall i \in S^k$). $\left(x_h^{(j)}, q_h^{(j)}, u_h^{(j)}\right)$ is a minimum of Problem (PBP_h) ($\forall h \in \{1, \ldots, s\}$) when $y = y^{(j)}$, and $\left(x_h^{(i)}, q_h^{(i)}, u_h^{(i)}\right)$ is a minimum of Problem (FP_h) ($\forall h \in \{1, \ldots, s\}$) when $y = y^{(i)}$. The last group of constraints represent a set of canonical integer cuts that prevent the previously examined integer realizations from becoming a solution [25]. In this work, these integer cuts are called "Balas cuts".

When no feasible integer realization for Problem (PBP) has been found (i.e. $T^k = \emptyset$), an alternative problem (RMFP^k), which yields a feasible solution for Problem

(RMP^k), is solved to allow the algorithm to proceed:

$$\begin{aligned}
\min_{y} \quad & \sum_{l=1}^{n_y} y_l \\
\text{s.t.} \quad & \gamma^{(i)} y + \theta^{(i)} \leq 0, \quad \forall i \in S^k, \\
& \sum_{l \in \{l: y_l^{(t)}=1\}} y_l - \sum_{l \in \{l: y_l^{(t)}=0\}} y_l \leq |\{l : y^{(t)} = 1\}| - 1, \quad \forall t \in S^k, \\
& y \in Y.
\end{aligned} \tag{RMPF^k}$$

5.3.4 Primal Problem

The primal problem (PP) is generated by fixing the integer variables in the original Problem (P) to $y^{(k)}$, which is the integer realization at the k^{th} iteration. Problem (PP) can be naturally decomposed into subproblems (PP$_h$) for the s scenarios:

$$\begin{aligned}
\text{obj}_{\text{PP}_h}\left(y^{(k)}\right) = \min_{x_h, q_h, u_h} \quad & c_{2,h}^{\text{T}} x_h + c_{3,h}^{\text{T}} q_h + c_{4,h}^{\text{T}} u_h \\
\text{s.t.} \quad & u_{h,l,t} = x_{h,l} q_{h,t}, \quad \forall (l,t) \in \Omega, \\
& A_{1,h} y^{(k)} + A_{2,h} x_h + A_{3,h} q_h + A_{4,h} u_h \leq b_h, \\
& (x_h, q_h, u_h) \in \Pi_h,
\end{aligned} \tag{PP$_h$}$$

where $\text{obj}_{\text{PP}_h}\left(y^{(k)}\right)$ is the optimal objective value of Problem (PP$_h$) for $y = y^{(k)}$, $h = 1, \ldots, s$. The objectives of Problem (PP) and (PP$_h$) satisfy the following relationship:

$$\text{obj}_{\text{PP}}\left(y^{(k)}\right) = c_1^{\text{T}} y^{(k)} + \sum_{h=1}^{s} \text{obj}_{\text{PP}_h}\left(y^{(k)}\right). \tag{5.2}$$

where $\text{obj}_{\text{PP}}\left(y^{(k)}\right)$ is the optimal objective value of Problem (PP) for $y = y^{(k)}$.

Remark 2. According to Ref [113], the solution of Problem (PP$_h$) can be accelerated with the inclusion of additional cuts.

5.4 Decomposition Algorithm

The decomposition algorithm is described as below [113]:

Initialize:

1. Iteration counters $k = 0$, $l = 1$, and the index sets $T^0 = \emptyset$, $S^0 = \emptyset$, $U^0 = \emptyset$.

2. Upper bound on the problem UBD $= +\infty$, upper bound on the lower bounding problem UBDPB $= +\infty$, lower bound on the lower bounding problem LBD $= -\infty$.

3. Set tolerances ϵ_h and ϵ such that $\sum_{h=1}^{s} \epsilon_h \leq \epsilon$.

4. Integer realization $y^{(1)}$ is given.

repeat

if $k = 0$ or (Problem (RMP^k) is feasible and LBD $<$ UBDPB and LBD $<$ UBD $- \epsilon$) **then**

repeat

Set $k = k + 1$

1. Solve the decomposed primal bounding problem (PBP$_h(y^{(k)})$) for each scenario $h = 1, ..., s$ sequentially. If Problem (PBP$_h(y^{(k)})$) is feasible for all the scenarios with Lagrange multipliers $\lambda_h^{(k)}$, add optimality cuts to the relaxed master problem (RMP^k) according to $\lambda_1^{(k)}, ..., \lambda_s^{(k)}$, set $T^k = T^{k-1} \cup \{k\}$. If obj$_{\text{PBP}}(y^{(k)})$ $<$ UBDPB, update UBDPB $=$ obj$_{\text{PBP}}(y^{(k)})$, $y^* = y^{(k)}$, $k^* = k$.

2. If Problem (PBP$_h(y^{(k)})$) is infeasible for one scenario, stop solving it for the remaining scenarios and set $S^k = S^{k-1} \cup \{k\}$. Then, solve the decomposed feasibility problem (FP$_h(y^{(k)})$) for $h = 1, ..., s$ and obtain the corresponding Lagrange multipliers $\mu_h^{(k)}$. Add feasibility cuts to Problem (RMP^k) according to these multipliers.

3. If $T^k = \emptyset$, solve the feasibility problem (RMFP^k); otherwise, solve Problem (RMP^k). In the latter case, if Problem (RMP^k) is feasible,

set LBD to its optimal objective value. In both cases, set $y^{(k+1)}$ to the y value at the solution of either problem.

until LBD $\geq$ UBDPB or (Problem (RMP^k) or (RMFP^k) is infeasible).

end if

if UBDPB $<$ UBD $- \epsilon$ **then**

1. Solve the decomposed primal problem (PP$_h(y^*)$) to ϵ_h-optimality for each scenario $h = 1, ..., s$ sequentially. Set $U^l = U^{l-1} \cup \{k^*\}$. If Problem (PP$_h(y^*)$) is feasible with optimum (x_h^*, q_h^*, u_h^*) for all the scenarios and obj$_{\text{PP}}(y^*)$ $<$ UBD, update UBD $=$ obj$_{\text{PP}}(y^*)$ and set $y_p^* = y^*$, $(x_{p,h}^*, q_{p,h}^*, u_{p,h}^*) = (x_h^*, q_h^*, u_h^*)$ for $h = 1, \ldots, s$.

2. If $T^k \setminus U^l = \emptyset$, set UBDPB $= +\infty$.

3. If $T^k \setminus U^l \neq \emptyset$, pick $i \in T^k \setminus U^l$ such that obj$_{\text{PBP}}(y^{(i)}) = \min_{j \in T^k \setminus U^l}\{\text{obj}_{\text{PBP}}(y^{(j)})\}$. Update UBDPB $=$ obj$_{\text{PBP}}(y^{(i)})$, $y^* = y^{(i)}$, $k^* = i$. Set $l = l + 1$.

end if

until UBDPB $\geq$ UBD $- \epsilon$ and ((Problem (RMP^k) or (RMFP^k) is infeasible) or LBD $\geq$ UBD $- \epsilon$).

An ϵ-global optimum of the original problem (P) is given by

$$(y_p^*, x_{p,1}^*, ..., x_{p,s}^*, q_{p,1}^*, ..., q_{p,s}^*, u_{p,1}^*, ..., u_{p,s}^*)$$

or (P) is infeasible.

The algorithm flowchart is shown in Figure 5-1 [110]. Note that the nested loops are designed to minimize the number of primal problems solved [100, 113].

The proof of the finite convergence of the decomposition algorithm can be found in Ref [113].

5.5 Conclusions

The decomposition algorithm is expected to be an efficiency algorithm for stochastic/multi-period optimization problems, and can potentially reduce significant amounts of com-

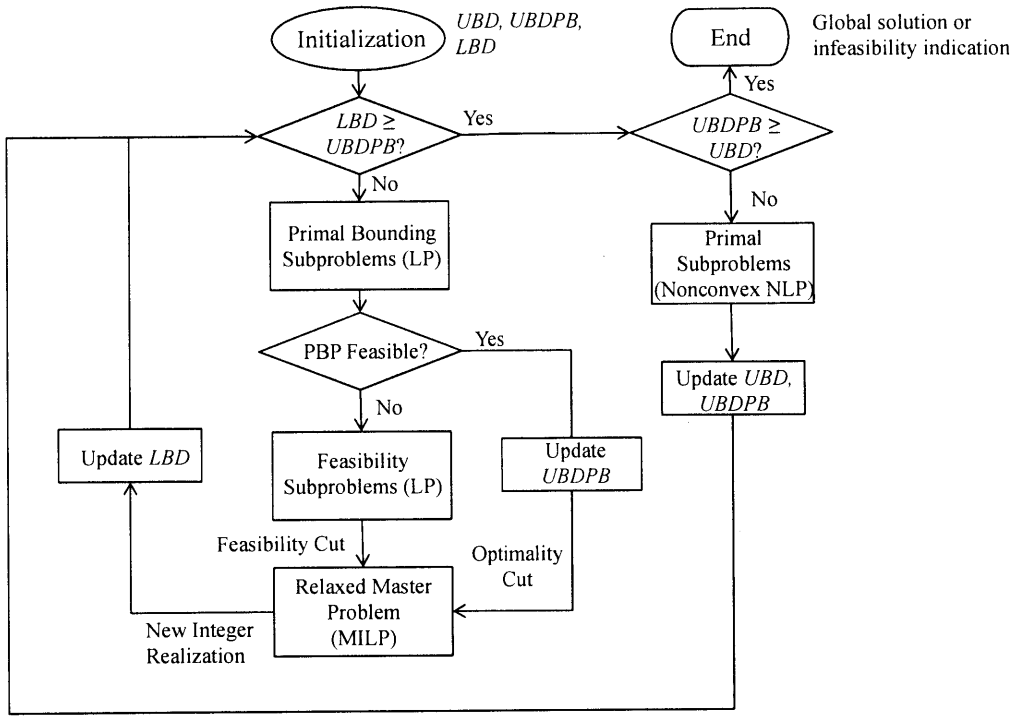

Figure 5-1: Flowchart for the decomposition algorithm.

putational times for large-scale problems compared to state-of-the-art global optimization solvers (as shown in case study results in Chapter 7). However, this method can suffer from a slow convergence rate for highly nonconvex problems, such as the polygeneration optimization problem, due to a large relaxation gap. In Chapter 6, the decomposition algorithm will be enhanced by several methods for faster convergence.

Chapter 6

Enhanced Nonconvex Generalized Benders Decomposition Algorithms

6.1 Overview of Enhancement Technologies

In NGBD, the lower bounding problem serves as a surrogate for Problem (P) for the purpose of valid decomposition, and the tightness of the convex relaxation (i.e., the closeness of the lower bounding problem to Problem (P)) determines the quality of the information generated through the decomposition. Therefore, the tighter the relaxation is, the faster the NGBD may converge. However, NGBD does not reduce the relaxation gap during the solution procedure because it does not branch on the variables in the full search space, so it may have to visit most or even all of the binary variable realizations when the relaxation gap is large. Therefore, NGBD may suffer from a slow convergence rate for highly nonconvex problems, including the polygeneration optimization problem. Several enhancement technologies can be incorporated into NGBD for tighter relaxation and faster convergence.

One enhancement technology is the incorporation of dual information of the primal problem into the relaxed master problem [49]. It has been demonstrated that the

Lagrangian relaxations of some nonconvex functions could be tighter than their convex relaxations [97, 102]. The enhanced NGBD with primal dual information will be discussed in Section 6.2.

Another enhancement technology is using piecewise McCormick relaxation in the lower bounding problem (and also Problem (PBP)) [111]. Recently, it has been recognized in the process systems engineering literature that piecewise linear relaxation enables much tighter relaxations of bilinear programs and can expedite global optimization significantly in the branch-and-bound framework [95, 133, 181, 74] (while the notion of piecewise linear relaxation dates back to the 1980s [150]). The enhanced NGBD with piecewise relaxation will be discussed in Section 6.3, and the enhanced NGBD with both primal dual information and piecewise relaxation will be discussed in Section 6.4.

The third enhancement technology is applying lift-and-project cuts to the lower bounding problem (and Problem (PBP)), instead of directly using piecewise relaxations. The lift-and-project cutting plain method has been successfully developed for the fast solution of MILPs [24, 164]. By using lift-and-project cuts, piecewise relaxation problems with a large number of pieces may be solved efficiently, and the relaxation gap between the original problem and the lower bounding problem can be potentially eliminated when the number of pieces is sufficiently large. The enhanced NGBD with lift-and-project cuts will be discussed in Section 6.5.

Some new subproblems will be added into the NGBD algorithm after applying enhancement technologies, and they will be introduced in each of the following sections.

6.2 Enhanced Decomposition Algorithm with Primal Dual Cuts

6.2.1 New Subproblems

Relaxed Dual of Primal Problem

Primal dual information can be obtained by solving the dual of Problem (PP), which is a quite difficult problem since it is a bilevel program. Instead, a restriction of the dual of Problem (PP) (called Problem (DPP)), which is generated by fixing the multipliers in the dual of Problem (PP) to some specified values, is solved here. The optimal value of Problem (DPP) is a lower bound of that of the dual of Problem (PP). Problem (DPP) can be naturally decomposed into subproblems (DPP_h) for the s scenarios:

$$\begin{aligned} \min_{x_h, q_h, u_h} \quad & c_{2,h}^{\mathrm{T}} x_h + c_{3,h}^{\mathrm{T}} q_h + c_{4,h}^{\mathrm{T}} u_h + \\ & \left(\kappa_h^{(k)}\right) \left(A_{1,h} y^{(k)} + A_{2,h} x_h + A_{3,h} q_h + A_{4,h} u_h - b_h\right) \\ \text{s.t.} \quad & u_{h,l,t} = x_{h,l} q_{h,t}, \quad \forall (l,t) \in \Omega, \\ & (x_h, q_h, u_h) \in \Pi_h, \end{aligned} \tag{DPP$_h$}$$

where $\kappa_h^{(k)}$ can be either $\lambda_h^{(k)}$, which denotes Karush-Kuhn-Tucker (KKT) multipliers of Problem (PBP_h) when $y = y^{(k)}$, or $\breve{\lambda}_h^{(k)}$, which denotes KKT multipliers of Problem (PP_h) when $y = y^{(k)}$. Problem (DPP_h) is solved for both values of the KKT multipliers in this work to obtain additional dual information from the primal problem.

Remark 3. Problem (DPP_h) is always feasible and its optimal objective value is finite because the set Π_h is compact. By weak duality [33], it provides a lower bound on Problem (PP_h).

Remark 4. Problem (DPP_h) is nonconvex, hence global optimization solvers, such as BARON, need to be used here to obtain ϵ-optimal solutions. As discussed later, solving Problem (DPP_h) is the most time-consuming step in the whole algorithm.

To reduce the overall solution time, Problem (DPP_h) is only solved for those integer realizations for which Problem (PP) is feasible and updates the current upper bound (UBD).

Enhanced Relaxed Master Problem with Primal Dual Cuts

The optimal solutions of Problem (DPP_h) together with the KKT multipliers of Problem (PBP_h) and (PP_h) provide additional cuts for the relaxed master problem (RMP^k) to obtain tighter lower bounds for Problem (P). The updated relaxed master problem, which is called the enhanced relaxed master problem with primal dual cuts ($DERMP^k$), is as follows:

$$
\begin{aligned}
\min_{y,\eta} \quad & \eta \\
\text{s.t.} \quad & \eta \geq \tilde{\alpha}^{(r)} y + \tilde{\beta}^{(r)}, \quad \forall r \in V^k, \\
& \eta \geq \breve{\alpha}^{(r)} y + \breve{\beta}^{(r)}, \quad \forall r \in V^k, \\
& \eta \geq \alpha^{(j)} y + \beta^{(j)}, \quad \forall j \in T^k \backslash V^k, \qquad \text{(DERMP}^k\text{)} \\
& \gamma^{(i)} y + \theta^{(i)} \leq 0, \quad \forall i \in S^k, \\
& \sum_{l \in \{l: y_l^{(t)} = 1\}} y_l - \sum_{l \in \{l: y_l^{(t)} = 0\}} y_l \leq |\{l : y^{(t)} = 1\}| - 1, \quad \forall t \in T^k \cup S^k, \\
& y \in Y, \ \eta \in \mathbb{R},
\end{aligned}
$$

where

$$\tilde{\alpha}^{(r)} = c_1^{\mathrm{T}} + \sum_{h=1}^{s} \left(\lambda_h^{(r)}\right)^{\mathrm{T}} A_{1,h},$$

$$\tilde{\beta}^{(r)} = \sum_{h=1}^{s} \left[c_{2,h}^{\mathrm{T}} \tilde{x}_h^{(r)} + c_{3,h}^{\mathrm{T}} \tilde{q}_h^{(r)} + c_{4,h}^{\mathrm{T}} \tilde{u}_h^{(r)}\right] + \sum_{h=1}^{s} \left[\left(\lambda_h^{(r)}\right)^{\mathrm{T}} \left(A_{2,h} \tilde{x}_h^{(r)} + A_{3,h} \tilde{q}_h^{(r)} + A_{4,h} \tilde{u}_h^{(r)} - b_h\right)\right],$$

$$\breve{\alpha}^{(r)} = c_1^{\mathrm{T}} + \sum_{h=1}^{s} \left(\breve{\lambda}_h^{(r)}\right)^{\mathrm{T}} A_{1,h},$$

$$\breve{\beta}^{(r)} = \sum_{h=1}^{s} \left[c_{2,h}^{\mathrm{T}} \breve{x}_h^{(r)} + c_{3,h}^{\mathrm{T}} \breve{q}_h^{(r)} + c_{4,h}^{\mathrm{T}} \breve{u}_h^{(r)}\right] + \sum_{h=1}^{s} \left[\left(\breve{\lambda}_h^{(r)}\right)^{\mathrm{T}} \left(A_{2,h} \breve{x}_h^{(r)} + A_{3,h} \breve{q}_h^{(r)} + A_{4,h} \breve{u}_h^{(r)} - b_h\right)\right],$$

$$V^k = \{r \in \{1, \ldots, k\} : \text{Problem PP } \left(y^{(r)}\right) \text{ is feasible and updates UBD}\} \subset T^k.$$

$\left(\tilde{x}_h^{(r)}, \tilde{q}_h^{(r)}, \tilde{u}_h^{(r)}\right)$ is a minimum of Problem (DPP_h) with the KKT multipliers of Problem (PBP_h) ($\forall h \in \{1, \ldots, s\}$) when $y = y^{(r)}$ and $\left(\breve{x}_h^{(r)}, \breve{q}_h^{(r)}, \breve{u}_h^{(r)}\right)$ is a minimum of Problem (DPP_h) with the KKT multipliers of Problem (PP_h) ($\forall h \in \{1, \ldots, s\}$) when $y = y^{(r)}$. The first two sets of constraints are called primal dual cuts since they are constructed according to the dual information of the primal problem.

Enhanced Relaxed Master Problem with Primal Dual Multicuts

The relaxed master problem (DERMP^k) can be further enhanced by replacing each single primal dual cut with s cuts for the s scenarios, following the multicut strategy in Ref [36]. The new primal dual cuts are called primal dual multicuts in this work. The enhanced relaxed master problem with primal dual multicuts (MDERMP^k) is constructed as follows (in which the optimality and feasibility cuts are also replaced

by multicuts):

$$
\begin{aligned}
\min_{\substack{y,\eta \\ \eta_1,\ldots,\eta_s}} \quad & \eta \\
\text{s.t.} \quad & \eta \geq c_1^{\mathrm{T}} y + \sum_{h=1}^{s} \eta_h, \\
& \eta_h \geq \tilde{\alpha}_h^{(r)} y + \tilde{\beta}_h^{(r)}, \quad \forall h \in \{1,\ldots,s\},\ \forall r \in V^k, \\
& \eta_h \geq \breve{\alpha}_h^{(r)} y + \breve{\beta}_h^{(r)}, \quad \forall h \in \{1,\ldots,s\},\ \forall r \in V^k, \\
& \eta_h \geq \alpha_h^{(j)} y + \beta_h^{(j)}, \quad \forall h \in \{1,\ldots,s\},\ \forall j \in T^k \backslash V^k, \\
& \gamma_h^{(i)} y + \theta_h^{(i)} \leq 0, \quad \forall h \in \{1,\ldots,s\},\ \forall i \in S^k, \\
& \sum_{l \in \{l: y_l^{(t)}=1\}} y_l \; - \sum_{l \in \{l: y_l^{(t)}=0\}} y_l \leq |\{l : y^{(t)} = 1\}| - 1, \quad \forall t \in T^k \cup S^k, \\
& y \in Y,\ \eta \in \mathbb{R},
\end{aligned}
\tag{MDERMP^k}
$$

where

$$
\begin{aligned}
\tilde{\alpha}_h^{(r)} &= \left(\lambda_h^{(r)}\right)^{\mathrm{T}} A_{1,h}, \\
\tilde{\beta}_h^{(r)} &= c_{2,h}^{\mathrm{T}} \tilde{x}_h^{(r)} + c_{3,h}^{\mathrm{T}} \tilde{q}_h^{(r)} + c_{4,h}^{\mathrm{T}} \tilde{u}_h^{(r)} + \\
&\qquad \left(\lambda_h^{(r)}\right)^{\mathrm{T}} \left(A_{2,h} \tilde{x}_h^{(r)} + A_{3,h} \tilde{q}_h^{(r)} + A_{4,h} \tilde{u}_h^{(r)} - b_h\right), \\
\breve{\alpha}_h^{(r)} &= \left(\breve{\lambda}_h^{(r)}\right)^{\mathrm{T}} A_{1,h}, \\
\breve{\beta}_h^{(r)} &= c_{2,h}^{\mathrm{T}} \breve{x}_h^{(r)} + c_{3,h}^{\mathrm{T}} \breve{q}_h^{(r)} + c_{4,h}^{\mathrm{T}} \breve{u}_h^{(r)} + \\
&\qquad \left(\breve{\lambda}_h^{(r)}\right)^{\mathrm{T}} \left(A_{2,h} \breve{x}_h^{(r)} + A_{3,h} \breve{q}_h^{(r)} + A_{4,h} \breve{u}_h^{(r)} - b_h\right), \\
\alpha_h^{(j)} &= \left(\lambda_h^{(j)}\right)^{\mathrm{T}} A_{1,h}, \\
\beta_h^{(j)} &= c_{2,h}^{\mathrm{T}} x_h^{(j)} + c_{3,h}^{\mathrm{T}} q_h^{(j)} + c_{4,h}^{\mathrm{T}} u_h^{(j)} + \\
&\qquad \left(\lambda_h^{(j)}\right)^{\mathrm{T}} \left(A_{2,h} x_h^{(j)} + A_{3,h} q_h^{(j)} + A_{4,h} u_h^{(j)} - b_h\right), \\
\gamma_h^{(i)} &= \left(\mu_h^{(i)}\right)^{\mathrm{T}} A_{1,h}, \\
\theta_h^{(i)} &= \left(\mu_h^{(i)}\right)^{\mathrm{T}} \left(A_{2,h} x_h^{(i)} + A_{3,h} q_h^{(i)} + A_{4,h} u_h^{(i)} - b_h\right).
\end{aligned}
$$

Remark 5. After incorporation of multicuts, the number of continuous variables in Problem (MDERMP^k) depends on the number of scenarios linearly while the number of binary variables, which dominates the solution time of MILPs, remains the same; on the other hand, the number of iterations (and hence the number of Problems (PP$_h$) and (DPP$_h$) to be solved) may be significantly reduced, as will be shown by the case study results.

6.2.2 Theoretical Properties

Remark 6. According to the separability in the integer and continuous variables, Problem (DERMP$^{\mathrm{k}}$) is equivalent to the following problem:

$$
\begin{aligned}
\min_{y,\eta} \quad & \eta \\
\text{s.t.} \quad & \eta \geq F_{\mathrm{P}}(y, \lambda_1^{(r)}, \ldots, \lambda_s^{(r)}), \quad \forall r \in V^k, \\
& \eta \geq F_{\mathrm{P}}(y, \breve{\lambda}_1^{(r)}, \ldots, \breve{\lambda}_s^{(r)}), \quad \forall r \in V^k, \\
& \eta \geq F(y, \lambda_1^{(j)}, \ldots, \lambda_s^{(j)}), \quad \forall j \in T^k \backslash V^k, \\
& G(y, \mu_1^{(i)}, \ldots, \mu_s^{(i)}) \leq 0, \quad \forall i \in S^k, \\
& \sum_{l \in \{l: y_l^{(t)} = 1\}} y_l - \sum_{l \in \{l: y_l^{(t)} = 0\}} y_l \leq |\{l : y^{(t)} = 1\}| - 1, \quad \forall t \in T^k \cup S^k, \\
& y \in Y, \ \eta \in \mathbb{R},
\end{aligned}
\tag{DERMP1^k}
$$

where

$$F_{\mathrm{P}}(y,\lambda_1^{(r)},\ldots,\lambda_s^{(r)}) = \inf_{\substack{(x_h,q_h,u_h)\in\tilde{\Pi}_h,\\ \forall h\in\{1,\ldots,s\}}} c_1^{\mathrm{T}}y + \sum_{h=1}^{s}\Big(c_{2,h}^{\mathrm{T}}x_h + c_{3,h}^{\mathrm{T}}q_h + c_{4,h}^{\mathrm{T}}u_h + (\lambda_h^{(r)})^{\mathrm{T}}\left(A_{1,h}y + A_{2,h}x_h + A_{3,h}q_h + A_{4,h}u_h - b_h\right)\Big),$$

$$F_{\mathrm{P}}(y,\breve{\lambda}_1^{(r)},\ldots,\breve{\lambda}_s^{(r)}) = \inf_{\substack{(x_h,q_h,u_h)\in\tilde{\Pi}_h,\\ \forall h\in\{1,\ldots,s\}}} c_1^{\mathrm{T}}y + \sum_{h=1}^{s}\Big(c_{2,h}^{\mathrm{T}}x_h + c_{3,h}^{\mathrm{T}}q_h + c_{4,h}^{\mathrm{T}}u_h + (\breve{\lambda}_h^{(r)})^{\mathrm{T}}\left(A_{1,h}y + A_{2,h}x_h + A_{3,h}q_h + A_{4,h}u_h - b_h\right)\Big),$$

$$F(y,\lambda_1^{(j)},\ldots,\lambda_s^{(j)}) = \inf_{\substack{(x_h,q_h,u_h)\in\hat{\Pi}_h,\\ \forall h\in\{1,\ldots,s\}}} c_1^{\mathrm{T}}y + \sum_{h=1}^{s}\Big(c_{2,h}^{\mathrm{T}}x_h + c_{3,h}^{\mathrm{T}}q_h + c_{4,h}^{\mathrm{T}}u_h + (\lambda_h^{(j)})^{\mathrm{T}}\left(A_{1,h}y + A_{2,h}x_h + A_{3,h}q_h + A_{4,h}u_h - b_h\right)\Big),$$

$$G(y,\mu_1^{(i)},\ldots,\mu_s^{(i)}) = \inf_{\substack{(x_h,q_h,u_h)\in\hat{\Pi}_h,\\ \forall h\in\{1,\ldots,s\}}} \sum_{h=1}^{s}(\mu_h^{(i)})^{\mathrm{T}}\left(A_{1,h}y + A_{2,h}x_h + A_{3,h}q_h + A_{4,h}u_h - b_h\right),$$

and the set

$$\tilde{\Pi}_h = \{(x_h,q_h,u_h)\in\Pi_h:\ u_{h,l,t} = x_{h,l}q_{h,t},\quad \forall(l,t)\in\Omega\ \}.$$

Proposition 1. *Any y that is feasible for Problem (P) augmented with the Balas cuts is also feasible for Problem (DERMP$^{\mathrm{k}}$), and the optimal objective of Problem (DERMP$^{\mathrm{k}}$) is a lower bound of that of Problem (P) augmented with the Balas cuts.*

Proof. According to the equivalency of Problems (DERMP$^{\mathrm{k}}$) and (DERMP1$^{\mathrm{k}}$), the following property is proved: any y that is feasible for Problem (P) augmented with the Balas cuts is also feasible for Problem (DERMP1$^{\mathrm{k}}$), and the optimal objective of Problem (DERMP1$^{\mathrm{k}}$) is a lower bound of that of Problem (P) augmented with the Balas cuts.

Define

$$\begin{aligned}\text{obj}_{\text{PP}}(y) \;=\; \min_{\substack{(x_h,q_h,u_h)\in\tilde{\Pi}_h,\\ \forall h\in\{1,\ldots,s\}}} \; & c_1^{\mathrm{T}}y + \sum_{h=1}^{s}\left(c_{2,h}^{\mathrm{T}}x_h + c_{3,h}^{\mathrm{T}}q_h + c_{4,h}^{\mathrm{T}}u_h\right) \\ \text{s.t.} \quad & A_{1,h}y + A_{2,h}x_h + A_{3,h}q_h + A_{4,h}u_h \le b_h, \quad \forall h \in \{1,\ldots,s\}.\end{aligned}$$

From weak duality,

$$F_{\text{P}}(y, \lambda_1^{(r)}, \ldots, \lambda_s^{(r)}) \le \text{obj}_{\text{PP}}(y), \quad \forall r \in V^k, \;\; \forall y \in Y, \tag{6.1}$$

$$F_{\text{P}}(y, \breve{\lambda}_1^{(r)}, \ldots, \breve{\lambda}_s^{(r)}) \le \text{obj}_{\text{PP}}(y), \quad \forall r \in V^k, \;\; \forall y \in Y. \tag{6.2}$$

For all $\hat{y}$ that is feasible for Problem (P) augmented with the Balas cuts, pick $\hat{\eta} = \text{obj}_{\text{PP}}(\hat{y})$, then

$$\hat{\eta} \ge F_{\text{P}}(\hat{y}, \lambda_1^{(r)}, \ldots, \lambda_s^{(r)}), \tag{6.3}$$

and

$$\hat{\eta} \ge F_{\text{P}}(\hat{y}, \breve{\lambda}_1^{(r)}, \ldots, \breve{\lambda}_s^{(r)}). \tag{6.4}$$

Define

$$\begin{aligned}\text{obj}_{\text{PBP}}(y) \;=\; \min_{\substack{(x_h,q_h,u_h)\in\hat{\Pi}_h,\\ \forall h\in\{1,\ldots,s\}}} \; & c_1^{\mathrm{T}}y + \sum_{h=1}^{s}\left(c_{2,h}^{\mathrm{T}}x_h + c_{3,h}^{\mathrm{T}}q_h + c_{4,h}^{\mathrm{T}}u_h\right) \\ \text{s.t.} \quad & A_{1,h}y + A_{2,h}x_h + A_{3,h}q_h + A_{4,h}u_h \le b_h, \quad \forall h \in \{1,\ldots,s\}.\end{aligned}$$

Due to their definitions, set $\hat{\Pi}_h$ is a convex relaxation of the set $\tilde{\Pi}_h$, hence

$$\tilde{\Pi}_h \subset \hat{\Pi}_h, \quad \forall h \in \{1,\ldots,s\}, \tag{6.5}$$

then

$$\text{obj}_{\text{PP}}(y) \ge \text{obj}_{\text{PBP}}(y), \quad \forall y \in Y. \tag{6.6}$$

From strong duality for linear programs [33],

$$F(y, \lambda_1^{(j)}, \ldots, \lambda_s^{(j)}) = \text{obj}_{\text{PBP}}(y), \quad \forall j \in T^k \backslash V^k, \;\; \forall y \in Y. \tag{6.7}$$

So

$$\hat{\eta} \geq F(\hat{y}, \lambda_1^{(j)}, \ldots, \lambda_s^{(j)}) \tag{6.8}$$

holds from Equations (6.6) and (6.7).

According to the definition of Problem (RMP^k), for all $\hat{y}$ that is feasible for Problem (P) augmented with the Balas cuts is also feasible for Problem (RMP^k) [113]. So

$$G(\hat{y}, \mu_1^{(i)}, \ldots, \mu_s^{(i)}) \leq 0 \tag{6.9}$$

holds.

Equations (6.3), (6.4), (6.8) and (6.9) imply that $(\hat{y}, \hat{\eta})$ is feasible for Problem (DERMP1^k), and

$$\text{obj}_{\text{DERMP1}^k} \leq \hat{\eta} = \text{obj}_{\text{PP}}(\hat{y}), \quad \forall \hat{y} \in \Phi, \tag{6.10}$$

where $\text{obj}_{\text{DERMP1}^k}$ is the optimal objective value of Problem (DERMP1^k), and the set

$$\Phi \equiv \{y \in Y : A_{1,h}y + A_{2,h}x_h + A_{3,h}q_h + A_{4,h}u_h \leq b_h \text{ for some } (x_h, q_h, u_h) \in \tilde{\Pi}_h\}$$

Hence,

$$\text{obj}_{\text{DERMP1}^k} \leq \min_{\hat{y} \in \Phi} \text{obj}_{\text{PP}}(\hat{y}) = \text{obj}_{\text{P}}, \tag{6.11}$$

where obj_{P} is the optimal objective of Problem (P). □

Proposition 2. *Problem (DERMP^k) is a tighter (or equal) underestimate of Problem (P) augmented with the Balas cuts compared to Problem (RMP^k).*

Proof. Problem (RMP^k) can be equivalently reformulated into the following problem

[113]:

$$
\begin{aligned}
\min_{y,\eta} \quad & \eta \\
\text{s.t.} \quad & \eta \geq F(y, \lambda_1^{(j)}, \ldots, \lambda_s^{(j)}), \quad \forall j \in T^k, \\
& G(y, \mu_1^{(i)}, \ldots, \mu_s^{(i)}) \leq 0, \quad \forall i \in S^k, \\
& \sum_{l \in \{l: y_l^{(t)}=1\}} y_l - \sum_{l \in \{l: y_l^{(t)}=0\}} y_l \leq |\{l : y^{(t)} = 1\}| - 1, \quad \forall t \in T^k \cup S^k, \\
& y \in Y, \ \eta \in \mathbb{R},
\end{aligned}
\tag{RMP1^k}
$$

According to the equivalency of Problems (RMP^k) and (RMP1^k) and the equivalency of Problems (DERMP^k) and (DERMP1^k), the following property is proved: problem (DERMP1^k) is a tighter (or equal) underestimate of Problem (P) augmented with the Balas cuts compared to Problem (RMP1^k).

For all $(\hat{y}, \hat{\eta})$ feasible for Problem (DERMP1^k),

$$\hat{\eta} \geq F(\hat{y}, \lambda_1^{(j)}, \ldots, \lambda_s^{(j)}), \quad \forall j \in T^k \backslash V^k, \tag{6.12}$$

$$G(\hat{y}, \mu_1^{(i)}, \ldots, \mu_s^{(i)}) \leq 0, \quad \forall i \in S^k, \tag{6.13}$$

and

$$\hat{\eta} \geq F_{\mathrm{P}}(\hat{y}, \lambda_1^{(r)}, \ldots, \lambda_s^{(r)}), \quad \forall r \in V^k, \tag{6.14}$$

Based on Equation (6.5), the following relationship holds:

$$F_{\mathrm{P}}(y, \lambda_1^{(r)}, \ldots, \lambda_s^{(r)}) \geq F(y, \lambda_1^{(r)}, \ldots, \lambda_s^{(r)}), \quad \forall r \in V^k, \ \forall y \in Y. \tag{6.15}$$

So $\hat{\eta} \geq F(\hat{y}, \lambda_1^{(r)}, \ldots, \lambda_s^{(r)})$ $(\forall r \in V^k)$. Hence $(\hat{y}, \hat{\eta})$ is also feasible for problem (RMP1^k).

Therefore, Problem (DERMP1^k) is a tighter (or equal) underestimate of Problem (P) augmented with the Balas cuts compared to Problem (RMP1^k). □

Remark 7. According to the separability in the integer and continuous variables,

Problem (MDERMP$^{\mathrm{k}}$) is equivalent to the following problem:

$$
\begin{aligned}
\min_{\substack{y,\eta \\ \eta_1,\ldots,\eta_s}} \quad & \eta \\
\text{s.t.} \eta \geq c_1^{\mathrm{T}} y + \sum_{h=1}^{s} \eta_h, & \\
& \eta_h \geq F_{\mathrm{P},h}(y, \lambda_h^{(r)}), \quad \forall h \in \{1,\ldots,s\},\ \forall r \in V^k, \\
& \eta_h \geq F_{\mathrm{P},h}(y, \breve{\lambda}_h^{(r)}), \quad \forall h \in \{1,\ldots,s\},\ \forall r \in V^k, \\
& \eta_h \geq F_h(y, \lambda_h^{(j)}), \quad \forall h \in \{1,\ldots,s\},\ \forall j \in T^k \backslash V^k, \\
& G_h(y, \mu_h^{(i)}) \leq 0, \quad \forall h \in \{1,\ldots,s\},\ \forall i \in S^k, \\
& \sum_{l \in \{l: y_l^{(t)}=1\}} y_l - \sum_{l \in \{l: y_l^{(t)}=0\}} y_l \leq |\{l : y^{(t)} = 1\}| - 1, \quad \forall t \in T^k \cup S^k, \\
& y \in Y,\ \eta \in \mathbb{R},
\end{aligned}
\tag{MDERMP1^k}
$$

where

$$
\begin{aligned}
F_{\mathrm{P},h}(y, \lambda_h^{(r)}) = \inf_{(x_h,q_h,u_h)\in\tilde{\Pi}_h} & c_{2,h}^{\mathrm{T}} x_h + c_{3,h}^{\mathrm{T}} q_h + c_{4,h}^{\mathrm{T}} u_h \\
& + \left(\lambda_h^{(r)}\right)^{\mathrm{T}} (A_{1,h} y + A_{2,h} x_h + A_{3,h} q_h + A_{4,h} u_h - b_h), \\
F_{\mathrm{P},h}(y, \breve{\lambda}_h^{(r)}) = \inf_{(x_h,q_h,u_h)\in\tilde{\Pi}_h} & c_{2,h}^{\mathrm{T}} x_h + c_{3,h}^{\mathrm{T}} q_h + c_{4,h}^{\mathrm{T}} u_h \\
& + \left(\breve{\lambda}_h^{(r)}\right)^{\mathrm{T}} (A_{1,h} y + A_{2,h} x_h + A_{3,h} q_h + A_{4,h} u_h - b_h), \\
F_h(y, \lambda_h^{(j)}) = \inf_{(x_h,q_h,u_h)\in\hat{\Pi}_h} & c_{2,h}^{\mathrm{T}} x_h + c_{3,h}^{\mathrm{T}} q_h + c_{4,h}^{\mathrm{T}} u_h \\
& + \left(\lambda_h^{(j)}\right)^{\mathrm{T}} (A_{1,h} y + A_{2,h} x_h + A_{3,h} q_h + A_{4,h} u_h - b_h), \\
G_h(y, \mu_h^{(i)}) = \inf_{(x_h,q_h,u_h)\in\hat{\Pi}_h} & \left(\mu_h^{(i)}\right)^{\mathrm{T}} (A_{1,h} y + A_{2,h} x_h + A_{3,h} q_h + A_{4,h} u_h - b_h).
\end{aligned}
$$

Proposition 3. *Any y that is feasible for Problem (P) augmented with the Balas cuts is also feasible for Problem (MDERMP$^{\mathrm{k}}$), and the optimal objective of Problem (MDERMP$^{\mathrm{k}}$) is a lower bound of that of the original problem (P) augmented with the Balas cuts.*

Proof. According to the idea in Ref [68], Problem (P) can be equivalently transformed into the following form by projection from the space of both continuous and integer variables to the space of only the integer variables:

$$\begin{aligned}
\min_{y} \quad & c_1^{\mathrm{T}} y + \sum_{h=1}^{s} v_h(y) \\
\text{s.t.} \quad & v_h(y) = \min_{x_h, q_h, u_h} \quad c_{2,h}^{\mathrm{T}} x_h + c_{3,h}^{\mathrm{T}} q_h + c_{4,h}^{\mathrm{T}} u_h \\
& \qquad\qquad \text{s.t.} \quad A_{1,h} y + A_{2,h} x_h + A_{3,h} q_h + A_{4,h} u_h \le b_h, \\
& \qquad\qquad\quad\ (x_h, q_h, u_h) \in \tilde{\Pi}_h, \\
& y \in \Phi.
\end{aligned} \qquad \left.\begin{array}{l} \\ \\ \\ \end{array}\right\} \ \forall h \in \{1, \ldots, s\} \tag{P1}$$

According to the equivalency of Problems (P) and (P1) and the equivalency of Problems (MDERMP^k) and (MDERMP1^k), the following property is proved: any y that is feasible for Problem (P1) augmented with the Balas cuts is also feasible for Problem (MDERMP1$^{\mathrm{k}}$), and the optimal objective of Problem (MDERMP1$^{\mathrm{k}}$) is a lower bound of that of Problem (P1) augmented with the Balas cuts.

Based on weak duality,

$$F_{\mathrm{P},h}(y, \lambda_h^{(r)}) \le v_h(y), \quad \forall h \in \{1, \ldots, s\},\ \forall r \in V^k,\ \forall y \in \Phi, \tag{6.16}$$

$$F_{\mathrm{P},h}(y, \breve{\lambda}_h^{(r)}) \le v_h(y), \quad \forall h \in \{1, \ldots, s\},\ \forall r \in V^k,\ \forall y \in \Phi. \tag{6.17}$$

For all $\hat{y}$ feasible for Problem (P1) augmented with the Balas cuts, pick $\hat{\eta}_h = v_h(\hat{y})$ and $\hat{\eta} = c_1^{\mathrm{T}} \hat{y} + \sum_{h=1}^{s} \hat{\eta}_h$, then

$$\hat{\eta}_h \ge F_{\mathrm{P},h}(\hat{y}, \lambda_h^{(r)}), \quad \forall h \in \{1, \ldots, s\}, \tag{6.18}$$

$$\hat{\eta}_h \ge F_{\mathrm{P},h}(\hat{y}, \breve{\lambda}_h^{(r)}), \quad \forall h \in \{1, \ldots, s\}, \tag{6.19}$$

and

$$\hat{\eta} \ge c_1^{\mathrm{T}} \hat{y} + \sum_{h=1}^{s} \hat{\eta}_h. \tag{6.20}$$

Define

$$\begin{aligned} v_h^{\mathrm{R}}(y) \;=\; & \min_{(x_h,q_h,u_h)\in\hat{\Pi}_h} \quad c_{2,h}^{\mathrm{T}}x_h + c_{3,h}^{\mathrm{T}}q_h + c_{4,h}^{\mathrm{T}}u_h \\ & \text{s.t.} \qquad A_{1,h}y + A_{2,h}x_h + A_{3,h}q_h + A_{4,h}u_h \le b_h, \end{aligned}$$

Based on Equation (6.5),

$$v_h(y) \ge v_h^{\mathrm{R}}(y), \quad \forall y \in \Phi. \tag{6.21}$$

According to strong duality for linear programs,

$$F_h(y, \lambda_h^{(j)}) = v_h^{\mathrm{R}}(y), \quad \forall h \in \{1, \ldots, s\},\ \forall j \in T^k \backslash V^k,\ \forall y \in Y. \tag{6.22}$$

Hence

$$\hat{\eta}_h \ge F_h(\hat{y}, \lambda_h^{(j)}), \quad \forall h \in \{1, \ldots, s\}, \tag{6.23}$$

from Equations (6.21) and (6.22).

In addition, $\hat{y} \in \Phi$ implies $\exists (x_h, q_h, u_h) \in \tilde{\Pi}_h \subset \hat{\Pi}_h$ (Equation (6.5)) such that

$$A_{1,h}\hat{y} + A_{2,h}x_h + A_{3,h}q_h + A_{4,h}u_h - b_h \le 0, \quad \forall h \in \{1, \ldots, s\}. \tag{6.24}$$

As Lagrange multipliers

$$\mu_h^{(i)} \ge 0, \quad \forall h \in \{1, \ldots, s\},\ \forall i \in S^k. \tag{6.25}$$

So

$$G_h(\hat{y}, \mu_h^{(i)}) \le 0, \quad \forall h \in \{1, \ldots, s\}. \tag{6.26}$$

Equations (6.18), (6.19), (6.23) and (6.26) imply $(\hat{y}, \hat{\eta}, \hat{\eta}_1, \ldots, \hat{\eta}_s)$ is feasible for Problem (MDERMP1^k), and

$$\mathrm{obj}_{\mathrm{MDERMP1}^k} \le \hat{\eta} = c_1^{\mathrm{T}}\hat{y} + \sum_{h=1}^{s} \hat{\eta}_h = c_1^{\mathrm{T}}\hat{y} + \sum_{h=1}^{s} v_h(\hat{y}), \quad \forall \hat{y} \in \Phi, \tag{6.27}$$

where $\text{obj}_{\text{MDERMP1}^k}$ is the optimal objective value of Problem (MDERMP1^k). Hence,

$$\text{obj}_{\text{MDERMP1}^k} \leq \min_{\hat{y}\in\Phi} \; c_1^{\mathrm{T}}\hat{y} + \sum_{h=1}^{s} v_h(\hat{y}) = \text{obj}_{\text{P1}}, \tag{6.28}$$

where obj_{P1} is the optimal objective value of Problem (P1). □

Proposition 4. *Problem (MDERMP^k) is a tighter (or equal) underestimate of Problem (P) augmented with the Balas cuts compared to Problem (DERMP^k).*

Proof. For all $(\hat{y}, \hat{\eta}, \hat{\eta}_1, \ldots, \hat{\eta}_s)$ feasible for Problem (MDERMP^k),

$$\hat{\eta} \geq c_1^{\mathrm{T}}\hat{y} + \sum_{h=1}^{s} \hat{\eta}_h, \tag{6.29}$$

$$\hat{\eta}_h \geq \tilde{\alpha}_h^{(r)}\hat{y} + \tilde{\beta}_h^{(r)}, \quad \forall h \in \{1,\ldots,s\},\ \forall r \in V^k, \tag{6.30}$$

$$\hat{\eta}_h \geq \breve{\alpha}_h^{(r)}\hat{y} + \breve{\beta}_h^{(r)}, \quad \forall h \in \{1,\ldots,s\},\ \forall r \in V^k, \tag{6.31}$$

$$\hat{\eta}_h \geq \alpha_h^{(j)}\hat{y} + \beta_h^{(j)}, \quad \forall h \in \{1,\ldots,s\},\ \forall j \in T^k \backslash V^k, \tag{6.32}$$

$$\gamma_h^{(i)}\hat{y} + \theta_h^{(i)} \leq 0, \quad \forall h \in \{1,\ldots,s\},\ \forall i \in S^k. \tag{6.33}$$

Sum Equation (6.30) over all the scenarios, then

$$\hat{\eta} \geq \tilde{\alpha}^{(r)}\hat{y} + \tilde{\beta}^{(r)}, \quad \forall r \in V^k. \tag{6.34}$$

Similarly, Equations (6.31), (6.32) and (6.33) imply

$$\hat{\eta} \geq \breve{\alpha}^{(r)}\hat{y} + \breve{\beta}^{(r)}, \quad \forall r \in V^k, \tag{6.35}$$

$$\hat{\eta} \geq \alpha^{(j)}\hat{y} + \beta^{(j)}, \quad \forall j \in T^k \backslash V^k, \tag{6.36}$$

$$\gamma^{(i)}\hat{y} + \theta^{(i)} \leq 0, \quad \forall i \in S^k. \tag{6.37}$$

Hence $(\hat{y}, \hat{\eta})$ is also feasible for Problem (DERMP^k).

Therefore, Problem (MDERMP^k) is a tighter (or equal) underestimate of Problem (P) augmented with the Balas cuts compared to Problem (DERMP^k). □

6.2.3 Enhanced Decomposition Algorithm with Primal Dual Cuts

Either the enhanced relaxed master problem with primal dual cuts (DERMP^k) or with primal dual multicuts (MDERMP^k) can be employed in the enhanced decomposition algorithm. The following algorithm is stated with Problem (DERMP^k) [49]:

Initialize:

1. Iteration counters $k = 0$, $l = 1$, and the index sets $T^0 = \emptyset$, $S^0 = \emptyset$, $U^0 = \emptyset$, $V^0 = \emptyset$.

2. Upper bound on the problem UBD $= +\infty$, upper bound on the lower bounding problem UBDPB $= +\infty$, lower bound on the lower bounding problem LBD $= -\infty$.

3. Set tolerances ϵ_h and ϵ such that $\sum_{h=1}^{s} \epsilon_h \leq \epsilon$.

4. Integer realization $y^{(1)}$ is given.

repeat

if $k = 0$ or (Problem (DERMP^k) is feasible and LBD $<$ UBDPB and LBD $<$ UBD $- \epsilon$) **then**

repeat

Set $k = k + 1$

1. Solve the decomposed primal bounding problem (PBP$_h(y^{(k)})$) for each scenario $h = 1, ..., s$ sequentially. If Problem (PBP$_h(y^{(k)})$) is feasible for all the scenarios with Lagrange multipliers $\lambda_h^{(k)}$, add optimality cuts to the enhanced relaxed master problem (DERMP^k) according to $\lambda_1^{(k)}, ..., \lambda_s^{(k)}$, set $T^k = T^{k-1} \cup \{k\}$. If obj$_{\text{PBP}}(y^{(k)}) <$ UBDPB, update UBDPB $=$ obj$_{\text{PBP}}(y^{(k)})$, $y^* = y^{(k)}$, $k^* = k$.

2. If Problem (PBP$_h(y^{(k)})$) is infeasible for one scenario, stop solving it for the remaining scenarios and set $S^k = S^{k-1} \cup \{k\}$. Then, solve the decomposed feasibility problem (FP$_h(y^{(k)})$) for $h = 1, ..., s$ and obtain

the corresponding Lagrange multipliers $\mu_h^{(k)}$. Add feasibility cuts to Problem (DERMP^k) according to these multipliers.

3. If $T^k = \emptyset$, solve the feasibility problem (RMFP^k); otherwise, solve Problem (DERMP^k). In the latter case, if Problem (DERMP^k) is feasible, set LBD to its optimal objective value. In both cases, set $y^{(k+1)}$ to the y value at the solution of either problem.

until LBD $\geq$ UBDPB or (Problem (DERMP^k) or (RMFP^k) is infeasible).

end if

if UBDPB $<$ UBD $- \epsilon$ **then**

1. Solve the decomposed primal problem (PP$_h(y^*)$) to ϵ_h-optimality for each scenario $h = 1, ..., s$ sequentially. Set $U^l = U^{l-1} \cup \{k^*\}$. If Problem (PP$_h(y^*)$) is feasible with optimum (x_h^*, q_h^*, u_h^*) for all the scenarios and obj$_{\text{PP}}(y^*) <$ UBD, obtain the corresponding KKT multipliers $\breve{\lambda}_h^{(k^*)}$, update UBD = obj$_{\text{PP}}(y^*)$ and set $y_p^* = y^*$, $(x_{p,h}^*, q_{p,h}^*, u_{p,h}^*) = (x_h^*, q_h^*, u_h^*)$ for $h = 1, \ldots, s$, set $V^k = V^{k-1} \cup \{k^*\}$.

2. If $k^* \in V^k$, solve the decomposed relaxed dual of primal problem (DPP$_h(y^*)$) to ϵ_h-optimality for each scenario $h = 1, ..., s$ sequentially with KKT multipliers $\lambda_h^{(k^*)}$ and $\breve{\lambda}_h^{(k^*)}$. Add primal dual cuts to Problem (DERMP^k) according to these multipliers and the optimal solutions of Problem (DPP$_h(y^*)$).

3. If $T^k \setminus U^l = \emptyset$, set UBDPB $= +\infty$.

4. If $T^k \setminus U^l \neq \emptyset$, pick $i \in T^k \setminus U^l$ such that obj$_{\text{PBP}}(y^{(i)}) = \min_{j \in T^k \setminus U^l}\{\text{obj}_{\text{PBP}}(y^{(j)})\}$. Update UBDPB = obj$_{\text{PBP}}(y^{(i)})$, $y^* = y^{(i)}$, $k^* = i$. Set $l = l + 1$.

end if

until UBDPB $\geq$ UBD $- \epsilon$ and ((Problem (DERMP^k) or (RMFP^k) is infeasible) or LBD $\geq$ UBD $- \epsilon$).

An ϵ-global optimum of the original problem (P) is given by

$$(y_p^*, x_{p,1}^*, ..., x_{p,s}^*, q_{p,1}^*, ..., q_{p,s}^*, u_{p,1}^*, ..., u_{p,s}^*)$$

or (P) is infeasible.

If the multicut enhanced relaxed master problem (MDERMP^k) is applied, replace Problem (DERMP^k) in the aforementioned algorithm by Problem (MDERMP^k).

The algorithm flowchart is shown in Figure 6-1 [49], in which differences between the enhanced decomposition algorithm and the original decomposition algorithm are highlighted in grey. Compared to the flowchart of the original decomposition algorithm, two new steps, "Solve DPP?" and "Relaxed Dual of Primal Problem", are added in this flowchart, and the step "Relaxed Master Problem" is replaced by "Enhanced Relaxed Master Problem".

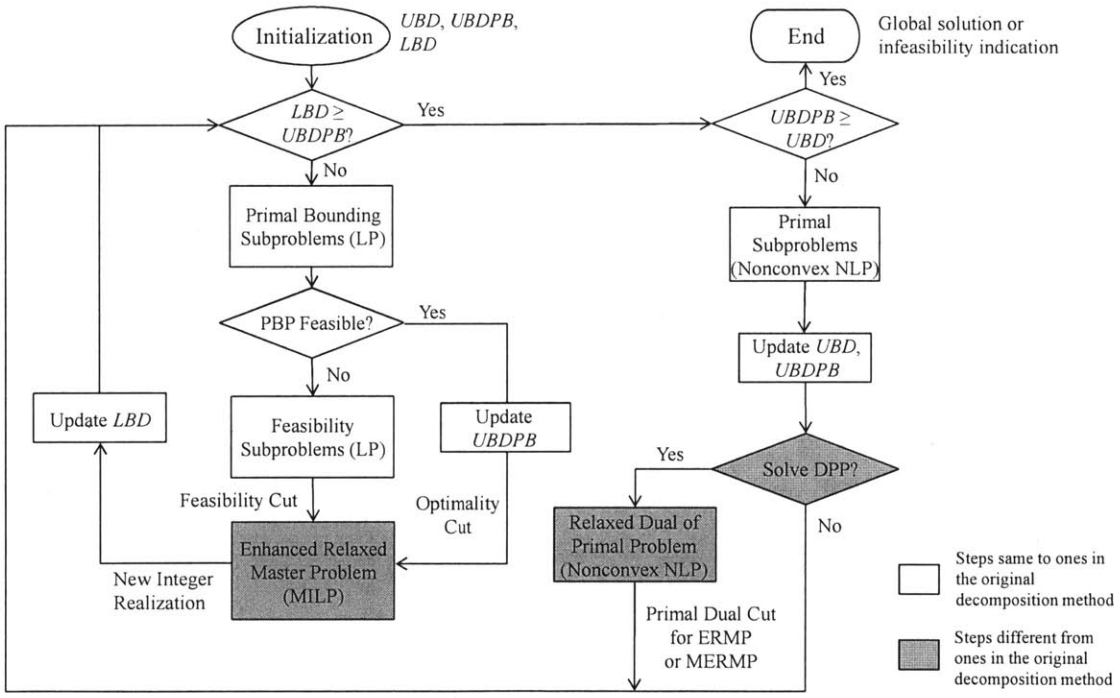

Figure 6-1: Flowchart for the enhanced decomposition algorithm with primal dual cuts.

Theorem 1. *If all the subproblems can be solved to ϵ-optimality in a finite number of steps, then the enhanced NGBD algorithm terminates in a finite number of steps with an ϵ-optimal solution of Problem (P) or an indication that Problem (P) is infeasible.*

Proof. The solution procedure in the enhanced NGBD is the same as that in NGBD except that the enhanced NGBD solves a finite number of additional subproblems

and it solves a different relaxed master problem. Since all these subproblems can be solved finitely, and the new relaxed master problem still prevents visiting the same integer realization twice, the convergence property holds for the enhanced NGBD as well according to the proof of NGBD convergence in Li et al [113, 114]. □

6.3 Enhanced Decomposition Algorithm with Piecewise Convex Relaxation

6.3.1 Piecewise Relaxation for Bilinear Functions

For the bilinear function $z = xy$, with known upper and lower bounds on x and y, say, x^{L}, x^{U}, y^{L}, y^{U}, the McCormick relaxation can be written as:

$$\begin{aligned} z^{\mathrm{r}} &\geq x^{\mathrm{U}}y + xy^{\mathrm{U}} - x^{\mathrm{U}}y^{\mathrm{U}}, \\ z^{\mathrm{r}} &\geq x^{\mathrm{L}}y + xy^{\mathrm{L}} - x^{\mathrm{L}}y^{\mathrm{L}}, \\ z^{\mathrm{r}} &\leq x^{\mathrm{U}}y + xy^{\mathrm{L}} - x^{\mathrm{U}}y^{\mathrm{L}}, \\ z^{\mathrm{r}} &\leq x^{\mathrm{L}}y + xy^{\mathrm{U}} - x^{\mathrm{L}}y^{\mathrm{U}}, \\ x^{\mathrm{L}} &\leq x \leq x^{\mathrm{U}}, \\ y^{\mathrm{L}} &\leq y \leq y^{\mathrm{U}} \end{aligned} \tag{6.38}$$

where z^{r} denotes the value of the relaxed bilinear function. Define the relaxation gap of a function over $\left[x^{\mathrm{L}},\ x^{\mathrm{U}}\right] \times \left[y^{\mathrm{L}},\ y^{\mathrm{U}}\right]$ to be the maximum difference of the function and its relaxation over this domain, then the relaxation gap of the bilinear function diminishes to zero as either $\left|x^{\mathrm{U}} - x^{\mathrm{L}}\right|$ or $\left|y^{\mathrm{U}} - y^{\mathrm{L}}\right|$ approaches zero, because according

to Eq (6.38) (and $z = xy$):

$$
\begin{aligned}
z^{\mathrm{r}} - z &\geq x^{\mathrm{U}}y + xy^{\mathrm{U}} - x^{\mathrm{U}}y^{\mathrm{U}} - xy = \left(x^{\mathrm{U}} - x\right)\left(y - y^{\mathrm{U}}\right) \geq \left(x^{\mathrm{U}} - x^{\mathrm{L}}\right)\left(y^{\mathrm{L}} - y^{\mathrm{U}}\right), \\
z^{\mathrm{r}} - z &\geq x^{\mathrm{L}}y + xy^{\mathrm{L}} - x^{\mathrm{U}}y^{\mathrm{L}} - xy = \left(x^{\mathrm{L}} - x\right)\left(y - y^{\mathrm{L}}\right) \geq \left(x^{\mathrm{L}} - x^{\mathrm{U}}\right)\left(y^{\mathrm{U}} - y^{\mathrm{L}}\right), \\
z^{\mathrm{r}} - z &\leq x^{\mathrm{U}}y + xy^{\mathrm{L}} - x^{\mathrm{U}}y^{\mathrm{L}} - xy = \left(x^{\mathrm{U}} - x\right)\left(y - y^{\mathrm{L}}\right) \leq \left(x^{\mathrm{U}} - x^{\mathrm{L}}\right)\left(y^{\mathrm{U}} - y^{\mathrm{L}}\right), \\
z^{\mathrm{r}} - z &\leq x^{\mathrm{L}}y + xy^{\mathrm{U}} - x^{\mathrm{L}}y^{\mathrm{U}} - xy = \left(x^{\mathrm{L}} - x\right)\left(y - y^{\mathrm{U}}\right) \leq \left(x^{\mathrm{L}} - x^{\mathrm{U}}\right)\left(y^{\mathrm{L}} - y^{\mathrm{U}}\right),
\end{aligned}
\tag{6.39}
$$

so

$$
\sup_{x^{\mathrm{L}} \leq x \leq x^{\mathrm{U}},\, y^{\mathrm{L}} \leq y \leq y^{\mathrm{U}}} \left|z^{\mathrm{r}} - z\right| \leq \left|x^{\mathrm{U}} - x^{\mathrm{L}}\right| \left|y^{\mathrm{U}} - y^{\mathrm{L}}\right| \tag{6.40}
$$

Therefore, the relaxation gap can be decreased by partitioning the x domain, $\left[x^{\mathrm{L}},\, x^{\mathrm{U}}\right]$ into M subdomains, i.e., picking $M+1$ points $x^1 < x^2 < \cdots < x^{M+1}$ such that $x^1 = x^{\mathrm{L}}$, $x^{M+1} = x^{\mathrm{U}}$ and performing McCormick relaxation on each individual subdomain. Furthermore, each subdomain is assigned a binary variable δ_m to determine if the McCormick relaxation on this subdomain is used or not, and $\sum_{m=1}^{M} \delta_m = 1$ is enforced. Thus the McCormick relaxation of the bilinear function can be upgraded into:

$$
\begin{aligned}
& z^{\mathrm{r}} = \sum_{m=1}^{M} z_m^{\mathrm{r}},\ x = \sum_{m=1}^{M} x_m,\ y = \sum_{m=1}^{M} y_m, \\
& z_m^{\mathrm{r}} \geq x^{m+1}y_m + x_m y^{\mathrm{U}} - x^{m+1}y^{\mathrm{U}}\delta_m, \\
& z_m^{\mathrm{r}} \geq x^{m}y_m + x_m y^{\mathrm{L}} - x^{m}y^{\mathrm{L}}\delta_m, \\
& z_m^{\mathrm{r}} \leq x^{m+1}y_m + x_m y^{\mathrm{L}} - x^{m+1}y^{\mathrm{L}}\delta_m, \\
& z_m^{\mathrm{r}} \leq x^{m}y_m + x_m y^{\mathrm{U}} - x^{m}y^{\mathrm{U}}\delta_m, \\
& \delta_m x^m \leq x_m \leq \delta_m x^{m+1}, \\
& \delta_m y^{\mathrm{L}} \leq y_m \leq \delta_m y^{\mathrm{U}}, \\
& \sum_{m=1}^{M} \delta_m = 1, \\
& m = 1, \ldots, M
\end{aligned}
\tag{6.41}
$$

Proposition 5. *If z^{r} is feasible for the constraints in Eq (6.41), then it is feasible for the constraints in Eq (6.38) as well.*

Proof. For any $\hat{z}_{\mathrm{r}}$ that is feasible for the constraints in Eq (6.41), say, corresponding to the McCormick relaxation on the i^{th} subdomain, there exist $\hat{\delta}_i$, $\hat{x}_i$ and $\hat{y}_i$ such that $\hat{\delta}_i = 1$, $\hat{z}_{\mathrm{r}} = \hat{z}_i^{\mathrm{r}}$, $x^{\mathrm{L}} \leq x^i \leq \hat{x}_i \leq x^{i+1} \leq x^{\mathrm{U}}$, $y^{\mathrm{L}} \leq \hat{y}_i \leq y^{\mathrm{U}}$ and

$$\begin{aligned} \hat{z}_{\mathrm{r}} &= \hat{z}_i^{\mathrm{r}} \\ &\geq x^{i+1}\hat{y}_i + \hat{x}_i y^{\mathrm{U}} - x^{i+1}y^{\mathrm{U}} \\ &= x^{i+1}\left(\hat{y}_i - y^{\mathrm{U}}\right) + \hat{x}_i y^{\mathrm{U}} \\ &\geq x^{\mathrm{U}}\left(\hat{y}_i - y^{\mathrm{U}}\right) + \hat{x}_i y^{\mathrm{U}} \quad \left(\text{noticing } x^{i+1} \leq x^{\mathrm{U}},\ \hat{y}_i \leq y^{\mathrm{U}}\right) \end{aligned} \tag{6.42}$$

Therefore, $\hat{z}_{\mathrm{r}}$, $\hat{x}_i$ and $\hat{y}_i$ satisfy the first constraint of relaxation Eq (6.38). Similarly, $\hat{z}_{\mathrm{r}}$, $\hat{x}_i$ and $\hat{y}_i$ also satisfy the second to the fourth constraint of relaxation Eq (6.38). Therefore, $\hat{z}_{\mathrm{r}}$ is also feasible for the constraints in Eq (6.38). □

The piecewise McCormick relaxation Eq (6.41) characterizes a disjunctive polyhedral set that contains the value of the bilinear function over its domain, and its continuous relaxation leads to the convex hull of the disjunctive set [23]. So this formulation is favorable for mixed-integer programming. Let n_{B} be the total number of bilinear functions and n_{PB} denotes the total number of variables whose domains need to be partitioned for the bilinear functions, then upgrading relaxation Eq (6.38) into Eq (6.41) incurs Mn_{PB} additional binary variables, $3(M-1)n_{\mathrm{B}}$ continuous variables, and $(8K-1)n_{\mathrm{B}}$ linear constraints provided all the partitioned domains are divided into M pieces. Note that only the domain of one variable in each bilinear function needs to be partitioned, according to Eq (6.40).

6.3.2 New Subproblems

Piecewise Primal Bounding Problem (PBP-PCR)

The piecewise primal bounding problem (PBP-PCR) is generated by fixing the integer variables in the piecewise lower bounding problem to $y^{(k)}$, which is the integer real-

ization at the k^{th} iteration. In Problem (PBP-PCR), the domain of q_h is selected to be partitioned into M (uniform) subdomains. Problem (PBP-PCR) can be naturally decomposed into subproblems (PBP-PCR$_h$) for the s scenarios:

$$\begin{aligned}\text{obj}_{\text{PBP-PCR}_h}\left(y^{(k)}\right) = \min_{\substack{x_h,q_h,u_h,\delta_h,\\ \bar{x}_h,\bar{q}_h,\bar{u}_h}} \; & c_{2,h}^{\mathrm{T}}x_h + c_{3,h}^{\mathrm{T}}q_h + c_{4,h}^{\mathrm{T}}u_h \\ \text{s.t.} \quad & A_{1,h}y^{(k)} + A_{2,h}x_h + A_{3,h}q_h + A_{4,h}u_h \le b_h, \\ & (x_h, q_h, u_h, \delta_h, \bar{x}_h, \bar{q}_h, \bar{u}_h) \in \bar{\Pi}_h \end{aligned} \tag{PBP-PCR$_h$}$$

where

$$\begin{aligned}\bar{\Pi}_h = \{ & (x_h, q_h, u_h) \in \Pi_h,\ \delta_h \in \{0,1\}^{Mn_q},\ (\bar{x}_h, \bar{q}_h, \bar{u}_h) \in \mathbb{R}^{Mn_x} \times \mathbb{R}^{Mn_q} \times \mathbb{R}^{Mn_u} : \\ & \sum_{m=1}^{M} \delta_{h,m} = 1, \\ & u_{h,l,t} = \sum_{m=1}^{M} \bar{u}_{h,l,t,m}, \quad \forall (l,t) \in \Omega, \\ & x_{h,l} = \sum_{m=1}^{M} \bar{x}_{h,l,m}, \quad \forall l \in \{1,\ldots,n_x\}, \\ & q_{h,t} = \sum_{m=1}^{M} \bar{q}_{h,t,m}, \quad \forall t \in \{1,\ldots,n_q\}, \\ & \bar{u}_{h,l,t,m} \ge x_{h,l}^{\mathrm{L}}\, \bar{q}_{h,t,m} + \bar{x}_{h,l,m}\, q_{h,t}^{m} - x_{h,l}^{\mathrm{L}} q_{h,t}^{m} \delta_{h,m}, \\ & \bar{u}_{h,l,t,m} \ge x_{h,l}^{\mathrm{U}}\, \bar{q}_{h,t,m} + \bar{x}_{h,l,m}\, q_{h,t}^{m+1} - x_{h,l}^{\mathrm{U}} q_{h,t}^{m+1} \delta_{h,m}, \\ & \bar{u}_{h,l,t,m} \le x_{h,l}^{\mathrm{U}}\, \bar{q}_{h,t,m} + \bar{x}_{h,l,m}\, q_{h,t}^{m} - x_{h,l}^{\mathrm{U}} q_{h,t}^{m} \delta_{h,m}, \\ & \bar{u}_{h,l,t,m} \le x_{h,l}^{\mathrm{L}}\, \bar{q}_{h,t,m} + \bar{x}_{h,l,m}\, q_{h,t}^{m+1} - x_{h,l}^{\mathrm{L}} q_{h,t}^{m+1} \delta_{h,m}, \\ & \quad \forall (l,t) \in \Omega,\ \ \forall m \in \{1,\ldots,M\}, \\ & \delta_{h,m} x_h^{\mathrm{L}} \le \bar{x}_{h,m} \le \delta_{h,m} x_h^{\mathrm{U}},\ \ \delta_{h,m} q_h^{m} \le \bar{q}_{h,m} \le \delta_{h,m} q_h^{m+1}, \quad \forall m \in \{1,\ldots,M\}, \\ & q_h^{\mathrm{L}} = q_h^1 \le q_h^2 \le \ldots \le q_h^M \le q_h^{M+1} = q_h^{\mathrm{U}} \ \} \end{aligned}$$

$\text{obj}_{\text{PBP-PCR}_h}\left(y^{(k)}\right)$ is the optimal objective value of Problem (PBP-PCR$_h$) for $y = y^{(k)}$, $h = 1,\ldots,s$. The objectives of Problem (PBP-PCR) and (PBP-PCR$_h$) satisfy

the following relationship:

$$\text{obj}_{\text{PBP-PCR}}\left(y^{(k)}\right) = c_1^{\text{T}} y^{(k)} + \sum_{h=1}^{s} \text{obj}_{\text{PBP-PCR}_h}\left(y^{(k)}\right) \tag{6.43}$$

where $\text{obj}_{\text{PBP-PCR}}\left(y^{(k)}\right)$ is the optimal objective value of Problem (PBP-PCR) for $y = y^{(k)}$.

With the piecewise convex relaxation, Problem (PBP-PCR$_h$) is a tighter relaxation of Problem (PP$_h$) compared to Problem (PBP$_h$), so

$$\text{obj}_{\text{PP}_h}\left(y^{(k)}\right) \geq \text{obj}_{\text{PBP-PCR}_h}\left(y^{(k)}\right) \geq \text{obj}_{\text{PBP}_h}\left(y^{(k)}\right) \tag{6.44}$$

Summing Eq (6.44) over $h = 1, \ldots, s$ yields

$$\text{obj}_{\text{PP}}\left(y^{(k)}\right) \geq \text{obj}_{\text{PBP-PCR}}\left(y^{(k)}\right) \geq \text{obj}_{\text{PBP}}\left(y^{(k)}\right) \tag{6.45}$$

Therefore, Problem (PBP-PCR$_h$) leads to a better estimate of the optimal objective value of Problem P for $y = y^{(k)}$ compared to Problem (PBP$_h$).

Relaxed Dual of PBP-PCR

Problem (PBP-PCR) is a nonconvex problem, and hence its solution cannot be directly used for optimality cuts in the enhanced relaxed master problem. Instead, a relaxed dual of Problem (PBP-PCR), called Problem (DPBP-PCR), is solved to construct optimality cuts. Problem (DPBP-PCR) can be naturally decomposed into subproblems (DPBP-PCR$_h$) for the s scenarios:

$$\begin{aligned}
\text{obj}_{\text{DPBP-PCR}_h}\left(y^{(k)}, \bar{\lambda}_h^{(k)}\right) = \min_{\substack{x_h, q_h, u_h, \delta_h, \\ \bar{x}_h, \bar{q}_h, \bar{u}_h}} \; & c_{2,h}^{\text{T}} x_h + c_{3,h}^{\text{T}} q_h + c_{4,h}^{\text{T}} u_h \\
& + \left(\bar{\lambda}_h^{(k)}\right)^{\text{T}} \left(A_{1,h} y^{(k)} + A_{2,h} x_h + A_{3,h} q_h + A_{4,h} u_h - b_h\right) \\
\text{s.t.} \quad & (x_h, q_h, u_h, \delta_h, \bar{x}_h, \bar{q}_h, \bar{u}_h) \in \bar{\Pi}_h
\end{aligned} \tag{DPBP-PCR$_h$}$$

where $\bar{\lambda}_h^{(k)}$ denotes the KKT multipliers obtained at the solution of Problem (PBP-PCR$_h$) when $y = y^{(k)}$. $\text{obj}_{\text{DPBP-PCR}_h}\left(y^{(k)}, \bar{\lambda}_h^{(k)}\right)$ is the optimal objective value of Problem (DPBP-PCR$_h$) for $y = y^{(k)}$, $h = 1, \ldots, s$. The objectives of Problem (DPBP-PCR) and (DPBP-PCR$_h$) satisfy the following relationship:

$$\text{obj}_{\text{DPBP-PCR}}\left(y^{(k)}, \bar{\lambda}^{(k)}\right) = c_1^{\mathrm{T}} y^{(k)} + \sum_{h=1}^{s} \text{obj}_{\text{DPBP-PCR}_h}\left(y^{(k)}, \bar{\lambda}_h^{(k)}\right) \tag{6.46}$$

where $\text{obj}_{\text{PBP-PCR}}\left(y^{(k)}, \bar{\lambda}^{(k)}\right)$ is the optimal objective value of Problem (DPBP-PCR) for $y = y^{(k)}$, $\bar{\lambda}^{(k)} = \left(\bar{\lambda}_1^{(k)}, \ldots, \bar{\lambda}_s^{(k)}\right)$.

Enhanced Relaxed Master problem with Piecewise Relaxation

The optimal solutions of Problem (DPBP-PCR$_h$) together with the KKT multipliers of Problem (PBP-PCR$_h$) construct enhanced optimality cuts for the relaxed master problem. The enhanced relaxed master problem with piecewise convex relaxation, called Problem (PERMP^k), is as follows:

$$\begin{aligned}
\min_{y,\eta} \quad & \eta \\
\text{s.t.} \quad & \eta \geq \bar{\alpha}^{(j)} y + \bar{\beta}^{(j)}, \quad \forall j \in \bar{T}^k, \\
& \eta \geq \alpha^{(j)} y + \beta^{(j)}, \quad \forall j \in T^k, \\
& \gamma^{(i)} y + \theta^{(i)} \leq 0, \quad \forall i \in S^k, \\
& \sum_{l \in \{l: y_l^{(t)} = 1\}} y_l - \sum_{l \in \{l: y_l^{(t)} = 0\}} y_l \leq |\{l : y^{(t)} = 1\}| - 1, \quad \forall t \in T^k \cup S^k, \\
& y \in Y, \ \eta \in \mathbb{R},
\end{aligned} \tag{PERMP^k}$$

where

$$\bar{\alpha}^{(j)} = c_1^{\mathrm{T}} + \sum_{h=1}^{s} \left(\bar{\lambda}_h^{(j)}\right)^{\mathrm{T}} A_{1,h},$$

$$\bar{\beta}^{(j)} = \sum_{h=1}^{s} \left[c_{2,h}^{\mathrm{T}} \bar{x}_h^{(j)} + c_{3,h}^{\mathrm{T}} \bar{q}_h^{(j)} + c_{4,h}^{\mathrm{T}} \bar{u}_h^{(j)}\right] + \sum_{h=1}^{s} \left[\left(\bar{\lambda}_h^{(j)}\right)^{\mathrm{T}} \left(A_{2,h} \bar{x}_h^{(j)} + A_{3,h} \bar{q}_h^{(j)} + A_{4,h} \bar{u}_h^{(j)} - b_h\right)\right],$$

$$\bar{T}^k = \{j \in \{1, \ldots, k\} : \text{Problem PBP-PCR } \left(y^{(k)}\right) \text{ is feasible}\}.$$

$\left(\bar{x}_h^{(j)}, \bar{q}_h^{(j)}, \bar{u}_h^{(j)}\right)$ is a minimum of Problem (DPBP-PCR$_h$) with the KKT multipliers of Problem (PBP-PCR$_h$) ($\forall h \in \{1, \ldots, s\}$) when $y = y^{(j)}$. Note that $\bar{T}^k \subset T^k$ due to the tighter relaxation. The first set of constraints are called enhanced optimality cuts with piecewise convex relaxation.

If $T^k = \emptyset$, Problem (PERMP^k) is unbounded, so the feasibility relaxed master Problem (RMFP^k) introduced in Chapter 5 is solved instead. In principle, the feasibility subproblem (FP$_h$) can also be upgraded with piecewise convex relaxations to generate additional valid feasibility cuts for the relaxed master problem, but our computational experience indicates that these cuts do not significantly accelerate the convergence, which may be because the Balas cuts in the problem (which prevent visiting an integer realization twice) are already strong enough. So these feasibility cuts are not addressed in this study.

6.3.3 Theoretical Properties

Proposition 6. *Compared to Problem (RMP^k), Problem (PERMP^k) is a tighter (or equal) relaxation of Problem (P) when Problem (P) is augmented with the Balas cuts.*

Proof. Considering that Problem (PERMP^k) differs from Problem (RMP^k) only with the first group of optimality cuts, it is obvious that Problem (PERMP^k) is a tighter relaxation if it is a valid relaxation of Problem (P). It is proved in Ref [113] that Problem (RMP^k) is a relaxation of Problem (P) when Problem (P) is augmented with

the Balas cuts excluding the previously examined integer realizations, so it remains to prove

$$\mathrm{obj}_{\mathrm{PP}}(y) \geq \bar{\alpha}^{(j)} y + \bar{\beta}^{(j)}, \quad \forall j \in \bar{T}^k, \ \forall y \in W \tag{6.47}$$

$$W = \{\hat{y} \in Y : \text{Problem P is feasible for } y = \hat{y}\}$$

For all $j \in \bar{T}^k$ and $h \in \{1, \ldots, s\}$,

$$\begin{aligned}
\bar{\alpha}^{(j)} y + \bar{\beta}^{(j)} &= c_1^{\mathrm{T}} y + \sum_{h=1}^{s} \Bigg[\inf_{\substack{(x_h, q_h, u_h, \delta_h, \\ \bar{x}_h, \bar{q}_h, \bar{u}_h) \in \bar{\Pi}_h}} c_{2,h}^{\mathrm{T}} x_h + c_{3,h}^{\mathrm{T}} q_h + c_{4,h}^{\mathrm{T}} u_h \\
&\qquad + \left(\bar{\lambda}_h^{(j)}\right)^{\mathrm{T}} \left(A_{1,h} y^{(j)} + A_{2,h} x_h + A_{3,h} q_h + A_{4,h} u_h - b_h\right) \Bigg] \\
&\qquad + \sum_{h=1}^{s} \left(\bar{\lambda}_h^{(j)}\right)^{\mathrm{T}} A_{1,h} \left(y - y^{(j)}\right) \\
&= c_1^{\mathrm{T}} y + \sum_{h=1}^{s} \Bigg[\inf_{\substack{(x_h, q_h, u_h, \delta_h, \\ \bar{x}_h, \bar{q}_h, \bar{u}_h) \in \bar{\Pi}_h}} c_{2,h}^{\mathrm{T}} x_h + c_{3,h}^{\mathrm{T}} q_h + c_{4,h}^{\mathrm{T}} u_h \\
&\qquad + \left(\bar{\lambda}_h^{(j)}\right)^{\mathrm{T}} \left(A_{1,h} y + A_{2,h} x_h + A_{3,h} q_h + A_{4,h} u_h - b_h\right) \Bigg] \\
&= c_1^{\mathrm{T}} y + \mathrm{obj}_{\mathrm{DPBP-PCR}_h}\left(y, \bar{\lambda}_h^{(j)}\right) \\
&= \mathrm{obj}_{\mathrm{DPBP-PCR}}\left(y, \bar{\lambda}^{(j)}\right)
\end{aligned} \tag{6.48}$$

where $\bar{\lambda}^{(j)} = \left(\bar{\lambda}_1^{(j)}, \ldots, \bar{\lambda}_s^{(j)}\right)$.

Eq (6.45) implies

$$\mathrm{obj}_{\mathrm{PP}}(y) \geq \mathrm{obj}_{\mathrm{PBP-PCR}}(y), \quad \forall y \in W \tag{6.49}$$

Due to weak duality, for all $y \in W$,

$$\begin{aligned}
\mathrm{obj}_{\mathrm{PBP-PCR}}(y) &\geq \sup_{\bar{\lambda} \geq 0} \mathrm{obj}_{\mathrm{DPBP-PCR}}\left(y, \bar{\lambda}\right) \\
&\geq \mathrm{obj}_{\mathrm{DPBP-PCR}}\left(y, \bar{\lambda}^{(j)}\right)
\end{aligned} \tag{6.50}$$

Eqs (6.48), (6.49) and (6.50) imply Eq (6.47). □

6.3.4 Enhanced Decomposition Algorithm with Piecewise Relaxation

The enhanced decomposition algorithm with piecewise convex relaxation is stated as below [111]:

Initialize:

1. Iteration counters $k = 0$, $l = 1$, and the index sets $T^0 = \emptyset$, $\bar{T}^0 = \emptyset$, $S^0 = \emptyset$, $U^0 = \emptyset$.

2. Upper bound on the problem UBD $= +\infty$, upper bound on the lower bounding problem UBDPB $= +\infty$, lower bound on the lower bounding problem LBD $= -\infty$.

3. Set tolerances ϵ_h and ϵ such that $\sum_{h=1}^{s} \epsilon_h \leq \epsilon$.

4. Integer realization $y^{(1)}$ is given.

repeat

if $k = 0$ or (Problem (PERMP^k) is feasible and LBD $<$ UBDPB and LBD $<$ UBD $- \epsilon$) **then**

repeat

Set $k = k + 1$

1. Solve the decomposed primal bounding problem (PBP$_h(y^{(k)})$) for each scenario $h = 1, ..., s$ sequentially. If Problem (PBP$_h(y^{(k)})$) is feasible for all the scenarios with Lagrange multipliers $\lambda_h^{(k)}$, add optimality cuts to the enhanced relaxed master problem (PERMP^k) according to $\lambda_1^{(k)}, ..., \lambda_s^{(k)}$, set $T^k = T^{k-1} \cup \{k\}$.

2. If Problem (PBP$_h(y^{(k)})$) is feasible for all the scenarios, solve subproblem (PBP-PCR$_h(y^{(k)})$) for each scenario $h = 1, ..., s$ sequentially. If Problem (PBP-PCR$_h(y^{(k)})$) is feasible with KKT multipliers $\bar{\lambda}_h^{(k)}$ for all the scenarios, set $\bar{T}^k = \bar{T}^{k-1} \cup \{k\}$. In this case, if obj$_{\text{PBP-PCR}}(y^{(k)}) <$ UBDPB, update UBDPB $=$ obj$_{\text{PBP-PCR}}(y^{(k)})$, $y^* = y^{(k)}$, $k^* = k$, solve

subproblem (DPBP-PCR$_h(y^{(k)})$) with $\bar{\lambda}_h^{(k)}$ for each scenario $h = 1, ..., s$ sequentially, add optimality cuts to Problem (PERMP^k).

3. If Problem (PBP$_h(y^{(k)})$) is infeasible for one scenario, stop solving it for the remaining scenarios and set $S^k = S^{k-1} \cup \{k\}$. Then, solve the decomposed feasibility subproblem (FP$_h(y^{(k)})$) for $h = 1, ..., s$ and obtain the corresponding Lagrange multipliers $\mu_h^{(k)}$. Add feasibility cuts to Problem (PERMP^k) according to these multipliers.

4. If $T^k = \emptyset$, solve the feasibility problem (RMFP^k); otherwise, solve Problem (PERMP^k). In the latter case, if Problem (PERMP^k) is feasible, set LBD to its optimal objective value. In both cases, set $y^{(k+1)}$ to the y value at the solution of either problem.

until LBD $\geq$ UBDPB or (Problem (PERMP^k) or (RMFP^k) is infeasible).

end if

if UBDPB $<$ UBD $- \epsilon$ **then**

1. Solve the decomposed primal subproblem (PP$_h(y^*)$) to ϵ_h-optimality for each scenario $h = 1, ..., s$ sequentially. Set $U^l = U^{l-1} \cup \{k^*\}$. If Problem (PP$_h(y^*)$) is feasible with optimum (x_h^*, q_h^*, u_h^*) for all the scenarios and obj$_{\text{PP}}(y^*) <$ UBD, update UBD = obj$_{\text{PP}}(y^*)$ and set $y_p^* = y^*$, $(x_{p,h}^*, q_{p,h}^*, u_{p,h}^*) = (x_h^*, q_h^*, u_h^*)$ for $h = 1, \ldots, s$.

2. If $\bar{T}^k \setminus U^l = \emptyset$, set UBDPB $= +\infty$.

3. If $\bar{T}^k \setminus U^l \neq \emptyset$, pick $i \in \bar{T}^k \setminus U^l$ such that obj$_{\text{PBP-PCR}}(y^{(i)}) = \min_{j \in \bar{T}^k \setminus U^l} \{\text{obj}_{\text{PBP-PCR}}(y^{(j)})$. Update UBDPB = obj$_{\text{PBP-PCR}}(y^{(i)})$, $y^* = y^{(i)}$, $k^* = i$. Set $l = l + 1$.

end if

until UBDPB $\geq$ UBD $- \epsilon$ and ((Problem (PERMP^k) or (RMFP^k) is infeasible) or LBD $\geq$ UBD $- \epsilon$).

An ϵ-global optimum of the original problem (P) is given by

$$(y_p^*, x_{p,1}^*, ..., x_{p,s}^*, q_{p,1}^*, ..., q_{p,s}^*, u_{p,1}^*, ..., u_{p,s}^*)$$

or (P) is infeasible.

The algorithm flowchart is shown in Figure 6-2 [111], in which differences between the enhanced decomposition algorithm and the original decomposition algorithm are highlighted in grey. Compared to the flowchart of the original decomposition algorithm, two new steps, "PBP-PCR (MILP)" and "DPBP-PCR (MILP)", are added in this flowchart, and the step "Relaxed Master Problem" is replaced by "Enhanced Relaxed Master Problem". Another important change (which is not shown in the figure) is that the selection of the integer realization $y^{(k)}$ for constructing primal subproblems (PP_h) is based on $\mathrm{obj}_{\mathrm{PBP-PCR}}(y^{(k)})$ instead of $\mathrm{obj}_{\mathrm{PBP}}(y^{(k)})$. According to Eq (6.45), the new selection criterion is more likely to locate a global optimum earlier.

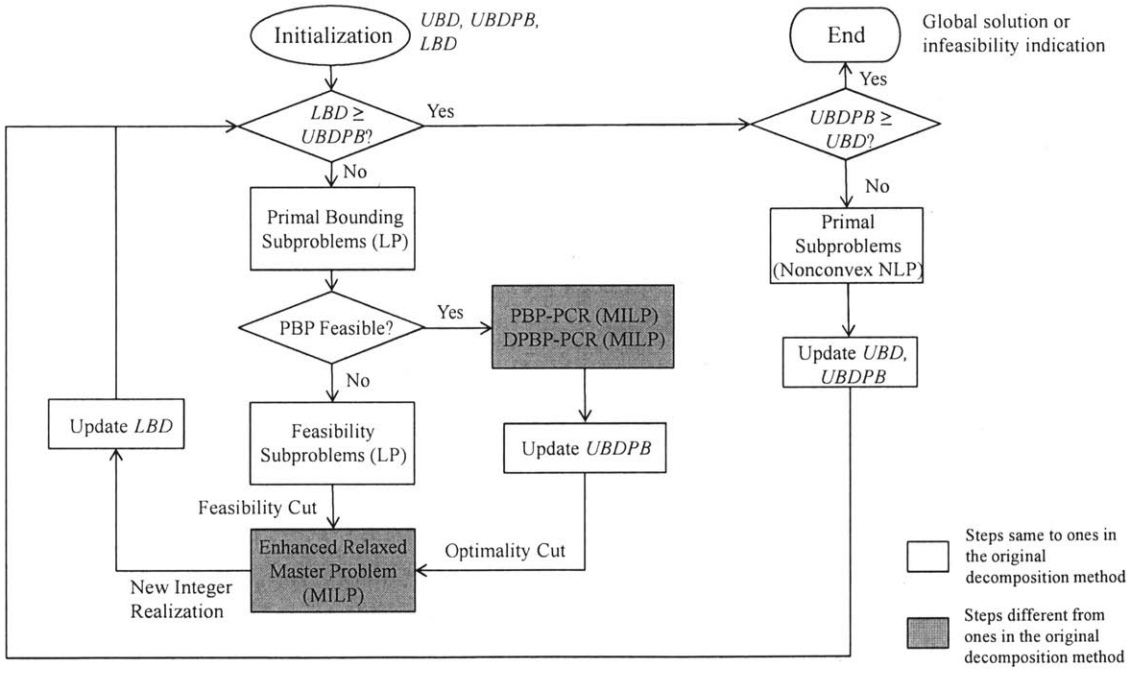

Figure 6-2: Flowchart for the enhanced decomposition algorithm with piecewise convex relaxation.

The convergence property for the enhanced NGBD holds according to Theorem 1.

6.3.5 Adaptive Piecewise Convex Relaxation & New Subproblems

Adaptive Subdomain Partition Strategy

There are several drawbacks of the aforementioned fixed subdomain partition strategy:

First, the number of subdomains needs to be pre-determined. From our computational experience, the performance of the enhanced NGBD strongly depends on the number of subdomains for partition variables, e.g., a larger number of subdomains will reduce total iteration numbers but increase the solution times for the piecewise primal bounding problems (as shown in Chapter 7). Hence, the optimal number of subdomains cannot be easily determined before solution.

Second, the points dividing subdomains need to be pre-determined and are usually uniformly distributed for convenience. A uniform partition may not be an optimal way for the fast solution of piecewise enhanced NGBD. In order to obtain tighter relaxation, more subdomains need to be partitioned in the region close to the global optimal solution, and fewer subdomains can be assigned in other regions. It is quite difficult to know this nonuniform partition pattern before solution.

Third, the numbers of subdomains for all partition variables are equal. Obviously, some variables need more subdomains than others, depending on the mathematical structure of the problem.

A heuristic that automatically partitions the domain of each variable by using information from subproblems solved by the algorithm, called the adaptive partition strategy, is proposed to address above issues. In this strategy, all variables are initially unpartitioned, and the algorithm starts as per the original NGBD. After Problem (PP) is solved and is feasible, the solution of Problem (PP) is then compared with the end points of subdomains for all partitioned variables. If the solution of Problem (PP) is different from (or outside the neighbourhood of) all end points of subdomains for some partition variable, a new subdomain is introduced, and the solution becomes the point dividing the new subdomain. The new subdomains are

then used for Problem (PBP-PCR) in the next iteration. The number of subdomains will increase iteratively, hence some maximum number of subdomains or some minimum radius for neighbourhoods must be enforced to prevent an unlimited increase of subdomains.

Under the adaptive partition strategy, no choice for the partition needs to be preselected before solution, and the appropriate number of subdomains for each variable will be determined by the feedback from the algorithm. More reasonable distributions of subdomains are also expected because more primal problems will be solved near the global optimal solution and more subdomains will be then partitioned there. The adaptive piecewise convex relaxation avoids possible bad subdomain partitions caused by human factors, and ensures fast convergence (as will be shown in Chapter 7).

Problems (PBP-PCR) and (DPBP-PCR) are modified to incorporate the adaptive partition strategy, as shown in the following sections.

Adaptive Piecewise Primal Bounding Problem (PBP-PCR-A)

The adaptive piecewise primal bounding problem, called Problem (PBP-PCR-A), is modified from Problem (PBP-PCR). Problem (PBP-PCR-A) can be naturally decomposed into subproblems (PBP-PCR-A$_h$) for the s scenarios:

$$\begin{aligned}
\mathrm{obj}_{\mathrm{PBP-PCR-A}_h}\left(y^{(k)}\right) = \min_{\substack{x_h, q_h, u_h, \delta_h, \\ \bar{x}_h, \bar{q}_h, \bar{u}_h}} \quad & c_{2,h}^{\mathrm{T}} x_h + c_{3,h}^{\mathrm{T}} q_h + c_{4,h}^{\mathrm{T}} u_h \\
\text{s.t.} \quad & A_{1,h} y^{(k)} + A_{2,h} x_h + A_{3,h} q_h + A_{4,h} u_h \leq b_h, \\
& (x_h, q_h, u_h, \delta_h, \bar{x}_h, \bar{q}_h, \bar{u}_h) \in \bar{\Pi}_h^{\mathrm{adp}}
\end{aligned} \tag{PBP-PCR-A$_h$}$$

where

$$\bar{\Pi}_h^{\text{adp}} = \{(x_h, q_h, u_h) \in \Pi_h,\ \delta_h \in \{0,1\}^{n_q n_{\delta,h,\max}},\ (\bar{x}_h, \bar{q}_h, \bar{u}_h) \in \mathbb{R}^{n_x n_{\delta,h,\max}} \times \mathbb{R}^{n_q n_{\delta,h,\max}} \times \mathbb{R}^{n_u n_{\delta,h,\max}} :$$

$$\sum_{m=1}^{n_{\delta,h,t}} \delta_{h,t,m} = 1, \quad \forall t \in \{1,\ldots,n_q\},\ \forall m \in \{1,\ldots,n_{\delta,h,t}\},$$

$$\delta_{h,t,m} = 0, \quad \forall t \in \{1,\ldots,n_q\},\ \forall m \in \{n_{\delta,h,t}+1,\ldots,n_{\delta,h,\max}\},$$

$$u_{h,l,t} = \sum_{m=1}^{n_{\delta,h,t}} \bar{u}_{h,l,t,m}, \quad \forall (l,t) \in \Omega,$$

$$x_{h,l} = \sum_{m=1}^{n_{\delta,h,t}} \bar{x}_{h,l,m}, \quad \forall (l,t) \in \Omega,$$

$$q_{h,t} = \sum_{m=1}^{n_{\delta,h,t}} \bar{q}_{h,t,m}, \quad \forall t \in \{1,\ldots,n_q\},$$

$$\bar{u}_{h,l,t,m} \geq x_{h,l}^{\text{L}}\, \bar{q}_{h,t,m} + \bar{x}_{h,l,m}\, q_{h,t}^{m} - x_{h,l}^{\text{L}} q_{h,t}^{m} \delta_{h,t,m},$$

$$\bar{u}_{h,l,t,m} \geq x_{h,l}^{\text{U}}\, \bar{q}_{h,t,m} + \bar{x}_{h,l,m}\, q_{h,t}^{m+1} - x_{h,l}^{\text{U}} q_{h,t}^{m+1} \delta_{h,t,m},$$

$$\bar{u}_{h,l,t,m} \leq x_{h,l}^{\text{U}}\, \bar{q}_{h,t,m} + \bar{x}_{h,l,m}\, q_{h,t}^{m} - x_{h,l}^{\text{U}} q_{h,t}^{m} \delta_{h,t,m},$$

$$\bar{u}_{h,l,t,m} \leq x_{h,l}^{\text{L}}\, \bar{q}_{h,t,m} + \bar{x}_{h,l,m}\, q_{h,t}^{m+1} - x_{h,l}^{\text{L}} q_{h,t}^{m+1} \delta_{h,t,m},$$

$$\forall (l,t) \in \Omega,\ \forall m \in \{1,\ldots,n_{\delta,h,t}\},$$

$$\delta_{h,t,m} x_h^{\text{L}} \leq \bar{x}_{h,t,m} \leq \delta_{h,t,m} x_h^{\text{U}},\ \ \delta_{h,t,m} q_{h,t}^{m} \leq \bar{q}_{h,t,m} \leq \delta_{h,t,m} q_{h,t}^{m+1},$$

$$\forall t \in \{1,\ldots,n_q\},\ \forall m \in \{1,\ldots,n_{\delta,h,t}\},$$

$$q_h^{\text{L}} = q_h^1 \leq q_h^2 \leq \ldots \leq q_h^{n_{\delta,h,t}} \leq q_h^{n_{\delta,h,t}+1} = q_h^{\text{U}}, \quad \forall t \in \{1,\ldots,n_q\}$$

$$\bar{u}_{h,l,t,m} = 0,\ \ \bar{x}_{h,l,m} = 0,\ \ \bar{q}_{h,t,m} = 0,$$

$$\forall (l,t) \in \Omega,\ \forall m \in \{n_{\delta,h,t}+1,\ldots,n_{\delta,h,\max}\}\ \}$$

$n_{\delta,h,\max}$ is the maximum number of pieces in scenario h, which is initially determined. $n_{\delta,h,t}$ is the number of pieces for the t^{th} partitioned variable $q_{h,t}$ in scenario h, which increases as more primal problems are solved. $q_{h,t}^m$ $(m = 2,\ldots,n_{\delta,h,t})$ are the points dividing pieces for $q_{h,t}$, which are provided by the solution of the primal problem. $\text{obj}_{\text{PBP-PCR-A}_h}\left(y^{(k)}\right)$ is the optimal objective value of Problem (PBP-PCR-A$_h$) for $y = y^{(k)}$, $h = 1,\ldots,s$. The objectives of Problem (PBP-PCR-A) and (PBP-PCR-A$_h$)

satisfy the following relationship:

$$\text{obj}_{\text{PBP-PCR-A}}\left(y^{(k)}\right) = c_1^{\text{T}} y^{(k)} + \sum_{h=1}^{s} \text{obj}_{\text{PBP-PCR-A}_h}\left(y^{(k)}\right) \tag{6.51}$$

where $\text{obj}_{\text{PBP-PCR-A}}\left(y^{(k)}\right)$ is the optimal objective value of Problem (PBP-PCR-A) for $y = y^{(k)}$.

Relaxed Dual of PBP-PCR-A

The relaxed dual of Problem (PBP-PCR-A), called Problem (DPBP-PCR-A), is modified from Problem (DPBP-PCR). Problem (DPBP-PCR-A) can be naturally decomposed into subproblems (DPBP-PCR-A$_h$) for the s scenarios:

$$\begin{aligned}
\text{obj}_{\text{DPBP-PCR-A}_h}\left(y^{(k)}, \bar{\lambda}_h^{(k)}\right) = \min_{\substack{x_h, q_h, u_h, \delta_h, \\ \bar{x}_h, \bar{q}_h, \bar{u}_h}} \; & c_{2,h}^{\text{T}} x_h + c_{3,h}^{\text{T}} q_h + c_{4,h}^{\text{T}} u_h \\
& + \left(\bar{\lambda}_h^{(k)}\right)^{\text{T}} \left(A_{1,h} y^{(k)} + A_{2,h} x_h + A_{3,h} q_h + A_{4,h} u_h - b_h\right) \\
\text{s.t.} \quad & \left(x_h, q_h, u_h, \delta_h, \bar{x}_h, \bar{q}_h, \bar{u}_h\right) \in \bar{\Pi}_h^{\text{adp}} \\
& \qquad\qquad\qquad\qquad\qquad\qquad\qquad\qquad \text{(DPBP-PCR-A}_h\text{)}
\end{aligned}$$

where $\bar{\lambda}_h^{(k)}$ denotes the KKT multipliers obtained at the solution of Problem (PBP-PCR-A$_h$) when $y = y^{(k)}$. $\text{obj}_{\text{DPBP-PCR-A}_h}\left(y^{(k)}, \bar{\lambda}_h^{(k)}\right)$ is the optimal objective value of Problem (DPBP-PCR-A$_h$) for $y = y^{(k)}$, $h = 1, \ldots, s$. The objectives of Problem (DPBP-PCR-A) and (DPBP-PCR-A$_h$) satisfy the following relationship:

$$\text{obj}_{\text{DPBP-PCR-A}}\left(y^{(k)}, \bar{\lambda}^{(k)}\right) = c_1^{\text{T}} y^{(k)} + \sum_{h=1}^{s} \text{obj}_{\text{DPBP-PCR-A}_h}\left(y^{(k)}, \bar{\lambda}_h^{(k)}\right) \tag{6.52}$$

where $\text{obj}_{\text{PBP-PCR-A}}\left(y^{(k)}, \bar{\lambda}^{(k)}\right)$ is the optimal objective value of Problem (DPBP-PCR-A) for $y = y^{(k)}$, $\bar{\lambda}^{(k)} = \left(\bar{\lambda}_1^{(k)}, \ldots, \bar{\lambda}_s^{(k)}\right)$.

6.3.6 Enhanced Decomposition Algorithm with Adaptive Piecewise Relaxation

The enhanced decomposition algorithm with adaptive piecewise convex relaxation is stated as below:

Initialize:

1. Iteration counters $k = 0$, $l = 1$, and the index sets $T^0 = \emptyset$, $\bar{T}^0 = \emptyset$, $S^0 = \emptyset$, $U^0 = \emptyset$.

2. Upper bound on the problem UBD $= +\infty$, upper bound on the lower bounding problem UBDPB $= +\infty$, lower bound on the lower bounding problem LBD $= -\infty$.

3. The number of pieces $n_{\delta,h} = 1$ for each scenario $h = 1, \ldots, s$. The maximum number of pieces $n_{\delta,h,\max}$ is given for each scenario $h = 1, \ldots, s$.

4. Set tolerances ϵ_h and ϵ such that $\sum_{h=1}^{s} \epsilon_h \leq \epsilon$.

5. Integer realization $y^{(1)}$ is given.

repeat

if $k = 0$ or (Problem (PERMP^k) is feasible and LBD $<$ UBDPB and LBD $<$ UBD $- \epsilon$) **then**

repeat

Set $k = k + 1$

1. Solve the decomposed primal bounding problem (PBP$_h(y^{(k)})$) for each scenario $h = 1, ..., s$ sequentially. If Problem (PBP$_h(y^{(k)})$) is feasible for all the scenarios with Lagrange multipliers $\lambda_h^{(k)}$, add optimality cuts to the enhanced relaxed master problem (PERMP^k) according to $\lambda_1^{(k)}, ..., \lambda_s^{(k)}$, set $T^k = T^{k-1} \cup \{k\}$.

2. If Problem (PBP$_h(y^{(k)})$) is feasible for all the scenarios, solve subproblem (PBP-PCR-A$_h(y^{(k)})$) for each scenario $h = 1, ..., s$ sequen-

tially. If Problem (PBP-PCR-A$_h(y^{(k)})$) is feasible with KKT multipliers $\bar{\lambda}_h^{(k)}$ for all the scenarios, set $\bar{T}^k = \bar{T}^{k-1} \cup \{k\}$. In this case, if $\text{obj}_{\text{PBP-PCR-A}}(y^{(k)}) < \text{UBDPB}$, update $\text{UBDPB} = \text{obj}_{\text{PBP-PCR-A}}(y^{(k)})$, $y^* = y^{(k)}$, $k^* = k$, solve subproblem (DPBP-PCR-A$_h(y^{(k)})$) with $\bar{\lambda}_h^{(k)}$ for each scenario $h = 1, ..., s$ sequentially, add optimality cuts to Problem (PERMP^k).

3. If Problem (PBP$_h(y^{(k)})$) is infeasible for one scenario, stop solving it for the remaining scenarios and set $S^k = S^{k-1} \cup \{k\}$. Then, solve the decomposed feasibility subproblem (FP$_h(y^{(k)})$) for $h = 1, ..., s$ and obtain the corresponding Lagrange multipliers $\mu_h^{(k)}$. Add feasibility cuts to Problem (PERMP^k) according to these multipliers.

4. If $T^k = \emptyset$, solve the feasibility problem (RMFP^k); otherwise, solve Problem (PERMP^k). In the latter case, if Problem (PERMP^k) is feasible, set LBD to its optimal objective value. In both cases, set $y^{(k+1)}$ to the y value at the solution of either problem.

until LBD $\geq$ UBDPB or (Problem (PERMP^k) or (RMFP^k) is infeasible).

end if

if UBDPB $<$ UBD $- \epsilon$ **then**

1. Solve the decomposed primal subproblem (PP$_h(y^*)$) to ϵ_h-optimality for each scenario $h = 1, ..., s$ sequentially. Set $U^l = U^{l-1} \cup \{k^*\}$. If Problem (PP$_h(y^*)$) is feasible with optimum (x_h^*, q_h^*, u_h^*) for all the scenarios and $\text{obj}_{\text{PP}}(y^*) < \text{UBD}$, update $\text{UBD} = \text{obj}_{\text{PP}}(y^*)$ and set $y_p^* = y^*$, $(x_{p,h}^*, q_{p,h}^*, u_{p,h}^*) = (x_h^*, q_h^*, u_h^*)$ for $h = 1, \ldots, s$.

2. If Problem (PP$_h(y^*)$) is feasible for all scenarios, for each scenario $h = 1, \ldots, s$ and $t = 1, \ldots, n_q$, if $n_{\delta,h,t} \leq n_{\delta,h,\max}$ and $q_{h,t}^m < q_{h,t}^* < q_{h,t}^{m+1}$ for some $m \in \{1, \ldots, n_{\delta,h,t}\}$, set $n_{\delta,h,t} = n_{\delta,h,t} + 1$, set $q_{h,t}^{j+1} = q_{h,t}^j$ for each $j = m+1, \ldots, n_{\delta,h,t}$, and set $q_{h,t}^{m+1} = q_{h,t}^*$.

3. If $\bar{T}^k \setminus U^l = \emptyset$, set $\text{UBDPB} = +\infty$.

4. If $\bar{T}^k \setminus U^l \neq \emptyset$, pick $i \in \bar{T}^k \setminus U^l$ such that $\text{obj}_{\text{PBP-PCR-A}}(y^{(i)}) = \min_{j \in \bar{T}^k \setminus U^l}\{\text{obj}_{\text{PBP-PCR-A}}(y^{(j)})\}$. Update UBDPB $= \text{obj}_{\text{PBP-PCR-A}}(y^{(i)})$, $y^* = y^{(i)}$, $k^* = i$. Set $l = l + 1$.

end if

until UBDPB $\geq$ UBD $- \epsilon$ and ((Problem (PERMP^k) or (RMFP^k) is infeasible) or LBD $\geq$ UBD $- \epsilon$).

An ϵ-global optimum of the original problem (P) is given by

$$(y_p^*, x_{p,1}^*, ..., x_{p,s}^*, q_{p,1}^*, ..., q_{p,s}^*, u_{p,1}^*, ..., u_{p,s}^*)$$

or (P) is infeasible.

The algorithm flowchart is shown in Figure 6-3, in which differences between the enhanced decomposition algorithm and the original decomposition algorithm are highlighted in grey. Compared to the flowchart of the original decomposition algorithm, three new steps, "PBP-PCR (MILP)", "DPBP-PCR (MILP)" and "Update pieces for PBP-PCR and DPBP-PCR", are added in this flowchart, and the step "Relaxed Master Problem" is replaced by "Enhanced Relaxed Master Problem". The selection of the integer realization $y^{(k)}$ for constructing primal subproblems (PP$_h$) is based on $\text{obj}_{\text{PBP-PCR-A}}(y^{(k)})$ here.

The convergence property for the enhanced NGBD holds according to Theorem 1.

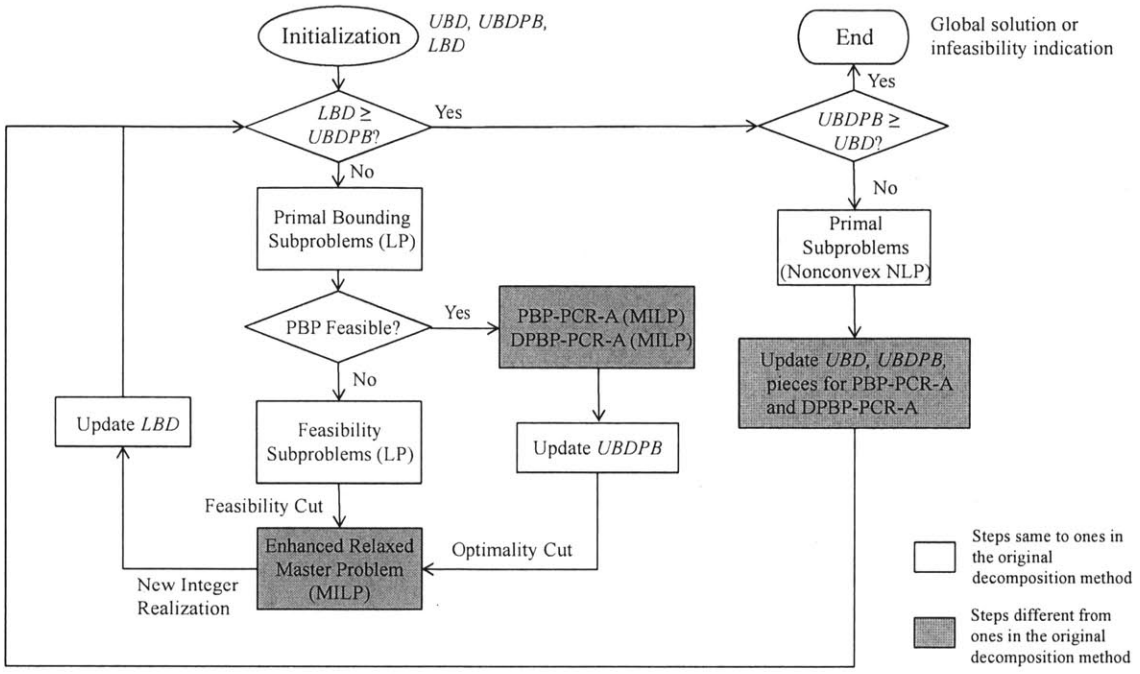

Figure 6-3: Flowchart for the enhanced decomposition algorithm with adaptive piecewise convex relaxation.

6.4 Enhanced Decomposition Algorithm with Primal Dual Cuts and Piecewise Convex Relaxation

6.4.1 New Subproblems

Enhanced Relaxed Master problem with Primal Dual Cuts and Piecewise Relaxation

The performance of decomposition algorithm can be further enhanced by incorporating both primal dual cuts and piecewise convex relaxations. The enhanced relaxed

master problem with both technologies, called the Problem (DPERMP^k), is as follows:

$$
\begin{aligned}
\min_{y,\eta} \quad & \eta \\
\text{s.t.} \quad & \eta \geq \tilde{\alpha}^{(r)} y + \tilde{\beta}^{(r)}, \quad \forall r \in V^k, \\
& \eta \geq \breve{\alpha}^{(r)} y + \breve{\beta}^{(r)}, \quad \forall r \in V^k, \\
& \eta \geq \bar{\alpha}^{(j)} y + \bar{\beta}^{(j)}, \quad \forall j \in \bar{T}^k, \\
& \eta \geq \alpha^{(j)} y + \beta^{(j)}, \quad \forall j \in T^k, \\
& \gamma^{(i)} y + \theta^{(i)} \leq 0, \quad \forall i \in S^k, \\
& \sum_{l \in \{l: y_l^{(t)} = 1\}} y_l - \sum_{l \in \{l: y_l^{(t)} = 0\}} y_l \leq |\{l : y^{(t)} = 1\}| - 1, \quad \forall t \in T^k \cup S^k, \\
& y \in Y, \ \eta \in \mathbb{R},
\end{aligned}
\tag{DPERMP^k}
$$

The first two groups of constraints are primal dual cuts, and the third group of constraints are piecewise enhanced optimality cuts.

Remark 8. Compared to Problem (RMP^k), Problem (DPERMP^k) is a tighter (or equal) relaxation of Problem (P) when Problem (P) is augmented with the Balas cuts according to Propositions 2 and 6.

6.4.2 Enhanced Decomposition Algorithm with Primal Dual Cuts and Piecewise Relaxation

The enhanced decomposition algorithm with primal dual cuts and piecewise convex relaxation is stated as below:

Initialize:

1. Iteration counters $k = 0$, $l = 1$, and the index sets $T^0 = \emptyset$, $\bar{T}^0 = \emptyset$, $S^0 = \emptyset$, $U^0 = \emptyset$, $V^0 = \emptyset$.

2. Upper bound on the problem UBD $= +\infty$, upper bound on the lower bounding problem UBDPB $= +\infty$, lower bound on the lower bounding problem

LBD $= -\infty$.

3. Set tolerances ϵ_h and ϵ such that $\sum_{h=1}^{s} \epsilon_h \leq \epsilon$.

4. Integer realization $y^{(1)}$ is given.

repeat

if $k = 0$ or (Problem (DPERMP^k) is feasible and LBD $<$ UBDPB and LBD $<$ UBD $- \epsilon$) **then**

repeat

Set $k = k + 1$

1. Solve the decomposed primal bounding problem (PBP$_h(y^{(k)})$) for each scenario $h = 1, ..., s$ sequentially. If Problem (PBP$_h(y^{(k)})$) is feasible for all the scenarios with Lagrange multipliers $\lambda_h^{(k)}$, add optimality cuts to the enhanced relaxed master problem (DPERMP^k) according to $\lambda_1^{(k)}, ..., \lambda_s^{(k)}$, set $T^k = T^{k-1} \cup \{k\}$.

2. If Problem (PBP$_h(y^{(k)})$) is feasible for all the scenarios, solve subproblem (PBP-PCR$_h(y^{(k)})$) for each scenario $h = 1, ..., s$ sequentially. If Problem (PBP-PCR$_h(y^{(k)})$) is feasible with KKT multipliers $\bar{\lambda}_h^{(k)}$ for all the scenarios, set $\bar{T}^k = \bar{T}^{k-1} \cup \{k\}$. In this case, if obj$_{\text{PBP-PCR}}(y^{(k)}) <$ UBDPB, update UBDPB = obj$_{\text{PBP-PCR}}(y^{(k)})$, $y^* = y^{(k)}$, $k^* = k$, solve subproblem (DPBP-PCR$_h(y^{(k)})$) with $\bar{\lambda}_h^{(k)}$ for each scenario $h = 1, ..., s$ sequentially, add optimality cuts to Problem (DPERMP^k).

3. If Problem (PBP$_h(y^{(k)})$) is infeasible for one scenario, stop solving it for the remaining scenarios and set $S^k = S^{k-1} \cup \{k\}$. Then, solve the decomposed feasibility subproblem (FP$_h(y^{(k)})$) for $h = 1, ..., s$ and obtain the corresponding Lagrange multipliers $\mu_h^{(k)}$. Add feasibility cuts to Problem (DPERMP^k) according to these multipliers.

4. If $T^k = \emptyset$, solve the feasibility problem (RMFP^k); otherwise, solve Problem (DPERMP^k). In the latter case, if Problem (DPERMP^k) is

feasible, set LBD to its optimal objective value. In both cases, set $y^{(k+1)}$ to the y value at the solution of either problem.

until LBD $\geq$ UBDPB or (Problem (DPERMP^k) or (RMFP^k) is infeasible).

end if

if UBDPB $<$ UBD $- \epsilon$ **then**

1. Solve the decomposed primal subproblem (PP$_h(y^*)$) to ϵ_h-optimality for each scenario $h = 1, ..., s$ sequentially. Set $U^l = U^{l-1} \cup \{k^*\}$. If Problem (PP$_h(y^*)$) is feasible with optimum (x_h^*, q_h^*, u_h^*) for all the scenarios and $\text{obj}_{\text{PP}}(y^*) <$ UBD, obtain the corresponding KKT multipliers $\breve{\lambda}_h^{(k^*)}$, update UBD $= \text{obj}_{\text{PP}}(y^*)$ and set $y_p^* = y^*$, $(x_{p,h}^*, q_{p,h}^*, u_{p,h}^*) = (x_h^*, q_h^*, u_h^*)$ for $h = 1, \ldots, s$, set $V^k = V^{k-1} \cup \{k^*\}$.

2. If $k^* \in V^k$, solve the decomposed relaxed dual of primal problem (DPP$_h(y^*)$) to ϵ_h-optimality for each scenario $h = 1, ..., s$ sequentially with KKT multipliers $\lambda_h^{(k^*)}$ and $\breve{\lambda}_h^{(k^*)}$. Add primal dual cuts to Problem (DPERMP^k) according to these multipliers and the optimal solutions of Problem (DPP$_h(y^*)$).

2. If $\bar{T}^k \setminus U^l = \emptyset$, set UBDPB $= +\infty$.

3. If $\bar{T}^k \setminus U^l \neq \emptyset$, pick $i \in \bar{T}^k \setminus U^l$ such that $\text{obj}_{\text{PBP-PCR}}(y^{(i)}) = \min_{j \in \bar{T}^k \setminus U^l} \{\text{obj}_{\text{PBP-PCR}}(y^{(j)})$ Update UBDPB $= \text{obj}_{\text{PBP-PCR}}(y^{(i)})$, $y^* = y^{(i)}$, $k^* = i$. Set $l = l + 1$.

end if

until UBDPB $\geq$ UBD $- \epsilon$ and ((Problem (DPERMP^k) or (RMFP^k) is infeasible) or LBD $\geq$ UBD $- \epsilon$).

An ϵ-global optimum of the original problem (P) is given by

$$(y_p^*, x_{p,1}^*, ..., x_{p,s}^*, q_{p,1}^*, ..., q_{p,s}^*, u_{p,1}^*, ..., u_{p,s}^*)$$

or (P) is infeasible.

If the adaptive piecewise convex relaxation is applied, replace Problems (PBP-PCR$_h$) and (DPBP-PCR$_h$) in the aforementioned algorithm by Problems (PBP-PCR-

A_h) and (DPBP-PCR-A_h), and update the pieces for Problems (PBP-PCR-A_h) and (DPBP-PCR-A_h) after solution of Problem (PP).

The flowcharts for the enhanced decomposition algorithm with primal dual cuts and piecewise convex relaxation are shown in Figures 6-4 and 6-5, in which differences between the enhanced decomposition algorithm and the original decomposition algorithm are highlighted in grey.

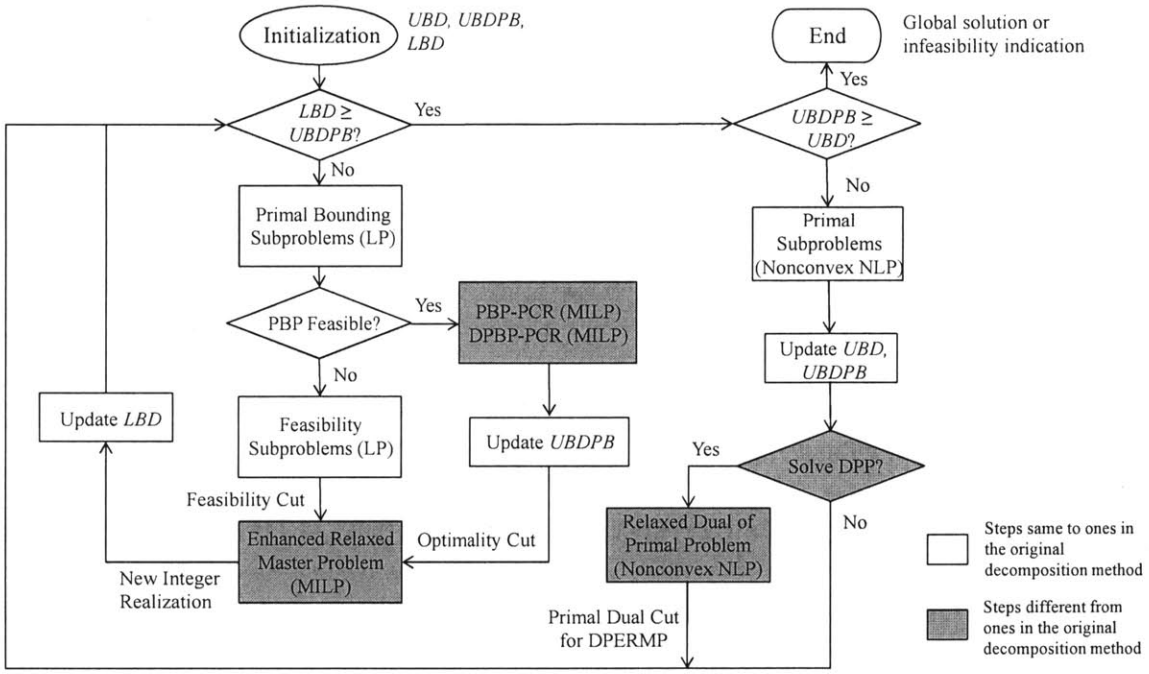

Figure 6-4: Flowchart for the enhanced decomposition algorithm with primal dual cuts and piecewise convex relaxation.

The convergence property for the enhanced NGBD holds according to Theorem 1.

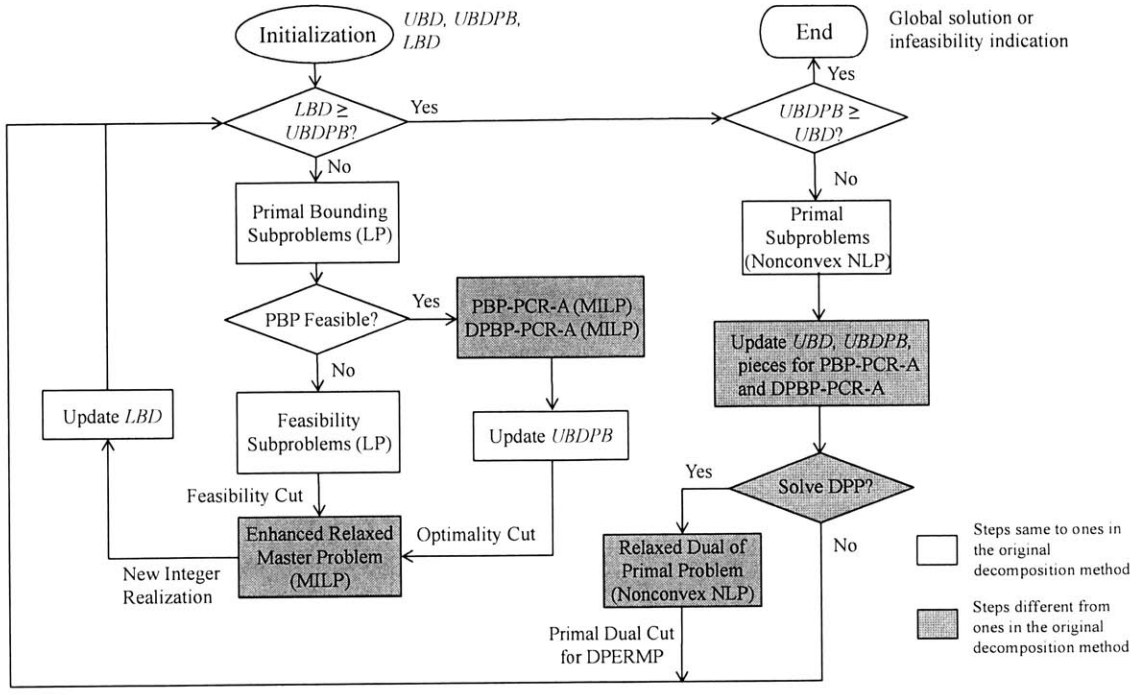

Figure 6-5: Flowchart for the enhanced decomposition algorithm with primal dual cuts and adaptive piecewise convex relaxation.

6.5 Enhanced Decomposition Algorithm with Lift-and-Project Cuts

6.5.1 Lift-and-Project Cuts for MILPs

Balas et al. [24] developed a cutting plane algorithm for mixed-integer programs, in which lift-and-project cuts were generated to strengthen the LP relaxation. This algorithm solves MILPs without branching on integer variables, instead, it iteratively solves a series of LPs, including LP relaxations with lift-and-project cuts and LPs generation corresponding cuts.

A MILP with the following general form is studied:

$$\begin{aligned} \min_{x} \ & c^{\mathrm{T}}x \\ \text{s.t.} \ & Ax \geq b \\ & x_j \in \{0,1\}, \quad j \in \{1,\ldots,p\} \\ & x_j^{\mathrm{L}} \leq x_j \leq x_j^{\mathrm{U}}, \quad j \notin \{1,\ldots,p\} \end{aligned} \tag{MIP}$$

where the first p components of x $(x_1,\ldots,x_p)$ are binary variables, and the remaining components of x are continuous variables. x^{L} and x^{U} are the lower and upper bounds for the continuous variables, respectively.

To solve Problem (MIP) by the cutting plane algorithm, Problem (MIP) is first relaxed to a LP problem as below:

$$\begin{aligned} \min_{x} \ & c^{\mathrm{T}}x \\ \text{s.t.} \ & Ax \geq b \\ & 0 \leq x_j \leq 1, \quad j \in \{1,\ldots,p\} \\ & x_j^{\mathrm{L}} \leq x_j \leq x_j^{\mathrm{U}}, \quad j \notin \{1,\ldots,p\} \end{aligned} \tag{RMIP}$$

For the ease of discussion, the formulation of Problem (RMIP) is simplified as:

$$\begin{aligned} \min_{x} \ & c^{\mathrm{T}}x \\ \text{s.t.} \ & \tilde{A}x \geq \tilde{b} \end{aligned} \tag{RMIP'}$$

Let $\hat{x}$ be the solution of Problem (RMIP) (or (RMIP')). For any $j \in \{1,\ldots,p\} \cap$

$\{j : 0 < \hat{x}_j < 1\}$ (or a subset of these j), solve the following cut generation problem:

$$\begin{aligned}
\min_{\alpha,\beta,u,v,u_0,v_0} \quad & \alpha^{\mathrm{T}}\hat{x} - \beta \\
\text{s.t.} \quad & \alpha - \tilde{A}^{\mathrm{T}}u - u_0 e_j \geq 0 \\
& \alpha - \tilde{A}^{\mathrm{T}}v - v_0 e_j \geq 0 \\
& \beta = \tilde{b}u \\
& \beta = \tilde{b}v + v_0 \\
& u \geq 0, \;\; v \geq 0 \\
& \sum_{i=1}^{n} |\alpha_i| \leq 1
\end{aligned} \tag{CGP$_j$}$$

where e_j is the unit vector with the j^{th} element equal to 1.

Then the cut $\alpha^{\mathrm{T}}x \geq \beta$, called the lift-and-project cut, is added to the constraints in Problem (RMIP).

The dual of Problem (CGP$_j$) is formulated as below:

$$\begin{aligned}
\min_{\gamma_1,\gamma_2,\gamma_3,\gamma_4,\gamma_5} \quad & \gamma_5 \\
\text{s.t.} \quad & \tilde{A}\gamma_1 \geq -\tilde{b}\gamma_3 \\
& \tilde{A}\gamma_2 \geq -\tilde{b}\gamma_4 \\
& -e_j^{\mathrm{T}}\gamma_1 \leq 0 \\
& e_j^{\mathrm{T}}\gamma_1 \leq 0 \\
& -e_j^{\mathrm{T}}\gamma_2 - \gamma_4 \leq 0 \\
& e_j^{\mathrm{T}}\gamma_2 + \gamma_4 \leq 0 \\
& \gamma_1 + \gamma_2 - \mathbf{1}\gamma_5 \leq \hat{x} \\
& -\gamma_1 - \gamma_2 - \mathbf{1}\gamma_5 \leq -\hat{x} \\
& \gamma_3 + \gamma_4 \leq -1 \\
& -\gamma_3 - \gamma_4 \leq 1 \\
& \gamma_1, \;\; \gamma_2, \;\; \gamma_5 \geq 0
\end{aligned} \tag{DCGP$_j$}$$

The last four groups of constraints in Problem (DCGP$_j$) are listed as below:

$$\gamma_1 + \gamma_2 - \mathbf{1}\gamma_5 \leq \hat{x} \tag{6.53}$$

$$-\gamma_1 - \gamma_2 - \mathbf{1}\gamma_5 \leq -\hat{x} \tag{6.54}$$

$$\gamma_3 + \gamma_4 \leq -1 \tag{6.55}$$

$$-\gamma_3 - \gamma_4 \leq 1 \tag{6.56}$$

The Lagrange multipliers of Constraints (6.53), (6.54), (6.55) and (6.56) are recorded as λ_{α^+}, λ_{α^-}, λ_{β^+} and λ_{β^-}, respectively. α and β are calculated as:

$$\alpha = \lambda_{\alpha^+} - \lambda_{\alpha^-} \tag{6.57}$$

$$\beta = \lambda_{\beta^+} - \lambda_{\beta^-} \tag{6.58}$$

Due to strong duality for LPs [33], Problem (DCGP$_j$) and (CGP$_j$) have the same optimal objective. Note that Problem (DCGP$_j$) is usually easier to be formulated from Problem (RMIP) compared to Problem (CGP$_j$), hence is selected for generating lift-and-project cuts in this work.

There are several strategies for adding lift-and-project cuts. For example, Problem (DCGP$_j$) can be solved for all x_j that violate integrality or just one x_j with the maximum violation to integer values, depending on the strength of lift-and-project cuts and the solution time for Problem (DCGP$_j$). In this work, lift-and-project cuts for all x_j are added in order to obtain tighter relaxation.

The cutting plane algorithm is stated as below:

Step 1: Solve Problem (RMIP). If $x_j \in \{0,1\}$ for $j = 1, \ldots, p$, **STOP**.

Step 2: For all $x_j \notin \{0,1\}$ $(j = 1, \ldots, p)$ (or x_j with the maximum integral violation), generate a lift-and-project cut $\alpha^{\mathrm{T}} x \geq \beta$ for each x_j by solving Problem (DCGP$_j$).

Step 3: Add the cuts $\alpha^{\mathrm{T}} x \geq \beta$ for all x_j to the constraints of Problem (RMIP). **Go to** Step 1.

Theorem 2. *The aforementioned cutting plane algorithm finds an optimal solution to Problem (MIP) in finitely many iterations.*

Proof. See Ref [24]. □

Remark 9. Lift-and-project cuts generated by the aforementioned cutting plane algorithm will not cut off any point in the convex hull of the feasible region for Problem (MIP) [24].

6.5.2 New Subproblems

Primal Bounding Problem with Lift-and-Project Cuts

In the enhanced NGBD with lift-and-project cuts, the enhanced primal bounding problem is still based on the piecewise convex relaxation. However, it is formulated as a LP augmented with lift-and-project cuts here, instead of a MILP in Section 6.3,. The new primal bounding problem is called Problem (PBP-LAP), and it can be naturally decomposed into subproblems (PBP-LAP$_h$) for the s scenarios:

$$
\begin{aligned}
\mathrm{obj}_{\mathrm{PBP-LAP}_h}\left(y^{(k)}\right) = \min_{\substack{x_h, q_h, u_h, \delta_h, \\ \bar{x}_h, \bar{q}_h, \bar{u}_h}} \quad & c_{2,h}^{\mathrm{T}} x_h + c_{3,h}^{\mathrm{T}} q_h + c_{4,h}^{\mathrm{T}} u_h \\
\text{s.t.} \quad & A_{1,h} y^{(k)} + A_{2,h} x_h + A_{3,h} q_h + A_{4,h} u_h \leq b_h, \\
& \left(\alpha_{1,h}^r\right)^{\mathrm{T}} y^{(k)} + \left(\alpha_{2,h}^r\right)^{\mathrm{T}} x_h + \left(\alpha_{3,h}^r\right)^{\mathrm{T}} q_h + \left(\alpha_{4,h}^r\right)^{\mathrm{T}} u_h \\
& \quad + \left(\alpha_{5,h}^r\right)^{\mathrm{T}} \delta_h + \left(\alpha_{6,h}^r\right)^{\mathrm{T}} \bar{x}_h + \left(\alpha_{7,h}^r\right)^{\mathrm{T}} \bar{q}_h + \left(\alpha_{8,h}^r\right)^{\mathrm{T}} \bar{u}_h \\
& \quad \geq \beta_h^r, \quad \forall r \in \{1, \ldots, n_{l,h}\}, \\
& (x_h, q_h, u_h, \delta_h, \bar{x}_h, \bar{q}_h, \bar{u}_h) \in \bar{\Pi}_h^{\mathrm{lap}}
\end{aligned}
\tag{PBP-LAP$_h$}
$$

where

$$\begin{aligned}
\bar{\Pi}_h^{\text{lap}} =& \{(x_h, q_h, u_h) \in \Pi_h,\ \delta_h \in [0,1]^{Mn_q},\ (\bar{x}_h, \bar{q}_h, \bar{u}_h) \in \mathbb{R}^{Mn_x} \times \mathbb{R}^{Mn_q} \times \mathbb{R}^{Mn_u} : \\
& \sum_{m=1}^{M} \delta_{h,m} = 1, \\
& u_{h,l,t} = \sum_{m=1}^{M} \bar{u}_{h,l,t,m}, \quad \forall (l,t) \in \Omega, \\
& x_{h,l} = \sum_{m=1}^{M} \bar{x}_{h,l,m}, \quad \forall l \in \{1, \ldots, n_x\}, \\
& q_{h,t} = \sum_{m=1}^{M} \bar{q}_{h,t,m}, \quad \forall t \in \{1, \ldots, n_q\}, \\
& \bar{u}_{h,l,t,m} \geq x_{h,l}^{\text{L}}\, \bar{q}_{h,t,m} + \bar{x}_{h,l,m}\, q_{h,t}^{m} - x_{h,l}^{\text{L}} q_{h,t}^{m} \delta_{h,m}, \\
& \bar{u}_{h,l,t,m} \geq x_{h,l}^{\text{U}}\, \bar{q}_{h,t,m} + \bar{x}_{h,l,m}\, q_{h,t}^{m+1} - x_{h,l}^{\text{U}} q_{h,t}^{m+1} \delta_{h,m}, \\
& \bar{u}_{h,l,t,m} \leq x_{h,l}^{\text{U}}\, \bar{q}_{h,t,m} + \bar{x}_{h,l,m}\, q_{h,t}^{m} - x_{h,l}^{\text{U}} q_{h,t}^{m} \delta_{h,m}, \\
& \bar{u}_{h,l,t,m} \leq x_{h,l}^{\text{L}}\, \bar{q}_{h,t,m} + \bar{x}_{h,l,m}\, q_{h,t}^{m+1} - x_{h,l}^{\text{L}} q_{h,t}^{m+1} \delta_{h,m}, \\
& \quad \forall (l,t) \in \Omega,\ \ \forall m \in \{1, \ldots, M\}, \\
& \delta_{h,m} x_h^{\text{L}} \leq \bar{x}_{h,m} \leq \delta_{h,m} x_h^{\text{U}},\ \ \delta_{h,m} q_h^{m} \leq \bar{q}_{h,m} \leq \delta_{h,m} q_h^{m+1}, \quad \forall m \in \{1, \ldots, M\}, \\
& q_h^{\text{L}} = q_h^1 \leq q_h^2 \leq \ldots \leq q_h^M \leq q_h^{M+1} = q_h^{\text{U}} \ \}
\end{aligned}$$

δ_h is the relaxed binary variable representing the choice of pieces for q_h in scenario h.

The second group of constraints in Problem (PBP-LAP$_h$) are lift-and-project cuts, and $n_{l,h}$ is the number of lift-and-project cuts in scenario h. By adding lift-and-project cuts, the values of relaxed binary variables δ_h will approach integers (0 or 1). The cut parameters α_h and β_h are obtained in cut generation problems, which will be discussed later.

$\text{obj}_{\text{PBP-LAP}_h}\left(y^{(k)}\right)$ is the optimal objective value of Problem (PBP-LAP$_h$) for $y = y^{(k)}$, $h = 1, \ldots, s$. The objectives of Problem (PBP-LAP) and (PBP-LAP$_h$) satisfy the following relationship:

$$\text{obj}_{\text{PBP-LAP}}\left(y^{(k)}\right) = c_1^{\text{T}} y^{(k)} + \sum_{h=1}^{s} \text{obj}_{\text{PBP-LAP}_h}\left(y^{(k)}\right) \tag{6.59}$$

where $\text{obj}_{\text{PBP-LAP}}\left(y^{(k)}\right)$ is the optimal objective value of Problem (PBP-LAP) for $y = y^{(k)}$.

Remark 10. Note that Problem (PBP-LAP$_h$) is a LP, which is convex. The optimal solution of Problem (PBP-LAP$_h$) can directly construct optimality cuts for the enhanced relaxed master problem, and no relaxed dual of Problem (PBP-LAP$_h$) needs to be solved.

Cut Generation Problem

After solving Problem (PBP-LAP$_h$), the integrality of relaxed binary variables δ_h is checked. If the value of one variable $\delta_{h,m}$ $(m = 1, \ldots, M)$ does not satisfy integrality, the corresponding cut generation problem (CGP) is solved. A new lift-and-project cut is then generated and added into Problem (PBP-LAP$_h$). The cut generation

problem for $\delta_{h,m}$ in scenario h at the k^{th} iteration is expressed as below:

$$
\begin{aligned}
\min_{\substack{\gamma^x_{1,h},\gamma^q_{1,h},\gamma^u_{1,h},\gamma^\delta_{1,h},\\ \gamma^{\bar{x}}_{1,h},\gamma^{\bar{q}}_{1,h},\gamma^{\bar{u}}_{1,h},\gamma^y_{1,h},\\ \gamma^x_{2,h},\gamma^q_{2,h},\gamma^u_{2,h},\gamma^\delta_{2,h},\\ \gamma^{\bar{x}}_{2,h},\gamma^{\bar{q}}_{2,h},\gamma^{\bar{u}}_{2,h},\gamma^y_{2,h},\\ \gamma_{3,h},\gamma_{4,h},\gamma_{5,h}}} \quad & \gamma_{5,h} \\
\text{s.t.} \quad & A_{1,h}\gamma^y_{1,h} + A_{2,h}\gamma^x_{1,h} + A_{3,h}\gamma^q_{1,h} + A_{4,h}\gamma^u_{1,h} \le -b_h\gamma_{3,h}, \\
& \left(\alpha^r_{1,h}\right)^{\mathrm{T}}\gamma^y_{1,h} + \left(\alpha^r_{2,h}\right)^{\mathrm{T}}\gamma^x_{1,h} + \left(\alpha^r_{3,h}\right)^{\mathrm{T}}\gamma^q_{1,h} + \left(\alpha^r_{4,h}\right)^{\mathrm{T}}\gamma^u_{1,h} + \left(\alpha^r_{5,h}\right)^{\mathrm{T}}\gamma^\delta_{1,h} + \\
& \quad \left(\alpha^r_{6,h}\right)^{\mathrm{T}}\gamma^{\bar{x}}_{1,h} + \left(\alpha^r_{7,h}\right)^{\mathrm{T}}\gamma^{\bar{q}}_{1,h} + \left(\alpha^r_{8,h}\right)^{\mathrm{T}}\gamma^{\bar{u}}_{1,h} \ge -\beta^r_h\gamma_{3,h}, \quad \forall r \in \{1,\ldots,n_{l,h}\}, \\
& A_{1,h}\gamma^y_{2,h} + A_{2,h}\gamma^x_{2,h} + A_{3,h}\gamma^q_{2,h} + A_{4,h}\gamma^u_{2,h} \le -b_h\gamma_{4,h}, \\
& \left(\alpha^r_{1,h}\right)^{\mathrm{T}}\gamma^y_{2,h} + \left(\alpha^r_{2,h}\right)^{\mathrm{T}}\gamma^x_{2,h} + \left(\alpha^r_{3,h}\right)^{\mathrm{T}}\gamma^q_{2,h} + \left(\alpha^r_{4,h}\right)^{\mathrm{T}}\gamma^u_{2,h} + \left(\alpha^r_{5,h}\right)^{\mathrm{T}}\gamma^\delta_{2,h} + \\
& \quad \left(\alpha^r_{6,h}\right)^{\mathrm{T}}\gamma^{\bar{x}}_{2,h} + \left(\alpha^r_{7,h}\right)^{\mathrm{T}}\gamma^{\bar{q}}_{2,h} + \left(\alpha^r_{8,h}\right)^{\mathrm{T}}\gamma^{\bar{u}}_{2,h} \ge -\beta^r_h\gamma_{4,h}, \quad \forall r \in \{1,\ldots,n_{l,h}\}, \\
& -e_m^{\mathrm{T}}\gamma^\delta_{1,h} \le 0, \quad e_m^{\mathrm{T}}\gamma^\delta_{1,h} \le 0, \quad -e_m^{\mathrm{T}}\gamma^\delta_{2,h} - \gamma_{4,h} \le 0, \quad e_m^{\mathrm{T}}\gamma^\delta_{2,h} + \gamma_{4,h} \le 0, \\
& \gamma^y_{1,h} + \gamma^y_{2,h} - \mathbf{1}\gamma_{5,h} \le y^{(k)}, \quad \gamma^x_{1,h} + \gamma^x_{2,h} - \mathbf{1}\gamma_{5,h} \le x^{(k)}_h, \quad \gamma^q_{1,h} + \gamma^q_{2,h} - \mathbf{1}\gamma_{5,h} \le q^{(k)}_h, \\
& \gamma^u_{1,h} + \gamma^u_{2,h} - \mathbf{1}\gamma_{5,h} \le u^{(k)}_h, \quad \gamma^\delta_{1,h} + \gamma^\delta_{2,h} - \mathbf{1}\gamma_{5,h} \le \delta^{(k)}_h, \quad \gamma^{\bar{x}}_{1,h} + \gamma^{\bar{x}}_{2,h} - \mathbf{1}\gamma_{5,h} \le \bar{x}^{(k)}_h, \\
& \gamma^{\bar{q}}_{1,h} + \gamma^{\bar{q}}_{2,h} - \mathbf{1}\gamma_{5,h} \le \bar{q}^{(k)}_h, \quad \gamma^{\bar{u}}_{1,h} + \gamma^{\bar{u}}_{2,h} - \mathbf{1}\gamma_{5,h} \le \bar{u}^{(k)}_h, \\
& -\gamma^y_{1,h} - \gamma^y_{2,h} - \mathbf{1}\gamma_{5,h} \le -y^{(k)}, \quad -\gamma^x_{1,h} - \gamma^x_{2,h} - \mathbf{1}\gamma_{5,h} \le -x^{(k)}_h, \\
& -\gamma^q_{1,h} - \gamma^q_{2,h} - \mathbf{1}\gamma_{5,h} \le -q^{(k)}_h, \quad -\gamma^u_{1,h} - \gamma^u_{2,h} - \mathbf{1}\gamma_{5,h} \le -u^{(k)}_h, \\
& -\gamma^\delta_{1,h} - \gamma^\delta_{2,h} - \mathbf{1}\gamma_{5,h} \le -\delta^{(k)}_h, \quad -\gamma^{\bar{x}}_{1,h} - \gamma^{\bar{x}}_{2,h} - \mathbf{1}\gamma_{5,h} \le -\bar{x}^{(k)}_h, \\
& -\gamma^{\bar{q}}_{1,h} - \gamma^{\bar{q}}_{2,h} - \mathbf{1}\gamma_{5,h} \le -\bar{q}^{(k)}_h, \quad -\gamma^{\bar{u}}_{1,h} - \gamma^{\bar{u}}_{2,h} - \mathbf{1}\gamma_{5,h} \le -\bar{u}^{(k)}_h, \\
& \gamma_{3,h} + \gamma_{4,h} \le -1, \quad -\gamma_{3,h} - \gamma_{4,h} \le 1, \\
& (\gamma^x_{1,h}, \gamma^q_{1,h}, \gamma^u_{1,h}, \gamma^\delta_{1,h}, \gamma^{\bar{x}}_{1,h}, \gamma^{\bar{q}}_{1,h}, \gamma^{\bar{u}}_{1,h}, \gamma^y_{1,h}, \gamma_{3,h}) \in \bar{\bar{\Pi}}^1_h, \\
& (\gamma^x_{2,h}, \gamma^q_{2,h}, \gamma^u_{2,h}, \gamma^\delta_{2,h}, \gamma^{\bar{x}}_{2,h}, \gamma^{\bar{q}}_{2,h}, \gamma^{\bar{u}}_{2,h}, \gamma^y_{2,h}, \gamma_{4,h}) \in \bar{\bar{\Pi}}^2_h, \\
& \gamma_{5,h} \in \mathbb{R}, \quad \gamma_{5,h} \ge 0
\end{aligned}
\tag{$\mathrm{CGP}_{h,m}$}
$$

where

$$
\begin{aligned}
\bar{\bar{\Pi}}_h^1 =& \{(\gamma_{1,h}^x, \gamma_{1,h}^q, \gamma_{1,h}^u, \gamma_{1,h}^\delta, \gamma_{1,h}^{\bar{x}}, \gamma_{1,h}^{\bar{q}}, \gamma_{1,h}^{\bar{u}}, \gamma_{1,h}^y, \gamma_{3,h}) \\
& \in \mathbb{R}^{n_x} \times \mathbb{R}^{n_q} \times \mathbb{R}^{n_u} \times \mathbb{R}^{Mn_q} \times \mathbb{R}^{Mn_x} \times \mathbb{R}^{Mn_q} \times \mathbb{R}^{Mn_u} \times \mathbb{R}^{n_y} \times \mathbb{R} : \\
& \tilde{A}_{2,h}\gamma_{1,h}^x + \tilde{A}_{3,h}\gamma_{1,h}^q + \tilde{A}_{4,h}\gamma_{1,h}^u \le -\tilde{b}_h\gamma_{3,h}, \\
& \sum_{m=1}^{M} \gamma_{1,h,m}^\delta = -\gamma_{3,h}, \\
& \gamma_{1,h,l,t}^u = \sum_{m=1}^{M} \gamma_{1,h,l,t,m}^{\bar{u}}, \quad \forall (l,t) \in \Omega, \\
& \gamma_{1,h,l}^x = \sum_{m=1}^{M} \gamma_{1,h,l,m}^{\bar{x}}, \quad \forall l \in \{1,\dots,n_x\}, \\
& \gamma_{1,h,t}^q = \sum_{m=1}^{M} \gamma_{1,h,t,m}^{\bar{q}}, \quad \forall t \in \{1,\dots,n_q\}, \\
& \gamma_{1,h,l,t,m}^{\bar{u}} \ge x_{h,l}^{\mathrm{L}}\gamma_{1,h,t,m}^{\bar{q}} + \gamma_{1,h,l,m}^{\bar{x}} q_{h,t}^m - x_{h,l}^{\mathrm{L}} q_{h,t}^m \gamma_{1,h,m}^\delta, \\
& \gamma_{1,h,l,t,m}^{\bar{u}} \ge x_{h,l}^{\mathrm{U}}\gamma_{1,h,t,m}^{\bar{q}} + \gamma_{1,h,l,m}^{\bar{x}} q_{h,t}^{m+1} - x_{h,l}^{\mathrm{U}} q_{h,t}^{m+1} \gamma_{1,h,m}^\delta, \\
& \gamma_{1,h,l,t,m}^{\bar{u}} \le x_{h,l}^{\mathrm{U}}\gamma_{1,h,t,m}^{\bar{q}} + \gamma_{1,h,l,m}^{\bar{x}} q_{h,t}^m - x_{h,l}^{\mathrm{U}} q_{h,t}^m \gamma_{1,h,m}^\delta, \\
& \gamma_{1,h,l,t,m}^{\bar{u}} \le x_{h,l}^{\mathrm{L}}\gamma_{1,h,t,m}^{\bar{q}} + \gamma_{1,h,l,m}^{\bar{x}} q_{h,t}^{m+1} - x_{h,l}^{\mathrm{L}} q_{h,t}^{m+1} \gamma_{1,h,m}^\delta, \\
& \quad \forall (l,t) \in \Omega, \ \ \forall m \in \{1,\dots,M\}, \\
& B\gamma_{1,h}^y \le -a\gamma_{3,h}, \\
& -x_h^{\mathrm{L}}\gamma_{3,h} \le \gamma_{1,h}^x \le -x_h^{\mathrm{U}}\gamma_{3,h}, \ \ -q_h^{\mathrm{L}}\gamma_{3,h} \le \gamma_{1,h}^q \le -q_h^{\mathrm{U}}\gamma_{3,h}, \\
& -x_h^{\mathrm{L}}\gamma_{1,h,m}^\delta \le \gamma_{1,h,m}^{\bar{x}} \le -x_h^{\mathrm{U}}\gamma_{1,h,m}^\delta, \ \ -q_h^m\gamma_{1,h,m}^\delta \le \gamma_{1,h,m}^{\bar{q}} \le -q_h^{m+1}\gamma_{1,h,m}^\delta, \quad \forall m \in \{1,\dots,M\}, \\
& -y^{\mathrm{L}}\gamma_{3,h} \le \gamma_{1,h}^y \le -y^{\mathrm{U}}\gamma_{3,h}, \\
& \gamma_{1,h}^x \ge 0, \ \ \gamma_{1,h}^q \ge 0, \ \ \gamma_{1,h}^u \ge 0, \ \ \gamma_{1,h}^\delta \ge 0, \ \ \gamma_{1,h}^{\bar{x}} \ge 0, \ \ \gamma_{1,h}^{\bar{q}} \ge 0, \ \ \gamma_{1,h}^{\bar{u}} \ge 0, \ \ \gamma_{1,h}^y \ge 0 \ \ \}
\end{aligned}
$$

and

$$
\begin{aligned}
\bar{\bar{\Pi}}_h^2 =& \{(\gamma_{2,h}^x, \gamma_{2,h}^q, \gamma_{2,h}^u, \gamma_{2,h}^\delta, \gamma_{2,h}^{\bar{x}}, \gamma_{2,h}^{\bar{q}}, \gamma_{2,h}^{\bar{u}}, \gamma_{2,h}^y, \gamma_{4,h}) \\
& \in \mathbb{R}^{n_x} \times \mathbb{R}^{n_q} \times \mathbb{R}^{n_u} \times \mathbb{R}^{Mn_q} \times \mathbb{R}^{Mn_x} \times \mathbb{R}^{Mn_q} \times \mathbb{R}^{Mn_u} \times \mathbb{R}^{n_y} \times \mathbb{R} : \\
& \tilde{A}_{2,h}\gamma_{2,h}^x + \tilde{A}_{3,h}\gamma_{2,h}^q + \tilde{A}_{4,h}\gamma_{2,h}^u \leq -\tilde{b}_h\gamma_{4,h}, \\
& \sum_{m=1}^{M} \gamma_{2,h,m}^\delta = -\gamma_{4,h}, \\
& \gamma_{2,h,l,t}^u = \sum_{m=1}^{M} \gamma_{2,h,l,t,m}^{\bar{u}}, \quad \forall (l,t) \in \Omega, \\
& \gamma_{2,h,l}^x = \sum_{m=1}^{M} \gamma_{2,h,l,m}^{\bar{x}}, \quad \forall l \in \{1,\ldots,n_x\}, \\
& \gamma_{2,h,t}^q = \sum_{m=1}^{M} \gamma_{2,h,t,m}^{\bar{q}}, \quad \forall t \in \{1,\ldots,n_q\}, \\
& \gamma_{2,h,l,t,m}^{\bar{u}} \geq x_{h,l}^{\mathrm{L}}\gamma_{2,h,t,m}^{\bar{q}} + \gamma_{2,h,l,m}^{\bar{x}} q_{h,t}^m - x_{h,l}^{\mathrm{L}} q_{h,t}^m \gamma_{2,h,m}^\delta, \\
& \gamma_{2,h,l,t,m}^{\bar{u}} \geq x_{h,l}^{\mathrm{U}}\gamma_{2,h,t,m}^{\bar{q}} + \gamma_{2,h,l,m}^{\bar{x}} q_{h,t}^{m+1} - x_{h,l}^{\mathrm{U}} q_{h,t}^{m+1} \gamma_{2,h,m}^\delta, \\
& \gamma_{2,h,l,t,m}^{\bar{u}} \leq x_{h,l}^{\mathrm{U}}\gamma_{2,h,t,m}^{\bar{q}} + \gamma_{2,h,l,m}^{\bar{x}} q_{h,t}^m - x_{h,l}^{\mathrm{U}} q_{h,t}^m \gamma_{2,h,m}^\delta, \\
& \gamma_{2,h,l,t,m}^{\bar{u}} \leq x_{h,l}^{\mathrm{L}}\gamma_{2,h,t,m}^{\bar{q}} + \gamma_{2,h,l,m}^{\bar{x}} q_{h,t}^{m+1} - x_{h,l}^{\mathrm{L}} q_{h,t}^{m+1} \gamma_{2,h,m}^\delta, \\
& \quad \forall (l,t) \in \Omega, \ \ \forall m \in \{1,\ldots,M\}, \\
& B\gamma_{2,h}^y \leq -a\gamma_{4,h}, \\
& -x_h^{\mathrm{L}}\gamma_{4,h} \leq \gamma_{2,h}^x \leq -x_h^{\mathrm{U}}\gamma_{4,h}, \ \ -q_h^{\mathrm{L}}\gamma_{4,h} \leq \gamma_{2,h}^q \leq -q_h^{\mathrm{U}}\gamma_{4,h}, \\
& -x_h^{\mathrm{L}}\gamma_{2,h,m}^\delta \leq \gamma_{2,h,m}^{\bar{x}} \leq -x_h^{\mathrm{U}}\gamma_{2,h,m}^\delta, \ \ -q_h^m\gamma_{2,h,m}^\delta \leq \gamma_{2,h,m}^{\bar{q}} \leq -q_h^{m+1}\gamma_{2,h,m}^\delta, \quad \forall m \in \{1,\ldots,M\}, \\
& -y^{\mathrm{L}}\gamma_{4,h} \leq \gamma_{2,h}^y \leq -y^{\mathrm{U}}\gamma_{4,h}, \\
& \gamma_{2,h}^x \geq 0, \ \ \gamma_{2,h}^q \geq 0, \ \ \gamma_{2,h}^u \geq 0, \ \ \gamma_{2,h}^\delta \geq 0, \ \ \gamma_{2,h}^{\bar{x}} \geq 0, \ \ \gamma_{2,h}^{\bar{q}} \geq 0, \ \ \gamma_{2,h}^{\bar{u}} \geq 0, \ \ \gamma_{2,h}^y \geq 0 \ \ \}
\end{aligned}
$$

e_m is the unit vector with the m^{th} element equal to 1. $x_h^{(k)}$, $q_h^{(k)}$, $u_h^{(k)}$, $\delta_h^{(k)}$, $\bar{x}_h^{(k)}$, $\bar{q}_h^{(k)}$ and $\bar{u}_h^{(k)}$ are the solutions of Problem (PBP-LAP$_h$) at the k^{th} iteration.

The last 18 groups of constraints in Problem ($\mathrm{CGP}_{h,m}$) are listed as below:

$$\gamma_{1,h}^{y} + \gamma_{2,h}^{y} - \mathbf{1}\gamma_{5,h} \leq y^{(k)} \tag{6.60}$$

$$\gamma_{1,h}^{x} + \gamma_{2,h}^{x} - \mathbf{1}\gamma_{5,h} \leq x_{h}^{(k)} \tag{6.61}$$

$$\gamma_{1,h}^{q} + \gamma_{2,h}^{q} - \mathbf{1}\gamma_{5,h} \leq q_{h}^{(k)} \tag{6.62}$$

$$\gamma_{1,h}^{u} + \gamma_{2,h}^{u} - \mathbf{1}\gamma_{5,h} \leq u_{h}^{(k)} \tag{6.63}$$

$$\gamma_{1,h}^{\delta} + \gamma_{2,h}^{\delta} - \mathbf{1}\gamma_{5,h} \leq \delta_{h}^{(k)} \tag{6.64}$$

$$\gamma_{1,h}^{\bar{x}} + \gamma_{2,h}^{\bar{x}} - \mathbf{1}\gamma_{5,h} \leq \bar{x}_{h}^{(k)} \tag{6.65}$$

$$\gamma_{1,h}^{\bar{q}} + \gamma_{2,h}^{\bar{q}} - \mathbf{1}\gamma_{5,h} \leq \bar{q}_{h}^{(k)} \tag{6.66}$$

$$\gamma_{1,h}^{\bar{u}} + \gamma_{2,h}^{\bar{u}} - \mathbf{1}\gamma_{5,h} \leq \bar{u}_{h}^{(k)} \tag{6.67}$$

$$-\gamma_{1,h}^{y} - \gamma_{2,h}^{y} - \mathbf{1}\gamma_{5,h} \leq -y^{(k)} \tag{6.68}$$

$$-\gamma_{1,h}^{x} - \gamma_{2,h}^{x} - \mathbf{1}\gamma_{5,h} \leq -x_{h}^{(k)} \tag{6.69}$$

$$-\gamma_{1,h}^{q} - \gamma_{2,h}^{q} - \mathbf{1}\gamma_{5,h} \leq -q_{h}^{(k)} \tag{6.70}$$

$$-\gamma_{1,h}^{u} - \gamma_{2,h}^{u} - \mathbf{1}\gamma_{5,h} \leq -u_{h}^{(k)} \tag{6.71}$$

$$-\gamma_{1,h}^{\delta} - \gamma_{2,h}^{\delta} - \mathbf{1}\gamma_{5,h} \leq -\delta_{h}^{(k)} \tag{6.72}$$

$$-\gamma_{1,h}^{\bar{x}} - \gamma_{2,h}^{\bar{x}} - \mathbf{1}\gamma_{5,h} \leq -\bar{x}_{h}^{(k)} \tag{6.73}$$

$$-\gamma_{1,h}^{\bar{q}} - \gamma_{2,h}^{\bar{q}} - \mathbf{1}\gamma_{5,h} \leq -\bar{q}_{h}^{(k)} \tag{6.74}$$

$$-\gamma_{1,h}^{\bar{u}} - \gamma_{2,h}^{\bar{u}} - \mathbf{1}\gamma_{5,h} \leq -\bar{u}_{h}^{(k)} \tag{6.75}$$

$$\gamma_{3,h} + \gamma_{4,h} \leq -1 \tag{6.76}$$

$$-\gamma_{3,h} - \gamma_{4,h} \leq 1 \tag{6.77}$$

The Lagrange multipliers of Eq (6.60), (6.61), (6.62), (6.63), (6.64), (6.65), (6.66) and (6.67) are recorded as $\lambda_{\alpha^+,1,h}$, $\lambda_{\alpha^+,2,h}$, $\lambda_{\alpha^+,3,h}$, $\lambda_{\alpha^+,4,h}$, $\lambda_{\alpha^+,5,h}$, $\lambda_{\alpha^+,6,h}$, $\lambda_{\alpha^+,7,h}$ and $\lambda_{\alpha^+,8,h}$, respectively; the Lagrange multipliers of Eq (6.68), (6.69), (6.70), (6.71), (6.72), (6.73), (6.74) and (6.75) are recorded as $\lambda_{\alpha^-,1,h}$, $\lambda_{\alpha^-,2,h}$, $\lambda_{\alpha^-,3,h}$, $\lambda_{\alpha^-,4,h}$, $\lambda_{\alpha^-,5,h}$, $\lambda_{\alpha^-,6,h}$, $\lambda_{\alpha^-,7,h}$ and $\lambda_{\alpha^-,8,h}$, respectively; and the Lagrange multipliers of Eq (6.76) and (6.77) are recorded as $\lambda_{\beta^+,h}$ and $\lambda_{\beta^-,h}$, respectively. Then parameters for the new lift-

and-project cut to be added into Problem (PBP-LAP$_h$) are calculated as below:

$$\alpha_{i,h} = \lambda_{\alpha^+,i,h} - \lambda_{\alpha^-,i,h}\ , \quad i = 1, \ldots, 8 \tag{6.78}$$

$$\beta_h = \lambda_{\beta^+,h} - \lambda_{\beta^-,h} \tag{6.79}$$

Enhanced Relaxed Master problem with Lift-and-Project Cuts

The optimal solutions and Lagrange multipliers of Problem (PBP-LAP$_h$) construct enhanced optimality cuts for the relaxed master problem. The enhanced relaxed master problem with lift-and-project, called Problem (LERMP^k), is as follows:

$$\begin{aligned}
\min_{y,\eta} \quad & \eta \\
\text{s.t.} \quad & \eta \geq \bar{\bar{\alpha}}^{(j)} y + \bar{\bar{\beta}}^{(j)}, \quad \forall j \in \bar{\bar{T}}^k, \\
& \eta \geq \alpha^{(j)} y + \beta^{(j)}, \quad \forall j \in T^k, \\
& \gamma^{(i)} y + \theta^{(i)} \leq 0, \quad \forall i \in S^k, \\
& \sum_{l \in \{l: y_l^{(t)} = 1\}} y_l \ - \sum_{l \in \{l: y_l^{(t)} = 0\}} y_l \leq |\{l : y^{(t)} = 1\}| - 1, \quad \forall t \in T^k \cup S^k, \\
& y \in Y,\ \eta \in \mathbb{R},
\end{aligned} \tag{LERMP^k}$$

where

$$\begin{aligned}
\bar{\bar{\alpha}}^{(j)} &= c_1^{\mathrm{T}} + \sum_{h=1}^{s} \left(\bar{\bar{\lambda}}_h^{(j)}\right)^{\mathrm{T}} A_{1,h}, \\
\bar{\bar{\beta}}^{(j)} &= \sum_{h=1}^{s} \left[c_{2,h}^{\mathrm{T}} \bar{\bar{x}}_h^{(j)} + c_{3,h}^{\mathrm{T}} \bar{\bar{q}}_h^{(j)} + c_{4,h}^{\mathrm{T}} \bar{\bar{u}}_h^{(j)}\right] + \\
&\quad \sum_{h=1}^{s} \left[\left(\bar{\bar{\lambda}}_h^{(j)}\right)^{\mathrm{T}} \left(A_{2,h} \bar{\bar{x}}_h^{(j)} + A_{3,h} \bar{\bar{q}}_h^{(j)} + A_{4,h} \bar{\bar{u}}_h^{(j)} - b_h\right)\right],
\end{aligned}$$

$$\bar{\bar{T}}^k = \{j \in \{1, \ldots, k\} : \text{Problem PBP-LAP } \left(y^{(k)}\right) \text{ is feasible}\}.$$

$\bar{\bar{\lambda}}_h^{(j)}$ denotes the Lagrange multipliers of Problem (PBP-LAP$_h$) ($\forall h \in \{1, \ldots, s\}$) when $y = y^{(j)}$ ($\forall j \in \bar{\bar{T}}^k$). $\left(\bar{\bar{x}}_h^{(j)}, \bar{\bar{q}}_h^{(j)}, \bar{\bar{u}}_h^{(j)}\right)$ is a minimum of Problem (PBP-LAP$_h$)

$(\forall h \in \{1, \ldots, s\})$ when $y = y^{(j)}$. Note that $\bar{\bar{T}}^k \subset T^k$ due to the tighter relaxation. The first set of constraints are called enhanced optimality cuts with lift-and-project cuts.

If $T^k = \emptyset$, the feasibility relaxed master Problem (RMFP^k) introduced in Chapter 5 is solved instead. The enhanced feasibility cuts with lift-and-project cuts are not considered here.

6.5.3 Theoretical Properties

Proposition 7. *Compared to Problem (RMP^k), Problem (LERMP^k) is a tighter (or equal) relaxation of Problem (P) when Problem (P) is augmented with the Balas cuts.*

Proof. Considering that Problem (LERMP^k) differs from Problem (RMP^k) only with the first group of optimality cuts, it is obvious that Problem (LERMP^k) is a tighter relaxation if it is a valid relaxation of Problem (P). It is proved in Ref [113] that Problem (RMP^k) is a relaxation of Problem (P) when Problem (P) is augmented with the Balas cuts excluding the previously examined integer realizations, so it remains to prove

$$\text{obj}_{\text{PP}}(y) \geq \bar{\bar{\alpha}}^{(j)} y + \bar{\bar{\beta}}^{(j)}, \quad \forall j \in \bar{\bar{T}}^k, \; \forall y \in W \tag{6.80}$$

$$W = \{\hat{y} \in Y : \text{Problem P is feasible for } y = \hat{y}\}$$

For all $j \in \bar{\bar{T}}^k$ and $h \in \{1, \ldots, s\}$, due to strong duality for linear programs:

$$\begin{aligned}
\bar{\bar{\alpha}}^{(j)} y + \bar{\bar{\beta}}^{(j)} &= c_1^{\mathrm{T}} y + \sum_{h=1}^{s} \left[\inf_{\substack{(x_h, q_h, u_h, \delta_h, \\ \bar{x}_h, \bar{q}_h, \bar{u}_h) \in \bar{\Pi}_h^{\mathrm{lap}}}} c_{2,h}^{\mathrm{T}} x_h + c_{3,h}^{\mathrm{T}} q_h + c_{4,h}^{\mathrm{T}} u_h \right. \\
&\qquad \left. + \left(\bar{\bar{\lambda}}_h^{(j)} \right)^{\mathrm{T}} \left(A_{1,h} y^{(j)} + A_{2,h} x_h + A_{3,h} q_h + A_{4,h} u_h - b_h \right) \right] \\
&\qquad + \sum_{h=1}^{s} \left(\bar{\bar{\lambda}}_h^{(j)} \right)^{\mathrm{T}} A_{1,h} \left(y - y^{(j)} \right) \\
&= c_1^{\mathrm{T}} y + \sum_{h=1}^{s} \left[\inf_{\substack{(x_h, q_h, u_h, \delta_h, \\ \bar{x}_h, \bar{q}_h, \bar{u}_h) \in \bar{\Pi}_h^{\mathrm{lap}}}} c_{2,h}^{\mathrm{T}} x_h + c_{3,h}^{\mathrm{T}} q_h + c_{4,h}^{\mathrm{T}} u_h \right. \\
&\qquad \left. + \left(\bar{\bar{\lambda}}_h^{(j)} \right)^{\mathrm{T}} \left(A_{1,h} y + A_{2,h} x_h + A_{3,h} q_h + A_{4,h} u_h - b_h \right) \right] \\
&= c_1^{\mathrm{T}} y + \mathrm{obj}_{\mathrm{PBP-LAP}_h}(y) \\
&= \mathrm{obj}_{\mathrm{PBP-LAP}}(y)
\end{aligned} \tag{6.81}$$

Since Problem (PBP-LAP) is a relaxation of Problem (PP),

$$\mathrm{obj}_{\mathrm{PP}}(y) \geq \mathrm{obj}_{\mathrm{PBP-LAP}}(y), \quad \forall y \in W \tag{6.82}$$

Eqs (6.81) and (6.82) imply Eq (6.80). □

6.5.4 Enhanced Decomposition Algorithm with Lift-and-Project Cuts

The enhanced decomposition algorithm with lift-and-project cuts is stated as below:

Initialize:

1. Iteration counters $k = 0$, $l = 1$, and the index sets $T^0 = \emptyset$, $\bar{\bar{T}}^0 = \emptyset$, $S^0 = \emptyset$, $U^0 = \emptyset$.

2. Upper bound on the problem UBD $= +\infty$, upper bound on the lower bounding problem UBDPB $= +\infty$, lower bound on the lower bounding problem LBD $= -\infty$.

3. The number of lift-and-project cuts $n_{l,h} = 0$ for each scenario $h = 1, \ldots, s$.

4. Set tolerances ϵ_h and ϵ such that $\sum_{h=1}^{s} \epsilon_h \leq \epsilon$.

5. Integer realization $y^{(1)}$ is given.

repeat

if $k = 0$ or (Problem (LERMP^k) is feasible and LBD $<$ UBDPB and LBD $<$ UBD $- \epsilon$) **then**

repeat

Set $k = k + 1$

1. Solve the decomposed primal bounding problem (PBP$_h(y^{(k)})$) for each scenario $h = 1, ..., s$ sequentially. If Problem (PBP$_h(y^{(k)})$) is feasible for all the scenarios with Lagrange multipliers $\lambda_h^{(k)}$, add optimality cuts to the enhanced relaxed master problem (LERMP^k) according to $\lambda_1^{(k)}, ..., \lambda_s^{(k)}$, set $T^k = T^{k-1} \cup \{k\}$.

2. If Problem (PBP$_h(y^{(k)})$) is feasible for all the scenarios, solve subproblem (PBP-LAP$_h(y^{(k)})$) for each scenario $h = 1, ..., s$ sequentially. If Problem (PBP-LAP$_h(y^{(k)})$) is feasible with Lagrange multipliers $\bar{\bar{\lambda}}_h^{(k)}$ for all the scenarios, add enhanced optimality cuts to Problem (LERMP^k) according to $\bar{\bar{\lambda}}_1^{(k)}, ..., \bar{\bar{\lambda}}_s^{(k)}$, set $\bar{\bar{T}}^k = \bar{\bar{T}}^{k-1} \cup \{k\}$, and record the optimal solutions $x_h^{(k)}$, $q_h^{(k)}$, $u_h^{(k)}$, $\delta_h^{(k)}$, $\bar{x}_h^{(k)}$, $\bar{q}_h^{(k)}$, $\bar{u}_h^{(k)}$ for all s scenarios. If obj$_{\text{PBP-LAP}}(y^{(k)}) <$ UBDPB, update UBDPB $=$ obj$_{\text{PBP-LAP}}(y^{(k)})$, $y^* = y^{(k)}$, $k^* = k$.

3. If Problem (PBP-LAP$_h(y^{(k)})$) is feasible, check the integrality of relaxed binary variables $\delta_h^{(k)}$ in all s scenario. For each scenario $h = 1, ..., s$, for each $m = 1, ..., M$, if $\delta_{h,m}^{(k)}$ does not satisfy integrality, solve the corresponding cut generation problem (CGP$_{h,m}$), record parameters α_h, β_h, set $n_{l,h} = n_{l,h}+1$, add the new lift-and-project cut into Problem (PBP-LAP$_h(y^{(k+1)})$).

4. If Problem ($\text{PBP}_h(y^{(k)})$) is infeasible for one scenario, stop solving it for the remaining scenarios and set $S^k = S^{k-1} \cup \{k\}$. Then, solve the decomposed feasibility subproblem ($\text{FP}_h(y^{(k)})$) for $h = 1, ..., s$ and obtain the corresponding Lagrange multipliers $\mu_h^{(k)}$. Add feasibility cuts to Problem (LERMP^k) according to these multipliers.

5. If $T^k = \emptyset$, solve the feasibility problem (RMFP^k); otherwise, solve Problem (LERMP^k). In the latter case, if Problem (LERMP^k) is feasible, set LBD to its optimal objective value. In both cases, set $y^{(k+1)}$ to the y value at the solution of either problem.

until LBD $\geq$ UBDPB or (Problem (LERMP^k) or (RMFP^k) is infeasible).

end if

if UBDPB $<$ UBD $- \epsilon$ **then**

1. Solve the decomposed primal subproblem ($\text{PP}_h(y^*)$) to ϵ_h-optimality for each scenario $h = 1, ..., s$ sequentially. Set $U^l = U^{l-1} \cup \{k^*\}$. If Problem ($\text{PP}_h(y^*)$) is feasible with optimum (x_h^*, q_h^*, u_h^*) for all the scenarios and $\text{obj}_{\text{PP}}(y^*) <$ UBD, update UBD $= \text{obj}_{\text{PP}}(y^*)$ and set $y_p^* = y^*$, $(x_{p,h}^*, q_{p,h}^*, u_{p,h}^*) = (x_h^*, q_h^*, u_h^*)$ for $h = 1, \ldots, s$.

2. If $\bar{\bar{T}}^k \setminus U^l = \emptyset$, set UBDPB $= +\infty$.

3. If $\bar{\bar{T}}^k \setminus U^l \neq \emptyset$, pick $i \in \bar{\bar{T}}^k \setminus U^l$ such that $\text{obj}_{\text{PBP-LAP}}(y^{(i)}) = \min_{j \in \bar{\bar{T}}^k \setminus U^l} \{\text{obj}_{\text{PBP-LAP}}(y^{(j)})\}$ Update UBDPB $= \text{obj}_{\text{PBP-LAP}}(y^{(i)})$, $y^* = y^{(i)}$, $k^* = i$. Set $l = l + 1$.

end if

until UBDPB $\geq$ UBD $- \epsilon$ and ((Problem (LERMP^k) or (RMFP^k) is infeasible) or LBD $\geq$ UBD $- \epsilon$).

An ϵ-global optimum of the original problem (P) is given by

$$(y_p^*, x_{p,1}^*, ..., x_{p,s}^*, q_{p,1}^*, ..., q_{p,s}^*, u_{p,1}^*, ..., u_{p,s}^*)$$

or (P) is infeasible.

The algorithm flowchart is shown in Figure 6-6, in which differences between the enhanced decomposition algorithm and the original decomposition algorithm are highlighted in grey. Compared to the flowchart of the original decomposition algorithm, three new steps, "PBP-LAP (LP)", "Cut Generation Problems (LP)" and "Update Lift-and-project Cuts", are added in this flowchart, and the step "Relaxed Master Problem" is replaced by "Enhanced Relaxed Master Problem". The dashed line in the flowchart means an information flow, instead of a step in the algorithm. The selection of the integer realization $y^{(k)}$ for constructing primal subproblems (PP_h) is based on $\mathrm{obj}_{\mathrm{PBP-LAP}}(y^{(k)})$.

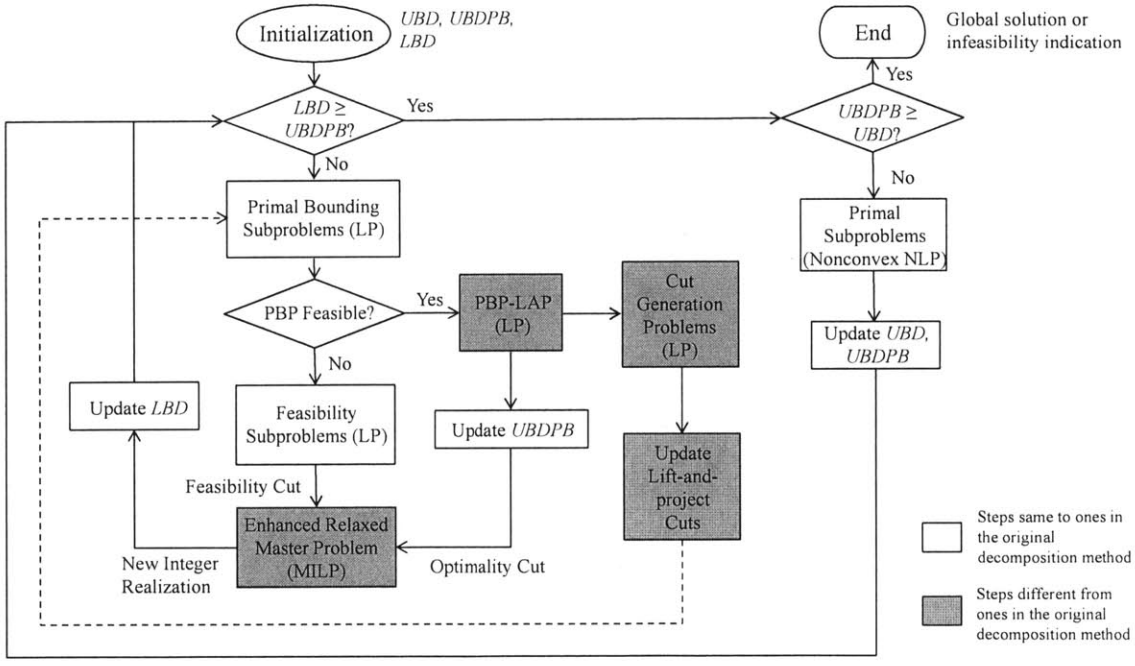

Figure 6-6: Flowchart for the enhanced decomposition algorithm with lift-and-project cuts.

The convergence property for the enhanced NGBD holds according to Theorem 1.

6.6 Conclusions

By employing enhancement technologies, the decomposition algorithm achieves much faster convergence rates, and solves large-scale polygeneration optimization problems in reasonable times. The computational performance of enhanced decomposition algorithms will be shown in Chapter 7.

Chapter 7

Case Studies of Polygeneration Problems with Decomposition Algorithms

7.1 Model Reformulations

The objective of the optimization model is to maximize the overall economic performance of the flexible polygeneration plant while satisfying all design constraints and operational constraints in all scenarios (here a scenario represents a time period in the year or a possible market/policy scenario, as described in the section of case study problems and implementation). The key design decision variables are equipment capacities. The key operational decision variables include the consumption rates of feedstocks (coal, biomass and water), the production rates of products (power, naphtha, diesel, methanol and sulfur), the CO_2 sequestration rate and the CO_2 emission rate. The mathematical model in this section is reformulated from the flexible polygeneration model in Chapter 4. The major reformulations, including the application of aggregate equipment and discrete equipment capacities, were implemented in the capital cost calculations in the original model and will be discussed in the remaining part of this section.

7.1.1 Aggregate Equipment

The concept of "aggregate equipment" is introduced in this model to simplify the economic analysis and reduce the complexity of the model. Aggregate equipment is a set of equipment within the same subsystem that follow a similar scaling-up relationship. In capital cost calculations, aggregate equipment can be treated as a single unit with a scaling-up factor equal to the weighted average of all equipment in the group. Therefore, the number of units in the economic analysis is reduced from thirty to seven sets of aggregate equipment whose capacities need to be determined, including Syngas Cleaning System 1 (for the liquid fuel production), Syngas Cleaning System 2 (for the power production), the CO_2 compressor, the Fischer-Tropsch synthesis system, the methanol synthesis system, the gas turbine system, and the steam turbine system. These are illustrated in Figure 7-1, where each set of aggregate equipment is placed in the same position as Figure 2-2. Optimization of equipment capacities is therefore based on the seven sets of aggregate equipment instead of the thirty individual pieces of equipment.

In this work, the dry mass capacity of the gasifier is fixed to 1042 ton/h or 7.815 Mt/yr on the basis of industrial experience of BP engineers [9] (Mt = million tons). Therefore, the accessory equipment of the gasifier (including the radiant cooler and the convective cooler) and upstream and downstream equipment whose capacities are determined by the gasifier (such as the air separation unit(ASU), the COS hydrolysis reactor, Selexol Unit 1, and the Claus plant), also have fixed capacities. All equipment with fixed capacities are grouped into one set of aggregate equipment (as shown in Figure 7-1 with the same position as in Figure 2-2), whose capacity is a specified parameter in the optimization model.

Note that the concept of aggregate equipment is only applied to the economic analysis, and all mass and energy balances are still based on individual equipment and are the same as those in Chapter 4.

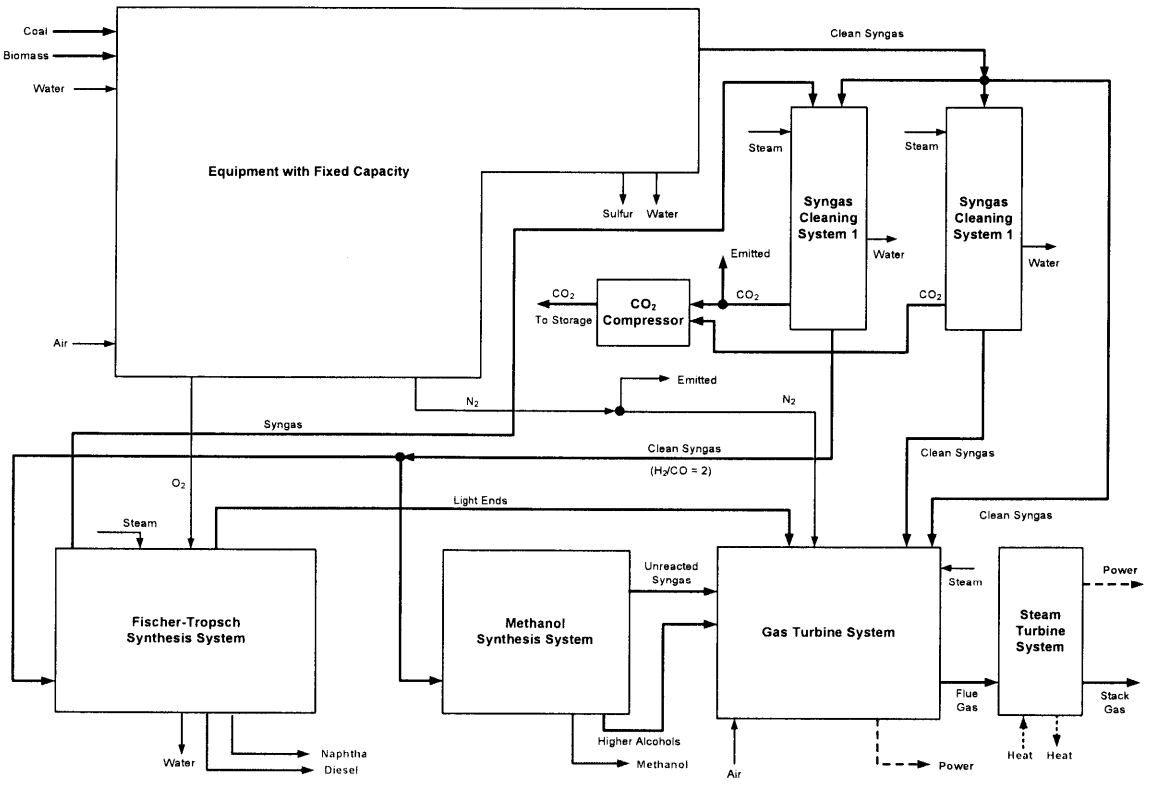

Figure 7-1: Illustration of aggregate equipment.

7.1.2 Discrete Capital Costs

The other major model reformulation is to change the equipment capacity variables in the optimization formulation from continuous variables to discrete variables. There are two reasons for this reformulation: (1) The current version of the decomposition method is developed for problems whose first stage decision variables (or design decision variables) contain only integer variables. Equipment capacities, which are design decision variables, need to be discretized to fit the framework of the decomposition method. A direction for future research is to develop new versions of the decomposition method that can also handle continuous design decision variables. (2) In real applications, only a limited number of sizes are available in the market for many kinds of equipment, including gas turbines and steam turbines. It is therefore more reasonable to model these equipment capacities as discrete choices instead of continuous variables.

The capacity of a set of aggregate equipment w is now expressed as

$$E_w = \sum_{v=1}^{d} \bar{E}_{w,v} y_{w,v}, \quad \forall w \in \{1, \ldots, e\}, \tag{7.1}$$

where $\bar{E}_{w,v}$ is the v^{th} choice for the capacity of the set of equipment w, which is a specified parameter; $y_{w,v}$ is a binary variable that determines whether the v^{th} choice for the capacity of the set of equipment w is selected or not. d is the number of all choices for each set of equipment; e is the number of sets of aggregate equipment without fixed capacity, which is equal to 7. In this work, in order to obtain sufficiently accurate economic analysis results while keeping the optimization problem tractable for the decomposition algorithm, d is set to be 10.

The choices for the capacity of the set of equipment w ($\bar{E}_{w,v}$) are assumed to be uniformly distributed and can be generated as follows

$$\bar{E}_{w,v} = \bar{E}_w^{\text{L}} + \frac{v-1}{d-1}\left(\bar{E}_w^{\text{U}} - \bar{E}_w^{\text{L}}\right), \quad \forall w \in \{1, \ldots, e\}, \tag{7.2}$$

where $\bar{E}_w^{\text{L}}$ and $\bar{E}_w^{\text{U}}$ are the minimum and maximum possible capacity for the set of equipment w in the process, respectively, which are specified parameters. $\bar{E}_w^{\text{L}}$ and $\bar{E}_w^{\text{U}}$ can be estimated by the rough mass balance calculations given the aforementioned gasifier capacity, and their values are listed in Table 7.1.

Table 7.1: Parameters for equipment capacities

Aggregate Equipment w	$\bar{E}_w^{\text{L}}$	$\bar{E}_w^{\text{U}}$	
Syngas Cleaning System 1	0	150	Mmol/h
Syngas Cleaning System 2	0	205	Mmol/h
CO_2 Compressor	0	2500	ton/h
Fischer-Tropsch Synthesis System	0	340	ton/h
Methanol Synthesis System	0	840	ton/h
Gas Turbine System	200	4750	MW
Steam Turbine System	600	1800	MW

Only one choice for capacity can be selected for each set of equipment, therefore

the following relationship holds

$$\sum_{v=1}^{d} y_{w,v} = 1, \quad \forall w \in \{1, \ldots, e\}. \tag{7.3}$$

The flow rate through each set of equipment is limited by its capacity, hence

$$F_{w,h} \leq E_w, \quad \forall w \in \{1, \ldots, e\}, \ \forall h \in \{1, \ldots, s\}, \tag{7.4}$$

where $F_{w,h}$ is the input (or output) flow rate of the set of equipment w in scenario h. s is the number of scenarios, which is a given number.

The capital cost of a set of equipment w is given by

$$C_w = \sum_{v=1}^{d} \bar{C}_{w,v} y_{w,v}, \quad \forall w \in \{1, \ldots, e\}, \tag{7.5}$$

where $\bar{C}_{w,v}$ is the v^{th} choice for the capital cost of the set of equipment w, which is a specified parameter.

The choices for the capital cost of the set of equipment w ($\bar{C}_{w,v}$) are estimated by the following power law scaling relationship

$$\bar{C}_{w,v} = \bar{C}_{\text{b},w} \left(\frac{\bar{E}_{w,v}}{\bar{E}_{\text{b},w}} \right)^{\text{sf}_w}, \quad \forall w \in \{1, \ldots, e\}, \ \forall v \in \{1, \ldots, d\}, \tag{7.6}$$

where $\bar{E}_{\text{b},w}$ is the capacity of the set of equipment w in the base case, $\bar{C}_{\text{b},w}$ is the capital cost of the set of equipment w in the corresponding base case, and sf_w is the sizing factor of the set of equipment w, which are specified parameters. The values of $\bar{E}_{\text{b},w}$, $\bar{C}_{\text{b},w}$ and sf_w for aggragate equipment, which are estimated from those for individual equipment in Appendix B, are provided in Table 7.2.

The total capital investment for the plant is given by

$$\text{Cap} = \sum_{w=1}^{e} C_w + \bar{C}_{\text{f}}, \tag{7.7}$$

where $\bar{C}_{\text{f}}$ is the total capital cost of equipment with fixed capacity, which is a specified

Table 7.2: Parameters for equipment capital costs

Aggregate Equipment w	$\bar{E}_{\mathrm{b},w}$		$\bar{C}_{\mathrm{b},w}{}^{a}$	sf_w
Syngas Cleaning System 1	28.2	Mmol/h	34.0	0.69
Syngas Cleaning System 2	28.2	Mmol/h	34.0	0.69
CO_2 Compressor	469.0	ton/h	75.1	0.80
Fischer-Tropsch Synthesis System	34.2	ton/h	183.4	0.70
Methanol Synthesis System	110.4	ton/h	220.3	0.67
Gas Turbine System	464.0	MW	136.4	0.76
Steam Turbine System	274.7	MW	123.3	0.69

[a] The unit is million dollars.

parameter. In this work, $\bar{C}_{\mathrm{f}} = 2978$ million dollars.

The net present value (NPV) is denoted by

$$\begin{aligned} \mathrm{NPV} = \mathrm{Cap}\left[-1 + \frac{R_{\mathrm{tax}}}{t_{\mathrm{dp}}}\frac{1}{r}\left(1 - \frac{1}{(1+r)^{t_{\mathrm{dp}}}}\right)\right] \\ + \sum_{h=1}^{s} \mathrm{Occu}_h\, \mathrm{Pro}_{\mathrm{net},h}\, \frac{1}{r}\left(1 - \frac{1}{(1+r)^{t_{\mathrm{lf}}}}\right), \end{aligned} \tag{7.8}$$

where $\mathrm{Pro}_{\mathrm{net},h}$ is the annualized net profit in scenario h. Occu_h is the fraction of occurrence of scenario h, R_{tax} is the tax rate (including both federal and state taxes), r is the annual discount rate, t_{dp} is the depreciation time of the project, and t_{lf} is the lifetime of the project, which are specified parameters. In this study, $R_{\mathrm{tax}} = 40\%$ [173, 174], $r = 12\%$ [173, 174], $t_{\mathrm{dp}} = 10\mathrm{yr}$ [158], and $t_{\mathrm{lf}} = 30\mathrm{yr}$ [173, 174].

For the ease of computation, the objective of this model is selected to be the scaled NPV, which is given as follows

$$\begin{aligned} \mathrm{NPV}_{\mathrm{scale}} &= \frac{\mathrm{NPV}}{\frac{1}{r}\left(1 - \frac{1}{(1+r)^{t_{\mathrm{lf}}}}\right)} \\ &= \sum_{h=1}^{s} \mathrm{Occu}_h\, \mathrm{Pro}_{\mathrm{net},h} + \mathrm{Cap}\,\frac{-1 + \frac{R_{\mathrm{tax}}}{t_{\mathrm{dp}}}\frac{1}{r}\left(1 - \frac{1}{(1+r)^{t_{\mathrm{dp}}}}\right)}{\frac{1}{r}\left(1 - \frac{1}{(1+r)^{t_{\mathrm{lf}}}}\right)}. \end{aligned} \tag{7.9}$$

The binary variables $y_{w,v}$ ($\forall w \in \{1,\ldots,e\}, \forall v \in \{1,\ldots,d\}$) are the only design

decision variables in this model. All other design variables, including E_w, C_w, and Cap, can be replaced by their expressions in terms of $y_{w,v}$ (such as Equations (7.1) (7.5) and (7.7)).

Therefore, the only design constraints in this model are

$$F_{w,h} \leq \sum_{v=1}^{d} \bar{E}_{w,v} y_{w,v}, \quad \forall w \in \{1,\ldots,e\},\ \forall h \in \{1,\ldots,s\}, \tag{7.10}$$

The objective function to be minimized is expressed as

$$-\mathrm{NPV}_{\mathrm{scale}} = -\sum_{h=1}^{s} \mathrm{Occu}_h\ \mathrm{Pro}_{\mathrm{net},h} - \left(\sum_{w=1}^{e}\sum_{v=1}^{d} \bar{C}_{w,v} y_{w,v} + \bar{C}_{\mathrm{f}}\right) \frac{-1 + \frac{R_{\mathrm{tax}}}{t_{\mathrm{dp}}} \frac{1}{r}\left(1 - \frac{1}{(1+r)^{t_{\mathrm{dp}}}}\right)}{\frac{1}{r}\left(1 - \frac{1}{(1+r)^{t_{\mathrm{lf}}}}\right)}. \tag{7.11}$$

Estimation of equipment capacity and cost parameters, including $\bar{E}_{w,v}$ and $\bar{C}_{w,v}$ ($\forall w \in \{1,\ldots,e\}, \forall v \in \{1,\ldots,d\}$), are provided in Appendix.

7.1.3 Other Reformulations

Topology constraints for aggregate equipment are added into the model to reduce the integer possibilities. The minimum capacity of equipment ($\bar{E}^{\mathrm{L}}_w$) (or the first choice for equipment capacity) is typically set to be zero (except for the gas turbine system and steam turbine system), which implies the set of equipment is not included in the process. The following topology constraint indicates that if an upstream unit is not included, all downstream equipment should not be included either:

$$y_{w_{\mathrm{u}},1} \leq y_{w_{\mathrm{d}},1} \tag{7.12}$$

where $y_{w_{\mathrm{u}},1}$ and $y_{w_{\mathrm{d}},1}$ are the 1$^{\mathrm{st}}$ choice for capacity of a set of upper stream equipment w_{u} and a set of downstream equipment w_{d}, respectively.

The reformulation-linearization technique is employed to generate redundant constraints for tighter convex relaxations. The resulting model is similar to the pq-formulation [168] for the pooling problem.

7.1.4 Model Summary

The optimization model for flexible polygeneration systems is a large-scale nonconvex MINLP, including 70 binary variables and $613s$ continuous variables. s is the number of scenarios. A scenario represents a time period in multi-period optimization problems or a possible realization in stochastic optimization problems. The nonconvexity originates from bilinear terms in mass balances. The overall model can be expressed in the form of Problem (P)

$$\begin{aligned}
\min_{\substack{y,x_1,\ldots,x_s,\\ q_1,\ldots,q_s,u_1,\ldots,u_s}} \quad & c_1^{\mathrm{T}} y + \sum_{h=1}^{s} \left(c_{2,h}^{\mathrm{T}} x_h + c_{3,h}^{\mathrm{T}} q_h + c_{4,h}^{\mathrm{T}} u_h \right) \\
\text{s.t.} \quad & u_{h,l,t} = x_{h,l} q_{h,t}, \quad \forall (l,t) \in \Omega, \ \forall h \in \{1,\ldots,s\}, \\
& A_{1,h} y + A_{2,h} x_h + A_{3,h} q_h + A_{4,h} u_h \leq b_h, \quad \forall h \in \{1,\ldots,s\}, \\
& (x_h, q_h, u_h) \in \Pi_h, \ \forall h \in \{1,\ldots,s\}, \quad y \in Y,
\end{aligned} \tag{7.13}$$

where x_h represents flow rates and heat/power consumption rates in scenario h, q_h represents split fractions in scenario h, and u_h represents intermediate variables introduced for bilinear terms in scenario h, which are all continuous variables; y represents the binary variables that determine equipment capacities (which is equivalent to $y_{w,v}$); the objective function is the general form of Equation (7.11); the first set of constraints represent the bilinear functions in mass balances, which are the only nonconvex functions in the model; the second set of constraints represent the design constraints (or equipment capacity constraints as shown in Equation (7.10)), which contain both the binary and continuous variables. The set for the continuous variables is

$$\begin{aligned}
\Pi_h = \{ (x_h, q_h, u_h) \in \mathbb{R}^{n_x} \times \mathbb{R}^{n_q} \times \mathbb{R}^{n_u} : \tilde{A}_{2,h} x_h + \tilde{A}_{3,h} q_h + \tilde{A}_{4,h} u_h \leq \tilde{b}_h, \\
x_h^{\mathrm{L}} \leq x_h \leq x_h^{\mathrm{U}}, \ q_h^{\mathrm{L}} \leq q_h \leq q_h^{\mathrm{U}} \ \},
\end{aligned}$$

where the inequality represents the linear operational constraints, including mass and energy balances, production and feedstock consumption rates, reactor feedstock specifications, and emission regulations; x_h^{L}, x_h^{U}, q_h^{L}, and q_h^{U} are the lower and upper

bounds for x_h, q_h, respectively. The set for the binary variables is

$$Y = \{y \in \{0,1\}^{n_y} : By \leq a\}.$$

where the inequality represents Equations (7.3) and (7.12).

7.2 Case Study Problems and Implementation

Three case study problems are investigated in this work, which are modified from the case study problems in Chapter 4. Case 1 and 2 are multiperiod optimization problems considering operations in different time periods during the project lifetime, and Case 3 is a stochastic optimization problem addressing both market/policy uncertainties and different time periods.

7.2.1 Description of Case 1 and 2

The description and problem sizes of Case 1 and 2 are listed in Table 7.3.

Table 7.3: Case study problems (Case 1 and 2)

	Case 1	**Case 2**
Settings	Middle oil price Middle carbon tax 100% operational flexibility	Middle oil price Middle carbon tax 100% operational flexibility
Number of Scenarios	8	24
Description of Scenarios	Peak and off-peak times in 4 seasons	Peak and off-peak times in 12 months
Number of Binary Variables	70	70
Number of Continuous Variables	4904	14712

The average feedstock prices, average product prices and carbon tax for Case 1 and 2, which are under the middle oil price and middle carbon tax, are provided in Chapter 4, and are listed in Table 7.4.

Table 7.4: Average market prices and carbon tax in Case 1 and 2

	Value	Unit
Feedstock Price		
Coal	39.5	\$/tonne
Biomass	59.2	\$/tonne
Water	0.8	\$/tonne
Product Price		
Electricity	98.9	\$/MWh
Naphtha	1012.8	\$/tonne
Diesel	1035.5	\$/tonne
Methanol	449.8	\$/tonne
Sulfur	100.0	\$/tonne
Carbon Tax	20.0	\$/tonne of CO_2

The peak time is defined to be 7 am - 11 pm on working days, and the off-peak time is the rest of the time in the year, including 11 pm - 7 am on weekdays, and the whole day on weekends and holidays. The fraction of occurrence of all scenarios over the lifetime of the plant for Cases 1 and 2 are given in Tables 7.5 and 7.6, respectively.

For simplicity, the feedstock prices and sulfur price are assumed to be constant in all scenarios for Case 1 and 2, whose values are equal to their average prices. The prices of other products, including power, naphtha, diesel, and methanol, vary seasonally, and the power price also changes between peak and off-peak. The product prices (except for sulfur) in each scenario are given by the following relationship

$$P^{\mathrm{p}}_{q,h} = P^{\mathrm{p}}_{q}\,\mathrm{ScF}_{q,h}, \quad \forall q \in \mathrm{Prod}/\{\mathrm{sulfur}\}, \ \forall h \in \{1,\ldots,s\}, \tag{7.14}$$

where $P^{\mathrm{p}}_{q,h}$ is the price of product q in scenario h, P^{p}_{q} is the average price of product q whose value is given in Table 7.4, $\mathrm{ScF}_{q,h}$ is the scale factor for the product q in scenario h. Prod $\equiv$ {electricity, naphtha, diesel, methanol, sulfur} is the set of products. The scale factors represent the degree of fluctuation of product prices in different scenarios. Their values for Cases 1 and 2, which are estimated from historical market data [3, 5, 4], are shown in Figures 7-2 and 7-3.

Table 7.5: Fractions of occurrence of all scenarios for Case 1

Scenario	Occurrence
Spring Peak [a]	12.01%
Spring Off-peak	13.21%
Summer Peak [b]	11.82%
Summer Off-peak	13.39%
Fall Peak [c]	11.32%
Fall Off-peak	13.61%
Winter Peak [d]	11.19%
Winter Off-peak	13.46%

[a] Spring ≡ {March, April, May}.
[b] Summer ≡ {June, July, August}.
[c] Fall ≡ {September, October, November}.
[d] Winter ≡ {December, January, February}.

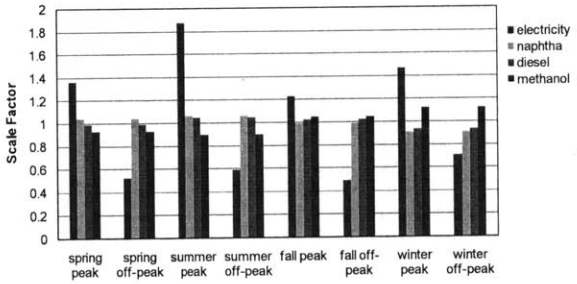

Figure 7-2: Scale factors of product prices in all scenarios for Case 1.

7.2.2 Description of Case 3

The description and problem sizes of Case 3 are listed in Table 7.7.

In total nine uncertain scenarios are considered in Case 3, including 3 oil price scenarios (low, middle and high oil prices) combined with 3 carbon tax scenarios (low, middle and high carbon taxes). Case 3 is viewed as an extension of Case 1 to stochastic optimization applications.

Other than Case 1 and 2, both feedstock and product prices change in different scenarios. The feedstock and product prices in all scenarios for Case 3 are expressed as

$$P^{\mathrm{f}}_{q,h} = P^{\mathrm{f}}_{q}\,\mathrm{ScF}_{q,h}, \quad \forall q \in \mathrm{Feed}, \ \forall h \in \{1,\ldots,s\}, \tag{7.15}$$

Table 7.6: Fractions of occurrence of all scenarios for Case 2

Scenario	**Occurrence**
January Peak	3.86%
January Off-peak	4.63%
February Peak	3.65%
February Off-peak	4.02%
March Peak	4.04%
March Off-peak	4.45%
April Peak	3.91%
April Off-peak	4.31%
May Peak	4.04%
May Off-peak	4.45%
June Peak	3.91%
June Off-peak	4.31%
July Peak	3.86%
July Off-peak	4.63%
August Peak	4.04%
August Off-peak	4.45%
September Peak	3.73%
September Off-peak	4.49%
October Peak	4.05%
October Off-peak	4.45%
November Peak	3.55%
November Off-peak	4.67%
December Peak	3.68%
December Off-peak	4.82%

$$P^{\mathrm{p}}_{q,h} = P^{\mathrm{p}}_{q}\ \mathrm{ScF}_{q,h}, \quad \forall q \in \mathrm{Prod}, \ \forall h \in \{1, \ldots, s\}, \tag{7.16}$$

where $P^{\mathrm{f}}_{q,h}$ is the price of feedstock q in scenario h, P^{f}_{q} is the average price of feedstock q, $\mathrm{ScF}_{q,h}$ is the scale factor for the feedstock or product q in scenario h. Feed $\equiv$ {coal, biomass, water} is the set of feedstocks.

The carbon tax in all scenarios for Case 3 are expressed as

$$P^{\mathrm{car}}_{\mathrm{tax},h} = P^{\mathrm{car}}_{\mathrm{tax}}\ \mathrm{ScF}^{\mathrm{car}}_{\mathrm{tax},h}, \quad \forall h \in \{1, \ldots, s\}, \tag{7.17}$$

where $P^{\mathrm{car}}_{\mathrm{tax},h}$ is the carbon tax in scenario h, $P^{\mathrm{car}}_{\mathrm{tax}}$ is the average carbon tax, $\mathrm{ScF}^{\mathrm{car}}_{\mathrm{tax},h}$

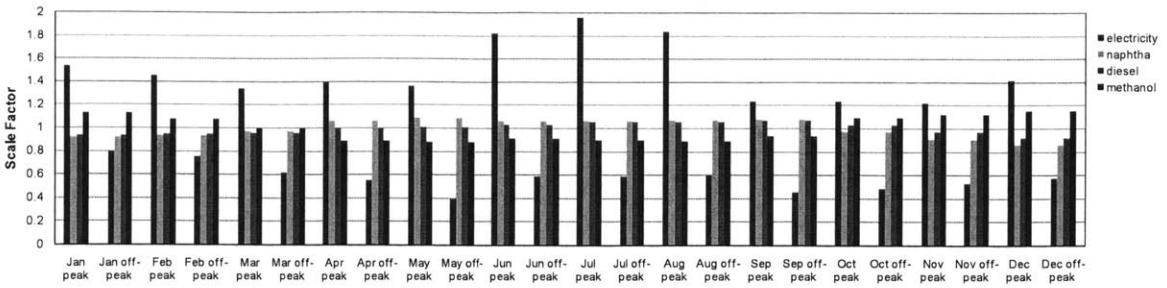

Figure 7-3: Scale factors of product prices in all scenarios for Case 2.

Table 7.7: Case study problem (Case 3)

	Case 3
Settings	Stochastic optimization for 9 market/policy scenarios 100% operational flexibility
Number of Scenarios	72
Description of Scenarios	3 oil price scenarios × 3 carbon tax scenarios × Peak and off-peak times in 4 seasons
Number of Binary Variables	70
Number of Continuous Variables	44136

is the scale factor for the carbon tax in scenario h.

The average feedstock prices, product prices and carbon tax over all uncertain market/policy scenarios and time periods for Case 3 are listed in Table 7.8.

The scale factors of feedstock and product prices in all scenarios for Case 3 are given as

$$\mathrm{ScF}_{q,h} = \mathrm{ScF}_{q,h'}\,\mathrm{ScF}_{q,h''},$$
$$\forall q \in \text{Feed} \cup \text{Prod},\ \forall h \in \{1,\ldots,s\},\ \forall h' \in \{1,\ldots,s'\},\ \forall h'' \in \{1,\ldots,s''\} \tag{7.18}$$

where h' and h'' are the indexes of scenarios representing market/policy uncertainties and time periods, respectively; s' and s'' are the numbers of uncertain scenarios and time periods, respectively. In Case 3, $s' = 9$, $s'' = 8$. $s = s' \times s''$ is the number of total scenarios. $\mathrm{ScF}_{q,h'}$ and $\mathrm{ScF}_{q,h''}$ are scale factors of market prices in uncertain scenario

Table 7.8: Average market prices and carbon tax in Case 3

	Value	Unit
Feedstock Price		
Coal	39.2	\$/tonne
Biomass	58.8	\$/tonne
Water	0.8	\$/tonne
Product Price		
Electricity	97.3	\$/MWh
Naphtha	990.2	\$/tonne
Diesel	1027.6	\$/tonne
Methanol	433.1	\$/tonne
Sulfur	100.0	\$/tonne
Carbon Tax	26.7	\$/tonne of CO_2

h' and time period h'', respectively. The values of $\mathrm{ScF}_{q,h''}$ in Case 3 are the same as those in Case 1, e.g., $\mathrm{ScF}_{q,h''} = 1$ for all feedstocks and sulfur, and $\mathrm{ScF}_{q,h''}$ for all products except sulfur are shown in Figure 7-2. The values of $\mathrm{ScF}_{q,h'}$ only change in different oil price scenarios, as provided in Table 7.9.

Table 7.9: Scale factors of market prices under different oil price scenarios

	Low Oil Price	Middle Oil Price	High Oil Price
Feedstock			
Coal	0.9351	1.0081	1.0568
Biomass	0.9351	1.0081	1.0568
Water	1	1	1
Product			
Electricity	0.6918	1.0161	1.2921
Naphtha	0.536	1.0228	1.4412
Diesel	0.5471	1.0077	1.4452
Methanol	0.6075	1.0387	1.3537
Sulfur	1	1	1

The scale factors of carbon tax in all scenarios for Case 3 are given as

$$\mathrm{ScF}^{\mathrm{car}}_{\mathrm{tax},h} = \mathrm{ScF}^{\mathrm{car}}_{\mathrm{tax},h'}\,\mathrm{ScF}^{\mathrm{car}}_{\mathrm{tax},h''}, \quad \forall h \in \{1,\ldots,s\},\ \forall h' \in \{1,\ldots,s'\},\ \forall h'' \in \{1,\ldots,s''\} \tag{7.19}$$

$\mathrm{ScF}^{\mathrm{car}}_{\mathrm{tax},h'}$ and $\mathrm{ScF}^{\mathrm{car}}_{\mathrm{tax},h''}$ are scale factors of the carbon tax in uncertain scenario h' and time period h'', respectively. $\mathrm{ScF}^{\mathrm{car}}_{\mathrm{tax},h''} = 1$ since the carbon tax remains the same in different time periods. The values of $\mathrm{ScF}^{\mathrm{car}}_{\mathrm{tax},h'}$ only change in different carbon tax scenarios, as provided in Table 7.10.

Table 7.10: Scale factors of the carbon tax under different carbon tax scenarios

	Low Carbon Tax	**Middle Carbon Tax**	**High Carbon Tax**
Carbon Tax	0.375	0.75	1.875

The fraction of occurrence of all scenarios for Cases 3 is given by the following relationship

$$\mathrm{Occu}_h = \mathrm{Occu}_{h'}\,\mathrm{Occu}_{h''}, \quad \forall h \in \{1,\ldots,s\},\ \forall h' \in \{1,\ldots,s'\},\ \forall h'' \in \{1,\ldots,s''\} \tag{7.20}$$

where $\mathrm{Occu}_{h'}$ and $\mathrm{Occu}_{h''}$ are fractions of occurrence of uncertain scenario h' and time period h'', respectively. The values of $\mathrm{Occu}_{h''}$ are provided in Table 7.5, which are the same as those in Case 1. Three oil price scenarios are assumed to have the same probability, i.e., the probability of each oil price scenario is equal to 1/3. Similar for three carbon tax scenarios. Hence, $\mathrm{Occu}_{h'} = 1/9$ for each combined oil price and carbon tax scenario h'.

7.2.3 Implementation

The solver times for the following six methods are compared for the aforementioned three case study problems: (1) branch-and-reduce method (realized by **BARON** 9.0.6 [169]), (2) **NGBD**, (3) enhanced NGBD with primal dual cuts (**NGBD-D**) (and also with primal dual multicuts, **NGBD-MD**), (4) enhanced NGBD with piecewise

convex relaxation (**NGBD-PCR**), (5) enhanced NGBD with both primal dual cuts and piecewise convex relaxation (**NGBD-D-PCR**), (6) enhanced NGBD with lift-and-project cuts (**NGBD-LAP**).

BARON 9.0.6 employs CONOPT 3.14 [55] for local NLP subproblems and CPLEX 12.2 [1] for LP subproblems. NGBD and enhanced NGBD algorithms employ BARON 9.0.6 (with the same settings described above) for NLP subproblems and CPLEX 12.2 for LP and MILP subproblems.

Case study problems are solved on a computer allocated a single 2.66 GHz CPU and running Linux kernel. GAMS 23.5.2 is used to formulate the models, program the NGBD and enhanced NGBD algorithms, and interface the various solvers for the subproblems. For all the methods, the absolute and relative termination criteria are 10^{-2} and the initial integer realization ($y^{(1)}$) is 0. Only the solver time reported by GAMS is reported here.

7.3 Optimization Results

7.3.1 Optimization for Different Time Periods

The optimal objective values (which are negative scaled NPVs) for Case 1 and Case 2 are -1123.017 and -1124.385 million dollars, respectively. The actual NPVs can be calculated from the scaled NPVs by Eq (7.9), and their values are shown in Table 7.14. The optimal equipment selections for Cases 1 and 2 are the same, whose values are listed in Table 7.11. The capacity choice means the selection of possible equipment capacities that are pre-determined in Section 7.1.2, e.g., choice 10 means the 10^{th} possible capacity is selected. The optimal feedstock consumption rates, production rates, CO_2 sequestration rates and CO_2 emission rates for Cases 1 and 2 are shown in Tables 7.12 and 7.13, respectively. Total capital investments, annual net profits and net present values of Cases 1 and 2 are compared in Table 7.14.

In both cases, power generation is preferred during peak times while methanol production is preferred during off-peak times because of the large variation of power

Table 7.11: Optimal equipment designs for Cases 1 and 2

Aggregate Equipment	Capacity Choice	Capacity	Capital Cost[d]
Syngas Cleaning System 1	1	0[a]	0
Syngas Cleaning System 2	7	137[a]	102
CO_2 Compressor	6	1389[b]	180
Fischer-Tropsch Synthesis System	1	0[b]	0
Methanol Synthesis System	10	840[b]	858
Gas Turbine System	10	4750[c]	799
Steam Turbine System	10	1800[c]	448

[a] The unit is Mmol/h.
[b] The unit is tonne/h.
[c] The unit is MW.
[d] The unit is million dollars.

prices between peak and off-peak. Liquid fuels, including naphtha and diesel, are not produced in any scenario due to their low prices compared to other products. CO_2 emissions are relatively high in peak times because all feedstocks are used for power generation and carbon sequestration is not implemented in order to save power for export. However, CO_2 emissions significantly drop in off-peak times since most of carbon in feedstocks now flows into the methanol and carbon sequestration becomes profitable to implement due to the low power price.

The fact that the equipment capacities are the same in Cases 1 and 2 (as shown in Table 7.11) implies that the operational flexibility of the polygeneration plant does not increase by considering monthly price variations instead of seasonal ones. Discussions in Chapter 4 indicated the degree of price fluctuations between peak and off-peak times had significant impacts on the optimal design and operation while the seasonal price changes, which were much smaller than those between peak and off-peak, had little or no influence. Although the monthly price changes are larger than the seasonal ones in this work, they are still not comparable with price differences between peak and off-peak. Therefore, monthly price fluctuations are not reflected in the optimal design and operation in both cases (except for the November peak

times in Case 2), and the economic improvement of Case 2 compared to Case 1 is not significant (as shown in Table 7.14).

7.3.2 Optimization under Market and Policy Uncertainties

The optimal objective value (which is the negative scaled NPV) for Case 3 is -1041.58 million dollars. The optimal equipment selections for Case 3 are listed in Table 7.15. The optimal feedstock consumption rates, production rates, CO_2 sequestration rates and CO_2 emission rates for Case 3 are shown in Tables 7.16, 7.17, 7.18 and 7.19, respectively. Total capital investment, expected annual net profit and expected net present value of Case 3 are shown in Table 7.20.

The stochastic optimization in Case 3 obtained the optimal design for the maximum expected NPV over all possible market and policy scenarios. In this optimal design, Syngas Cleaning System 1 (used for power generation with CCS) and the Fischer-Tropsch synthesis system are not installed due to their high capital costs and low profitability, and the methanol synthesis system, the gas turbine system and the steam turbine system are designed at their maximum capacities to introduce the operation flexibility for both market/policy uncertainties and different time periods.

Operations in different oil price and carbon tax scenarios are also optimized. In high carbon tax scenarios, electricity production is somewhat suppressed due to its high CO_2 emissions, while methanol production is promoted during peak times. Carbon capture and sequestration (CCS) is only implemented under middle and high carbon taxes, and in high carbon tax scenarios CCS is also encouraged during some peak times. The optimal CO_2 emissions decrease significantly with the increase of the carbon tax because CCS and methanol production are encouraged under higher carbon taxes.

7.4 Computational Performance

7.4.1 NGBD and Enhanced NGBD with Primal Dual Cuts (NGBD-D and NGBD-MD)

The computational performance of BARON, NGBD, NGBD-D and NGBD-MD for Cases 1 and 2 are compared in Tables 7.21 and 7.22, respectively. BARON did not return a global solution within 30 CPU days for either problem, while NGBD and enhanced NGBD all obtained a global solution within 18 CPU hours for Case 1 and within 60 CPU hours for Case 2. These results demonstrate that viability of the decomposition strategy for the global optimization of flexible polygeneration systems.

Note that the solution time for Problem (PP) dominates the total solution time within NGBD, because Problem (PP) is the only nonconvex NLP subproblem in NGBD and the solution time for it is much longer than that for other subproblems. By introducing extra dual information from the primal problem to form a tighter relaxed master problem, NGBD-D significantly reduced the number of iterations for convergence and it solved much fewer Problem (PBP) and (more importantly) Problem (PP). The solution time with NGBD-D was reduced by almost an order of magnitude compared to that with NGBD for both cases, although it spent a fairly large amount of time to solve Problem (DPP) to obtain extra dual information for a tighter relaxation. In addition, by adopting the multicut strategy for an even tighter relaxation, NGBD-MD achieved faster convergence than NGBD-D and further reduced the solution time for both cases.

Also note that the number of scenarios in Case 2 is three times of that in Case 1, and the solution time for Case 2 was around 2-4 times of that for Case 1 for all of the three decomposition methods. This indicates the favorable scalability of the decomposition strategy with respect to the number of scenarios, as also shown by the case studies in Ref [110].

The computational performance of BARON, NGBD and NGBD-D for Cases 3 are compared in Tables 7.23. Due to the large problem size of Case 3, even NGBD

cannot return a global solution within a reasonable time. Meanwhile, NGBD-D practically solved this problem in less than 45 CPU hours. It demonstrates that enhanced NGBD with primal dual cuts can efficiently solve large-scale nonconvex stochastic/multiperiod problems.

7.4.2 Enhanced NGBD with Piecewise Convex Relaxation (NGBD-PCR)

The computational performance of NGBD and NGBD-PCR for Cases 1 and 2 are compared in Tables 7.24 and 7.25, respectively. Both the fixed and adaptive partition strategies are studied for NGBD-PCR. Tables 7.24 and 7.25 show that NGBD-PCR reduced the solution time by one order of magnitude compared to NGBD, because much fewer Problem (PP) were solved.

In the fixed partition strategy, the domains of the variables to be partitioned are assumed to be partitioned uniformly into the same number of subdomains, denoted by M, and NGBD-PCR was implemented for three different M values, say $M =$ 5, 10 or 15, to show the effect of M on the performance of NGBD-PCR. As the piecewise relaxation helped to generate improved lower bounding problems that have a better chance to locate an optimal integer realization earlier, the NGBD-PCR method with more finely partitioned subdomains led to fewer Problem (PP) to be solved. On the other hand, integrating piecewise relaxation requires solving an additional MILP problem (PBP-PCR) (and sometimes (DPBP-PCR) as well) for each integer realization visited, and these MILPs are expensive to solve compared to Problem (PBP) in NGBD (although they are much easier than Problem (PP)). As M increases, these additional MILPs contain more integer variables and are more difficult to solve. Therefore, the solution time by NGBD-PCR depends on both the solution time for Problem (PP) and the solution time for the additional MILPs, and these two times are in principle negatively correlated. In this study, NGBD-PCR with $M = 15$ had the fastest solution because it achieved the best trade-off between the two times in three M values.

In the adaptive partition strategy, the number of subdomains for partition variables does not need to be pre-determined. Instead, the partition is implemented within the algorithm based on the solution of Problem (PP). Case study results show that the number of subdomains for different variables ranged from 1 to 15 in Case 1, and from 1 to 16 in Case 2, and exhibited a flexible partition pattern. The performance of the adaptive NGBD-PCR might be worse than the fixed NGBD-PCR with some optimal choice of M ($M = 15$), but it was better than the fixed NGBD-PCR with other choices of M, as shown in Tables 7.24 and 7.25. In reality, the optimal value for M is difficult to know in advance for general problems. The adaptive NGBD-PCR could achieve fast convergence for problems without much prior information.

Note that the results in the two tables indicate the scalability of NGBD and NGBD-PCR, whose solution time increased moderately with the number of scenarios.

The computational performance of NGBD and NGBD-PCR for Case 3 is compared in Table 7.26. In order to achieve fast convergence for Case 3, only the fixed partition strategy with the optimal selection of M ($M = 15$) was studied for NGBD-PCR here. The results show that NGBD-PCR could solve large-scale stochastic/multiperiod problems in reasonable times.

7.4.3 Enhanced NGBD with Primal Dual Cuts and Piecewise Convex Relaxation (NGBD-D-PCR)

The computational performance of NGBD and NGBD-D-PCR for Cases 1, 2 and 3 are compared in Tables 7.27, 7.28 and 7.29, respectively. NGBD-D-PCR reduced the solution time by one order of magnitude compared to NGBD. Compared with the results in previous two sections, the performance of NGBD-D-PCR was better than both NGBD-D and NGBD-PCR. Note that under some choices of subdomains numbers (e.g., $M = 15$), the performance improvement of NGBD-D-PCR compared to NGBD-PCR was not significant since the solution time of Problem (DPP) accounted for a large portion of the total solution time.

7.4.4 Enhanced NGBD with Lift-and-Project Cuts (NGBD-LAP)

The computational performance of NGBD and NGBD-LAP for Cases 1 and 2 are compared in Tables 7.30 and 7.31, respectively, in which the solution times of cut generation problems (CGP) are grouped into those of Problem (PBP). Results show that NGBD-LAP reduced the solution time by one order of magnitude compared to NGBD.

In this study, only the fixed subdomain partition strategy is considered for NGBD-LAP. The effect of subdomain numbers M on the computational performance was studied. With the increase of M, tighter relaxation of the original problem can be obtained, leading to fewer iterations for the whole algorithm; on the other hand, more Problem (CGP) need to be solved, resulting in more solution times for Problem (CGP) (and Problem (PBP) here). Note that the solution time of Problem (PBP) and (CGP) dominated the total solution time for Case 1 and 2, hence large numbers of subdomains had the negative effect on the performance of NGBD-LAP here.

Table 7.12: Optimal operations in Case 1

	Value	Unit
Feedstock Consumption Rate		
Coal		
All Seasons, Peak and Off-peak	1172	tonne/h
Biomass		
All Seasons, Peak and Off-peak	0	tonne/h
Water		
All Seasons, Peak	205	tonne/h
All Seasons, Off-peak	412	tonne/h
Production Rate		
Electricity		
All Seasons, Peak	3966	MW
All Seasons, Off-peak	72	MW
Naphtha		
All Seasons, Peak and Off-peak	0	tonne/h
Diesel		
All Seasons, Peak and Off-peak	0	tonne/h
Methanol		
All Seasons, Peak	0	tonne/h
All Seasons, Off-peak	831	tonne/h
Sulfur		
All Seasons, Peak and Off-peak	29	tonne/h
Carbon Dioxide		
Sequestration Rate		
All Seasons, Peak	0	tonne/h
All Seasons, Off-peak	1389	tonne/h
Emission Rate		
All Seasons, Peak	2684	tonne/h
All Seasons, Off-peak	153	tonne/h

Table 7.13: Optimal Operations in Case 2

	Value	Unit
Feedstock Consumption Rate		
Coal		
All Months, Peak and Off-peak	1172	tonne/h
Biomass		
All Months, Peak and Off-peak	0	tonne/h
Water		
All Months except November, Peak	205	tonne/h
November, Peak	87	tonne/h
All Months, Off-peak	412	tonne/h
Production Rate		
Electricity		
All Months except November, Peak	3966	MW
November, Peak	3630	MW
All Months, Off-peak	72	MW
Naphtha		
All Months, Peak and Off-peak	0	tonne/h
Diesel		
All Months, Peak and Off-peak	0	tonne/h
Methanol		
All Months except November, Peak	0	tonne/h
November, Peak	74	tonne/h
All Months, Off-peak	831	tonne/h
Sulfur		
All Months, Peak and Off-peak	29	tonne/h
Carbon Dioxide		
Sequestration Rate		
All Months except November, Peak	0	tonne/h
November, Peak	131	tonne/h
All Months, Off-peak	1389	tonne/h
Emission Rate		
All Months except November, Peak	2684	tonne/h
November, Peak	2450	tonne/h
All Months, Off-peak	153	tonne/h

Table 7.14: Economics of Cases 1 and 2

	Case 1	**Case 2**	**Unit**
Capital Investment	5363	5363	million dollars
Annual Net Profit	1638	1640	million dollars per year
Net Present Value	9046	9057	million dollars

Table 7.15: Optimal equipment designs for Cases 3

Aggregate Equipment	**Capacity Choice**	**Capacity**	**Capital Cost**[d]
Syngas Cleaning System 1	1	0[a]	0
Syngas Cleaning System 2	7	137[a]	102
CO_2 Compressor	6	1389[b]	180
Fischer-Tropsch Synthesis System	1	0[b]	0
Methanol Synthesis System	10	840[b]	858
Gas Turbine System	10	4750[c]	799
Steam Turbine System	10	1800[c]	448

[a] The unit is Mmol/h.
[b] The unit is tonne/h.
[c] The unit is MW.
[d] The unit is million dollars.

Table 7.16: Optimal feedstock consumption rates in Case 3

	Value	Unit
Coal		
All Oil Prices, All Carbon Taxes		
All Seasons, Peak and Off-peak	1172	tonne/h
Biomass		
All Oil Prices, All Carbon Taxes		
All Seasons, Peak and Off-peak	0	tonne/h
Water		
All Oil Prices, Low and Middle Carbon Tax		
All Seasons, Peak	205	tonne/h
All Seasons, Off-peak	412	tonne/h
Low Oil Price, High Carbon Tax		
Spring, Fall and Winter, Peak	408	tonne/h
Summer, Peak	205	tonne/h
All Seasons, Off-peak	412	tonne/h
Middle and High Oil Prices, High Carbon Tax		
Spring, Summer and Winter, Peak	205	tonne/h
Fall, Peak	408	tonne/h
All Seasons, Off-peak	412	tonne/h

Table 7.17: Optimal production rates in Case 3 (electricity, naphtha and diesel)

	Value	Unit
Electricity		
All Oil Prices, Low Carbon Tax		
All Seasons, Peak	3966	MW
All Seasons, Off-peak	174	MW
All Oil Prices, Middle Carbon Tax		
All Seasons, Peak	3966	MW
All Seasons, Off-peak	72	MW
Low Oil Price, High Carbon Tax		
Spring, Fall and Winter, Peak	2445	MW
Summer, Peak	3966	MW
All Seasons, Off-peak	72	MW
Middle Oil Price, High Carbon Tax		
Spring, Summer and Winter, Peak	3966	MW
Fall, Peak	380	MW
All Seasons, Off-peak	72	MW
High Oil Price, High Carbon Tax		
Spring, Summer and Winter, Peak	3966	MW
Fall, Peak	405	MW
All Seasons, Off-peak	72	MW
Naphtha		
All Oil Prices, All Carbon Taxes		
All Seasons, Peak and Off-peak	0	tonne/h
Diesel		
All Oil Prices, All Carbon Taxes		
All Seasons, Peak and Off-peak	0	tonne/h

Table 7.18: Optimal production rates in Case 3 (methanol and sulfur)

	Value	Unit
Methanol		
All Oil Prices, Low and Middle Carbon Tax		
All Seasons, Peak	0	tonne/h
All Seasons, Off-peak	831	tonne/h
Low Oil Price, High Carbon Tax		
Spring, Fall and Winter, Peak	279	tonne/h
Summer, Peak	0	tonne/h
All Seasons, Off-peak	831	tonne/h
Middle Oil Price, High Carbon Tax		
Spring, Summer and Winter, Peak	0	tonne/h
Fall, Peak	766	tonne/h
All Seasons, Off-peak	831	tonne/h
High Oil Price, High Carbon Tax		
Spring, Summer and Winter, Peak	0	tonne/h
Fall, Peak	760	tonne/h
All Seasons, Off-peak	831	tonne/h
Sulfur		
All Oil Prices, All Carbon Taxes		
All Seasons, Peak and Off-peak	29	tonne/h

Table 7.19: Optimal CO_2 sequestration rates and emission rates in Case 3

	Value	Unit
CO_2 Sequestration Rates		
All Oil Prices, Low Carbon Tax		
All Seasons, Peak and Off-peak	0	tonne/h
All Oil Prices, Middle Carbon Tax		
All Seasons, Peak	0	tonne/h
All Seasons, Off-peak	1389	tonne/h
Low Oil Price, High Carbon Tax		
Spring, Fall and Winter, Peak	1389	tonne/h
Summer, Peak	0	tonne/h
All Seasons, Off-peak	1389	tonne/h
Middle and High Oil Price, High Carbon Tax		
Spring, Summer and Winter, Peak	0	tonne/h
Fall, Peak	1389	tonne/h
All Seasons, Off-peak	1389	tonne/h
CO_2 Emission Rates		
All Oil Prices, Low Carbon Tax		
All Seasons, Peak	2684	tonne/h
All Seasons, Off-peak	1542	tonne/h
All Oil Prices, Middle Carbon Tax		
All Seasons, Peak	2684	tonne/h
All Seasons, Off-peak	153	tonne/h
Low Oil Price, High Carbon Tax		
Spring, Fall and Winter, Peak	911	tonne/h
Summer, Peak	2684	tonne/h
All Seasons, Off-peak	153	tonne/h
Middle Oil Price, High Carbon Tax		
Spring, Summer and Winter, Peak	2684	tonne/h
Fall, Peak	243	tonne/h
All Seasons, Off-peak	153	tonne/h
High Oil Price, High Carbon Tax		
Spring, Summer and Winter, Peak	2684	tonne/h
Fall, Peak	251	tonne/h
All Seasons, Off-peak	153	tonne/h

Table 7.20: Economics of Cases 3

	Case 3	Unit
Capital Investment	5363	million dollars
Expected Annual Net Profit	1557	million dollars per year
Expected Net Present Value	8390	million dollars

Table 7.21: Computational performance of BARON, NGBD, NGBD-D and NGBD-MD for Case 1 (70 binary variables and 4904 continuous variables)

	BARON	NGBD	NGBD-D	NGBD-MD
Solver Time (CPU seconds)				
Total	—[b]	64316.5	7898.7	7426.4
Problem (PBP_h)	n/a	17.3	8.9	1.8
Problem (FP_h)	n/a	0.3	1.1	1.1
Relaxed Master Problem[a]	n/a	282.2	20.0	7.1
Problem (PP_h)	n/a	64016.7	4750.8	2631.7
Problem (DPP_h)	n/a	n/a	3118.0	4784.7
Integer Realizations Visited				
Problem (PBP_h)	n/a	464	128	53
Problem (PP_h)	n/a	396	73	15
Problem (DPP_h)	n/a	n/a	5	3

[a] The relaxed master problem is Problem (RMP) or (DERMP) or (MDERMP).
[b] No global solution was returned within 30 CPU days.

Table 7.22: Computational Performance of BARON, NGBD, NGBD-D and NGBD-MD for Case 2 (70 binary variables and 14712 continuous variables)

	BARON	NGBD	NGBD-D	NGBD-MD
Solver Time (CPU seconds)				
Total	—[b]	215280.2	26390.0	15158.6
Problem (PBP_h)	n/a	202.2	39.7	1.2
Problem (FP_h)	n/a	6.6	2.4	0.8
Relaxed Master Problem[a]	n/a	612.5	26.3	10.3
Problem (PP_h)	n/a	214458.9	12454.7	4519.8
Problem (DPP_h)	n/a	n/a	13867.0	10626.5
Integer Realizations Visited				
Problem (PBP_h)	n/a	613	132	46
Problem (PP_h)	n/a	537	77	14
Problem (DPP_h)	n/a	n/a	6	3

[a] The relaxed master problem is Problem (RMP) or (DERMP) or (MDERMP).
[b] No global solution was returned within 30 CPU days.

Table 7.23: Computational Performance of BARON, NGBD and NGBD-D for Case 3 (70 binary variables and 44136 continuous variables)

	BARON	NGBD	NGBD-D
Solver Time (CPU seconds)			
Total	—[b]	—[b]	153192.8
Problem (PBP_h)	n/a	n/a	38.1
Problem (FP_h)	n/a	n/a	21.5
Relaxed Master Problem[a]	n/a	n/a	344.5
Problem (PP_h)	n/a	n/a	117300.4
Problem (DPP_h)	n/a	n/a	35488.3
Integer Realizations Visited			
Problem (PBP_h)	n/a	n/a	416
Problem (PP_h)	n/a	n/a	313
Problem (DPP_h)	n/a	n/a	2

[a] The relaxed master problem is Problem (RMP) or (DERMP) or (MDERMP).
[b] No global solution was returned within 1000000 CPU seconds.

Table 7.24: Computational performance of NGBD and NGBD-PCR for Case 1 (70 binary variables and 4904 continuous variables)

	NGBD	NGBD-PCR			
		$M = 5$	$M = 10$	$M = 15$	Adaptive
Solver Time (CPU seconds)					
Total	64316.5	19055.1	8004.2	3652.9	5294.4
Problem (PBP_h)	17.3	781.9	2519.8	2357.1	1002.7
Problem (FP_h)	0.3	0.4	0.2	0.2	1.0
Relaxed Master Problem[a]	282.2	63.2	50.3	6.7	47.8
Problem (PP_h)	64016.7	18209.5	5434.0	1289.0	4242.9
Integer Realizations Visited					
Problem (PBP_h)	464	277	207	99	179
Problem (PP_h)	396	207	92	28	22

[a] The relaxed master problem is Problem (RMP) or (PERMP).

Table 7.25: Computational performance of NGBD and NGBD-PCR for Case 2 (70 binary variables and 14712 continuous variables)

	NGBD	NGBD-PCR			
		$M = 5$	$M = 10$	$M = 15$	Adaptive
Solver Time (CPU seconds)					
Total	215280.2	52052.9	29863.7	9328.9	22106.4
Problem (PBP_h)	202.2	3014.5	11463.7	7090.0	4048.5
Problem (FP_h)	6.6	0.9	0.3	0.3	0.4
Relaxed Master Problem[a]	612.5	103.8	82.7	7.7	68.8
Problem (PP_h)	214458.9	48933.7	18317.0	2230.7	17988.7
Integer Realizations Visited					
Problem (PBP_h)	613	324	304	103	243
Problem (PP_h)	537	233	107	27	41

[a] The relaxed master problem is Problem (RMP) or (PERMP).

Table 7.26: Computational performance of NGBD and NGBD-PCR for Case 3 (70 binary variables and 44136 continuous variables)

	NGBD	NGBD-PCR $M = 15$
Solver Time (CPU seconds)		
Total	—[b]	116123.4
Problem (PBP_h)	n/a	79366.9
Problem (FP_h)	n/a	11.1
Relaxed Master Problem[a]	n/a	130.6
Problem (PP_h)	n/a	36614.9
Integer Realizations Visited		
Problem (PBP_h)	n/a	342
Problem (PP_h)	n/a	57

[a] The relaxed master problem is Problem (RMP) or (PERMP).
[b] No global solution was returned within 1000000 CPU seconds.

Table 7.27: Computational performance of NGBD and NGBD-D-PCR for Case 1 (70 binary variables and 4904 continuous variables)

	NGBD	NGBD-D-PCR			
		$M = 5$	$M = 10$	$M = 15$	Adaptive
Solver Time (CPU seconds)					
Total	64316.5	5488.7	6191.6	3600.1	5390.8
Problem (PBP_h)	17.3	355.9	1905.2	2253.0	132.1
Problem (FP_h)	0.3	0.2	0.3	0.4	0.3
Relaxed Master Problem[a]	282.2	9.6	23.2	4.2	7.2
Problem (PP_h)	64016.7	3526.0	3681.3	636.6	3346.7
Problem (DPP_h)	64016.7	1596.9	581.8	705.9	1904.6
Integer Realizations Visited					
Problem (PBP_h)	464	121	163	86	84
Problem (PP_h)	396	70	75	19	18
Problem (DPP_h)	n/a	4	1	1	2

[a] The relaxed master problem is Problem (RMP) or (DPERMP).

Table 7.28: Computational performance of NGBD and NGBD-D-PCR for Case 2 (70 binary variables and 14712 continuous variables)

	NGBD	NGBD-D-PCR			
		$M = 5$	$M = 10$	$M = 15$	Adaptive
Solver Time (CPU seconds)					
Total	215280.2	16078.2	20678.9	9154.1	15150.0
Problem (PBP_h)	202.2	1218.1	6696.9	6448.5	1778.0
Problem (FP_h)	6.6	0.7	0.4	0.5	0.4
Relaxed Master Problem[a]	612.5	13.4	26.7	5.2	35.8
Problem (PP_h)	214458.9	10827.8	12856.4	1573.4	6248.0
Problem (DPP_h)	64016.7	4018.3	581.8	1126.5	7087.8
Integer Realizations Visited					
Problem (PBP_h)	613	130	195	84	170
Problem (PP_h)	537	72	82	21	13
Problem (DPP_h)	n/a	4	1	1	3

[a] The relaxed master problem is Problem (RMP) or (DPERMP).

Table 7.29: Computational performance of NGBD and NGBD-D-PCR for Case 3 (70 binary variables and 44136 continuous variables)

	NGBD	NGBD-D-PCR
		$M = 15$
Solver Time (CPU seconds)		
Total	—[b]	68392.6
Problem (PBP_h)	n/a	43070.7
Problem (FP_h)	n/a	9.2
Relaxed Master Problem[a]	n/a	28.1
Problem (PP_h)	n/a	12626.5
Problem (DPP_h)	n/a	12658.1
Integer Realizations Visited		
Problem (PBP_h)	n/a	230
Problem (PP_h)	n/a	21
Problem (DPP_h)	n/a	1

[a] The relaxed master problem is Problem (RMP) or (DPERMP).
[b] No global solution was returned within 1000000 CPU seconds.

Table 7.30: Computational performance of NGBD and NGBD-LAP for Case 1 (70 binary variables and 4904 continuous variables)

	NGBD	NGBD-LAP		
		$M = 5$	$M = 10$	$M = 15$
Solver Time (CPU seconds)				
Total	64316.5	2368.3	4970.4	17830.3
Problem (PBP_h)	17.3	1325.4	3463.3	9381.5
Problem (FP_h)	0.3	1.0	0.7	0.6
Relaxed Master Problem[a]	282.2	30.2	8.0	11.7
Problem (PP_h)	64016.7	1011.7	1498.4	8436.6
Integer Realizations Visited				
Problem (PBP_h)	464	281	111	108
Problem (PP_h)	396	3	8	29

[a] The relaxed master problem is Problem (RMP) or (LERMP).

Table 7.31: Computational performance of NGBD and NGBD-LAP for Case 2 (70 binary variables and 14712 continuous variables)

	NGBD	NGBD-LAP
		$M = 5$
Solver Time (CPU seconds)		
Total	215280.2	18213.3
Problem (PBP_h)	202.2	9209.1
Problem (FP_h)	6.6	7.5
Relaxed Master Problem[a]	612.5	146.6
Problem (PP_h)	214458.9	8850.1
Integer Realizations Visited		
Problem (PBP_h)	613	394
Problem (PP_h)	537	11

[a] The relaxed master problem is Problem (RMP) or (LERMP).

Chapter 8

Conclusions and Future Work

8.1 Conclusions

Energy polygeneration processes with high efficiency and low emissions are promising in the energy industries, serving as possible supplements to the current oil-based processes. Compared to the conventional single-product processes, polygeneration processes have advantages of higher profits, lower economic risks and higher energy efficiency.

In this thesis, an energy polygeneration system using coal and biomass as feedstocks and co-producing electricity, liquid fuels (naphtha and diesel) and chemicals (methanol) is studied. This system comprises a gasifier, an air separation unit, syngas clean-up units, Selexol units, a Claus plant, water gas shift reactors, Fischer-Tropsch (FT) synthesis reactors, hydrocarbon separation units, hydrocracking reactors, autothermal reforming reactors, methanol synthesis reactors, methanol separation units, gas turbines, steam turbines, compressors, pumps and heat exchangers.

The optimal design and operation of a static energy polygeneration system under different market and policy scenarios is investigated. A mathematical model is developed for this purpose, in which mass and energy balances in all unit operations, enthalpy calculations, reduced unit operation models, reactor feedstock specifications, emissions regulations, capital cost estimations and economic analyses are addressed. The optimal product distributions, NPVs and CO_2 emissions of the static polygen-

eration system are obtained under different product prices and carbon taxes. The results provide suggestions for planning production strategies and CO_2 emissions in polygeneration systems. The preference of power generation versus liquids production is strongly dependent on the ratio of the naphtha price to the power price, and the preference of liquid fuels production or methanol production is highly dependent on the ratio of the naphtha price to the methanol price. The co-production of electricity and liquids or liquid fuels and methanol is usually not the optimal choice under the static operation pattern due to its high capital investment. CO_2 emissions are mostly dependent on the level of carbon tax, and carbon capture and sequestration is only profitable above a certain level of carbon tax. Biomass usage is dependent on both the carbon tax and the biomass price. High carbon tax will be the major factor that promotes the usage of biomass. Polygeneration processes with a certain amount of biomass usage will achieve zero or negative net CO_2 emissions. Product distributions are also influenced by the type of carbon tax policy, e.g., whether the tax charges the CO_2 emissions only from the production process or from both the process and all downstream usages. The static polygeneration plant always has a higher (or equal) net present value than the single-product plants. However, the economic benefit from static polygeneration is not significant based on the case study results.

Flexible operations are further considered in the energy polygeneration process. In the flexible polygeneration process, the production rates change during different time periods in response to the market conditions in order to achieve higher profits. The major challenge in this flexible design is determination of the optimal trade-off between flexibility and capital cost because higher flexibility typically implies both higher product revenues and larger equipment sizes. A two-stage optimization framework, in which design decision variables (equipment sizes) and operational decision variables in all scenarios (flow rates, split fractions and temperatures) are optimized simultaneously to achieve the best overall economic performance, is hence incorporated into the mathematical model for the polygeneration system. The global optimization solver, BARON, is applied to the polygeneration optimization problem to ensure the global optimal solution. The optimal product distributions, equipment capacity

usages, NPVs and CO_2 emissions of the flexible polygeneration system are studied under different product prices and carbon taxes. Case study results show that the net present values of flexible polygeneration plants are higher than static polygeneration systems for the same oil price and carbon tax, although the capital investments for flexible polygeneration systems are also higher. The economic improvement of the flexible operations can be quite significant, e.g., the NPVs of flexible plants are 10%-60% higher than static plants under some market scenarios. With an increase in operational flexibility, the capital investment, the net profits and the net present value all increase as well. Hence, this analysis suggests that flexible designs are generally more profitable than static designs for polygeneration systems when sufficient capital is available for investment. The optimal product portfolios of flexible systems are quite different from those of static systems. For example, co-production of different products, such as electricity and liquids, becomes common in the optimal operation of flexible systems. The annual CO_2 emissions of flexible systems can be higher or lower than static systems depending on the product distributions.

The flexible polygeneration optimization problem is potentially a large-scale nonconvex MINLP with high computational burden. State-of-the-art global optimization solvers, such as BARON, cannot solve problems with a large number of scenarios in reasonable times. The nonconvex generalized Benders decomposition (NGBD) algorithm, which exploits the special mathematical structure of the two-stage program, is developed for efficient solution of large-scale nonconvex stochastic/multiperiod optimization problems. In NGBD, the original problem is reformulated by projection and dualization. A sequence of nondecreasing lower bounds and a sequence of nonincreasing upper bounds are generated by iteratively solving several subproblems whose sizes are independent of the number of scenarios, including decomposed primal bounding problems (PBP), decomposed feasibility problems (FP), decomposed primal problems (PP) and relaxed master problems (RMP). The global optimal solution is obtained when the lower and upper bounds coincide. NGBD guarantees finite termination with an ϵ-optimal solution or infeasibility indication. The CPU time for NGBD is expected to increase linearly with the number of scenarios. The case study results indicate that

the decomposition algorithm achieved much shorter computational times compared to BARON in the polygeneration application.

Several enhancement technologies are incorporated into NGBD for faster convergence, including primal dual information, piecewise convex relaxation and lift-and-project cuts. In NGBD with primal dual information (NGBD-D), primal dual cuts are obtained by solving a relaxed dual or Lagrangian relaxation of Problem (PP) and are then added into Problem (DERMP) for tighter relaxation. By introducing the primal dual multicuts, the performance of decomposition algorithm is further improved. In NGBD with piecewise convex relaxation (NGBD-PCR), the domains of variables in bilinear functions are partitioned into subdomains, and piecewise McCormick relaxation is performed for Problem (PBP-PCR) on these subdomains. The relaxed dual of Problem (PBP-PCR) is then solved to generate enhanced optimality cuts for Problem (PERMP). With the piecewise convex relaxation technique, a tighter relaxation is generated that provides improved information for NGBD to converge. In NGBD with lift-and-project cuts (NGBD-LAP), piecewise convex relaxation is performed, and a cutting plane algorithm that generates lift-and-project cuts is implemented for solving Problem (PBP-LAP). Again, enhanced optimality cuts generated from Problem (PBP-LAP) are introduced to Problem (LERMP). In NGBD-LAP, a certain amount of cut generation problems (CGP) need to be solved to obtain the lift-and-project cuts. Note that although all three enhanced decomposition algorithms obtain tighter relaxations than the original NGBD, they introduce some additional subproblems that may be difficult to solve, such as Problem (DPP) in NGBD-D, Problems (PBP-PCR) and (DPBP-PCR) in NGBD-PCR, and Problems (PBP-LAP) and (CGP) in NGBD-LAP. There is a trade-off between the tightness of the relaxation and solution times for additional subproblems. In order to introduce the appropriate number of enhanced cuts for fast solution, some heuristics determining whether or not to solve the additional subproblems for tighter relaxations are used. For example, in NGBD-D, Problem (DPP) is only solved when Problem (PP) is feasible and updates the current upper bound; while in NGBD-PCR or NGBD-LAP, Problems (PBP-PCR), (DPBP-PCR) or Problems (PBP-LAP), (CGP) are solved at every iteration when

Problem (PBP) is feasible. The case study results demonstrate that the enhanced decomposition algorithms reduced the solution time by about one order of magnitude compared to the original NGBD. The global optimal solutions of polygeneration optimization problems can be obtained by the enhanced NGBD in relatively short times.

After applying NGBD and enhanced NGBD to the polygeneration application, energy polygeneration problems with larger numbers of scenarios are studied, including flexible polygeneration considering more time periods and stochastic optimization under the market and policy uncertainties. After more time periods are considered, the economic performance of the flexible polygeneration system can be slightly improved due to the increase of operational flexibility. When the stochastic optimization is performed, the optimal design is obtained to achieve the best expected net present value under 3 oil price and 3 carbon tax scenarios. Note that in this case the basic NGBD algorithm could not solve this problem in a reasonable time, but the various enhanced NGBD algorithms could.

8.2 Future Work

8.2.1 Polygeneration Model

Several improvements for the mathematical model of the polygeneration system are potential subjects of future study.

First, a polygeneration model encompassing a superstructure with multiple technical alternatives needs to be develop. Recently, several new technologies related to energy polygeneration have been studied. For example, membrane technology has been developed for efficient CO_2 capture [124] and hydrogen separation [11]; solid oxide fuel cells (SOFCs) have shown great promise in reducing CO_2 emissions for electricity production [8]; and the incorporation of natural gas as a third possible feedstock has also shown economic benefits [9], especially considering the abundance of shale gas in the U.S. and elsewhere. These novel alternatives may help to achieve

higher energy efficiency and better economic performance for the energy polygeneration process, and need to be incorporated into the future optimization model. In addition, different conventional technologies need to be compared in the future study, such as a gasifier with slurry feed vs. a gasifier with dry feed, radiant cooler vs. quench, Selexol vs. Rectisol for acid gas removal, gas-phase FT or methanol reactor vs. slurry-phase FT or methanol reactor, and iron-based catalyst vs. cobalt-based catalyst for the FT reactor. Technical and economical parameters for these new technologies, e.g., conversions and selectivity for reactors, split fractions for separation units, operating temperatures and pressures and equipment capital costs, need to be estimated. They can be obtained from process or unit simulations, experimental data or the literature. After comparing different technologies, an optimal design with higher profits and lower emissions is expected to be obtained compared to the design in this work. Note that additional integer variables will be introduced to address different technical choices, which will increase the computational complexity for the model. More efficient global optimization algorithms will possibly be required for fast solution of this larger-scale problem.

Second, the cost of the flexible operation needs to be considered for more accurate economic analysis. In this work, the performance of all equipment is assumed to remain constant under all operating conditions, e.g., constant conversions and efficiency are assumed for reactors and turbines under different flow rates, respectively. In real applications, the performance of equipment may drop when operated below its design capacity. For example, the efficiency of the gas turbine under the off-design mode can be much lower than under its design mode. A possible way of addressing this issue is to incorporate some correlations that express equipment performance as a function of operating conditions or equipment capacity usage. Note that these correlations can be highly nonlinear and nonconvex functions, and advanced optimization algorithms might be needed for this new computational complexity. Another cost comes from the transition between different operational conditions. In this model, operations are considered to be at steady state at all times, and the transition times are neglected. However, chemical units (including reactors and separation units) typically require

some time to change from one steady state to another steady state, and off-spec products may be produced during these times. This profit loss can be estimated by the models representing change-over performance of unit operations. Dynamic optimization algorithms [188, 157] can be developed to find the optimal transition strategy for flexible operations. In addition, operational reliability suffers when deviating from steady state because control systems are generally designed to operate best at steady states and additional manual interventions are normally required to start up, shut down or change rates. This reliability loss may need to be addressed in future models.

Third, more sophisticated unit operation models may be incorporated in the future polygeneration models. For example, linear reactor models in the current model will be replaced by more accurate nonlinear models, in which reactor conversions will be expressed by some nonlinear functions of operating conditions (such as molar compositions and temperatures), instead of being fixed as parameters. Similarly for separation units, compressors and turbines. In addition, temperatures and pressures in unit operations, which are fixed in the current model, can be relaxed as decisions in the future models. If this update is applied to the model, more profitable polygeneration systems will be designed, but more computational difficulty is also expected.

Fourth, more detailed energy integration can be addressed. The heat balance calculation in this model may lead to an overestimation of energy efficiency for the whole system, as temperatures of some heat generation units are lower than those of heat consumption units and part of heat actually cannot be utilized in the process. Pinch analysis can be incorporated into the model addressing the detailed heat network design.

Finally, stochastic optimization for the polygeneration system needs to be further studied. Uncertainties for more economic and technical parameters will be considered, e.g., the supply and price of biomass could be quite unstable, and the performance and capital cost of new technologies are also quite uncertain. Sensitivity analysis needs to be performed to identify uncertain parameters that potentially have significant influence on the economic performance of the system. Uncertainties in these parameters should be addressed in the future models.

8.2.2 Decomposition Algorithm

Several issues will be addressed in the future development of decomposition algorithms.

First, enhancement technologies can be incorporated into NGBD in a more efficient and effective manner so that the solution can be further accelerated. So far some heuristics are employed for determining whether or not to add enhanced cuts for the relaxed master problem, e.g., primal dual cuts are added only when Problem (PP) is feasible and update the current upper bound, and piecewise optimality cuts are added when Problem (PBP) is feasible. These heuristics are developed based on our previous computational experience, and may not be the optimal choice for the best computational performance. In the future study, some systematic ways should be developed for effectively adding those enhanced cuts. For example, in NGBD-D, a better heuristic may be developed to determine whether to solve Problem (DPP) or not at each iteration so that this difficult nonconvex NLP is only solved when it can provide strong primal dual cuts to accelerate the solution; in NGBD-PCR, Problem (PBP-PCR) and (DPBP-PCR) may be only solved when strong piecewise optimality cuts are obtained, and this heuristic could significantly reduce the solution time of piecewise subproblems especially when the number of subdomains is large.

Second, more effective partition strategies should be developed for tighter piecewise relaxation in NGBD-PCR and NGBD-LAP. The case study results indicate that the number of partitioned subdomains impacts the efficiency of NGBD-PCR and NGBD-LAP. So it will be an interesting work to develop a systematic approach to improve the selection of this number. The adaptive partition strategy developed in this thesis has been demonstrated as an efficient approach. In the future work, the adaptive partition approach can be further improved by incorporating more intermediate solution information and introducing more flexibility for domain partitioning.

Third, lift-and-project cuts may be generated in a more efficient way for NGBD-LAP. The solution time for cut generation problems (CGP) accounts for a large portion of the total solution time. The computational performance of NGBD-LAP can

be further improved if fewer Problem (CGP) are solved without losing the tightness of relaxations. Some heuristics will be compared for this purpose, including solving Problem (CGP) for all relaxed integer variables vs. for only one variable with the maximum integrality violation, and solving Problem (CGP) once per iteration vs. several times per iteration.

Four, a new generation of NGBD addressing continuous complicating variables could be developed. Convergence of the current NGBD is guaranteed by the Balas cuts excluding previous examined integer realizations. However, this convergence property cannot hold for problems with continuous complicating variables, as no previous visited value can be excluded for continuous variables. Therefore, new approaches need to be developed to address this issue. One possible way is to apply the adaptive partition strategy to NGBD-LAP. As more finely partitioned subdomains are obtained, tighter lower bounding problems are solved, and finally the solution of the relaxed master problem and the primal problem will coincide without any duality gap. Another way is to introduce the idea of parametric programming [60, 69, 145, 56, 135, 58] into NGBD-PCR, by which the previously visited regions for continuous variables can be effectively excluded as done by the Balas cuts.

Finally, parallel computation architectures could be considered for NGBD. Note that there is no interaction between decomposed subproblems for each scenario. Hence, parallel computation can be employed for solving subproblems simultaneously, and the computational speed can be greatly accelerated if multiple CPUs are available.

Appendix A

Detailed Mathematical Model for Static Polygeneration Systems

A.1 Mathematical Model

A.1.1 Mass Balance

Air Separation Unit

The input rate of each species of air is denoted by:

$$F^{\text{asu}}_{\text{air},j} = x_{\text{air},j}\, F^{\text{asu}}_{\text{air}} \;, \quad \forall j \in J_{\text{air}} \tag{A.1}$$

where $F^{\text{asu}}_{\text{air},j}$ is the molar flow rate of species j in air, $F^{\text{asu}}_{\text{air}}$ is the total molar flow rate of input air; $x_{\text{air},j}$ is the mole fraction of species j in air; $J_{\text{air}} \equiv \{\text{N}_2,\ \text{O}_2,\ \text{Ar}\}$ is the set of species in air.

The mass balances of the ASU are given by:

$$F^{\text{asu}}_{\text{oxy},j} = x_{\text{oxy},j}\, F^{\text{asu}}_{\text{oxy}} \;, \quad \forall j \in J_{\text{air}} \tag{A.2}$$

$$F^{\text{asu}}_{\text{oxy},\text{O}_2} = S^{\text{asu}}_{\text{O}_2}\, F^{\text{asu}}_{\text{air},\text{O}_2} \tag{A.3}$$

$$F^{\text{asu}}_{\text{air},j} = F^{\text{asu}}_{\text{oxy},j} + F^{\text{asu}}_{\text{nit},j} \;, \quad \forall j \in J_{\text{air}} \tag{A.4}$$

where $F^{\text{asu}}_{\text{oxy},j}$ and $F^{\text{asu}}_{\text{nit},j}$ are the molar flow rate of species j in the oxygen rich stream and nitrogen rich stream from the ASU, $F^{\text{asu}}_{\text{oxy}}$ is the total molar flow rate of the oxygen rich stream; $x_{\text{oxy},j}$ is the mole fraction of species j in the oxygen rich stream, $S^{\text{asu}}_{\text{O}_2}$ is the split fraction of O_2 in air to the oxygen rich stream, which are specified parameters.

The oxygen stream is split for different downstream processes. The mass balance of the split is denoted by:

$$F^{\text{asu}}_{\text{oxy}} = F^{\text{gas}}_{\text{oxy}} + F^{\text{cls}}_{\text{oxy}} + F^{\text{atr}}_{\text{oxy}} \tag{A.5}$$

where $F^{\text{gas}}_{\text{oxy}}$, $F^{\text{cls}}_{\text{oxy}}$ and $F^{\text{atr}}_{\text{oxy}}$ are the total molar flow rates of the oxygen stream sent to the gasifier, the Claus plant and the auto-thermal reforming reactor in the Fischer-Tropsch process. All above oxygen streams have the same species compositions as the oxygen stream from the ASU.

Gasifier

The mass balance in the gasifier is given by:

$$\begin{aligned} & R^{\text{gas}}_i \left[w_{\text{coal},i} \left(1 - w_{\text{coal},\text{H}_2\text{O}}\right) m^{\text{gas}}_{\text{coal}} + w_{\text{bio},i} \left(1 - w_{\text{bio},\text{H}_2\text{O}}\right) m^{\text{gas}}_{\text{bio}} \right] \\ & \quad + w_{\text{H}_2\text{O},i} \left(w_{\text{coal},\text{H}_2\text{O}}\, m^{\text{gas}}_{\text{coal}} + w_{\text{bio},\text{H}_2\text{O}}\, m^{\text{gas}}_{\text{bio}} \right) + n_{i,\text{H}_2\text{O}}\, \text{MW}_{\text{H}_2\text{O}}\, F^{\text{gas}}_{\text{w,in}} + \sum_j n_{i,j}\, \text{MW}_i\, F^{\text{gas}}_{\text{oxy},j} \\ & \quad = \sum_j n_{i,j}\, \text{MW}_i\, F^{\text{gas}}_{\text{rsyn},j} \,, \quad \forall i \in I_{\text{feed}} \,, \ \forall j \in J_{\text{rsyn}} \end{aligned} \tag{A.6}$$

And

$$\left(1 - w_{\text{bio},\text{H}_2\text{O}}\right) m^{\text{gas}}_{\text{bio}} = R_{\text{b/f}} \left[\left(1 - w_{\text{coal},\text{H}_2\text{O}}\right) m^{\text{gas}}_{\text{coal}} + \left(1 - w_{\text{bio},\text{H}_2\text{O}}\right) m^{\text{gas}}_{\text{bio}} \right] \tag{A.7}$$

where $m^{\text{gas}}_{\text{coal}}$ and $m^{\text{gas}}_{\text{bio}}$ are the mass flow rates of coal and biomass fed into the gasifier respectively, $F^{\text{gas}}_{\text{rsyn},j}$ and $F^{\text{gas}}_{\text{oxy},j}$ are the molar flow rates of species j in the raw syngas produced from the gasifier and the oxygen stream fed into the gasifier respectively,

$F^{\text{gas}}_{\text{w,in}}$ is the molar flow rate of the water stream fed into the gasifier, $R_{\text{b/f}}$ is the dry mass fraction of biomass in the total feedstock; R^{gas}_{i} is the conversion of element i in the gasifier, $w_{\text{coal,H}_2\text{O}}$ and $w_{\text{bio,H}_2\text{O}}$ are the mass fraction of water in the coal and biomass fed into the gasifier, $w_{\text{coal},i}$ and $w_{\text{bio},i}$ are the dry mass fractions of element i in the coal and biomass, which are specified parameters and assumed to be unchanged throughout the project period; $w_{\text{H}_2\text{O},i}$ is the mass fraction of element i in the water, MW_i is the molar weight of element i, and $n_{i,j}$ is the number of atoms of element i in one molecule of species j, which are constants; $I_{\text{feed}} \equiv \{\text{C, H, O, N, S, Cl}\}$ is the set of elements in the feedstock of the gasifier, $J_{\text{rsyn}} \equiv \{\text{CO, H}_2\text{, CO}_2\text{, H}_2\text{O, CH}_4\text{, N}_2\text{, Ar, H}_2\text{S, COS, NH}_3\text{, HCl}\}$ is the set of species in the raw syngas from the gasifier.

The mole flow rates of species in the raw syngas are expressed as:

$$F^{\text{gas}}_{\text{rsyn},j} = \left[\frac{R_{\text{b/f}}}{R_{\text{b/f,max}}}\left(R^{\text{rsyn}}_{j/\text{key,bio}} - R^{\text{rsyn}}_{j/\text{key}}\right) + R^{\text{rsyn}}_{j/\text{key}}\right] F^{\text{gas}}_{\text{rsyn,key}} \ , \quad \forall j \in J'_{\text{rsyn}} \ , \ \forall \text{key} \in J_{\text{rsyn,key}} \tag{A.8}$$

where $F^{\text{gas}}_{\text{rsyn,key}}$ is the molar flow rates of key species in the raw syngas; $R_{\text{b/f,max}}$ is the maximum mass fraction of biomass in the feedstock (= 30% here), $R^{\text{rsyn}}_{j/\text{key}}$ and $R^{\text{rsyn}}_{j/\text{key,bio}}$ are the ratios of molar flow rates of species j and the key species in the raw syngas produced from 100% of coal and the coal/biomass mixture with 30% (mass based) of biomass, which are specified parameters; $J'_{\text{rsyn}} \equiv \{\text{H}_2\text{, CO}_2\text{, H}_2\text{O, CH}_4\text{, COS, NH}_3\} \subset J_{\text{rsyn}}$ is the set of part of species in the raw syngas, $J_{\text{rsyn,key}} \equiv \{\text{CO, H}_2\text{S, N}_2\}$ is the set of key species in the raw syngas. For $j \in \{\text{H}_2\text{, CO}_2\text{, H}_2\text{O, CH}_4\}$, key = CO; if j = COS, key = H_2S; if $j = \text{NH}_3$, key = N_2. So far, the mass balance equations for the gasifier are complete.

Scrubber

The mass balance is denoted by:

$$F^{\text{sr}}_{\text{tsyn},j} = F^{\text{sc}}_{\text{rsyn},j} \ , \quad \forall j \in J_{\text{tsyn}} \tag{A.9}$$

where $F^{\text{sc}}_{\text{rsyn},j}$ and $F^{\text{sr}}_{\text{tsyn},j}$ are the molar flow rates of species j in the raw syngas exiting the syngas convective cooler and the treated syngas exiting the scrubber respectively; $J_{\text{tsyn}} \equiv \{\text{CO, } H_2\text{, } CO_2\text{, } H_2O\text{, } CH_4\text{, } N_2\text{, Ar, } H_2S\text{, COS}\}$ is the set of species in the treated syngas exiting the scrubber.

COS Hydrolysis Reactor

The mass balance in the hydrolysis reactor is denoted by:

$$F^{\text{hy}}_{\text{tsyn},j} = F^{\text{sr}}_{\text{tsyn},j} + \text{Sto}^{\text{hy}}_{j}\, F^{\text{sr}}_{\text{tsyn,COS}}\,, \quad \forall j \in J_{\text{tsyn}} \tag{A.10}$$

where $F^{\text{hy}}_{\text{tsyn},j}$ is the molar flow rate of species j in the treated syngas exiting the COS hydrolysis reactor; $\text{Sto}^{\text{hy}}_{j}$ is the stoichiometric coefficient of species j in the hydrolysis reaction (2.1).

Selexol Units

The mass balance in Selexol Unit 1 is given by:

$$F^{\text{sel}}_{\text{csyn},j} = S^{\text{sel}}_{j}\left(F^{\text{col}}_{\text{tsyn},j} + F^{\text{cls}}_{\text{tail},j}\right)\,, \quad \forall j \in J_{\text{csyn}} \tag{A.11}$$

$$F^{\text{sel}}_{\text{sul},j} = F^{\text{col}}_{\text{tsyn},j} + F^{\text{cls}}_{\text{tail},j} - F^{\text{sel}}_{\text{csyn},j}\,, \quad \forall j \in J_{\text{sul}} \tag{A.12}$$

$$F^{\text{sel}}_{\text{sul,}H_2S} = x_{\text{sul,}H_2S}\left(F^{\text{sel}}_{\text{sul,}H_2S} + F^{\text{sel}}_{\text{sul,}CO_2}\right) \tag{A.13}$$

where $F^{\text{sel}}_{\text{csyn},j}$, $F^{\text{sel}}_{\text{sul},j}$, $F^{\text{col}}_{\text{tsyn},j}$ and $F^{\text{cls}}_{\text{tail},j}$ are the molar flow rates of species j in the clean syngas from Selexol Unit 1, the H_2S rich stream from Selexol Unit 1, the treated syngas from Syngas Cooler 1 and the tail gas from the Claus plant, respectively; S^{sel}_{j} is the split fraction of species j to the clean syngas in Selexol Unit 1, $x_{\text{sul,}H_2S}$ is the mole fraction of H_2S in the H_2S rich stream, which are specified parameters; $J_{\text{csyn}} \equiv \{\text{CO, } H_2\text{, } CO_2\text{, } H_2O\text{, } CH_4\text{, } N_2\text{, Ar, } H_2S\}$ is the set of species in the clean syngas exiting Selexol Unit 1, $J_{\text{sul}} \equiv CO_2$, H_2S is the set of species in the H_2S rich stream exiting the Selexol unit. S^{sel}_{j} is set to be 1 for all species except H_2S.

The mass balance in Selexol Unit 2 is given by:

$$F^{\text{se2}}_{\text{csyn},j} = S^{\text{se2}}_{j}\ F^{\text{co2}}_{\text{csyn},j}\ , \quad \forall j \in J_{\text{csyn}} \tag{A.14}$$

$$F^{\text{se2}}_{\text{car}} = F^{\text{co2}}_{\text{csyn},\text{CO}_2} - F^{\text{se2}}_{\text{csyn},\text{CO}_2} \tag{A.15}$$

where $F^{\text{se2}}_{\text{csyn},j}$ and $F^{\text{co2}}_{\text{csyn},j}$ are the molar flow rates of the clean syngas from Selexol Unit 2 and Syngas Cooler 2 respectively, $F^{\text{se2}}_{\text{car}}$ is the total molar flow rate of CO_2 stream from Selexol Unit 2; S^{se2}_{j} is the split fraction of species j to the clean syngas in Selexol Unit 2, which is a specified parameter. S^{se2}_{j} is set to be 1 for all species except CO_2. The mass balance in Selexol Unit 3 is similar.

All above parameters are estimated from the rigorous Aspen simulation models.

Claus Plant

The mass balance is denoted by:

$$F^{\text{cls}}_{\text{tail},j} = F^{\text{cls}}_{\text{oxy},j} + F^{\text{sel}}_{\text{sul},j} + \text{Sto}^{\text{cls}}_{j}\ R^{\text{cls}}_{\text{H}_2\text{S}}\ F^{\text{sel}}_{\text{sul},\text{H}_2\text{S}}\ , \quad \forall j \in J_{\text{tail}} \tag{A.16}$$

$$F^{\text{cls}}_{\text{oxy},\text{O}_2} - \frac{1}{2}\ R^{\text{cls}}_{\text{H}_2\text{S}}\ F^{\text{sel}}_{\text{sul},\text{H}_2\text{S}} = 0 \tag{A.17}$$

$$F^{\text{cls}}_{\text{es}} = R^{\text{cls}}_{\text{H}_2\text{S}}\ F^{\text{sel}}_{\text{sul},\text{H}_2\text{S}} \tag{A.18}$$

where $F^{\text{cls}}_{\text{oxy},j}$ and $F^{\text{cls}}_{\text{tail},j}$ are the molar flow rates of species j in the oxygen stream from the ASU injected into the Claus plant and the tail gas exiting the Claus plant, $F^{\text{cls}}_{\text{es}}$ is the molar flow rate of elemental sulfur produced by the Claus plant; $R^{\text{cls}}_{\text{H}_2\text{S}}$ is the conversion of H_2S in the Claus reaction, which is a specified parameter; $\text{Sto}^{\text{cls}}_{j}$ is the stoichiometric coefficient of species j in the Claus reaction (2.2); $J_{\text{tail}} \equiv \{CO_2, H_2O, N_2, Ar, H_2S\}$ is the set of species in the tail gas exiting the Claus plant.

Water-gas Shift Reactors

The mass balance in WGS Reactor 1 is denoted by:

$$F_{\mathrm{pd},j}^{\mathrm{wgs1}} = F_{\mathrm{fd},j}^{\mathrm{wgs1}} + \mathrm{Sto}_j^{\mathrm{wgs}}\, R_{\mathrm{CO}}^{\mathrm{wgs1}}\, F_{\mathrm{fd,CO}}^{\mathrm{wgs1}}\,, \quad \forall j \in J_{\mathrm{csyn}}/\{\mathrm{H_2O}\} \tag{A.19}$$

$$F_{\mathrm{pd,H_2O}}^{\mathrm{wgs1}} = F_{\mathrm{fd,H_2O}}^{\mathrm{wgs1}} + F_{\mathrm{w,in}}^{\mathrm{wgs1}} - R_{\mathrm{CO}}^{\mathrm{wgs1}}\, F_{\mathrm{fd,CO}}^{\mathrm{wgs1}} \tag{A.20}$$

where $F_{\mathrm{fd},j}^{\mathrm{wgs1}}$ and $F_{\mathrm{pd},j}^{\mathrm{wgs1}}$ are the molar flow rates of species j in the feedstock stream and product stream of WGS Reactor 1, $F_{\mathrm{w,in}}^{\mathrm{wgs1}}$ is the molar flow rate of steam injected into WGS Reactor 1, and $R_{\mathrm{CO}}^{\mathrm{wgs1}}$ is the conversion of CO in WGS Reactor 1; $\mathrm{Sto}_j^{\mathrm{wgs}}$ is the stoichiometric coefficient of species j in the WGS reaction (2.3).

The product molar flow rates of the WGS reaction is constrained by the following nonlinear correlation:

$$F_{\mathrm{pd,H_2}}^{\mathrm{wgs1}}\, F_{\mathrm{pd,CO_2}}^{\mathrm{wgs1}} + A^{\mathrm{wgs}}\, F_{\mathrm{pd,CO}}^{\mathrm{wgs1}}\, F_{\mathrm{pd,H_2O}}^{\mathrm{wgs1}} = 0 \tag{A.21}$$

where A^{wgs} is a factor regressed from the simulation results of the detailed WGS reactor model.

The mass balance of WGS Reactor 2 is similar.

The H_2 to CO mole ratio in the product of WGS Reactor 1 is required to be 2, thus an additional specification equation is given:

$$F_{\mathrm{pd,H_2}}^{\mathrm{wgs1}} = 2F_{\mathrm{pd,CO}}^{\mathrm{wgs1}} \tag{A.22}$$

There is no product requirement for WGS Reactor 2.

Pressure-swing Adsorption Unit

The mass balance in PSA is given by:

$$F_{\mathrm{tail},j}^{\mathrm{psa}} = F_{\mathrm{csyn},j}^{\mathrm{psa}}\,, \quad \forall j \in J_{\mathrm{csyn}}/\{\mathrm{H_2}\} \tag{A.23}$$

$$F^{\text{psa}}_{\text{tail},\text{H}_2} = \left(1 - S^{\text{psa}}_{\text{H}_2}\right) F^{\text{psa}}_{\text{csyn},\text{H}_2} \tag{A.24}$$

$$F^{\text{psa}}_{\text{hyd}} = S^{\text{psa}}_{\text{H}_2}\, F^{\text{psa}}_{\text{csyn},\text{H}_2} \tag{A.25}$$

where $F^{\text{psa}}_{\text{csyn},j}$ and $F^{\text{psa}}_{\text{tail},j}$ are the molar flow rates of species j in the clean syngas fed into the PSA and the tail gas exiting the PSA, and $F^{\text{psa}}_{\text{hyd}}$ is the molar flow rate of the pure hydrogen stream produced by the PSA; $S^{\text{psa}}_{\text{H}_2}$ is the split fraction of H_2 to the hydrogen product stream from the PSA (or H_2 recovery ratio), which is a specified parameter.

Fischer-Tropsch Synthesis Reactor

The mass balance in the FT synthesis reactor is denoted by:

$$F^{\text{fts}}_{\text{pd},\text{CO}} = \left(1 - R^{\text{fts}}_{\text{CO}}\right) F^{\text{fts}}_{\text{fd},\text{CO}} \tag{A.26}$$

$$F^{\text{fts}}_{\text{pd},\text{H}_2} = F^{\text{fts}}_{\text{fd},\text{H}_2} - R^{\text{fts}}_{\text{CO}} \sum_j \left[\left(\frac{n_{\text{H},j}}{2n_{\text{C},j}} + 1\right) S^{\text{fts}}_j\, F^{\text{fts}}_{\text{fd},\text{CO}}\right] + R^{\text{fts}}_{\text{CO}}\, S^{\text{fts}}_{\text{CO}_2}\, F^{\text{fts}}_{\text{fd},\text{CO}}\,, \quad \forall j \in J_{\text{fts}} \tag{A.27}$$

$$F^{\text{fts}}_{\text{pd},j} = F^{\text{fts}}_{\text{fd},j} + \frac{1}{n_{\text{C},j}}\, R^{\text{fts}}_{\text{CO}}\, S^{\text{fts}}_j\, F^{\text{fts}}_{\text{fd},\text{CO}}\,, \quad \forall j \in J_{\text{fts}} \tag{A.28}$$

$$F^{\text{fts}}_{\text{pd},\text{H}_2\text{O}} = F^{\text{fts}}_{\text{fd},\text{H}_2\text{O}} + R^{\text{fts}}_{\text{CO}} \left(1 - 2S^{\text{fts}}_{\text{CO}_2}\right) F^{\text{fts}}_{\text{fd},\text{CO}} \tag{A.29}$$

$$F^{\text{fts}}_{\text{pd},j} = F^{\text{fts}}_{\text{fd},j}\,, \quad \forall j \in \{\text{N}_2, \text{Ar}\} \tag{A.30}$$

where $F^{\text{fts}}_{\text{fd},j}$ and $F^{\text{fts}}_{\text{pd},j}$ are the molar flow rates of species j in the feedstock and product streams of the FT synthesis reactor respectively; $R^{\text{fts}}_{\text{CO}}$ is the conversion of CO in the FT reaction, and S^{fts}_j is the carbon selectivity to species j in the FT reaction, which are specified parameters; $J_{\text{fts}} \equiv \{\text{CH}_4, \text{C}_2\text{H}_4, \text{C}_2\text{H}_6, \text{C}_3\text{H}_6, \text{C}_3\text{H}_8, \text{C}_4\text{H}_8, \text{C}_4\text{H}_{10}, \text{C}_6\text{H}_{14}, \text{C}_8\text{H}_{18}, \text{C}_{16}\text{H}_{34}, \text{C}_{33}\text{H}_{68}, \text{CO}_2\}$ is the set of species produced from the FT reaction.

The feedstock specification for the FT synthesis reactor is given by:

$$F^{\text{fts}}_{\text{fd},\text{CO}_2} \leq x^{\text{fts}}_{\text{CO}_2,\text{max}}\, F^{\text{fts}}_{\text{fd}} \tag{A.31}$$

where $F^{\text{fts}}_{\text{fd}}$ and $F^{\text{fts}}_{\text{fd},\text{CO}_2}$ are the total molar flow rate and the CO_2 molar flow in

the feedstock stream of the FT synthesis reactor respectively; $x^{\text{fts}}_{\text{CO}_2,\max}$ is the upper bound of the mole fraction of CO_2 in the FT reactor feedstock, which is a specified parameter. $F^{\text{fts}}_{\text{fd}} = \sum_j F^{\text{fts}}_{\text{fd},j}$, $\forall j \in J_{\text{ftfd}}$, where $J_{\text{ftfd}} \equiv \{\text{CO}, \text{H}_2, \text{CO}_2, \text{H}_2\text{O}, \text{N}_2, \text{Ar}, \text{CH}_4, \text{C}_2\text{H}_4, \text{C}_2\text{H}_6, \text{C}_3\text{H}_6, \text{C}_3\text{H}_8, \text{C}_4\text{H}_8, \text{C}_4\text{H}_{10}, \text{C}_6\text{H}_{14}\}$ is the set of species in the FT reactor feedstock stream.

Hydrocarbon Separation Unit

The mass balance in the hydrocarbon separation unit is given by:

$$F^{\text{hs}}_{\text{lig},j} = F^{\text{fts}}_{\text{pd},j}\ , \quad \forall j \in J_{\text{lig}}/\{\text{C}_6\text{H}_{14}\} \tag{A.32}$$

$$F^{\text{hs}}_{\text{lig},\text{C}_6\text{H}_{14}} = \left(1 - S^{\text{hs}}_{\text{nap},\text{C}_6\text{H}_{14}}\right) F^{\text{fts}}_{\text{pd},\text{C}_6\text{H}_{14}} \tag{A.33}$$

$$F^{\text{hs}}_{\text{nap},\text{C}_6\text{H}_{14}} = S^{\text{hs}}_{\text{nap},\text{C}_6\text{H}_{14}}\ F^{\text{fts}}_{\text{pd},\text{C}_6\text{H}_{14}} \tag{A.34}$$

$$F^{\text{hs}}_{\text{nap},\text{C}_8\text{H}_{18}} = F^{\text{fts}}_{\text{pd},\text{C}_8\text{H}_{18}} + F^{\text{hc}}_{\text{pd},\text{C}_8\text{H}_{18}} \tag{A.35}$$

$$F^{\text{hs}}_{\text{dis}} = F^{\text{fts}}_{\text{pd},\text{C}_{16}\text{H}_{34}} + F^{\text{hc}}_{\text{pd},\text{C}_{16}\text{H}_{34}} \tag{A.36}$$

$$F^{\text{hs}}_{\text{wax}} = F^{\text{fts}}_{\text{pd},\text{C}_{33}\text{H}_{68}} + F^{\text{hc}}_{\text{pd},\text{C}_{33}\text{H}_{68}} \tag{A.37}$$

$$F^{\text{hs}}_{\text{w,out}} = F^{\text{fts}}_{\text{pd},\text{H}_2\text{O}} \tag{A.38}$$

where $F^{\text{hs}}_{\text{lig},j}$ and $F^{\text{hs}}_{\text{nap},j}$ is the molar flow rate of species j in the light ends stream and the naphtha (C_6H_{14} and C_8H_{18}) stream, $F^{\text{hs}}_{\text{dis}}$ is the molar flow rate of the diesel (pure $C_{16}H_{34}$) stream, $F^{\text{hs}}_{\text{wax}}$ is the molar flow rate of the wax (pure $C_{33}H_{68}$) stream, $F^{\text{hs}}_{\text{w,out}}$ is the molar flow rate of the output water (pure H_2O) stream, and $F^{\text{hc}}_{\text{pd},j}$ is the molar flow rate of species j in the product stream of the hydrocracking reactor; $S^{\text{hs}}_{\text{nap},\text{C}_6\text{H}_{14}}$ is the split fraction of C_6H_{14} to the naphtha stream, which is a specified parameter estimated from the Aspen simulation model; $J_{\text{lig}} \equiv \{\text{CH}_4, \text{C}_2\text{H}_4, \text{C}_2\text{H}_6, \text{C}_3\text{H}_6, \text{C}_3\text{H}_8, \text{C}_4\text{H}_8, \text{C}_4\text{H}_{10}, \text{C}_6\text{H}_{14}, \text{CO}, \text{H}_2, \text{CO}_2, \text{H}_2\text{O}, \text{N}_2, \text{Ar}\}$ is the set of species in the light ends stream.

Hydrocracking Reactor

Mass balance is given by:

$$F^{\text{hc}}_{\text{pd},C_{33}H_{68}} = R^{\text{hc}}_{\text{wax}}\, F^{\text{hs}}_{\text{wax}} \tag{A.39}$$

$$F^{\text{hc}}_{\text{pd},C_8H_{18}} = \frac{33}{8}\, R^{\text{hc}}_{\text{wax}}\, S^{\text{hc}}_{\text{nap}}\, F^{\text{hs}}_{\text{wax}} \tag{A.40}$$

$$F^{\text{hc}}_{\text{pd},C_{16}H_{34}} = \frac{33}{16}\, R^{\text{hc}}_{\text{wax}} \left(1 - S^{\text{hc}}_{\text{nap}}\right) F^{\text{hs}}_{\text{wax}} \tag{A.41}$$

$$F^{\text{hc}}_{\text{pd},H_2} = F^{\text{psa}}_{\text{hyd}} + 34F^{\text{hs}}_{\text{wax}} - 9F^{\text{hc}}_{\text{pd},C_8H_{18}} - 17F^{\text{hc}}_{\text{pd},C_{16}H_{34}} - 34F^{\text{hc}}_{\text{pd},C_{33}H_{68}} \tag{A.42}$$

$$F^{\text{hc}}_{\text{pd},H_2} = \left(1 - R^{\text{hc}}_{H_2}\right) F^{\text{psa}}_{\text{hyd}} \tag{A.43}$$

where $R^{\text{hc}}_{\text{wax}}$ is the conversion of wax, $R^{\text{hc}}_{H_2}$ is the conversion of H_2, and $S^{\text{hc}}_{\text{nap}}$ is the carbon selectivity to naphtha, which are specified parameters.

Auto-thermal Reforming Reactor

The mass balance is established as:

$$F^{\text{atr}}_{\text{pd,CO}} = \left(1 - R^{\text{atr}}_{\text{cm,CO}}\right) F^{\text{atr}}_{\text{fd,CO}} + \sum_j n_{C,j}\, R^{\text{atr}}_{\text{rf},j} \left(1 - R^{\text{atr}}_{\text{cm},j}\right) F^{\text{atr}}_{\text{fd},j}\,, \quad \forall j \in J_{\text{atr}} \tag{A.44}$$

$$F^{\text{atr}}_{\text{pd},H_2} = \left(1 - R^{\text{atr}}_{\text{cm},H_2}\right) F^{\text{atr}}_{\text{fd},H_2} + \sum_j \left(n_{C,j} + \frac{n_{H,j}}{2}\right) R^{\text{atr}}_{\text{rf},j} \left(1 - R^{\text{atr}}_{\text{cm},j}\right) F^{\text{atr}}_{\text{fd},j}\,, \quad \forall j \in J_{\text{atr}} \tag{A.45}$$

$$F^{\text{atr}}_{\text{pd},H_2O} = F^{\text{atr}}_{\text{w,in}} + R^{\text{atr}}_{\text{cm},H_2}\, F^{\text{atr}}_{\text{fd},H_2} + \sum_j \frac{n_{H,j}}{2}\, R^{\text{atr}}_{\text{cm},j}\, F^{\text{atr}}_{\text{fd},j} - \sum_j n_{C,j}\, R^{\text{atr}}_{\text{rf},j} \left(1 - R^{\text{atr}}_{\text{cm},j}\right) F^{\text{atr}}_{\text{fd},j}\,, \quad \forall j \in J_{\text{atr}} \tag{A.46}$$

$$F^{\text{atr}}_{\text{pd},CO_2} = F^{\text{atr}}_{\text{fd},CO_2} + R^{\text{atr}}_{\text{cm,CO}}\, F^{\text{atr}}_{\text{fd,CO}} + \sum_j n_{C,j}\, R^{\text{atr}}_{\text{cm},j}\, F^{\text{atr}}_{\text{fd},j}\,, \quad \forall j \in J_{\text{atr}} \tag{A.47}$$

$$F^{\text{atr}}_{\text{pd},j} = \left(1 - R^{\text{atr}}_{\text{cm},j}\right) \left(1 - R^{\text{atr}}_{\text{rf},j}\right) F^{\text{atr}}_{\text{fd},j}\,, \quad \forall j \in J_{\text{atr}} \tag{A.48}$$

$$0 = F^{\text{atr}}_{\text{oxy},O_2} - \frac{1}{2}\, R^{\text{atr}}_{\text{cm,CO}}\, F^{\text{atr}}_{\text{fd,CO}} - \frac{1}{2}\, R^{\text{atr}}_{\text{cm},H_2}\, F^{\text{atr}}_{\text{fd},H_2} - \sum_j \left(n_{C,j} + \frac{n_{H,j}}{4}\right) R^{\text{atr}}_{\text{cm},j}\, F^{\text{atr}}_{\text{fd},j}\,, \quad \forall j \in J_{\text{atr}} \tag{A.49}$$

$$F^{\text{atr}}_{\text{pd},j} = F^{\text{atr}}_{\text{fd},j} + F^{\text{atr}}_{\text{oxy},j}\,, \quad \forall j \in \{N_2, \text{Ar}\} \tag{A.50}$$

where $F^{\text{atr}}_{\text{fd},j}$, $F^{\text{atr}}_{\text{pd},j}$ and $F^{\text{atr}}_{\text{oxy},j}$ are the molar flow rates of species j in the feedstock stream of the ATR reactor, the product stream of the ATR reactor and the oxygen stream from the ASU injected into the ATR reactor, and $F^{\text{atr}}_{\text{w,in}}$ is the molar flow rate of steam injected in the ATR reactor; $R^{\text{atr}}_{\text{cm},j}$ is the conversion of species j in the combustion reaction, which is defined as a variable dependent on the amount of input oxygen; $R^{\text{atr}}_{\text{rf},j}$ is the conversion of species j in the steam reforming reaction (after the combustion reaction), which is a specified parameter; $J_{\text{atr}} \equiv \{CH_4, C_2H_4, C_2H_6, C_3H_6, C_3H_8, C_4H_8, C_4H_{10}, C_6H_{14}\}$ is the set of hydrocarbon species reacted in the ATR reactor. For simplicity, we assume all combustible species in the ATR reactor including CO, H_2 and hydrocarbons have the same percent conversion, thus $R^{\text{atr}}_{\text{cm},j}$ is assumed to be equal for all reactant species, and all $R^{\text{atr}}_{\text{cm},j}$ can be reduced to one variable $R^{\text{atr}}_{\text{cm}}$. $R^{\text{atr}}_{\text{rf},j}$ is set to be 1 for all hydrocarbon species except CH_4.

Excess steam needs to be added to achieve high conversion in the steam reforming reactor. The appropriate steam injection rate should be determined by the detailed ATR reactor model. Here, a fixed fraction of input water is assumed to be consumed in the ATR reactor. Hence, the amount of injected steam is simply calculated by:

$$F^{\text{atr}}_{\text{pd},H_2O} = \left(1 - R^{\text{atr}}_{\text{w}}\right)\left(F^{\text{atr}}_{\text{w,in}} + R^{\text{atr}}_{\text{cm},H_2}\, F^{\text{atr}}_{\text{fd},H_2} + \sum_j \frac{n_{\text{H},j}}{2}\, R^{\text{atr}}_{\text{cm},j}\, F^{\text{atr}}_{\text{fd},j}\right), \quad \forall j \in J_{\text{atr}} \tag{A.51}$$

where $R^{\text{atr}}_{\text{w}}$ is the water conversion in the ATR reactor, which is a specified parameter.

Methanol Synthesis Reactor

The mass balance in the MeOH reactor is given by:

$$F^{\text{mes}}_{\text{pd},j} = F^{\text{mes}}_{\text{fd},j} + R^{\text{mes}}_{\text{CO}}\, S^{\text{mes}}_{\text{m}}\, \text{Sto}^{\text{mes}}_{\text{m},j}\, F^{\text{mes}}_{\text{fd,CO}} + R^{\text{mes}}_{\text{CO}}\left(1 - S^{\text{mes}}_{\text{m}}\right)\text{Sto}^{\text{mes}}_{\text{s},j}\, F^{\text{mes}}_{\text{fd,CO}}, \quad \forall j \in J_{\text{mes}} \tag{A.52}$$

where $F^{\text{mes}}_{\text{fd},j}$ and $F^{\text{mes}}_{\text{pd},j}$ is the molar flow rates of species j in the feedstock stream and the product stream of the MeOH reactor respectively; $R^{\text{mes}}_{\text{CO}}$ is the conversion of CO in the MeOH reactor, $S^{\text{mes}}_{\text{m}}$ is the selectivity to the main reaction (or mole ratio of CO reacted in the main reaction to total reacted CO); $\text{Sto}^{\text{mes}}_{\text{m},j}$ and $\text{Sto}^{\text{mes}}_{\text{s},j}$ are

the stoichiometric coefficients of species j in the main reaction and the side reaction respectively; $J_{\text{mes}} \equiv \{\text{CO, H}_2\text{, CO}_2\text{, H}_2\text{O, CH}_4\text{, N}_2\text{, Ar, CH}_3\text{OH, C}_2\text{H}_5\text{OH}\}$ is the set of species involved in the MeOH reactor.

CO_2 content in the feedstock of MeOH reactor is constrained by an up limit, which is given by:

$$F^{\text{mes}}_{\text{fd,CO}_2} \leq x^{\text{mes}}_{\text{CO}_2,\text{max}}\, F^{\text{mes}}_{\text{fd}} \tag{A.53}$$

where $F^{\text{mes}}_{\text{fd}}$ and $F^{\text{mes}}_{\text{fd,CO}_2}$ are the total molar flow rate and the CO_2 molar flow in the feedstock stream of the MeOH synthesis reactor respectively; $x^{\text{mes}}_{\text{CO}_2,\text{max}}$ is the upper bound of the mole fraction of CO_2 in the MeOH reactor feedstock, which is a specified parameter. $F^{\text{mes}}_{\text{fd}} = \sum_j F^{\text{mes}}_{\text{fd},j}$, $\forall j \in J_{\text{mefd}}$, where $J_{\text{mefd}} \equiv \{\text{CO, H}_2\text{, CO}_2\text{, H}_2\text{O, N}_2\text{, Ar, CH}_4\text{, CH}_3\text{OH}\}$ is the set of species in the MeOH reactor feedstock stream.

Methanol Separation Unit

The mass balance in the methanol separation unit is given by:

$$F^{\text{ms}}_{\text{unr},j} = F^{\text{mes}}_{\text{pd},j}\,, \quad \forall j \in J_{\text{unr}}/\{\text{CH}_3\text{OH}\} \tag{A.54}$$

$$F^{\text{ms}}_{\text{unr,CH}_3\text{OH}} = S^{\text{ms}}_{\text{unr,CH}_3\text{OH}}\, F^{\text{mes}}_{\text{pd,CH}_3\text{OH}} \tag{A.55}$$

$$F^{\text{ms}}_{\text{met}} = S^{\text{ms}}_{\text{met,CH}_3\text{OH}}\, F^{\text{mes}}_{\text{pd,CH}_3\text{OH}} \tag{A.56}$$

$$F^{\text{ms}}_{\text{alc,CH}_3\text{OH}} = \left(1 - S^{\text{ms}}_{\text{unr,CH}_3\text{OH}} - S^{\text{ms}}_{\text{met,CH}_3\text{OH}}\right) F^{\text{mes}}_{\text{pd,CH}_3\text{OH}} \tag{A.57}$$

$$F^{\text{ms}}_{\text{alc},j} = F^{\text{mes}}_{\text{pd},j}\,, \quad \forall j \in J_{\text{alc}}/\{\text{CH}_3\text{OH}\} \tag{A.58}$$

where $F^{\text{ms}}_{\text{unr},j}$ and $F^{\text{ms}}_{\text{alc},j}$ are the molar flow rates of species j in the unreacted syngas stream and the higher alcohols stream, and $F^{\text{ms}}_{\text{met}}$ is the molar flow rate of the methanol (pure CH_3OH) stream; $S^{\text{ms}}_{\text{unr,CH}_3\text{OH}}$ and $S^{\text{ms}}_{\text{met,CH}_3\text{OH}}$ are the split fractions of CH_3OH to the unreacted syngas stream and the methanol stream, which are specified parameters estimated from the Aspen simulation model; $J_{\text{unr}} \equiv \{\text{CO, H}_2\text{, CO}_2\text{, CH}_4\text{, N}_2\text{, Ar, CH}_3\text{OH}\}$ is the set of species in the unreacted syngas stream, and $J_{\text{alc}} \equiv \{\text{CH}_3\text{OH, H}_2\text{O, C}_2\text{H}_5\text{OH}\}$ is the set of species in the higher alcohols stream.

Gas Turbine

The mass balance is denoted by:

$$F^{\text{gtc}}_{\text{pd,CO}_2} = F^{\text{gtc}}_{\text{fd,CO}_2} + \sum_j n_{\text{C},j}\, F^{\text{gtc}}_{\text{fd},j}\,, \quad \forall j \in J_{\text{gtc}} \tag{A.59}$$

$$F^{\text{gtc}}_{\text{pd,SO}_2} = \sum_j n_{\text{S},j}\, F^{\text{gtc}}_{\text{fd},j}\,, \quad \forall j \in J_{\text{gtc}} \tag{A.60}$$

$$F^{\text{gtc}}_{\text{pd,H}_2\text{O}} = F^{\text{gtc}}_{\text{fd,H}_2\text{O}} + \frac{1}{2}\sum_j n_{\text{H},j}\, F^{\text{gtc}}_{\text{fd},j}\,, \quad \forall j \in J_{\text{gtc}} \tag{A.61}$$

$$F^{\text{gtc}}_{\text{pd,O}_2} = F^{\text{gtc}}_{\text{fd,O}_2} - \sum_j \left(n_{\text{C},j} + n_{\text{S},j} + \frac{1}{4}\, n_{\text{H},j} - \frac{1}{2}\, n_{\text{O},j}\right) F^{\text{gtc}}_{\text{fd},j}\,, \quad \forall j \in J_{\text{gtc}} \tag{A.62}$$

$$F^{\text{gtc}}_{\text{pd},j} = F^{\text{gtc}}_{\text{fd},j}\,, \quad \forall j \in \{\text{N}_2, \text{Ar}\} \tag{A.63}$$

$$F^{\text{gtc}}_{\text{pd,H}_2\text{O}} = R^{\text{gtc}}_{\text{O}_2}\, F^{\text{gtc}}_{\text{fd,H}_2\text{O}} \tag{A.64}$$

where $F^{\text{gtc}}_{\text{fd},j}$ and $F^{\text{gtc}}_{\text{pd},j}$ are the molar flow rates of species j in the feedstock stream and the product stream of the gas turbine combustor; $R^{\text{gtc}}_{\text{O}_2}$ is the excess ratio of O_2 in the gas turbine combustor, which is a specified parameter; $J_{\text{gtc}} \equiv \{\text{CO}, \text{H}_2, \text{CH}_4, \text{C}_2\text{H}_4, \text{C}_2\text{H}_6, \text{C}_3\text{H}_6, \text{C}_3\text{H}_8, \text{C}_4\text{H}_8, \text{C}_4\text{H}_{10}, \text{C}_6\text{H}_{14}, \text{CH}_3\text{OH}, \text{H}_2\text{S}\}$ is the set of combusted species in the gas turbine combustor.

The high temperature flue gas produced from the gas turbine combustor expands in the gas turbine, passes through the HRSG, and then is discharged. The mass balance in the gas turbine and HRSG is given by:

$$F^{\text{gt}}_{\text{pd},j} = F^{\text{gtc}}_{\text{pd},j}\,, \quad \forall j \in J_{\text{gt}} \tag{A.65}$$

$$F^{\text{sg}}_{\text{fl},j} = F^{\text{gt}}_{\text{pd},j}\,, \quad \forall j \in J_{\text{gt}} \tag{A.66}$$

where $F^{\text{gt}}_{\text{pd},j}$ and $F^{\text{sg}}_{\text{fl},j}$ are the molar flow rates of species j in the product stream (or flue gas) of the gas turbine and the HRSG respectively; $J_{\text{gt}} \equiv \{\text{N}_2, \text{O}_2, \text{Ar}, \text{CO}_2, \text{H}_2\text{O}, \text{SO}_2\}$ is the set of species in the gas turbine flue gas.

The SO_2 molar flow rate in the flue gas is limited by the following sulfur regulation:

$$\mathrm{MW_S}\ F^{\mathrm{sg}}_{\mathrm{fl,SO_2}} \leq R^{\mathrm{fl}}_{\mathrm{S,max}} \left[w_{\mathrm{coal,S}} \left(1 - w_{\mathrm{coal,H_2O}}\right) m^{\mathrm{gas}}_{\mathrm{coal}} + w_{\mathrm{bio,S}} \left(1 - w_{\mathrm{bio,H_2O}}\right) m^{\mathrm{gas}}_{\mathrm{bio}} \right] \tag{A.67}$$

where $R^{\mathrm{fl}}_{\mathrm{S,max}}$ is the upper bound of the ratio of the sulfur mass flow rate in the flue gas to the sulfur mass flow rate in the feedstock of the entire process, which is a specified parameter.

Gas Coolers and Heaters

In the gas coolers without water output and gas heaters, the mass balance in the general form is simply given by:

$$F^k_{\mathrm{out},j} = F^k_{\mathrm{in},j}\ , \quad \forall j \in J_{\mathrm{spe}(k)}\ , \ \forall k \in K_{\mathrm{co}} \cup K_{\mathrm{rh}} \tag{A.68}$$

where $F^k_{\mathrm{in},j}$ and $F^k_{\mathrm{out},j}$ are the molar flow rates of species j in the input stream and output stream of unit operation k respectively; $J_{\mathrm{spe}(k)}$ is the set of species in the unit operation k, $K_{\mathrm{co}} \equiv \{\mathrm{rc, sc, atrpdco}\}$ is the set of gas coolers without water output, and $K_{\mathrm{rh}} \equiv \{\mathrm{rh1, wgs1ht, wgs2ht, rh2, rh3, atrfdh, nh, gtcwh}\}$ is the set of gas heaters.

In the gas coolers with water output, the mass balance in the general form is given by:

$$F^k_{\mathrm{out},j} = F^k_{\mathrm{in},j}\ , \quad \forall j \in J_{\mathrm{spe}(k)}/\{\mathrm{H_2O}\}\ , \ \forall k \in K_{\mathrm{cow}} \tag{A.69}$$

$$F^k_{\mathrm{out,H_2O}} = x^{\mathrm{co}}_{\mathrm{w}}\ F^k_{\mathrm{out}}\ , \quad \forall k \in K_{\mathrm{cow}} \tag{A.70}$$

$$F^k_{\mathrm{out}} = \sum_j F^k_{\mathrm{out},j}\ , \quad \forall j \in J_{\mathrm{spe}(k)}\ , \ \forall k \in K_{\mathrm{cow}} \tag{A.71}$$

$$F^k_{\mathrm{w,out}} = F^k_{\mathrm{in,H_2O}} - F^k_{\mathrm{out,H_2O}}\ , \quad \forall k \in K_{\mathrm{cow}} \tag{A.72}$$

where F^k_{out} is the total molar flow rates of the output stream of unit operation k; $x^{\mathrm{co}}_{\mathrm{w}}$ is the mole fraction of water in the output stream of gas coolers, which is a specified parameter; $K_{\mathrm{cow}} \equiv \{\mathrm{co1, co2, co3, clsc}\}$ is the set of gas coolers with water output.

Compressors and Turbines

For all compressors and turbines, the mass balance in the general form is simply given by:

$$F^{k}_{\text{out},j} = F^{k}_{\text{in},j} \ , \quad \forall j \in J_{\text{spe}(k)} \ , \ \forall k \in K_{\text{cp}} \cup K_{\text{tb}} \tag{A.73}$$

Where $K_{\text{cp}} \equiv$ {oxyc, clsc, cc, psagtc, atrscc, ligc1, ligc2, oxycr, unrc1, unrc2, nc, ac} is the set of compressors, and $K_{\text{tb}} \equiv$ {sntft, sntgt1, sntgt2, gt} is the set of turbines.

Mixers

In the polygeneration process, the mixers are placed before reactors, blending the reactor feedstock from different sources. The mass balance in mixers is given by:

$$F^{k}_{\text{fd},j} = \sum_{k'} F^{k'}_{\text{out},j} \ , \quad \forall j \in J_{\text{spe}(k)} \ , \ \forall k \in K_{\text{rtf}} \ , \ \forall k' \in K_{\text{fed}(k)} \tag{A.74}$$

where $F^{k}_{\text{fd},j}$ is the molar flow rate of species j in the feed stream of unit operation k; $K_{\text{rtf}} \equiv$ {wgs1, fts, atr, mes, gtc} is the set of reactors requiring feedstock mixer, $K_{\text{fed}(k)}$ is the set of unit operations providing the feedstock to reactor k.

Splitters

The mass balance in splitters is given by:

$$F^{k'}_{\text{in},j} = S^{k'} \ F^{k}_{\text{in},j} \ , \quad \forall j \in J_{\text{spe}(k)} \ , \ \forall k \in K_{\text{spl}} \ , \ \forall k', k'' \in K_{\text{out}(k)} \tag{A.75}$$

$$F^{k''}_{\text{in},j} = F^{k}_{\text{in},j} - F^{k'}_{\text{in},j} \ , \quad \forall j \in J_{\text{spe}(k)} \ , \ \forall k \in K_{\text{spl}} \ , \ \forall k', k'' \in K_{\text{out}(k)} \tag{A.76}$$

where $S^{k'}$ is the split fraction of the splitter output stream to unit operation k'; $K_{\text{spl}} \equiv$ {splsyn1, splsyn2, splcar, splpsa, spllig, splatr, splunr} is the set of splitters, $K_{\text{out}(k)}$ is the set of unit operations receiving the output of the splitter k.

A.1.2 Energy Balance

Gas Coolers and Heaters

The heat generation of the gas coolers without water output is equal to the difference of input enthalpy and output enthalpy:

$$Q_{\mathrm{g}}^{k} = \sum_{j} F_{\mathrm{in},j}^{k}\, h_j\left(T_{\mathrm{in}}^{k}\right) - \sum_{j} F_{\mathrm{out},j}^{k}\, h_j\left(T_{\mathrm{out}}^{k}\right) \ , \quad \forall j \in J_{\mathrm{spe}(k)} \ , \ \forall k \in K_{\mathrm{co}} \tag{A.77}$$

where Q_{g}^{k} is the heat generation rate of the unit operation k. h_j is the molar enthalpy of species j, which is a function of temperature. T_{in}^{k} and T_{out}^{k} are temperatures of the input stream and the output stream of unit operation k respectively, which are specified parameters. In energy balance calculations, all temperatures except the temperature of gas turbine input stream are specified parameters. $h_j\left(T_{\mathrm{in}}^{k}\right)$ and $h_j\left(T_{\mathrm{out}}^{k}\right)$ are the molar enthalpy of species j in the input stream and the output stream of unit operation k respectively, which will be calculated in Section A.1.3.

The heat consumption of the gas heaters is given by:

$$Q_{\mathrm{c}}^{k} = \sum_{j} F_{\mathrm{out},j}^{k}\, h_j\left(T_{\mathrm{out}}^{k}\right) - \sum_{j} F_{\mathrm{in},j}^{k}\, h_j\left(T_{\mathrm{in}}^{k}\right) \ , \quad \forall j \in J_{\mathrm{spe}(k)} \ , \ \forall k \in K_{\mathrm{rh}} \tag{A.78}$$

where Q_{c}^{k} is the heat consumption rate of the unit operation k.

Reactors

The heat generation of the reactors in the general form is denoted by:

$$Q_{\mathrm{g}}^{k} = \sum_{k'} \sum_{j} F_{\mathrm{out},j}^{k'}\, h_j\left(T_{\mathrm{out}}^{k'}\right) - \sum_{j} F_{\mathrm{out},j}^{k}\, h_j\left(T_{\mathrm{out}}^{k}\right) \ , \quad \forall j \in J_{\mathrm{spe}(k)} \ , \ \forall k \in K_{\mathrm{rt}} \ , \ \forall k' \in K_{\mathrm{fed}(k)} \tag{A.79}$$

where $K_{\mathrm{rt}} \equiv \{\mathrm{hy}, \mathrm{cls}, \mathrm{wgs1}, \mathrm{wgs2}, \mathrm{fts}, \mathrm{hc}, \mathrm{atr}, \mathrm{mes}, \mathrm{gtc}\}$ is the set of reactors.

The ATR reactor is required to satisfy the auto-thermal constraint:

$$Q_{\mathrm{g}}^{\mathrm{atr}} \geq 0 \tag{A.80}$$

The temperature of gas turbine combustor product (or output) stream is a variable, whose value is dependent on the input rates of nitrogen and steam dilution stream. Its value is limited by:

$$T_{\text{out}}^{\text{gtc}} \leq T_{\text{max}}^{\text{gtc}} \tag{A.81}$$

where $T_{\text{max}}^{\text{gtc}}$ is the upper bound of the allowable temperatures of the gas turbine combustor product, which is a specified parameter estimated from the NETL report. And the gas turbine combustor is assumed to be an adiabatic reactor:

$$Q_{\text{g}}^{\text{gtc}} = 0 \tag{A.82}$$

Separation Units

The heat and power consumption in the Selexol units for H_2S removal are given by:

$$Q_{\text{c}}^{k} = \text{QC}_{\text{c}}^{\text{sesul}} \, F_{\text{fd}}^{k} \,, \quad \forall k \in \{\text{se1}\} \tag{A.83}$$

$$E_{\text{c}}^{k} = \text{EC}_{\text{c}}^{\text{sesul}} \, F_{\text{fd}}^{k} \,, \quad \forall k \in \{\text{se1}\} \tag{A.84}$$

where E_{c}^{k} is the power consumption rate in the unit operation k, and F_{fd}^{k} is the total molar flow rate of the feedstock stream of unit operation k. $F_{\text{fd}}^{k} = \sum_j F_{\text{fd},j}^{k}$, $\forall j \in J_{\text{spe}(k)}$. In this case, $F_{\text{fd}}^{\text{se1}} = F_{\text{tsyn}}^{\text{col}} = \sum_j F_{\text{tsyn},j}^{\text{col}}$, $\forall j \in J_{\text{tsyn}}$. $\text{QC}_{\text{c}}^{\text{sesul}}$ and $\text{EC}_{\text{c}}^{\text{sesul}}$ are the coefficients of the heat consumption rate and the power consumption rate in the Selexol unit for H_2S removal, which are specified parameters regressed from the Aspen simulation results.

The power consumption in the Selexol units for CO_2 removal is given by:

$$E_{\text{c}}^{k} = \text{EC}_{\text{c}}^{\text{secar}} \, F_{\text{car}}^{k} \,, \quad \forall k \in \{\text{se2}, \text{se3}\} \tag{A.85}$$

where F_{car}^{k} is the molar flow rate of the CO_2 stream produced from unit operation k; $\text{EC}_{\text{c}}^{\text{secar}}$ is the coefficient of the power consumption rate in the Selexol unit for CO_2 removal, which is a specified parameter regressed from the Aspen simulation results. Heat consumption in the Selexol units for CO_2 removal is neglected.

The heat and power consumption in the hydrocarbon separation unit are given by:

$$Q_{\mathrm{c}}^{\mathrm{hs}} = \mathrm{QC}_{\mathrm{c,A}}^{\mathrm{hs}}\ F_{\mathrm{pd}}^{\mathrm{fts}} + \mathrm{QC}_{\mathrm{c,B}}^{\mathrm{hs}}\ F_{\mathrm{fd,CO}}^{\mathrm{fts}} \tag{A.86}$$

$$E_{\mathrm{c}}^{\mathrm{hs}} = \mathrm{EC}_{\mathrm{c}}^{\mathrm{hs}}\ F_{\mathrm{fd,CO}}^{\mathrm{fts}} \tag{A.87}$$

where $F_{\mathrm{pd}}^{\mathrm{fts}}$ is the total molar flow rate of the product stream of the FT synthesis reactor, and $F_{\mathrm{fd,CO}}^{\mathrm{fts}}$ is the molar flow rate of CO in the feedstock stream of the FT synthesis reactor; $\mathrm{QC}_{\mathrm{c,A}}^{\mathrm{hs}}$ and $\mathrm{QC}_{\mathrm{c,B}}^{\mathrm{hs}}$ are the coefficients of the heat consumption rate in the hydrocarbon separation unit, and $\mathrm{EC}_{\mathrm{c}}^{\mathrm{hs}}$ is the coefficient of the power consumption rate in the hydrocarbon separation unit, which are specified parameters regressed from the Aspen simulation results. $F_{\mathrm{pd}}^{\mathrm{fts}} = \sum_j F_{\mathrm{pd},j}^{\mathrm{fts}},\ \forall j \in J_{\mathrm{ftpd}}$, where $J_{\mathrm{ftpd}} \equiv \{\mathrm{CO}$, $\mathrm{H_2}$, $\mathrm{CO_2}$, $\mathrm{H_2O}$, $\mathrm{N_2}$, Ar, $\mathrm{CH_4}$, $\mathrm{C_2H_4}$, $\mathrm{C_2H_6}$, $\mathrm{C_3H_6}$, $\mathrm{C_3H_8}$, $\mathrm{C_4H_8}$, $\mathrm{C_4H_{10}}$, $\mathrm{C_6H_{14}}$, $\mathrm{C_8H_{18}}$, $\mathrm{C_{16}H_{34}}$, $\mathrm{C_{33}H_{68}}\}$ is the set of species in the FT reactor product stream.

The heat and power consumption in the methanol separation unit are given by:

$$Q_{\mathrm{c}}^{\mathrm{ms}} = \mathrm{QC}_{\mathrm{c,A}}^{\mathrm{ms}}\ F_{\mathrm{pd}}^{\mathrm{mes}} + \mathrm{QC}_{\mathrm{c,B}}^{\mathrm{ms}}\ F_{\mathrm{fd,CO}}^{\mathrm{mes}} \tag{A.88}$$

$$E_{\mathrm{c}}^{\mathrm{ms}} = \mathrm{EC}_{\mathrm{c}}^{\mathrm{ms}}\ F_{\mathrm{pd}}^{\mathrm{mes}} \tag{A.89}$$

where $F_{\mathrm{pd}}^{\mathrm{mes}}$ is the total molar flow rate of the product stream of the MeOH synthesis reactor, and $F_{\mathrm{fd,CO}}^{\mathrm{mes}}$ is the molar flow rate of CO in the feedstock stream of the MeOH synthesis reactor; $\mathrm{QC}_{\mathrm{c,A}}^{\mathrm{ms}}$ and $\mathrm{QC}_{\mathrm{c,B}}^{\mathrm{ms}}$ are the coefficients of the heat consumption rate in the methanol separation unit, and $\mathrm{EC}_{\mathrm{c}}^{\mathrm{ms}}$ is the coefficient of the power consumption rate in the methanol separation unit, which are specified parameters regressed from the Aspen simulation results. $F_{\mathrm{pd}}^{\mathrm{mes}} = \sum_j F_{\mathrm{pd},j}^{\mathrm{mes}},\ \forall j \in J_{\mathrm{mepd}}$, where $J_{\mathrm{mepd}} \equiv \{\mathrm{CO}$, $\mathrm{H_2}$, $\mathrm{CO_2}$, $\mathrm{H_2O}$, $\mathrm{N_2}$, Ar, $\mathrm{CH_4}$, $\mathrm{CH_3OH}$, $\mathrm{C_2H_5OH}\}$ is the set of species in the MeOH reactor product stream.

Compressors and Turbines

The power consumption in compressors is given by:

$$E_{\mathrm{c}}^{k} = E_{\mathrm{c},0}^{k} \, \frac{F_{\mathrm{in}}^{k}}{F_{\mathrm{in},0}^{k}} \,, \quad \forall k \in K_{\mathrm{cp}} \tag{A.90}$$

where F_{in}^{k} is the total molar flow rate of the input stream of unit operation k; $F_{\mathrm{in},0}^{k}$ is the total molar flow rate of the input stream of unit operation k in the base case, $E_{\mathrm{c},0}^{k}$ is the power consumption rate of unit operation k in the corresponding base case, which are specified parameters. $F_{\mathrm{in}}^{k} = \sum_{j} F_{\mathrm{in},j}^{k}$, $\forall j \in J_{\mathrm{spe}(k)}$.

The power consumption rates in the ASU and gasifier are calculated in the same way:

$$E_{\mathrm{c}}^{k} = E_{\mathrm{c},0}^{k} \, \frac{F_{\mathrm{in}}^{k}}{F_{\mathrm{in},0}^{k}} \,, \quad \forall k \in \{\mathrm{asu}, \mathrm{gas}\} \tag{A.91}$$

The power generation in turbines except the gas turbine and steam turbine is given by:

$$E_{\mathrm{g}}^{k} = E_{\mathrm{g},0}^{k} \, \frac{F_{\mathrm{in}}^{k}}{F_{\mathrm{in},0}^{k}} \,, \quad \forall k \in K_{\mathrm{tb}}/\{\mathrm{gt}\} \tag{A.92}$$

where $F_{\mathrm{in},0}^{k}$ is the total molar flow rate of the input stream of unit operation k in the base case, $E_{\mathrm{g},0}^{k}$ is the power generation rate of unit operation k in the corresponding base case, which are specified parameters.

The power generation in the gas turbine is denoted by:

$$E_{\mathrm{g}}^{\mathrm{gt}} = \eta^{\mathrm{gt}} \, Q_{\mathrm{c}}^{\mathrm{gt}} \tag{A.93}$$

where $E_{\mathrm{g}}^{\mathrm{gt}}$ is the power generation rate in the gas turbine and $Q_{\mathrm{c}}^{\mathrm{gt}}$ is the heat consumption rate in the gas turbine; η^{gt} is the mechanical efficiency in the gas turbine, which is a specified parameter estimated from the Aspen simulation model.

The heat consumption in the gas turbine is given by:

$$Q_{\mathrm{c}}^{\mathrm{gt}} = Q_{\mathrm{g}}^{\mathrm{gt}} \tag{A.94}$$

$$Q_{\mathrm{g}}^{\mathrm{gt}} = \sum_{j} F_{\mathrm{pd},j}^{\mathrm{gtc}}\, h_j\left(T_{\mathrm{pd}}^{\mathrm{gtc}}\right) - \sum_{j} F_{\mathrm{pd},j}^{\mathrm{gt}}\, h_j\left(T_{\mathrm{pd}}^{\mathrm{gt}}\right)\ , \quad \forall j \in J_{\mathrm{gt}} \tag{A.95}$$

where $Q_{\mathrm{g}}^{\mathrm{gt}}$ is the heat generation rate in the gas turbine, $T_{\mathrm{pd}}^{\mathrm{gtc}}$ is the temperature of the product stream of the gas turbine combustor; $T_{\mathrm{pd}}^{\mathrm{gt}}$ is the temperature of the product stream of the gas turbine, which is a specified parameter estimated from the Aspen simulation model.

The power generated in the steam turbine is divided into two parts: power generated from the high quality heat and the low quality heat, whose energy conversion efficiency are different. The power generation in the steam turbine is then given by:

$$E_{\mathrm{g}}^{\mathrm{sthi}} = \eta^{\mathrm{sthi}}\, Q_{\mathrm{c}}^{\mathrm{sthi}} \tag{A.96}$$

$$E_{\mathrm{g}}^{\mathrm{stlo}} = \eta^{\mathrm{stlo}}\, Q_{\mathrm{c}}^{\mathrm{stlo}} \tag{A.97}$$

where $E_{\mathrm{g}}^{\mathrm{sthi}}$ and $E_{\mathrm{g}}^{\mathrm{stlo}}$ are the power generation rates in the steam turbine from the high quality heat and the low quality heat respectively, $Q_{\mathrm{c}}^{\mathrm{sthi}}$ and $Q_{\mathrm{c}}^{\mathrm{stlo}}$ are the high quality heat consumption rate and the low quality heat consumption rate in the steam turbine; η^{sthi} and η^{stlo} are the energy conversion efficiency of the high quality heat and low quality heat respectively, which are specified parameters estimated from Aspen simulation model.

High quality heat only includes the heat generated under relatively high temperatures. In this model, it is given by:

$$Q_{\mathrm{c}}^{\mathrm{sthi}} \leq Q_{\mathrm{g}}^{\mathrm{rc}} + Q_{\mathrm{g}}^{\mathrm{sc}} + Q_{\mathrm{g}}^{\mathrm{sg}} + Q_{\mathrm{g}}^{\mathrm{atrpdco}} - Q_{\mathrm{c}}^{\mathrm{strfdh}} - Q_{\mathrm{c}}^{\mathrm{wgs1ht}} - Q_{\mathrm{c}}^{\mathrm{wgs2ht}} \tag{A.98}$$

where $Q_{\mathrm{g}}^{\mathrm{rc}}$, $Q_{\mathrm{g}}^{\mathrm{sc}}$, $Q_{\mathrm{g}}^{\mathrm{sg}}$ and $Q_{\mathrm{g}}^{\mathrm{atrpdco}}$ are the heat generation rates in the gasifier radiant cooler, the gasifier convective cooler, the gas turbine flue gas cooler in the HRSG and the ATR reactor product cooler; $Q_{\mathrm{c}}^{\mathrm{strfdh}}$, $Q_{\mathrm{c}}^{\mathrm{wgs1ht}}$, $Q_{\mathrm{c}}^{\mathrm{wgs2ht}}$ are the heat consumption rates in the ATR feedstock heater, the heater for WGS Reactor 1 injected steam and the heater for WGS Reactor 2 injected steam.

Low quality heat is supplied by all other heat generated in the process.

Heat Recovery Steam Generator

The heat recovery from the gas turbine flue gas in the HRSG is given by:

$$Q_{\mathrm{g}}^{\mathrm{sg}} = \sum_{j} F_{\mathrm{pd},j}^{\mathrm{gt}}\, h_j\left(T_{\mathrm{pd}}^{\mathrm{gt}}\right) - \sum_{j} F_{\mathrm{fl},j}^{\mathrm{sg}}\, h_j\left(T_{\mathrm{fl}}^{\mathrm{sg}}\right) \ , \quad \forall j \in J_{\mathrm{gt}} \tag{A.99}$$

where $T_{\mathrm{fl}}^{\mathrm{sg}}$ is the temperature of the flue gas discharged from the HRSG, which is a specified parameter estimated from the Aspen simulation model.

The heat balance of the whole system is established as:

$$\sum_{k} Q_{\mathrm{g}}^{k} - \sum_{k'} Q_{\mathrm{c}}^{k'} = 0 \ , \quad \forall k \in K_{\mathrm{qg}} \ , \ \forall k' \in K_{\mathrm{qc}} \tag{A.100}$$

where $K_{\mathrm{qg}} \equiv$ {rc, sc, wgs1, wgs2, cls, fts, atr, atrpdco, mes, gt, sg} is the set of unit operations with heat generation and $K_{\mathrm{qc}} \equiv$ {sel, rh1, wgs1ht, wgs2ht, rh2, rh3, hs, atrfdh, ms, nh, gtcwh, gt, sthi, stlo} is the set of unit operations with heat consumption.

A.1.3 Enthalpy Calculation

The molar enthalpy of each species is expressed as the polynomial function of temperature:

$$h_j(T) = h_{\mathrm{A},j}\, T^2 + h_{\mathrm{B},j}\, T + h_{\mathrm{C},j} \ , \quad \forall j \in J_{\mathrm{spe}} \tag{A.101}$$

where $h_{\mathrm{A},j}$, $h_{\mathrm{B},j}$ and $h_{\mathrm{C},j}$ are molar enthalpy coefficients, which are specified parameters regressed from the Aspen Plus property analysis data and are functions of pressure. J_{spe} is the set of all species in the entire system.

A.1.4 Production Rates and Feedstock Consumption Rates

The power generation rate of the whole system is given as follows:

$$m_{\mathrm{ele}}^{\mathrm{p}} = \sum_{k} E_{\mathrm{g}}^{k} - \sum_{k'} E_{\mathrm{c}}^{k'} \ , \quad \forall k \in K_{\mathrm{eg}} \ , \ \forall k' \in K_{\mathrm{ec}} \tag{A.102}$$

where $K_{eg} \equiv$ {sntft, sntgt1, sntgt2, gt, sthi, stlo} is the set of unit operations with power generation and $K_{ec} \equiv$ {asu, oxyc, gas, sel, clsc, se2, se3, cc, psagtc, hs, atrscc, lig1, lig2, oxycr, ms, unrc1, unrc2, nc, ac} is the set of unit operations with power consumption.

The naphtha production rate (mass based) is given by:

$$m^{p}_{nap} = MW_{C_6H_{14}} F^{hs}_{nap,C_6H_{14}} + MW_{C_8H_{18}} F^{hs}_{nap,C_8H_{18}} \tag{A.103}$$

The diesel production rate (mass based) is given by:

$$m^{p}_{dis} = MW_{C_{16}H_{34}} F^{hs}_{dis} \tag{A.104}$$

The methanol production rate (mass based) is given by:

$$m^{p}_{met} = MW_{CH_3OH} F^{ms}_{met} \tag{A.105}$$

The sulfur production rate (mass based) is given by:

$$m^{p}_{es} = MW_{S} F^{cls}_{es} \tag{A.106}$$

The CO_2 sequestration rate (mass based) is given by:

$$m^{p}_{car} = MW_{CO_2} F^{cc}_{car} \tag{A.107}$$

where F^{cc}_{car} is the molar flow rate of the CO_2 stream sent to the CO $_2$ compressor.

$$F^{cc}_{car} = S_{seq} F^{se2}_{car} + F^{se3}_{car} \tag{A.108}$$

where F^{se2}_{car} and F^{se3}_{car} are the molar flow rates of CO_2 streams exiting Selexol Unit 2 and Selexol Unit 3 respectively, S_{seq} is the split fraction of CO_2 stream to sequestration.

The coal consumption rate (mass based) is given by:

$$m^{\mathrm{f}}_{\mathrm{coal}} = m^{\mathrm{gas}}_{\mathrm{coal}} \tag{A.109}$$

The biomass consumption rate (mass based) is given by:

$$m^{\mathrm{f}}_{\mathrm{bio}} = m^{\mathrm{gas}}_{\mathrm{bio}} \tag{A.110}$$

The water consumption rate (mass based) is given by:

$$m^{\mathrm{f}}_{\mathrm{w}} = \mathrm{MW}_{\mathrm{H_2O}} \left(\sum_{k} F^{k}_{\mathrm{w,in}} - \sum_{k'} F^{k'}_{\mathrm{w,out}} \right) , \quad \forall k \in K_{\mathrm{wi}};, \ \forall k' \in K_{\mathrm{wo}} \tag{A.111}$$

where $F^{k}_{\mathrm{w,in}}$ and $F^{k'}_{\mathrm{w,out}}$ are the molar flow rates of the input water in unit operation k and the output water in unit operation k' respectively; $K_{\mathrm{wi}} \equiv$ {gas, wgs1, wgs2, atrfdh, gtc} is the set of unit operations with water input and $K_{\mathrm{wo}} \equiv$ {co1, co2, co3, clsc, hs} is the set of unit operations with water output.

A.1.5 Capital Costs

The capital costs of feedstock preparing equipments are given by:

$$C^{l} = C^{l}_{\mathrm{b}} \left(\frac{m^{\mathrm{gas}}_{\mathrm{fd}}}{F^{l}_{\mathrm{b}}} \right)^{\mathrm{sf}^{l}} , \quad \forall l \in \{\mathrm{fdh}, \mathrm{fdp}\} \tag{A.112}$$

where C^{l} is the capital cost of equipment l, $m^{\mathrm{gas}}_{\mathrm{fd}}$ is the mass flow rate of total feedstock fed into the gasifier;

$$m^{\mathrm{gas}}_{\mathrm{fd}} = m^{\mathrm{gas}}_{\mathrm{coal}} + m^{\mathrm{gas}}_{\mathrm{bio}} \tag{A.113}$$

F^{l}_{b} is the total mass (or molar) flow rate of the input stream of equipment l in the base case, C^{l}_{b} is the capital cost of equipment l in the corresponding base case, and sf^{l} is the sizing factor of equipment l, which are all specified parameters.

The capital costs of gasification related equipments are given by:

$$C^l = C^l_{\mathrm{b}} \left(\frac{m^{\mathrm{gas}}_{\mathrm{fd,dry}}}{F^l_{\mathrm{b}}} \right)^{\mathrm{sf}^l} \quad , \quad \forall l \in \{\mathrm{gas}, \mathrm{ash}, \mathrm{sr}, \mathrm{oth}\} \tag{A.114}$$

where $m^{\mathrm{gas}}_{\mathrm{fd,dry}}$ is the dry mass flow rate of total feedstock fed into the gasifier.

$$m^{\mathrm{gas}}_{\mathrm{fd,dry}} = (1 - w_{\mathrm{coal,H_2O}})\, m^{\mathrm{gas}}_{\mathrm{coal}} + (1 - w_{\mathrm{bio,H_2O}})\, m^{\mathrm{gas}}_{\mathrm{bio}} \tag{A.115}$$

The dry mass flow rate of gasifier feedstock is limited by:

$$m^{\mathrm{gas}}_{\mathrm{fd,dry}} \leq m^{\mathrm{gas}}_{\mathrm{ca}} \tag{A.116}$$

where $m^{\mathrm{gas}}_{\mathrm{ca}}$ is the upper limit of dry mass flow rate of total feedstock fed into the gasifier or the maximum capacity of the gasifier, which is a specified parameter.

The capital cost of CO_2 compressor is given by:

$$C^{\mathrm{cc}} = C^{\mathrm{cc}}_{\mathrm{b}} \left(\frac{m^{\mathrm{p}}_{\mathrm{car}}}{F^{\mathrm{cc}}_{\mathrm{b}}} \right)^{\mathrm{sf}^{\mathrm{cc}}} \tag{A.117}$$

The capital costs of equipments in the hydrocarbon separation process are given by:

$$C^l = C^l_{\mathrm{b}} \left(\frac{m^{\mathrm{p}}_{\mathrm{fue}}}{F^l_{\mathrm{b}}} \right)^{\mathrm{sf}^l} \quad , \quad \forall l \in \{\mathrm{hs}, \mathrm{hc}\} \tag{A.118}$$

where $m^{\mathrm{p}}_{\mathrm{fue}}$ is the mass based liquid fuels production rate of the whole process.

$$m^{\mathrm{p}}_{\mathrm{fue}} = m^{\mathrm{p}}_{\mathrm{nap}} + m^{\mathrm{p}}_{\mathrm{dis}} \tag{A.119}$$

The capital costs of the methanol separation unit are given by:

$$C^{\mathrm{ms}} = C^{\mathrm{ms}}_{\mathrm{b}} \left(\frac{m^{\mathrm{p}}_{\mathrm{met}}}{F^{\mathrm{ms}}_{\mathrm{b}}} \right)^{\mathrm{sf}^{\mathrm{ms}}} \tag{A.120}$$

The capital costs of the gas turbine and steam turbine are given by:

$$C^l = C^l_{\mathrm{b}} \left(\frac{E^l_{\mathrm{g}}}{F^l_{\mathrm{b}}} \right)^{\mathrm{sf}^l} , \quad \forall l \in \{\mathrm{gt}, \mathrm{st}\} \tag{A.121}$$

where $E^{\mathrm{st}}_{\mathrm{g}}$ is the power generation rate in the steam turbine, and

$$E^{\mathrm{st}}_{\mathrm{g}} = E^{\mathrm{sthi}}_{\mathrm{g}} + E^{\mathrm{stlo}}_{\mathrm{g}} \tag{A.122}$$

The capital cost of the HRSG is given by:

$$C^{\mathrm{sg}} = C^{\mathrm{sg}}_{\mathrm{b}} \left(\frac{E^{\mathrm{st}}_{\mathrm{g}}}{F^{\mathrm{sg}}_{\mathrm{b}}} \right)^{\mathrm{sf}^{\mathrm{sg}}} \tag{A.123}$$

The capital costs of the Selexol units for CO_2 removal are calculated as two parts: the first part is related to the total molar flow rate of input stream, which is given by:

$$C^l = C^l_{\mathrm{b}} \left(\frac{F^l_{\mathrm{in}}}{F^l_{\mathrm{b}}} \right)^{\mathrm{sf}^l} , \quad \forall l \in \{\mathrm{se2tot}, \mathrm{se3tot}\} \tag{A.124}$$

and the second part is related to the molar flow rate of the output CO_2 stream, which is given by:

$$C^l = C^l_{\mathrm{b}} \left(\frac{F^l_{\mathrm{car}}}{F^l_{\mathrm{b}}} \right)^{\mathrm{sf}^l} , \quad \forall l \in \{\mathrm{se2car}, \mathrm{se3car}\} \tag{A.125}$$

where, F^l_{in} is the total molar flow rate of the input stream of equipment l, and F^l_{car} is the molar flow rate of CO_2 stream exiting the equipment l.

The capital costs of all remaining equipment in the system can be expressed as the general form:

$$C^l = C^l_{\mathrm{b}} \left(\frac{F^l_{\mathrm{in}}}{F^l_{\mathrm{b}}} \right)^{\mathrm{sf}^l} , \quad \forall l \in \{\mathrm{asu}, \mathrm{hy}, \mathrm{se1}, \mathrm{cls}, \mathrm{wgs1}, \mathrm{wgs2}, \mathrm{psa}, \mathrm{sco}, \mathrm{fts}, \mathrm{atr}, \mathrm{fto}, \mathrm{mes}, \mathrm{meo}\} \tag{A.126}$$

The total capital investment of the process is given by:

$$\mathrm{Cap} = \sum_l C^l , \quad \forall l \in L_{\mathrm{eq}} \tag{A.127}$$

where Cap is the total capital investment; $L_{\text{eq}} \equiv$ {fdh, fdp, asu, gas, ash, sr, hy, sel, cls, wgs1, se2tot, se2car, wgs2 se3tot, se3car, cc, psa, sco, fts, hs, hc, atr, fto, mes, ms, meo, gt, st, sg, oth} is set of equipments with capital cost.

A.1.6 Economic Analysis

The total annual cost is:

$$\text{Cost} = \text{Cost}_{\text{fed}} + \text{Cost}_{\text{tax}}^{\text{car}} + \text{Cost}_{\text{ccs}}^{\text{car}} + \text{Cost}_{\text{ope}} \tag{A.128}$$

where Cost is the total annual cost, Cost_{fed} is the cost of purchasing the feedstock, $\text{Cost}_{\text{tax}}^{\text{car}}$ is the carbon emissions tax, $\text{Cost}_{\text{ccs}}^{\text{car}}$ is the cost of carbon sequestration and Cost_{ope} is the operational cost.

The feedstock cost is given by:

$$\text{Cost}_{\text{fed}} = \left(\sum_{q} P_q^{\text{f}} \, m_q^{\text{f}} \right) t_{\text{op}} \, , \quad \forall q \in \text{Feed} \tag{A.129}$$

where m_q^{f} is the consumption rate of feedstock q; P_q^{f} is the market price of feedstock q, and t_{op} is the annual operating time, which are specified parameters; Feed $\equiv$ {coal, bio, w} is the set of feedstocks.

The carbon tax is given by:

$$\text{Cost}_{\text{tax}}^{\text{car}} = P_{\text{tax}}^{\text{car}} \, \text{Emis}_{\text{net}} \tag{A.130}$$

where Emis_{net} is the annual net CO_2 emissions; $P_{\text{tax}}^{\text{car}}$ is the carbon tax per tonne of CO_2 emitted, which is a specified parameter. CO_2 emissions are calculated by:

$$\text{Emis}_{\text{gro}} = \text{MW}_{\text{CO}_2} \left[F_{\text{fl,CO}_2}^{\text{sg}} + (1 - S_{\text{seq}}) \, F_{\text{car}}^{\text{se2}} \right] t_{\text{op}} \tag{A.131}$$

$$\text{Emis}_{\text{net}} = \text{Emis}_{\text{gro}} - \frac{\text{MW}_{\text{CO}_2}}{\text{MW}_{\text{C}}} \left(1 - w_{\text{bio,H}_2\text{O}}\right) w_{\text{bio,C}} \, m_{\text{bio}}^{\text{gas}} \, t_{\text{op}} \tag{A.132}$$

where Emis_{gro} is the annual gross CO_2 emissions. If the carbon tax policy also taxes

the carbon in the liquid fuels (since they will ultimately be burned in their final use), the annual net CO_2 emissions are given by:

$$\begin{aligned}\mathrm{Emis_{net}} =& \mathrm{Emis_{gro}} - \frac{\mathrm{MW_{CO_2}}}{\mathrm{MW_C}} \left(1 - w_{\mathrm{bio,H_2O}}\right) w_{\mathrm{bio,C}}\, m_{\mathrm{bio}}^{\mathrm{gas}}\, t_{\mathrm{op}} \\ &+ \mathrm{MW_{CO_2}} \left(6F_{\mathrm{nap,C_6H_{14}}}^{\mathrm{hs}} + 8F_{\mathrm{nap,C_8H_{18}}}^{\mathrm{hs}} + 16F_{\mathrm{dis}}^{\mathrm{hs}}\right) t_{\mathrm{op}}\end{aligned} \tag{A.133}$$

The carbon sequestration cost is given by:

$$\mathrm{Cost}_{\mathrm{ccs}}^{\mathrm{car}} = P_{\mathrm{ccs}}^{\mathrm{car}}\, m_{\mathrm{car}}^{\mathrm{p}} \tag{A.134}$$

where $P_{\mathrm{ccs}}^{\mathrm{car}}$ is the carbon sequestration fee per tonne CO_2, which is a specified parameter.

The operational cost is given by:

$$\mathrm{Cost_{ope}} = \mathrm{Cost}_{\mathrm{ope}}^{\mathrm{fix}} + \mathrm{Cost}_{\mathrm{ope}}^{\mathrm{var}} \tag{A.135}$$

where $\mathrm{Cost}_{\mathrm{ope}}^{\mathrm{fix}}$ is the fixed annual operational cost, which is a specified parameter; $\mathrm{Cost}_{\mathrm{ope}}^{\mathrm{var}}$ is variable annual operational cost, which is calculated by the linear scaling up relationship:

$$\mathrm{Cost}_{\mathrm{ope}}^{\mathrm{var}} = \mathrm{Cost}_{\mathrm{ope,b}}^{\mathrm{var}}\, \frac{m_{\mathrm{fd}}^{\mathrm{gas}}}{m_{\mathrm{fd,b}}^{\mathrm{gas}}} \tag{A.136}$$

where $m_{\mathrm{fd,b}}^{\mathrm{gas}}$ is the mass flow rate of the total feedstock fed into the gasifier in the base case, and $\mathrm{Cost}_{\mathrm{ope,b}}^{\mathrm{var}}$ is the annual variable operational cost in the corresponding base case, which are specified parameters.

The revenue is denoted by:

$$\mathrm{Reve} = \left(\sum_q P_q^{\mathrm{p}}\, m_q^{\mathrm{p}}\right) t_{\mathrm{op}}\ , \quad \forall q \in \mathrm{Prod} \tag{A.137}$$

where m_q^{p} is the production rate of product q; P_q^{p} is the market price of product q, which are specified parameters; $\mathrm{Prod} \equiv \{\mathrm{ele, nap, dis, met, es}\}$ is the set of products.

The profit is calculated by:

$$\mathrm{Pro}_{\mathrm{gro}} = \mathrm{Reve} - \mathrm{Cost} \tag{A.138}$$

$$\mathrm{Pro}_{\mathrm{net}} = (1 - R_{\mathrm{tax}})\,\mathrm{Pro}_{\mathrm{gro}} \tag{A.139}$$

where $\mathrm{Pro}_{\mathrm{gro}}$ and $\mathrm{Pro}_{\mathrm{net}}$ are the annual gross profit and the annual net profit respectively; R_{tax} is the tax rate, which is a specified parameter.

The net present value, which is the objective function of this model, is denoted by:

$$\mathrm{NPV} = -\mathrm{Cap} + \mathrm{Pro}_{\mathrm{net}}\,\frac{1}{r}\left(1 - \frac{1}{(1+r)^{t_{\mathrm{lf}}}}\right) + \frac{R_{\mathrm{tax}}\,\mathrm{Cap}}{t_{\mathrm{dp}}}\,\frac{1}{r}\left(1 - \frac{1}{(1+r)^{t_{\mathrm{dp}}}}\right) \tag{A.140}$$

where NPV is the net present value of the polygeneration project; r is the annual discount rate, t_{lf} is the life time of the project, and t_{dp} is the depreciation time of the project, which are specified parameters.

A.2 Parameter Tables

Table A.1: Mole/mass compositions

Parameter	Value
$x_{\text{air,N}_2}$	0.7719
$x_{\text{air,O}_2}$	0.2076
$x_{\text{air,Ar}}$	0.0205
$x_{\text{oxy,N}_2}$	0.018
$x_{\text{oxy,O}_2}$	0.95
$x_{\text{oxy,Ar}}$	0.032
$x_{\text{sul,H}_2\text{S}}$	0.48
$x^{\text{fts}}_{\text{CO}_2,\text{max}}$	0.05
$x^{\text{mes}}_{\text{CO}_2,\text{max}}$	0.1
x^{co}_{w}	0.0016
$w_{\text{coal,H}_2\text{O}}$	0.1112
$w_{\text{bio,H}_2\text{O}}$	0.082
$w_{\text{coal,C}}$	0.7172
$w_{\text{coal,H}}$	0.0506
$w_{\text{coal,O}}$	0.0775
$w_{\text{coal,N}}$	0.0141
$w_{\text{coal,S}}$	0.0282
$w_{\text{coal,Cl}}$	0.0033
$w_{\text{bio,C}}$	0.476
$w_{\text{bio,H}}$	0.058
$w_{\text{bio,O}}$	0.4012
$w_{\text{bio,N}}$	0.005
$w_{\text{bio,S}}$	0.0008
$w_{\text{bio,Cl}}$	0.001
$w_{\text{H}_2\text{O,H}}$	0.1119
$w_{\text{H}_2\text{O,O}}$	0.8881

Table A.2: Mass/molar ratios

Parameter	Value
$R_{\mathrm{b/f,max}}$	0.3
$R^{\mathrm{rsyn}}_{\mathrm{H_2/CO}}$	0.756
$R^{\mathrm{rsyn}}_{\mathrm{H_2O/CO}}$	0.478
$R^{\mathrm{rsyn}}_{\mathrm{CO_2/CO}}$	0.27
$R^{\mathrm{rsyn}}_{\mathrm{CH_4/CO}}$	0.00039
$R^{\mathrm{rsyn}}_{\mathrm{COS/H_2S}}$	0.0586
$R^{\mathrm{rsyn}}_{\mathrm{NH_3/N_2}}$	0.00406
$R^{\mathrm{rsyn}}_{\mathrm{H_2/CO,bio}}$	0.7825
$R^{\mathrm{rsyn}}_{\mathrm{H_2O/CO,bio}}$	0.7145
$R^{\mathrm{rsyn}}_{\mathrm{CO_2/CO,bio}}$	0.3792
$R^{\mathrm{rsyn}}_{\mathrm{CH_4/CO,bio}}$	1.56×10^{-5}
$R^{\mathrm{rsyn}}_{\mathrm{COS/H_2S,bio}}$	0.05647
$R^{\mathrm{rsyn}}_{\mathrm{NH_3/N_2,bio}}$	0.003525
$R^{\mathrm{fl}}_{\mathrm{S,max}}$	0.001

Table A.3: Conversions

Parameter	Value
$R^{\mathrm{gas}}_{\mathrm{C}}$	0.98
R^{gas}_{i} $(i \neq \mathrm{C})$	1
$R^{\mathrm{cls}}_{\mathrm{H_S}}$	0.975
$R^{\mathrm{fts}}_{\mathrm{CO}}$	0.65
$R^{\mathrm{hc}}_{\mathrm{wax}}$	0.3333
$R^{\mathrm{hc}}_{\mathrm{H_2}}$	0.7495
$R^{\mathrm{atr}}_{\mathrm{rf,CH_4}}$	0.96
$R^{\mathrm{atr}}_{\mathrm{rf},j}$ $(j \neq \mathrm{CH_4})$	1
$R^{\mathrm{atr}}_{\mathrm{w}}$	0.5
$R^{\mathrm{mes}}_{\mathrm{CO}}$	0.33
$R^{\mathrm{gtc}}_{\mathrm{O_2}}$	0.647
A^{wgs}	42.766

Table A.4: Efficiency

Parameter	Value
η^{gt}	0.985
η^{sthi}	0.4407
η^{stlo}	0.1542

Table A.5: Selectivity

Parameter	Value
$S^{\mathrm{fts}}_{\mathrm{CH_4}}$	0.05
$S^{\mathrm{fts}}_{\mathrm{C_2H_4}}$	0.0005
$S^{\mathrm{fts}}_{\mathrm{C_2H_6}}$	0.01
$S^{\mathrm{fts}}_{\mathrm{C_3H_6}}$	0.02
$S^{\mathrm{fts}}_{\mathrm{C_3H_8}}$	0.01
$S^{\mathrm{fts}}_{\mathrm{C_4H_8}}$	0.02
$S^{\mathrm{fts}}_{\mathrm{C_4H_{10}}}$	0.01
$S^{\mathrm{fts}}_{\mathrm{C_6H_{14}}}$	0.08
$S^{\mathrm{fts}}_{\mathrm{C_8H_{18}}}$	0.11
$S^{\mathrm{fts}}_{\mathrm{C_{16}H_{34}}}$	0.22
$S^{\mathrm{fts}}_{\mathrm{C_{33}H_{68}}}$	0.46
$S^{\mathrm{fts}}_{\mathrm{CO_2}}$	0.0095
$S^{\mathrm{hc}}_{\mathrm{nap}}$	0.1053
$S^{\mathrm{mes}}_{\mathrm{m}}$	0.99

Table A.6: Split fractions

Parameter	**Value**
$S^{asu}_{O_2}$	0.94
$S^{sel}_{H_2S}$	6×10^{-7}
S^{sel}_{j} $(j \neq H_2S)$	1
$S^{se2}_{CO_2}$, $S^{se3}_{CO_2}$	0.031
S^{se2}_{j}, S^{se3}_{j} $(j \neq CO_2)$	1
$S^{psa}_{H_2}$	0.9
$S^{hs}_{nap,C_6H_{14}}$	0.986
S^{ms}_{unr,CH_3OH}	0.031
S^{ms}_{met,CH_3OH}	0.959

Table A.7: Temperatures (°C)

Parameter	**Value**
T^{asu}	32.2
T^{gas}	1370
T^{rc}	593
T^{sc}	205
T^{co1}, T^{co2}, T^{co3}	39
$T^{\text{se1}}_{\text{csyn}}$, $T^{\text{se2}}_{\text{hyg}}$, $T^{\text{se3}}_{\text{hyg}}$	22.5
$T^{\text{se1}}_{\text{sul}}$	49
$T^{\text{cls}}_{\text{tail}}$	35
$T^{\text{cls}}_{\text{w}}$	39.7
$T^{\text{cls}}_{\text{es}}$	189.2
T^{rh1}, T^{rh2}, T^{rh3}	240
$T^{\text{wgs}}_{\text{w,in}}$	270
T^{wgs}	232
$T^{\text{fts}}_{\text{pd}}$	240
$T^{\text{atr}}_{\text{fd}}$	550
$T^{\text{atr}}_{\text{pd}}$	1000
T^{sntft}	131.3
$T^{\text{mes}}_{\text{pd}}$	240
$T^{\text{ms}}_{\text{alc}}$	84.7
T^{sntgt1}, T^{sntgt2}	187.5
T^{nh}	196
T^{ac}	405
$T^{\text{gtc}}_{\text{max}}$	1200
$T^{\text{gt}}_{\text{pd}}$	563.3
$T^{\text{sg}}_{\text{fl}}$	131.9

Table A.8: Base case flow rates for power consumption/generation (Mmol/hr)

Parameter	**Value**
$F_{\text{air},0}^{\text{asu}}$	29.138
$F_{\text{oxy},0}^{\text{oxyc}}$	5.8975
$m_{\text{fd},0}^{\text{gas}}$ *	226.97
$F_{\text{tail},0}^{\text{clsc}}$	0.2931
$F_{\text{car},0}^{\text{cc}}$	11.357
$F_{\text{tail},0}^{\text{psa}}$	1
$F_{\text{fd},0}^{\text{sntft}}$	30
$F_{\text{lig},0}^{\text{ligc1}}$	4.7551
$F_{\text{lig},0}^{\text{ligc2}}$	2.3775
$F_{\text{oxy},0}^{\text{oxycr}}$	0.2812
$F_{\text{fd},0}^{\text{strscc}}$	10
$F_{\text{unr},0}^{\text{unrc1}}$	19.5507
$F_{\text{unr},0}^{\text{unrc2}}$	17.6034
$F_{\text{fd},0}^{\text{sntgt}}$	18.4207
$F_{\text{nit},0}^{\text{nc}}$	19.38
$F_{\text{air},0}^{\text{ac}}$	110.664

* : the unit is tonne/hr.

Table A.9: Base case power consumption/generation rates (MW)

Parameter	Value
$E_{c,0}^{asu}$	72.2496
$E_{c,0}^{oxyc}$	11.422
$E_{c,0}^{gas}$	5.17
$E_{c,0}^{clsc}$	1.087
$E_{c,0}^{cc}$	36.943
$E_{c,0}^{psagtc}$	2.1681
$E_{c,0}^{sntft}$	26.484
$E_{c,0}^{ligc1}$	9.598
$E_{c,0}^{ligc2}$	1.1479
$E_{c,0}^{oxycr}$	0.1805
$E_{c,0}^{strscc}$	9.7352
$E_{c,0}^{unrc1}$	9.6435
$E_{c,0}^{unrc2}$	11.8344
$E_{c,0}^{sntgt}$	8.1863
$E_{c,0}^{nc}$	35.7034
$E_{c,0}^{ac}$	364.425

Table A.10: Heat/power consumption coefficients

Parameter	Value	Unit
QC_c^{sesul}	3.8496	kJ/mol
EC_c^{sesul}	0.1061	W·hr/mol
EC_c^{secar}	1.6981	W·hr/mol
$QC_{c,A}^{hs}$	-0.8581	kJ/mol
$QC_{c,B}^{hs}$	9.1778	kJ/mol
EC_c^{hs}	0.0421	W·hr/mol
$QC_{c,A}^{ms}$	0	kJ/mol
$QC_{c,B}^{ms}$	39.9528	kJ/mol
EC_c^{ms}	-0.8806	W·hr/mol

Table A.11: Molar weight (kg/kmol)

Parameter	**Value**
MW_C	12.01
MW_H	1.008
MW_O	16
MW_N	14.01
MW_S	32.07
MW_{Cl}	35.45
MW_{H_2O}	18.01
MW_{CO_2}	44.01
$MW_{C_6H_{14}}$	86.18
$MW_{C_8H_{18}}$	114.23
$MW_{C_{16}H_{34}}$	226.44
MW_{CH_3OH}	32.04

Table A.12: Coefficients for enthalpy calculations under 5.5 MPa

Component	h_A	h_B	h_C
N_2	2.179×10^{-6}	2.957×10^{-2}	-1.047
O_2	2.143×10^{-6}	3.16×10^{-2}	-1.349
Ar	-4.263×10^{-7}	2.172×10^{-2}	-0.922
CO	2.176×10^{-6}	3×10^{-2}	-111.65
H_2	1.526×10^{-6}	2.826×10^{-2}	-0.577
CO_2	4.066×10^{-6}	4.872×10^{-2}	-397.65
H_2O	1.66×10^{-6}	4.223×10^{-2}	-248.06
H_2S	3.734×10^{-6}	4.177×10^{-2}	-25.069
COS	1.405×10^{-6}	5.658×10^{-2}	-148.24
HCl	-1.586×10^{-7}	3.348×10^{-2}	-95.529
NH_3	8.433×10^{-6}	4.548×10^{-2}	-50.837
CH_3OH	-4.879×10^{-5}	1.147×10^{-1}	-219.53
CH_4	1.985×10^{-5}	4.218×10^{-2}	-77.124
C_2H_4	3.169×10^{-5}	5.269×10^{-2}	48.556
C_2H_6	4.173×10^{-5}	6.514×10^{-2}	-88.944
C_3H_6	3.415×10^{-5}	9.2×10^{-2}	11.092
C_3H_8	4.634×10^{-5}	1.061×10^{-1}	-115.16
C_4H_8	3.34×10^{-5}	1.391×10^{-1}	-16.869
C_4H_{10}	3.458×10^{-5}	1.631×10^{-1}	-145.1
C_6H_{14}	-1.401×10^{-4}	4.109×10^{-1}	-235.58
$H_2O(l)$ *	3.54×10^{-5}	7.663×10^{-2}	-289.58
C_2H_5OH	-6.327×10^{-4}	4.984×10^{-1}	-308.94

* : (l) represents the liquid phase.

Table A.13: Coefficients for enthalpy calculations under 3.2 MPa

Component	h_A	h_B	h_C
N_2	2.489×10^{-6}	2.906×10^{-2}	-0.9
O_2	2.755×10^{-6}	3.074×10^{-2}	-1.109
Ar	-3.743×10^{-7}	2.147×10^{-2}	-0.778
CO	2.584×10^{-6}	2.937×10^{-2}	-111.47
H_2	1.289×10^{-6}	2.849×10^{-2}	-0.638
CO_2	6.39×10^{-6}	4.483×10^{-2}	-396.19
H_2O	3.587×10^{-6}	3.736×10^{-2}	-245.22
H_2S	6.026×10^{-6}	3.74×10^{-2}	-23.128
CH_3OH	-9.242×10^{-5}	1.199×10^{-1}	-215.7
CH_4	2.285×10^{-5}	3.86×10^{-2}	-76.325
C_2H_4	3.582×10^{-5}	4.873×10^{-2}	49.689
C_2H_6	4.802×10^{-5}	5.932×10^{-2}	-87.356
C_3H_6	4.84×10^{-5}	7.91×10^{-2}	14.46
C_3H_8	5.91×10^{-5}	9.382×10^{-2}	-111.72
C_4H_8	5.509×10^{-5}	1.179×10^{-1}	-10.928
C_4H_{10}	6.085×10^{-5}	1.375×10^{-1}	-138.08
C_6H_{14}	3.814×10^{-5}	2.503×10^{-1}	-197.68

Table A.14: Coefficients for enthalpy calculations under 2 MPa

Component	h_A	h_B	h_C
N_2	2.62×10^{-6}	2.883×10^{-2}	-0.827
O_2	2.898×10^{-6}	3.048×10^{-2}	-1.011
Ar	-2.358×10^{-7}	2.122×10^{-2}	-0.683
CO	2.732×10^{-6}	2.911×10^{-2}	-111.4
H_2	1.305×10^{-6}	2.847×10^{-2}	-0.647
CO_2	7.194×10^{-6}	4.345×10^{-2}	-395.64
H_2O	4.373×10^{-6}	3.572×10^{-2}	-244.28
CH_4	2.311×10^{-5}	3.813×10^{-2}	-76.129
C_2H_4	2.822×10^{-5}	5.295×10^{-2}	49.659
C_2H_6	3.97×10^{-5}	6.398×10^{-2}	-87.344
C_3H_6	4.2×10^{-5}	8.272×10^{-2}	14.769
C_3H_8	5.229×10^{-5}	9.733×10^{-2}	-111.22
C_4H_8	5.285×10^{-5}	1.182×10^{-1}	-9.78
C_4H_{10}	6.288×10^{-5}	1.345×10^{-1}	-136.14
C_6H_{14}	8.068×10^{-5}	2.128×10^{-1}	-187.95
C_8H_{18}	9.959×10^{-4}	-7.626×10^{-2}	-222.71
$C_{16}H_{34}$	4.592×10^{-4}	4.402×10^{-1}	-459.54
$C_{33}H_{68}$	6.88×10^{-4}	8.708×10^{-1}	-822.94
H_2O(l) *	3.722×10^{-5}	7.646×10^{-2}	-289.63
CH_3OH(l) *	1.63×10^{-4}	9.512×10^{-2}	-243.62
C_2H_5OH(l) *	1.808×10^{-4}	1.264×10^{-1}	-281.34

* : (l) represents the liquid phase.

Table A.15: Coefficients for enthalpy calculations under 1.6 MPa

Component	h_A	h_B	h_C
N_2	2.456×10^{-6}	2.897×10^{-2}	-0.84
O_2	2.453×10^{-6}	3.092×10^{-2}	-1.062
Ar	-1.277×10^{-7}	2.107×10^{-2}	-0.641
CO_2	6.235×10^{-6}	4.431×10^{-2}	-395.67
H_2O	5.07×10^{-6}	3.461×10^{-2}	-243.83
SO_2	3.409×10^{-6}	4.93×10^{-2}	-300.17

Table A.16: Coefficients for enthalpy calculations under 1 MPa

Component	h_A	h_B	h_C
N_2	-1.236×10^{-6}	2.972×10^{-2}	-0.818
O_2	1.283×10^{-6}	2.984×10^{-2}	-0.841
Ar	-1.635×10^{-6}	2.141×10^{-2}	-0.626

Table A.17: Coefficients for enthalpy calculations under 0.1 MPa

Component	h_A	h_B	h_C
N_2	2.532×10^{-6}	2.858×10^{-2}	-0.711
O_2	4.584×10^{-6}	2.903×10^{-2}	-0.74
Ar	-3.414×10^{-8}	2.082×10^{-2}	-0.529
CO_2	1.245×10^{-5}	3.873×10^{-2}	-394.57
H_2O	5.152×10^{-6}	3.316×10^{-2}	-242.73
H_2S	8.474×10^{-6}	3.356×10^{-2}	-21.516
SO_2	1.162×10^{-5}	4.106×10^{-2}	-298.01
S(l) *	-3.892×10^{-6}	6.492×10^{-2}	180.08

* : (l) represents the liquid phase.

Table A.18: Base case flow rates for capital costs

Parameter	Value	Unit
F_b^{fdh}	226.97	tonne/hr
F_b^{fdp}	226.97	tonne/hr
F_b^{asu}	29.18	Mmol/hr
F_b^{gas}	201.73	tonne/hr
F_b^{ash}	201.73	tonne/hr
F_b^{sr}	201.73	tonne/hr
F_b^{hy}	27.34	Mmol/hr
F_b^{se1}	19.77	Mmol/hr
F_b^{se2tot}, F_b^{se3tot}	38.84	Mmol/hr
F_b^{se2car}, F_b^{se3car}	10.66	Mmol/hr
F_b^{cls}	0.3878	Mmol/hr
F_b^{wgs1}, F_b^{wgs2}	36.73	Mmol/hr
F_b^{psa}	28.18	Mmol/hr
F_b^{cc}	469.04	tonne/hr
F_b^{sco}	30.7	Mmol/hr
F_b^{fts}	87.93	Mmol/hr
F_b^{hs}	34.18	tonne/hr
F_b^{hc}	243.67	tonne/h
F_b^{atr}	18.9	Mmol/hr
F_b^{fto}	57.69	Mmol/hr
F_b^{mes}	38.92	Mmol/hr
F_b^{ms}	110.35	tonne/hr
F_b^{meo}	61.76	Mmol/hr
F_b^{gt}	464.01	MW
F_b^{sg}	274.69	MW
F_b^{st}	274.69	MW
F_b^{oth}	824.21	tonne/hr

Table A.19: Base case capital costs ($MM)

Parameter	Value
C_b^{fdh}	36.35
C_b^{fdp}	58.41
C_b^{asu}	195.69
C_b^{gas}	234.84
C_b^{ash}	45.89
C_b^{sr}	50.37
C_b^{hy}	7.86
C_b^{se1}	24.85
C_b^{se2tot}, C_b^{se3tot}	18.38
C_b^{se2car}, C_b^{se3car}	36.38
C_b^{cls}	33.77
C_b^{wgs1}, C_b^{wgs2}	15.66
C_b^{psa}	82.02
C_b^{cc}	38.69
C_b^{sco}	19.86
C_b^{fts}	285.59
C_b^{hs}	31.82
C_b^{hc}	80.83
C_b^{atr}	35.33
C_b^{fto}	104.47
C_b^{mes}	94.79
C_b^{ms}	66.91
C_b^{meo}	64.56
C_b^{gt}	136.37
C_b^{sg}	56.72
C_b^{st}	66.55
C_b^{oth}	279.29

Table A.20: Sizing factors for capital costs

Parameter	Value
sf^{fdh}	0.85
sf^{fdp}	0.81
sf^{asu}	0.75
sf^{gas}	0.82
sf^{ash}	0.93
sf^{sr}	0.82
sf^{hy}	0.65
sf^{sel}	0.7
sf^{se2tot}, sf^{se3tot}	0.8
sf^{se2car}, sf^{se3car}	0.75
sf^{cls}	0.67
sf^{wgs1}, sf^{wgs2}	0.65
sf^{psa}	0.7
sf^{cc}	0.85
sf^{sco}	0.67
sf^{fts}	0.72
sf^{hs}	0.7
sf^{hc}	0.7
sf^{atr}	0.6
sf^{fto}	0.67
sf^{mes}	0.65
sf^{ms}	0.7
sf^{meo}	0.67
sf^{gt}	0.76
sf^{sg}	0.67
sf^{st}	0.7
sf^{oth}	0.67

Table A.21: Maximum capacity (tonne/hr)

Parameter	Value
$m_{\text{ca}}^{\text{gas}}$	1042

Table A.22: Economic parameters

Parameter	Value	Unit
$\text{Cost}_{\text{ope}}^{\text{fix}}$	25.061	\$MM/yr
$m_{\text{fd,b}}^{\text{gas}}$	824.206	tonne/hr
$\text{Cost}_{\text{ope,b}}^{\text{var}}$	207.295	\$MM/yr
$P_{\text{ccs}}^{\text{car}}$	10	\$/tonne CO_2
t_{op}	7500	hr
R_{tax}	0.4	
r	0.12	
t_{lf}	30	yr
t_{dp}	10	yr

Appendix B

Detailed Mathematical Model for Flexible Polygeneration Systems

B.1 Mathematical Model

The mathematical model in this paper is similar to the static polygeneration model in Appendix A, hence only the differences between the current model and the previous model are described here.

B.1.1 Mass Balance

This section is similar to the mass balance in the previous model (Appendix A.1.1). Differences are described below.

Replace $m^{\text{gas}}_{\text{coal}}$ and $m^{\text{gas}}_{\text{bio}}$ by $m^{\text{gas}}_{\text{coal},h}$ and $m^{\text{gas}}_{\text{bio},h}$ respectively, where $m^{\text{gas}}_{\text{coal},h}$ and $m^{\text{gas}}_{\text{bio},h}$ are the mass flow rates of coal and biomass fed into the gasifier in scenario h respectively.

Replace $R_{\text{b/f}}$ by $R_{\text{b/f},h}$, where $R_{\text{b/f},h}$ is the dry mass fraction of biomass in the total feedstock in the gasifier in scenario h.

Replace $F^k_{r,j}$ and F^k_r by $F^k_{r,j,h}$ and $F^k_{r,h}$ respectively, where $F^k_{r,j,h}$ is the molar flow rate of species j in the stream r exiting (or entering) unit operation k in scenario h, and $F^k_{r,h}$ is the total molar flow rate of stream r exiting (or entering) unit operation

k in scenario h.

Replace $F^k_{\mathrm{w,in}}$ and $F^k_{\mathrm{w,out}}$ by $F^k_{\mathrm{w,in},h}$ and $F^k_{\mathrm{w,out},h}$ respectively, where $F^k_{\mathrm{w,in},h}$ and $F^k_{\mathrm{w,out},h}$ are the molar flow rates of input water and output water of unit operation k in scenario h respectively.

Replace $F^{\mathrm{atr}}_{\mathrm{cm},j}$ by $F^{\mathrm{atr}}_{\mathrm{cm},j,h}$, where $F^{\mathrm{atr}}_{\mathrm{cm},j,h}$ is the conversion of species j in the combustion reaction in the ATR reactor in scenario h.

Replace S^k by S^k_h, where S^k_h is the split fraction of the splitter output stream to unit operation k in scenario h.

Apply all above related equations to all scenarios ($\forall h \in N_h$), where $N_h \equiv \{\mathrm{spp}, \mathrm{spo}, \mathrm{sup}, \mathrm{suo}, \mathrm{fap}, \mathrm{fao}, \mathrm{wip}, \mathrm{wio}\}$ is the set of scenarios in the project life time.

B.1.2 Energy Balance

This section is similar to the energy balance in the previous model (Appendix A.1.2). Differences are described below.

Replace Q^k_{c}, Q^k_{g}, E^k_{c} and E^k_{g} by $Q^k_{\mathrm{c},h}$, $Q^k_{\mathrm{g},h}$, $E^k_{\mathrm{c},h}$ and $E^k_{\mathrm{g},h}$, and apply the related equations to all scenarios ($\forall h \in N_h$), where $Q^k_{\mathrm{c},h}$, $Q^k_{\mathrm{g},h}$, $E^k_{\mathrm{c},h}$ and $E^k_{\mathrm{g},h}$ are the heat consumption rate, heat generation rate, power consumption rate and power generation rate in unit operation k in scenario h respectively.

All temperatures except $T^{\mathrm{gtc}}_{\mathrm{out}}$, which is the output temperature of the gas turbine combustor. Replace $T^{\mathrm{gtc}}_{\mathrm{out}}$ by $T^{\mathrm{gtc}}_{\mathrm{out},h}$, where $T^{\mathrm{gtc}}_{\mathrm{out},h}$ is the output temperature of the gas turbine combustor in scenario h, and apply the related equations to all scenarios ($\forall h \in N_h$).

B.1.3 Enthalpy Calculation

This section is exactly the same as the enthalpy calculation in the previous model (Appendix A.1.3).

B.1.4 Production Rates and Feedstock Consumption Rates

This section is similar to the part of production rates and feedstock consumption rates in the previous model (Appendix A.1.4). Differences are described below.

Replace m_q^{f} and m_q^{p} by $m_{q,h}^{\mathrm{f}}$ and $m_{q,h}^{\mathrm{p}}$ respectively, and apply the related equations to all scenarios ($\forall h \in N_h$), where $m_{q,h}^{\mathrm{f}}$ is the consumption rate of feedstock q in scenario h and $m_{q,h}^{\mathrm{p}}$ is the production rate of product q in scenario h.

B.1.5 Capital Costs

The capital costs of feedstock preparing equipments are given by:

$$C^l = C_{\mathrm{b}}^l \left(\frac{\bar{m}^{\mathrm{gas}}}{\bar{F}_{\mathrm{b}}^l} \right)^{\mathrm{sf}^l} , \quad \forall l \in \{\mathrm{fdh}, \mathrm{fdp}\} \tag{B.1}$$

where C^l is the capital cost of equipment l, $\bar{m}^{\mathrm{gas}}$ is the mass capacity of the gasifier; $\bar{F}_{\mathrm{b}}^l$ is the mass (or molar) capacity of equipment l in the base case (which is equal to F_{b}^l in Appendix A), C_{b}^l is the capital cost of equipment l in the corresponding base case, and sf^l is the sizing factor of equipment l, which are all specified parameters.

The mass capacity of the gasifier is calculated by:

$$m_{\mathrm{coal},h}^{\mathrm{gas}} + m_{\mathrm{bio},h}^{\mathrm{gas}} \leq \bar{m}^{\mathrm{gas}} , \quad \forall h \in N_h \tag{B.2}$$

$$m_{\mathrm{coal},h}^{\mathrm{gas}} + m_{\mathrm{bio},h}^{\mathrm{gas}} \geq \mathrm{Ca}_{\min}\, \bar{m}^{\mathrm{gas}} , \quad \forall h \in N_h \tag{B.3}$$

where $\mathrm{Ca}_{\min}$ is the lower limit of the flow-rate/capacity ratio, which is a specified parameter representing the operational flexibility.

The capital costs of gasification related equipments are given by:

$$C^l = C_{\mathrm{b}}^l \left(\frac{\bar{m}_{\mathrm{dry}}^{\mathrm{gas}}}{\bar{F}_{\mathrm{b}}^l} \right)^{\mathrm{sf}^l} , \quad \forall l \in \{\mathrm{gas}, \mathrm{ash}, \mathrm{sr}, \mathrm{oth}\} \tag{B.4}$$

where is the dry mass capacity the gasifier.

$$(1 - w_{\mathrm{coal},\mathrm{H_2O}})\, m_{\mathrm{coal},h}^{\mathrm{gas}} + (1 - w_{\mathrm{bio},\mathrm{H_2O}})\, m_{\mathrm{bio},h}^{\mathrm{gas}} \leq \bar{m}_{\mathrm{dry}}^{\mathrm{gas}} , \quad \forall h \in N_h \tag{B.5}$$

$$(1 - w_{\text{coal,H}_2\text{O}})\, m^{\text{gas}}_{\text{coal},h} + (1 - w_{\text{bio,H}_2\text{O}})\, m^{\text{gas}}_{\text{bio},h} \geq \text{Ca}_{\min}\, \bar{m}^{\text{gas}}_{\text{dry}} \,, \quad \forall h \in N_h \tag{B.6}$$

The dry mass capacity of gasifier feedstock is limited by:

$$\bar{m}^{\text{gas}}_{\text{dry}} \leq \bar{m}^{\text{gas}}_{\text{ca}} \tag{B.7}$$

where $\bar{m}^{\text{gas}}_{\text{ca}}$ is the upper limit of dry mass capacity of the gasifier or the maximum capacity of the gasifier, which is a specified parameter and is equal to $m^{\text{gas}}_{\text{ca}}$ in Appendix A.

The capital cost of CO_2 compressor is given by:

$$C^{\text{cc}} = C^{\text{cc}}_{\text{b}} \left(\frac{\bar{m}^{\text{cc}}}{\bar{F}^{\text{cc}}_{\text{b}}} \right)^{\text{sf}^{\text{cc}}} \tag{B.8}$$

where $\bar{m}^{\text{cc}}$ is the mass capacity of the CO_2 compressor, which is given by:

$$m^{\text{p}}_{\text{car},h} \leq \bar{m}^{\text{cc}} \,, \quad \forall h \in N_h \tag{B.9}$$

$$m^{\text{p}}_{\text{car},h} \geq \text{Ca}_{\min}\, \bar{m}^{\text{cc}} \,, \quad \forall h \in N_h \tag{B.10}$$

The capital costs of equipments in the hydrocarbon separation process are given by:

$$C^{l} = C^{l}_{\text{b}} \left(\frac{\bar{m}^{\text{hs}}}{\bar{F}^{l}_{\text{b}}} \right)^{\text{sf}^{l}} \,, \quad \forall l \in \{\text{hs}, \text{hc}\} \tag{B.11}$$

where $\bar{m}^{\text{hs}}$ is the mass capacity of the hydrocarbon separation unit, which is calculated by:

$$m^{\text{p}}_{\text{nap},h} + m^{\text{p}}_{\text{dis},h} \leq \bar{m}^{\text{hs}} \,, \quad \forall h \in N_h \tag{B.12}$$

$$m^{\text{p}}_{\text{nap},h} + m^{\text{p}}_{\text{dis},h} \geq \text{Ca}_{\min}\, \bar{m}^{\text{hs}} \,, \quad \forall h \in N_h \tag{B.13}$$

The capital costs of the methanol separation unit are given by:

$$C^{\text{ms}} = C^{\text{ms}}_{\text{b}} \left(\frac{\bar{m}^{\text{ms}}}{\bar{F}^{\text{ms}}_{\text{b}}} \right)^{\text{sf}^{\text{ms}}} \tag{B.14}$$

where $\bar{m}^{\text{ms}}$ is the mass capacity of the methanol separation unit, which is calculated

by:

$$m^{\mathrm{p}}_{\mathrm{met},h} \leq \bar{m}^{\mathrm{ms}} \ , \quad \forall h \in N_h \tag{B.15}$$

$$m^{\mathrm{p}}_{\mathrm{met},h} \geq \mathrm{Ca}_{\min}\ \bar{m}^{\mathrm{ms}} \ , \quad \forall h \in N_h \tag{B.16}$$

The capital costs of the gas turbine and steam turbine are given by:

$$C^l = C^l_{\mathrm{b}} \left(\frac{\bar{E}^l_{\mathrm{g}}}{\bar{F}^l_{\mathrm{b}}} \right)^{\mathrm{sf}^l} \ , \quad \forall l \in \{\mathrm{gt}, \mathrm{st}\} \tag{B.17}$$

where $\bar{E}^l_{\mathrm{g}}$ is the power generation capacity of equipment l.

The capacity of the gas turbine is calculated by:

$$E^{\mathrm{gt}}_{\mathrm{g},h} \leq \bar{E}^{\mathrm{gt}}_{\mathrm{g}} \ , \quad \forall h \in N_h \tag{B.18}$$

$$E^{\mathrm{gt}}_{\mathrm{g},h} \geq \mathrm{Ca}_{\min}\ \bar{E}^{\mathrm{gt}}_{\mathrm{g}} \ , \quad \forall h \in N_h \tag{B.19}$$

The capacity of the steam turbine is calculated by:

$$E^{\mathrm{sthi}}_{\mathrm{g},h} + E^{\mathrm{stlo}}_{\mathrm{g},h} \leq \bar{E}^{\mathrm{st}}_{\mathrm{g}} \ , \quad \forall h \in N_h \tag{B.20}$$

$$E^{\mathrm{sthi}}_{\mathrm{g},h} + E^{\mathrm{stlo}}_{\mathrm{g},h} \geq \mathrm{Ca}_{\min}\ \bar{E}^{\mathrm{st}}_{\mathrm{g}} \ , \quad \forall h \in N_h \tag{B.21}$$

The capital cost of the HRSG is given by:

$$C^{\mathrm{sg}} = C^{\mathrm{sg}}_{\mathrm{b}} \left(\frac{\bar{E}^{\mathrm{st}}_{\mathrm{g}}}{\bar{F}^{\mathrm{sg}}_{\mathrm{b}}} \right)^{\mathrm{sf}^{\mathrm{sg}}} \tag{B.22}$$

The capital costs of the Selexol units for CO_2 removal are calculated as two parts: the first part is related to the total molar flow rate of input stream, which is given by:

$$C^l = C^l_{\mathrm{b}} \left(\frac{\bar{F}^l_{\mathrm{A}}}{\bar{F}^l_{\mathrm{b}}} \right)^{\mathrm{sf}^l} \ , \quad \forall l \in \{\mathrm{se2tot}, \mathrm{se3tot}\} \tag{B.23}$$

and the second part is related to the molar flow rate of the output CO_2 stream, which

is given by:

$$C^l = C^l_{\mathrm{b}} \left(\frac{\bar{F}^l_{\mathrm{B}}}{\bar{F}^l_{\mathrm{b}}} \right)^{\mathrm{sf}^l} , \quad \forall l \in \{\mathrm{se2car}, \mathrm{se3car}\} \tag{B.24}$$

where $\bar{F}^l_{\mathrm{A}}$ and $\bar{F}^l_{\mathrm{B}}$ are the molar capacity of equipment l related to above two parts of cost, which are given by:

$$F^l_{\mathrm{in},h} \leq \bar{F}^l_{\mathrm{A}} , \quad \forall h \in N_h \tag{B.25}$$

$$F^l_{\mathrm{in},h} \geq \mathrm{Ca}_{\min} \bar{F}^l_{\mathrm{A}} , \quad \forall h \in N_h \tag{B.26}$$

$$F^l_{\mathrm{car},h} \leq \bar{F}^l_{\mathrm{B}} , \quad \forall h \in N_h \tag{B.27}$$

$$F^l_{\mathrm{car},h} \geq \mathrm{Ca}_{\min} \bar{F}^l_{\mathrm{B}} , \quad \forall h \in N_h \tag{B.28}$$

where, $F^l_{\mathrm{in},h}$ is the total molar flow rate of the input stream of equipment l in scenario h, and $F^l_{\mathrm{car},h}$ is the molar flow rate of CO_2 stream exiting the equipment l in scenario h.

The capital costs of all remaining equipment in the system can be expressed as the general form:

$$C^l = C^l_{\mathrm{b}} \left(\frac{\bar{F}^l}{\bar{F}^l_{\mathrm{b}}} \right)^{\mathrm{sf}^l} , \quad \forall l \in \{\mathrm{asu}, \mathrm{hy}, \mathrm{se1}, \mathrm{cls}, \mathrm{wgs1}, \mathrm{wgs2}, \mathrm{psa}, \mathrm{sco}, \mathrm{fts}, \mathrm{atr}, \mathrm{fto}, \mathrm{mes}, \mathrm{meo}\} \tag{B.29}$$

where $\bar{F}^l$ is the molar capacity of equipment l, which is calculated by:

$$F^l_{\mathrm{in},h} \leq \bar{F}^l , \quad \forall h \in N_h \tag{B.30}$$

$$F^l_{\mathrm{in},h} \geq \mathrm{Ca}_{\min} \bar{F}^l , \quad \forall h \in N_h \tag{B.31}$$

The total capital investment of the process is given by:

$$\mathrm{Cap} = \sum_l C^l , \quad \forall l \in L_{\mathrm{eq}} \tag{B.32}$$

where Cap is the total capital investment; $L_{\mathrm{eq}} \equiv \{$fdh, fdp, asu, gas, ash, sr, hy, se1,

cls, wgs1, se2tot, se2car, wgs2 se3tot, se3car, cc, psa, sco, fts, hs, hc, atr, fto, mes, ms, meo, gt, st, sg, oth} is set of equipments with capital cost.

B.1.6 Economic Analysis

The total annual cost is

$$\text{Cost} = \text{Cost}_{\text{fed}} + \text{Cost}^{\text{car}}_{\text{tax}} + \text{Cost}^{\text{car}}_{\text{ccs}} + \text{Cost}_{\text{ope}} \tag{B.33}$$

where Cost is the total annual cost, Cost_{fed} is the cost of purchasing the feedstock, $\text{Cost}^{\text{car}}_{\text{tax}}$ is the carbon emissions tax, $\text{Cost}^{\text{car}}_{\text{ccs}}$ is the cost of carbon sequestration, and Cost_{ope} is the operational cost.

The feedstock cost in given by:

$$\text{Cost}_{\text{fed}} = \sum_{h} \text{Occu}_h \left(\sum_{q} P^{\text{f}}_{q} \, m^{\text{f}}_{q,h} \right) t_{\text{op}} \ , \quad \forall q \in \text{Feed}, \ \forall h \in N_h \tag{B.34}$$

where $m^{\text{f}}_{q,h}$ is the consumption rate of feedstock q in scenario h. P^{f}_{q} is the annual average market price of feedstock q, t_{op} is the annual operating time, and Occu_h is the fraction of occurrence of scenario h, which are specified parameters. Feed $\equiv$ {coal, bio, w} is the set of feedstocks.

The carbon tax is given by

$$\text{Cost}^{\text{car}}_{\text{tax}} = P^{\text{car}}_{\text{tax}} \, \text{Emis}_{\text{net}} \tag{B.35}$$

where Emis_{net} is the annual net CO_2 emissions; $P^{\text{car}}_{\text{tax}}$ is the carbon tax per tonne of CO_2 emitted, which is a specified parameter. CO_2 emissions are calculated by

$$\text{Emis}_{\text{gro}} = \text{MW}_{\text{CO}_2} \sum_{h} \text{Occu}_h \left[F^{\text{sg}}_{\text{fl,CO}_2,h} + (1 - S_{\text{seq},h}) \, F^{\text{se2}}_{\text{car},h} \right] t_{\text{op}} \ , \quad \forall h \in N_h \tag{B.36}$$

$$\text{Emis}_{\text{net}} = \text{Emis}_{\text{gro}} - \frac{\text{MW}_{\text{CO}_2}}{\text{MW}_{\text{C}}} \left(1 - w_{\text{bio,H}_2\text{O}}\right) w_{\text{bio,C}} \sum_{h} \text{Occu}_h \, m^{\text{gas}}_{\text{bio},h} \, t_{\text{op}} \ , \quad \forall h \in N_h \tag{B.37}$$

where $\mathrm{Emis}_{\mathrm{gro}}$ is the annual gross CO_2 emissions. If the carbon tax policy also taxes the carbon in the liquid fuels, the annual net CO_2 emissions are given by:

$$\begin{aligned}\mathrm{Emis}_{\mathrm{net}} =& \mathrm{Emis}_{\mathrm{gro}} - \frac{\mathrm{MW}_{\mathrm{CO_2}}}{\mathrm{MW}_{\mathrm{C}}}\left(1 - w_{\mathrm{bio,H_2O}}\right) w_{\mathrm{bio,C}} \sum_h \mathrm{Occu}_h \, m^{\mathrm{gas}}_{\mathrm{bio},h} \, t_{\mathrm{op}} \\ &+ \mathrm{MW}_{\mathrm{CO_2}} \sum_h \mathrm{Occu}_h \left(6F^{\mathrm{hs}}_{\mathrm{nap,C_6H_{14}},h} + 8F^{\mathrm{hs}}_{\mathrm{nap,C_8H_{18}},h} + 16F^{\mathrm{hs}}_{\mathrm{dis},h}\right) t_{\mathrm{op}} \ , \quad \forall h \in N_h\end{aligned} \tag{B.38}$$

where $F^{\mathrm{sg}}_{\mathrm{fl,CO_2},h}$ is the molar flow rate of CO_2 in the gas turbine flue gas in scenario h, $F^{\mathrm{se2}}_{\mathrm{car},h}$ is the molar flow rate of CO_2 stream exiting Selexol Unit 2 in scenario h, $F^{\mathrm{hs}}_{\mathrm{nap,C_6H_{14}},h}$ and $F^{\mathrm{hs}}_{\mathrm{nap,C_8H_{18}},h}$ are the molar flow rates of C_6H_{14} and C_8H_{18} in the naphtha stream exiting the hydrocarbon separation unit in scenario h, respectively, and $F^{\mathrm{hs}}_{\mathrm{dis},h}$ is the molar flow rate of the diesel stream exiting the hydrocarbon separation unit in scenario h, $m^{\mathrm{gas}}_{\mathrm{bio},h}$ is the mass flow rate of biomass fed into the gasifier in scenario h, and $S_{\mathrm{seq},h}$ is the split fraction of CO_2 stream to sequestration in scenario h. $w_{\mathrm{bio,H_2O}}$ is the mass fraction of water in the wet biomass, and $w_{\mathrm{bio,C}}$ is the mass fraction of C in the dry biomass, which are specified parameters.

The carbon sequestration cost is given by:

$$\mathrm{Cost}^{\mathrm{car}}_{\mathrm{ccs}} = P^{\mathrm{car}}_{\mathrm{ccs}} \sum_h \mathrm{Occu}_h \, m^{\mathrm{p}}_{\mathrm{car},h} \ , \quad \forall h \in N_h \tag{B.39}$$

where $m^{\mathrm{p}}_{\mathrm{car},h}$ is the CO_2 production rate in scenario h; $P^{\mathrm{car}}_{\mathrm{ccs}}$ is the carbon sequestration fee per tonne CO_2, which is a specified parameter.

The operational cost is given by:

$$\mathrm{Cost}_{\mathrm{ope}} = \mathrm{Cost}^{\mathrm{fix}}_{\mathrm{ope}} + \mathrm{Cost}^{\mathrm{var}}_{\mathrm{ope}} \tag{B.40}$$

where $\mathrm{Cost}^{\mathrm{fix}}_{\mathrm{ope}}$ is the fixed annual operational cost, which is a specified parameter; $\mathrm{Cost}^{\mathrm{var}}_{\mathrm{ope}}$ is variable annual operational cost, which is calculated by the linear scaling up relationship:

$$\mathrm{Cost}^{\mathrm{var}}_{\mathrm{ope}} = \mathrm{Cost}^{\mathrm{var}}_{\mathrm{ope,b}} \sum_h \mathrm{Occu}_h \, \frac{m^{\mathrm{gas}}_{\mathrm{fd},h}}{m^{\mathrm{gas}}_{\mathrm{fd,b}}} \tag{B.41}$$

where $m^{\text{gas}}_{\text{fd,b}}$ is the mass flow rate of the total feedstock fed into the gasifier in the base case, and $\text{Cost}^{\text{var}}_{\text{ope,b}}$ is the annual variable operational cost in the corresponding base case, which are specified parameters.

The revenue is given by

$$\text{Reve} = \sum_{h} \text{Occu}_h \left(\sum_{q} P^{\text{p}}_{q,h}\, m^{\text{p}}_{q,h} \right) t_{\text{op}} \ , \quad \forall q \in \text{Prod},\ \forall h \in N_h \tag{B.42}$$

where $m^{\text{p}}_{q,h}$ is the production rate of product q in scenario h. $P^{\text{p}}_{q,h}$ is the market price of product q in scenario h, which are specified parameters. Prod $\equiv$ {ele, nap, dis, met, es} is the set of products.

The profit is calculated by:

$$\text{Pro}_{\text{gro}} = \text{Reve} - \text{Cost} \tag{B.43}$$

$$\text{Pro}_{\text{net}} = (1 - R_{\text{tax}})\, \text{Pro}_{\text{gro}} \tag{B.44}$$

where Pro_{gro} and Pro_{net} are the annual gross profit and the annual net profit respectively; R_{tax} is the tax rate, which is a specified parameter.

The net present value, which is the objective function of this model, is denoted by:

$$\text{NPV} = -\text{Cap} + \text{Pro}_{\text{net}}\, \frac{1}{r} \left(1 - \frac{1}{(1+r)^{t_{\text{lf}}}} \right) + \frac{R_{\text{tax}}\, \text{Cap}}{t_{\text{dp}}}\, \frac{1}{r} \left(1 - \frac{1}{(1+r)^{t_{\text{dp}}}} \right) \tag{B.45}$$

where NPV is the net present value of the polygeneration project; r is the annual discount rate, t_{lf} is the life time of the project, and t_{dp} is the depreciation time of the project, which are specified parameters.

B.2 Parameter Tables

Table B.1: Base case flow rates for capital costs

Parameter	Value	Unit
$\bar{F}_b^{fdh}$	226.97	tonne/hr
$\bar{F}_b^{fdp}$	226.97	tonne/hr
$\bar{F}_b^{asu}$	29.18	Mmol/hr
$\bar{F}_b^{gas}$	201.73	tonne/hr
$\bar{F}_b^{ash}$	201.73	tonne/hr
$\bar{F}_b^{sr}$	201.73	tonne/hr
$\bar{F}_b^{hy}$	27.34	Mmol/hr
$\bar{F}_b^{se1}$	19.77	Mmol/hr
$\bar{F}_b^{se2tot}$, $\bar{F}_b^{se3tot}$	38.84	Mmol/hr
$\bar{F}_b^{se2car}$, $\bar{F}_b^{se3car}$	10.66	Mmol/hr
$\bar{F}_b^{cls}$	0.3878	Mmol/hr
$\bar{F}_b^{wgs1}$, $\bar{F}_b^{wgs2}$	36.73	Mmol/hr
$\bar{F}_b^{psa}$	28.18	Mmol/hr
$\bar{F}_b^{cc}$	469.04	tonne/hr
$\bar{F}_b^{sco}$	30.7	Mmol/hr
$\bar{F}_b^{fts}$	87.93	Mmol/hr
$\bar{F}_b^{hs}$	34.18	tonne/hr
$\bar{F}_b^{hc}$	243.67	tonne/h
$\bar{F}_b^{atr}$	18.9	Mmol/hr
$\bar{F}_b^{fto}$	57.69	Mmol/hr
$\bar{F}_b^{mes}$	38.92	Mmol/hr
$\bar{F}_b^{ms}$	110.35	tonne/hr
$\bar{F}_b^{meo}$	61.76	Mmol/hr
$\bar{F}_b^{gt}$	464.01	MW
$\bar{F}_b^{sg}$	274.69	MW
$\bar{F}_b^{st}$	274.69	MW
$\bar{F}_b^{oth}$	824.21	tonne/hr

Table B.2: Base case capital costs ($MM)

Parameter	Value
C_b^{fdh}	36.35
C_b^{fdp}	58.41
C_b^{asu}	195.69
C_b^{gas}	234.84
C_b^{ash}	45.89
C_b^{sr}	50.37
C_b^{hy}	7.86
C_b^{se1}	24.85
C_b^{se2tot}, C_b^{se3tot}	18.38
C_b^{se2car}, C_b^{se3car}	36.38
C_b^{cls}	33.77
C_b^{wgs1}, C_b^{wgs2}	15.66
C_b^{psa}	82.02
C_b^{cc}	38.69
C_b^{sco}	19.86
C_b^{fts}	285.59
C_b^{hs}	31.82
C_b^{hc}	80.83
C_b^{atr}	35.33
C_b^{fto}	104.47
C_b^{mes}	94.79
C_b^{ms}	66.91
C_b^{meo}	64.56
C_b^{gt}	136.37
C_b^{sg}	56.72
C_b^{st}	66.55
C_b^{oth}	279.29

Table B.3: Sizing factors for capital costs

Parameter	Value
sf^{fdh}	0.85
sf^{fdp}	0.81
sf^{asu}	0.75
sf^{gas}	0.82
sf^{ash}	0.93
sf^{sr}	0.82
sf^{hy}	0.65
sf^{se1}	0.7
sf^{se2tot}, sf^{se3tot}	0.8
sf^{se2car}, sf^{se3car}	0.75
sf^{cls}	0.67
sf^{wgs1}, sf^{wgs2}	0.65
sf^{psa}	0.7
sf^{cc}	0.85
sf^{sco}	0.67
sf^{fts}	0.72
sf^{hs}	0.7
sf^{hc}	0.7
sf^{atr}	0.6
sf^{fto}	0.67
sf^{mes}	0.65
sf^{ms}	0.7
sf^{meo}	0.67
sf^{gt}	0.76
sf^{sg}	0.67
sf^{st}	0.7
sf^{oth}	0.67

Table B.4: Maximum capacity (tonne/hr)

Parameter	Value
$\bar{m}_{\text{ca}}^{\text{gas}}$	1042

Table B.5: Economic parameters

Parameter	Value	Unit
$\text{Cost}_{\text{ope}}^{\text{fix}}$	25.061	\$MM/yr
$m_{\text{fd,b}}^{\text{gas}}$	824.206	tonne/hr
$\text{Cost}_{\text{ope,b}}^{\text{var}}$	207.295	\$MM/yr
$P_{\text{ccs}}^{\text{car}}$	10	\$/tonne CO_2
t_{op}	7500	hr
R_{tax}	0.4	
r	0.12	
t_{lf}	30	yr
t_{dp}	10	yr

Nomenclature

Sets

Feed	set of feedstocks
I	set of elements
J	set of species
J'	set of species
K	set of unit operations
L	set of equipment
N_h	set of scenarios
Prod	set of products

Variables

C	capital cost
Cap	capital investment
Cost	cost
E_c	power consumption rate
E_g	power generation rate
Emis	CO_2 emissions
F	molar flow rate

h^{gtc}	molar enthalpy of the gas turbine combustor product
m	mass flow rate
m^{f}	feedstock consumption rate
m^{p}	production rate
NPV	net present value
Pro	profit
Q_{c}	heat consumption rate
Q_{g}	heat generation rate
$R_{\mathrm{b/f}}$	dry mass fraction of biomass in the total feedstock in the gasifier
$R_{\mathrm{cm}}^{\mathrm{atr}}$	conversion in the combustion reaction in the ATR reactor
Reve	revenue
S	split fraction
$T_{\mathrm{out}}^{\mathrm{gtc}}$	output temperature of the gas turbine combustor

Parameters

η	energy conversion efficiency
A^{wgs}	factor for the conversion in the WGS reactor
C_{b}	capital cost in the base case
$\mathrm{Cost}_{\mathrm{ope}}^{\mathrm{fix}}$	annual fixed operational cost
$\mathrm{Cost}_{\mathrm{ope,b}}^{\mathrm{var}}$	annual variable operational cost in the base case
$E_{\mathrm{c,0}}$	power consumption rate in the base case
$E_{\mathrm{g,0}}$	power generation rate in the base case
EC_{c}	coefficient of the power consumption rate
F_{b}	total mass (or molar) flow rate of the input stream in the base case
F_0	molar flow rate in the base case
$\bar{F}_{\mathrm{b}}$	mass (or molar) capacity in the base case

h	molar enthalpy
h_{A}	molar enthalpy coefficient
h_{B}	molar enthalpy coefficient
h_{C}	molar enthalpy coefficient
$m_{\mathrm{ca}}^{\mathrm{gas}}$	upper limit of dry mass flow rate of total feedstock fed into the gasifier
$m_{\mathrm{fd,b}}^{\mathrm{gas}}$	mass flow rate of the total feedstock fed into the gasifier in the base case
$\bar{m}_{\mathrm{ca}}^{\mathrm{gas}}$	upper limit of dry mass capacity of the gasifier
MW	molar weight
n	number of atoms in one molecule
Occu	frequency of occurrence
P^{f}	feedstock price
P^{p}	product price
$P_{\mathrm{ccs}}^{\mathrm{car}}$	CO_2 sequestration fee
$P_{\mathrm{tax}}^{\mathrm{car}}$	carbon tax
$\mathrm{QC_c}$	coefficient of the heat consumption rate
r	annual discount rate
$R_{\mathrm{b/f,max}}$	maximum dry mass fraction of biomass in the total feedstock in the gasifier
R_{tax}	tax rate
$R_{\mathrm{rf}}^{\mathrm{atr}}$	conversion in the steam reforming reaction in the ATR reactor
$R_{\mathrm{w}}^{\mathrm{atr}}$	water conversion in the ATR reactor
$R_{\mathrm{H_2S}}^{\mathrm{cls}}$	H_2S conversion in the Claus plant
$R_{\mathrm{S,max}}^{\mathrm{fl}}$	upper limit of the ratio of sulfur mass flow rate in flue gas to the feedstock
$R_{\mathrm{CO}}^{\mathrm{fts}}$	CO conversion in the FT reactor
R^{gas}	conversion in the gasifier
$R_{\mathrm{O_2}}^{\mathrm{gtc}}$	excess ratio of O_2 in the gas turbine combustor

R^{hc}	conversion in hydrocracking reactor
R^{rsyn}	ratio of molar flow rates of species in the raw syngas produced from coal
$R^{\mathrm{rsyn}}_{\mathrm{bio}}$	ratio of molar flow rates of species in the raw syngas produced from the coal/biomass mixture with 30% of biomass
$R^{\mathrm{wgs1}}_{\mathrm{CO}}$	CO conversion in WGS Reactor 1
$S^{\mathrm{asu}}_{\mathrm{O_2}}$	split fraction of O_2 in air to the oxygen rich stream in the ASU
S^{fts}	carbon selectivity in the FT reactor
$S^{\mathrm{hc}}_{\mathrm{nap}}$	carbon selectivity to naphtha in the hydrocracking reactor
$S^{\mathrm{hs}}_{\mathrm{nap}}$	split fraction to the naphtha stream in the hydrocarbon separation unit
$S^{\mathrm{ms}}_{\mathrm{met}}$	split fraction to the methanol stream in the methanol separation unit
$S^{\mathrm{ms}}_{\mathrm{unr}}$	split fraction to the unreacted syngas stream in the methanol separation unit
$S^{\mathrm{psa}}_{\mathrm{H_2}}$	split fraction of H_2 to the H_2 product stream in the PSA unit
S^{se1}	split fraction in Selexol Unit 1
S^{se2}	split fraction in Selexol Unit 2
ScF	scale factor for the price of product
sf	sizing factor
Sto	stoichiometric coefficient
T	temperature
$T^{\mathrm{gtc}}_{\mathrm{max}}$	upper limit of the gas turbine combustor output temperature
t_{dp}	depreciation time of the project
t_{lf}	life time of the project
t_{op}	annual operating time
w	mass fraction
x	mole fraction

Superscripts

ac	air compressor in the gas turbine
ash	ash handling unit
asu	air saparation unit
atr	autothermal reforming reactor
atrscc	ATR product compressor
atrfdh	ATR feedstock heater
strpdco	ATR product cooler
car	carbon
cc	CO_2 stream compressor
cls	Claus unit
clsc	Claus unit tail gas compressor
co	gas cooler
co1	Syngas Cooler 1
co2	Syngas Cooler 2
co3	Syngas Cooler 3
fao	fall off-peak time
fap	fall peak time
fdh	feedstock handling unit
fdp	feedstock preparation unit
fix	fixed part
fl	flue has
fto	other equipment in the FT process
fts	Fischer-Tropsch synthesis reactor
gas	gasifier

gt	gas turbine
gtc	gas turbine combustor
gtcwh	gas turbine combustor water heater
hc	hydrocracking reactor
hs	hydrocarbon separation unit
hy	COS hydrolysis reactor
k	unit operation
k'	unit operation
k''	unit operation
l	equipment
ligc1	Light Ends Compressor 1 in the FT process
ligc2	Light Ends Compressor 2 in the FT process
meo	other equipment in the MeOH process
mes	methanol synthesis reactor
ms	methanol separation unit
nc	N_2 stream compressor
nh	N_2 stream heater
oth	other equipment in the process
oxyc	O_2 stream (to the gasifier) compressor
oxycr	O_2 stream (to the ATR reactor) compressor
psa	pressure-swing adsorption unit
psagtc	PSA tail gas compressor
rc	syngas radiant cooler after the gasifier
rh1	Syngas Heater 1
rh2	Syngas Heater 2

rh3	Syngas Heater 3
rsyn	raw syngas stream
sc	syngas convective cooler after the gasifier
sco	other equipment in the syngas cleaning process
se1	Selexol Unit 1
se2	Selexol Unit 2
se2car	the part of Selexol Unit 2 related to the molar flow rate of CO_2 stream
se2tot	the part of Selexol Unit 2 related to the total molar flow rate of input stream
se3	Selexol Unit 3
se3car	the part of Selexol Unit 3 related to the molar flow rate of CO_2 stream
se3tot	the part of Selexol Unit 3 related to the total molar flow rate of input stream
secar	Selexol unit for CO_2 removal
sesul	Selexol unit for H_2S removal
sg	heat recovery steam generator
sntft	syngas turbine before the FT process
sntgt1	Syngas Turbine 1 before the gas turbine
sntgt2	Syngas Turbine 2 before the gas turbine
splatr	splitter for the ATR product in the FT process
splcar	CO_2 stream splitter
spllig	splitter for the light ends in the FT process
splpsa	spliter for the PSA
splsyn1	Syngas Splitter 1 (to liquid production branch) in Syngas Cleaning Process
splsyn2	Syngas Splitter 2 (to power production with CCS branch) in Syngas Cleaning Process
splunr	splitter for the unreacted syngas in the MeOH process

spo	spring off-peak time
spp	spring peak time
sr	scrubber
st	steam turbine
sthi	steam turbine for the high quality heat
stlo	steam turbine for the low quality heat
suo	summer off-peak time
sup	summer peak time
unrc1	Unreacted Syngas Compressor 1 in the MeOH process
unrc2	Unreacted Syngas Compressor 2 in the MeOH process
var	variable part
wgs	water gas shift reactor
wgs1	Water Gas Shift Reactor 1
wgs2	Water Gas Shift Reactor 2
wgs1ht	WGS Reactor 1 steam heater
wgs2ht	WGS Reactor 2 steam heater
wio	winter off-peak time
wip	winter peak time

Subscripts

air	air stream
alc	higher alcohol stream
atr	autothermal reforming reactor
bio	biomass
ca	capacity
car	CO_2

ccs	carbon capture and sequestration
cm	combustion reaction
co	gas cooler without water output
coal	coal
cow	gas cooler with water output
cp	compressor
csyn	clean syngas stream
dis	diesel
dry	dry feedstock
ec	unit operation with power consumption
eg	unit operation with power generation
ele	electricity
eq	equipment
es	elemental sulfur
fd	feedstock stream
fed	feedstock
feed	feedstock
fl	flue gas
ftfd	feedstock of the FT reaction
ftpd	product of the FT reaction
fts	FT synthesis reaction
fue	liquid fuels
gro	gross
gt	gas turbine
gtc	gas turbine combustor

h	scenario
hyd	H_2 rich stream
i	element
in	input stream
j	species
k	unit operation
key	key species
lig	light ends
m	main reaction
max	upper limit
mefd	feedstock of the MeOH reaction
mepd	product of the MeOH reaction
mes	methanol synthesis reactor
met	methanol
min	lower limit
nap	naphtha
net	net
nit	N_2 rich stream
ope	operational
out	output stream
oxy	O_2 rich stream
pd	product stream
q	feedstock or product
qc	unit operation with heat consumption
qg	unit operation with heat generation

unr	unreacted syngas stream
r	stream
rf	steam reforming reactor
rh	gas heater
rsyn	raw syngas stream
rt	reactor
rtf	reactor with feedstock mixer
s	side reaction
seq	sequestration
spe	species
spl	splitter
sul	H_2S rich stream
tail	tail gas stream
tax	tax
tb	turbine
tsyn	treated syngas stream
w	water
wax	wax stream
wi	unit operation with water input
wo	unit operation with water output

Bibliography

[1] CPLEX 12. Available at: http://www.gams.com/docs/document/cplex.pdf (2008).

[2] BP statistical review of world energy (June 2010). Available at http://www.bp.com/productlanding.do?categoryId=6929&contentId=7044622, August, 2010.

[3] Intercontinental Exchange (ICE) report data. Available at: https://www.theice.com/marketdata/reports/ReportCenter.shtml, December, 2010.

[4] Methanex monthly average regional posted contract price history. Available at: http://www.methanex.com/products/methanolprice.html, December, 2010.

[5] U.S. Energy Information Administration. Petroleum Navigator: Monthly spot prices. Available at: http://tonto.eia.doe.gov/dnav/pet/pet_pri_spt_s1_m.htm, December, 2010.

[6] J. Aaltola. Simultaneous synthesis of flexible heat exchanger network. *Applied Thermal Engineering*, 22(8):907–918, 2002.

[7] T. A. Adams II and P. I. Barton. A dynamic two-dimensional heterogeneous model for water gas shift reactors. *International Journal of Hydrogen Energy*, 34(21):8877–8891, 2009.

[8] T. A. Adams II and P. I. Barton. High-efficiency power production from coal with carbon capture. *AIChE Journal*, 56(12):3120–3136, 2010.

[9] T. A. Adams II and P. I. Barton. Combining coal gasification and natural gas reforming for efficient polygeneration. *Fuel Processing Technology*, 92(3):639–655, 2011.

[10] T. A. Adams II and P. I. Barton. Combining coal gasification, natural gas reforming, and solid oxide fuel cells for efficient polygeneration with CO_2 capture and sequestration. *Fuel Processing Technology*, 92(10):2105–2115, 2011.

[11] S. Adhikari and S. Fernando. Hydrogen membrane separation techniques. *Industrial & Engineering Chemistry Research*, 45(3):875–881, 2006.

[12] C. S. Adjiman, I. P. Androulakis, and C. A. Floudas. A global optimization method, αBB, for general twice-differentiable constrained NLPs - II. Implementation and computational results. *Computers & Chemical Engineering*, 22(9):1159–1179, 1998.

[13] C. S. Adjiman, I. P. Androulakis, and C. A. Floudas. Global optimization of mixed-integer nonlinear problems. *AIChE Journal*, 46(9):1769–1797, 2000.

[14] C. S. Adjiman, S. Dallwig, C. A. Floudas, and A. Neumaier. A global optimization method, αBB, for general twice-differentiable constrained NLPs - I. Theoretical advances. *Computers & Chemical Engineering*, 22(9):1137–1158, 1998.

[15] H. Aki, T. Oyama, and K. Tsuji. Analysis of energy pricing in urban energy service systems considering a multiobjective problem of environmental and economic impact. *IEEE Transactions on Power Systems*, 18(4):1275–1282, 2003.

[16] W. B. E. Al-Othman, H. M. S. Lababidi, I. M. Alatiqi, and K. Al-Shayji. Supply chain optimization of petroleum organization under uncertainty in market demands and prices. *European Journal of Operational Research*, 189(3):822–840, 2008.

[17] S. A. Al-Redhwan, B. D. Crittender, and H. M. S. Lababidi. Wastewater minimization under uncertain operational conditions. *Computers & Chemical Engineering*, 29(5):1009–1021, 2005.

[18] A. Al-Shammari and M. S. Ba-Shammakh. Uncertainty analysis for refinery production planning. *Industrial & Engineering Chemistry Research*, 50(11):7065–7072, 2011.

[19] I. P. Androulakis, C. D. Maranas, and C. A. Floudas. αBB: A global optimization method for general constrained nonconvex problems. *Journal of Global Optimization*, 7(4):337–363, 1995.

[20] S. Ansolabehere, J. Beer, J. Deutch, A. D. Ellerman, S. J. Friedmann, H. Herzog, H..D. Jacoby, P. L. Joskow, G. Mcrae, R. Lester, E. J. Moniz, E. Steinfeld, and J. Katzer. The future of coal: Options for a carbon-constrained world. Technical report, Massachusetts Institute of Technology, Cambridge, MA, 2007.

[21] P. Arcuri, G. Florio, and P. Firagiacomo. A mixed integer programming model for optimal design of trigeneration in a hospital complex. *Energy*, 32(8):1430–1447, 2007.

[22] A. Babayan, Z. Kapelan, D. Savic, and G. Walters. Least-cost design of water distribution networks under demand uncertainty. *Journal of Water Resources Planning and Management*, 131(5):375–382, 2005.

[23] E. Balas. Disjunctive programming and a hierachy of relaxations for discrete optimization problems. *SIAM J. Algebraic Discrete Methods*, 6:466486, 1985.

[24] E. Balas, S. Ceria, and G. Cornuéjols. A lift-and-project cutting plane algorithm for mixed 0-1 programs. *Mathematical Programming*, 58(3):295–324, 1993.

[25] E. Balas and R. Jeroslow. Canonical cuts on the unit hypercube. *SIAM Journal on Applied Mathematics*, 23(1):61–69, 1972.

[26] J. Balasubramanian and I. E. Grossmann. A novel branch and bound algorithm for scheduling flowshop plants with uncertain processing times. *Computers & Chemical Engineering*, 26(1):41, 2002.

[27] R. C. Baliban, J. A. Elia, and C. A. Floudas. Toward novel hybrid biomass, coal, and natural gas processes for satisfying current transportation fuel demands, 1: Process alternatives, gasification modeling, process simulation, and economic analysis. *Industrial & Engineering Chemistry Research*, 49(16):7343–7370, 2010.

[28] R. C. Baliban, J. A. Elia, and C. A. Floudas. Optimization framework for the simultaneous process synthesis, heat and power integration of a thermochemical hybrid biomass, coal, and natural gas facility. *Computers & Chemical Engineering*, 35(9):1647–1690, 2011.

[29] R. C. Baliban, J. A. Elia, and C. A. Floudas. Simultaneous process synthesis, heat, power, and water integration of thermochemical hybrid biomass, coal, and natural gas facilities. *Computers & Chemical Engineering*, 37:297–327, 2012.

[30] R. C. Baliban, J. A. Elia, R. Misener, and C. A. Floudas. Global optimization of a MINLP process synthesis model for thermochemical based conversion of hybrid coal, biomass, and natural gas to liquid fuels. *Computers & Chemical Engineering*, 42:64–86, 2012.

[31] S. Bashadi and H. Herzog. Using Aspen Icarus to simulate CO_2 capture economics of IGCC Selexol process. In *BP-MIT Advanced Conversion Research Program Technical Review Meeting*, Cambridge, MA, 2009.

[32] J. F. Benders. Partitioning procedures for solving mixed-variables programming problems. *Numerische Mathematik*, 4:238–252, 1962.

[33] D. P. Bertsekas. *Nonlinear Programming.* Athena Scientific, Cambridge, MA, 1999.

[34] J. R. Birge. Decomposition and partitioning methods for multistage stochastic linear programs. *Operations Research*, 33(5):9891007, 1985.

[35] J. R. Birge and F. Louveaux. *Introduction to Stochastic Programming.* Springer, New York, NY, 1997.

[36] J. R. Birge and F. V. Louveaux. A multicut algorithm for two-stage stochastic linear programs. *European Journal of Operational Research*, 34(3):384–392, 1988.

[37] F. Birol. World energy outlook 2011. Technical report, International Energy Agency, Paris, France, 2011.

[38] J. K. Bok, I. E. Grossmann, and S. Park. Supply chain optimization in continuous flexible process networks. *Industrial & Engineering Chemistry Research*, 39(5):1279–1290, 2000.

[39] B. Botros, K. DiGenova, and J. Brisson. Task 6: Innovation and optimization: Heat integration. In *BP-MIT Advanced Conversion Research Program Technical Review Meeting*, London, UK, 2010.

[40] A. Botterud, M. D. Ilic, and I. Wangensteen. Optimal investments in power generation under centralized and decentralized decision making. *IEEE Transactions on Power Systems*, 20(1):254–263, 2005.

[41] Brooke, Kendrick, Meeraus, and Raman. *GAMS - A User's Guide.* Available at: http://www.gams.com/docs/document/GAMSUsersGuide.pdf (2008).

[42] M. Burer, K. Tanaka, D. Favrat, and K. Yamada. Multi-criteria optimization of a district cogeneration plant integrating a solid oxide fuel cell-gas turbine combined cycle, heat pumps and chillers. *Energy*, 28(6):497–518, 2003.

[43] Y. P. Cai, G. H. Huang, Z. F. Yang, and Q. Tan. Identification of optimal strategies for energy management systems planning under multiple uncertainties. *Applied Energy*, 86(4):480–495, 2009.

[44] E. Cardona, A. Piacentino, and F. Cardona. Matching economical, energetic and environmental benefits: An analysis for hybrid CHCP-heat pump systems. *Energy Conversion and Management*, 47(20):3530–3542, 2006.

[45] M. C. Carneiro, G. P. Ribas, and S. Hamacher. Risk management in the oil supply chain: A CVaR approach. *Industrial & Engineering Chemistry Research*, 49(7):3286–3294, 2010.

[46] C. L. Chen, B. W. Wang, and W. C. Lee. Multiobjective optimization for a multienterprise supply chain network. *Industrial & Engineering Chemistry Research*, 42(9):1879–1889, 2003.

[47] Y. Chen, T. A. Adams II, and P. I. Barton. Optimal design and operation of flexible energy polygeneration systems. *Industrial & Engineering Chemistry Research*, 50(8):4553–4566, 2011.

[48] Y. Chen, T. A. Adams II, and P. I. Barton. Optimal design and operation of static energy polygeneration systems. *Industrial & Engineering Chemistry Research*, 50(9):5099–5113, 2011.

[49] Y. Chen, X. Li, T. A. Adams II, and P. I. Barton. Decomposition strategy for the global optimization of flexible energy polygeneration systems. *AIChE Journal*, 58(10):3080–3095, 2012.

[50] G. Chicco and P. Mancarella. Distributed multi-generation: A comprehensive view. *Renewable and Sustainable Energy Reviews*, 13(3):535–551, 2009.

[51] D. Cocco, A. Pettinau, and G. Cau. Energy and economic assessment of IGCC power plants integrated with DME synthesis processes. *Proceedings of the Institution of Mechanical Engineers Part A - Journal of Power and Energy*, 220(2):95–102, 2006.

[52] J. J. Conti, P. D. Holtberg, J. A. Beamon, A. M. Schaal, J. C. Ayoub, and J. T. Turnure. Annual energy outlook 2011: with projections to 2035. Technical report, U.S. Energy Information Administration, Washington, DC, 2011.

[53] J. J. Conti, P. D. Holtberg, J. A. Beamon, A. M. Schaal, G. E. Sweetnam, and A. S. Kydes. Annual energy outlook 2009: with projections to 2030. Technical report, U.S. Energy Information Administration, Washington, DC, 2009.

[54] J. J. Dooley and R. T. Dahowski. Large-scale U.S. unconventional fuels production and the role of carbon dioxide capture and storage technologies in reducing their greenhouse gas emissions. *Energy Procedia*, 1(1):4225–4232, 2009.

[55] A. Drud. *CONOPT*. ARKI Consulting and Development A/S, Bagsvaerd, Denmark. Available at: http://www.gams.com/docs/document/conopt.pdf.

[56] V. Dua and E. N. Pistikopoulos. An algorithm for the solution of multiparametric mixed integer linear programming problems. *Annals of Operations Research*, 99:123–139, 2000.

[57] M. Duran and I. E. Grossmann. An outer-approximation algorithm for a class of mixed nonlinear programs. *Mathematical Programming*, 36(3):307–339, 1986.

[58] N. P. Faísca, V. D. Kosmidis, B. Rustem, and E. N. Pistikopoulos. Global optimization of multi-parametric MILP problems. *Journal of Global Optimization*, 45(1):131–151, 2009.

[59] R. Fletcher and S. Leyffer. Solving mixed integer nonlinear programs by outer approximation. *Mathematical Programming*, 66(3):327349, 1994.

[60] T. Gal and J. Nedoma. Multiparametric linear programming. *Management Science*, 18(7):406–422, 1972.

[61] P. Gangadharan, A. Zanwar, K. L. Zheng, J. Gossage, and H. H. Lou. Sustainability assessment of polygeneration processes based on syngas derived from coal and natural gas. *Computers & Chemical Engineering*, 39:105–117, 2012.

[62] M. Gassner and F. Marechal. Thermo-economic optimisation of the polygeneration of synthetic natural gas (SNG), power and heat from lignocellulosic biomass by gasification and methanation. *Energy & Environmental Science*, 5(2):5768–5789, 2012.

[63] M. Gassner, F. Vogel, G. Heyen, and F. Marechal. Optimal process design for the polygeneration of SNG, power and heat by hydrothermal gasification of waste biomass: Process optimisation for selected substrates. *Energy & Environmental Science*, 4(5):1742–1758, 2011.

[64] M. Gassner, F. Vogel, G. Heyen, and F. Marechal. Optimal process design for the polygeneration of SNG, power and heat by hydrothermal gasification of waste biomass: Thermo-economic process modelling and integration. *Energy & Environmental Science*, 4(5):1726–1741, 2011.

[65] B. H. Gebreslassie, G. Guillen-Gosalbez, L. Jimenez, and D. Boer. Economic performance optimization of an absorption cooling system under uncertainty. *Applied Thermal Engineering*, 29(17-18):3491–3500, 2009.

[66] A. M. Geoffrion. Elements of large-scale mathematical programming: Part I: Concepts. *Management Science*, 16(11):652–675, 1970.

[67] A. M. Geoffrion. Elements of large-scale mathematical programming: Part II: Synthesis of algorithms and bibliography. *Management Science*, 16(11):676–691, 1970.

[68] A. M. Geoffrion. Generalized Benders decomposition. *Journal of Optimization Theory and Applications*, 10(4):237–260, 1972.

[69] A. M. Geoffrion and R. Nauss. Parametric and postoptimality analysis in integer linear programming. *Management Science*, 23(5):453–466, 1977.

[70] P. E. Gill, W. Murray, and M. A. Saunders. SNOPT: An SQP algorithm for large-scale constrained optimization. *SIAM Journal on Optimization*, 12(4):979–1006, 2002.

[71] O. Giustolisi, D. Laucelli, and A. F. Colombo. Deterministic versus stochastic design of water distribution networks. *Journal of Water Resources Planning and Management*, 135(2):117–127, 2009.

[72] V. Goel and I. E. Grossmann. A stochastic programming approach to planning of offshore gas field developments under uncertainty in reserves. *Computers & Chemical Engineering*, 28(8):1409–1429, 2004.

[73] B. G. Gorenstin, N. M. Campodonico, J. P. Costa, M. V. F. Pereira, and N. Deeb. Power-system expansion planning under uncertainty. *IEEE Transactions on Power Systems*, 8(1):129–136, 1993.

[74] C. E. Gounaris, R. Misener, and C. A. Floudas. Computational comparison of piecewise-linear relaxations for pooling problems. *Industrial & Engineering Chemistry Research*, 48(12):5742–5766, 2009.

[75] I. Grossmann. Enterprise-wide optimization: A new frontier in process systems engineering. *AIChE Journal*, 51(7):1846–1857, 2005.

[76] I. E. Grossmann. Review of nonlinear mixed-integer and disjunctive programming techniques. *Optimization and Engineering*, 3(3):227–252, 2002.

[77] M. Guignard and S. Kim. Lagrangean decomposition: A model yielding stronger Lagrangean bounds. *Mathematical Programming*, 39(2):215–228, 1987.

[78] G. Guillen, E. Mele, M. J. Bagajewicz, A. Espuna, and L. Puigjaner. Multiobjective supply chain design under uncertainty. *Chemical Engineering Science*, 60(6):1535–1553, 2005.

[79] G. Guillen-Gosalbez and I. E. Grossmann. Optimal design and planning of sustainable chemical supply chains under uncertainty. *AIChE Journal*, 55(1):99–121, 2009.

[80] A. Gupta and C. D. Maranas. Managing demand uncertainty in supply chain planning. *Computers & Chemical Engineering*, 27(8-9):1219–1227, 2003.

[81] C. N. Hamelinck, A. P. C. Faaij, H. den Uil, and H. Boerrigter. Production of FT transportation fuels from biomass: Technical options, process analysis and optimization, and development potential. Technical Report NWS-E-2003-08, Universiteit Utrecht, Utrecht, Netherlands, 2003.

[82] C. N. Hamelinck, A. P. C. Faaij, H. den Uil, and H. Boerrigter. Production of FT transportation fuels from biomass: technical options, process analysis and optimization, and development potential. *Energy*, 29(11):17431771, 2004.

[83] K. Hemmes, J. L. Zachariah-Wolff, M. Geidl, and G. Andersson. Towards multi-source multi-product energy systems. *International Journal of Hydrogen Energy*, 32(10-11):1332–1338, 2007.

[84] H. Herzog and D. Golomb. *Encyclopedia of Energy*, chapter Carbon Capture and Storage from Fossil Fuel Use. Elsevier, Boston, MA, 2004.

[85] G. H. Huang. A hybrid inexact-stochastic water management model. *European Journal of Operational Research*, 107(1):137–158, 1998.

[86] D. D. Ilic, E. Dotzauer, and L. Trygg. District heating and ethanol production through polygeneration in Stockholm. *Applied Energy*, 91(1):214–221, 2012.

[87] R. R. Iyer and I. E. Grossmann. Optimal multiperiod operational planning for utility systems. *Computers & Chemical Engineering*, 21(8):787–800, 1997.

[88] R. R. Iyer and I. E. Grossmann. Synthesis and operational planning of utility systems for multiperiod operation. *Computers & Chemical Engineering*, 22(7-8):979–993, 1998.

[89] J. R. Jackson and I. E. Grossmann. Temporal decomposition scheme for nonlinear multisite production planning and distribution models. *Industrial & Engineering Chemistry Research*, 42(13):3045–3055, 2003.

[90] J. Jacobs, G. Freeman, J. Grygier, D. Morton, G. Schultz, K. Staschus, and J. Stedinger. SOCRATES - A system for scheduling hydroelectric generation under uncertainty. *Annals of Operations Research*, 59:99–133, 1995.

[91] T. W. Jonsbraten. Oil field optimization under price uncertainty. *Journal of the Operational Research Society*, 49(8):811–818, 1998.

[92] J. Y. Jung, G. Blau, J. F. Pekny, G. V. Reklaitis, and D. Eversdyk. A simulation based optimization approach to supply chain management under demand uncertainty. *Computers & Chemical Engineering*, 28(10):2087–2106, 2004.

[93] P. Kall and S. Wallace. *Stochastic Programming*. John Wiley & Sons, New York, NY, 1995.

[94] U. Kaplan, M. Turkay, B. Karasozen, and L. T. Biegler. Optimization of supply chain systems with price elasticity of demand. *INFORMS Journal on Computing*, 23(4):557–568, 2011.

[95] R. Karuppiah and I. E. Grossmann. Global optimization for the synthesis of integrated water systems in chemical processes. *Computers & Chemical Engineering*, 30(4):650–673, 2006.

[96] R. Karuppiah and I. E. Grossmann. Global optimization of multiscenario mixed integer nonlinear programming models arising in the synthesis of integrated water networks under uncertainty. *Computers & Chemical Engineering*, 32(1-2):145–160, 2008.

[97] R. Karuppiah and I. E. Grossmann. A Lagrangean based branch-and-cut algorithm for global optimization of nonconvex mixed-integer nonlinear programs with decomposable structures. *Journal of Global Optimization*, 41(2):163–186, 2008.

[98] R. Karuppiah, A. Peschel, and I. E. Grossmann. Energy optimization for the design of corn-based ethanol plants. *AIChE Journal*, 54(6):1499–1525, 2008.

[99] R. S. Kempegowda, P. P. Selvam, O. Skreiberg, and K. Q. Tran. Process synthesis and economics of combined biomethanol and CHP energy production derived from biomass wastes. *Journal of Chemical Technology and Biotechnology*, 87(7):897–902, 2012.

[100] P. Kesavan, R. J. Allgor, E. P. Gatzke, and P. I. Barton. Outer approximation algorithms for separable nonconvex mixed-integer nonlinear programs. *Mathematical Programming*, 100(3):517–535, 2004.

[101] P. Kesavan and P. I. Barton. Decomposition algorithms for nonconvex mixed-integer nonlinear programs. *AIChE Symposium Series*, 96(323):458461, 2000.

[102] A. Khajavirad and J. J. Michalek. A deterministic Lagrangian-based global optimization approach for quasiseparable nonconvex mixed-integer nonlinear programs. *Journal of Mechanical Design*, 131(5):051009, 2009.

[103] R. Khalilpour and I. A. Karimi. Investment portfolios under uncertainty for utilizing natural gas resources. *Computers & Chemical Engineering*, 35(9):1827–1837, 2011.

[104] C. S. Khor, A. Elkamel, K. Ponnambalam, and P. L. Douglas. Two-stage stochastic programming with fixed recourse via scenario planning with economic and operational risk management for petroleum refinery planning under uncertainty. *Chemical Engineering and Processing*, 47(9-10):1744–1764, 2008.

[105] H. Lakkhanawat and M. J. Bagajewicz. Financial risk management with product pricing in the planning of refinery operations. *Industrial & Engineering Chemistry Research*, 47(17):6622–6639, 2008.

[106] E. D. Larson and T. Ren. Synthetic fuel production by indirect coal liquefaction. *Energy for Sustainable Development*, 7(4):79–102, 2003.

[107] C. Li, X. He, B. Chen, Q. Xu, and C. Liu. A hybrid programming model for optimal production planning under demand uncertainty in refinery. *Chinese Journal of Chemical Engineering*, 16(2):241–246, 2008.

[108] F. Li and L. Fan. Clean coal conversion processes - progress and challenges. *Energy & Environmental Science*, 1(2):248–267, 2008.

[109] H. Q. Li, H. Hong, H. G. Jin, and R. X. Cai. Analysis of a feasible polygeneration system for power and methanol production taking natural gas and biomass as materials. *Applied Energy*, 87(9):2846–2853, 2010.

[110] X. Li, E. Armagan, A. Tomasgard, and P. I. Barton. Stochastic pooling problem for natural gas production network design and operation under uncertainty. *AIChE Journal*, 57(8):2120–2135, 2011.

[111] X. Li, Y. Chen, and P. I. Barton. Nonconvex generalized Benders decomposition with piecewise convex relaxations for global optimization of integrated process design and operation problems. *Industrial & Engineering Chemistry Research*, 51(21):7287–7299, 2012.

[112] X. Li, A. Tomasgard, and P. I. Barton. Decomposition strategy for natural gas production network design under uncertainty. In *Proceedings of the 49th IEEE Conference on Decision and Control*, pages 188–193, 2010.

[113] X. Li, A. Tomasgard, and P. I. Barton. Decomposition strategy for the stochastic pooling problem. *Journal of Global Optimization*, 2011. DOI: 10.1007/s10898-011-9792-0.

[114] X. Li, A. Tomasgard, and P. I. Barton. Nonconvex generalized Benders decomposition for stochastic separable mixed-integer nonlinear programs. *Journal of Optimization Theory and Applications*, 151(3):425–454, 2011.

[115] Z. Li, P. Liu, F. He, M. H. Wang, and E. N. Pistikopoulos. Simulation and exergoeconomic analysis of a dual-gas sourced polygeneration process with integrated methanol/DME/DMC catalytic synthesis. *Computers & Chemical Engineering*, 35(9):1857–1862, 2011.

[116] H. Lin, H. G. Jin, L. Gao, and W. Han. Techno-economic evaluation of coal-based polygeneration systems of synthetic fuel and power with CO_2 recovery. *Energy Conversion and Management*, 52(1):274–283, 2011.

[117] M. Liszka and A. Ziebik. Economic optimization of the combined cycle integrated with multi-product gasification system. *Energy Conversion and Management*, 50(2):309–318, 2009.

[118] P. Liu, D. I. Gerogiorgis, and E. N. Pistikopoulos. Modeling and optimization of polygeneration energy systems. *Catalysis Today*, 127(1-4):347–359, 2007.

[119] P. Liu, E. N. Pistikopoulos, and Z. Li. A mixed-integer optimization approach for polygeneration energy systems design. *Computers and Chemical Engineering*, 33(3):759–768, 2009.

[120] P. Liu, E. N. Pistikopoulos, and Z. Li. Decomposition based stochastic programming approach for polygeneration energy systems design under uncertainty. *Industrial & Engineering Chemistry Research*, 49(7):3295–3305, 2010.

[121] P. Liu, E. N. Pistikopoulos, and Z. Li. A multi-objective optimization approach to polygeneration energy systems design. *AIChE Journal*, 56(5):1218–1234, 2010.

[122] X. Luo, B. Zhang, Y. Chen, and S. Mo. Operational planning optimization of multiple interconnected steam power plants considering environmental costs. *Energy*, 37(1):549–561, 2012.

[123] H. C. Mantripragada and E. S. Rubin. CO_2 reduction potential of coal-to-liquids (CTL) plants. *Energy Procedia*, 1(1):4331–4338, 2009.

[124] J. J. Marano and J. P. Ciferino. Integration of gas separation membranes with IGCC identifying the right membrane for the right job. *Energy Procedia*, 1(1):361–368, 2009.

[125] C. T. Maravelias and I. E. Grossmann. Simultaneous planning for new product development and batch manufacturing facilities. *Industrial & Engineering Chemistry Research*, 40(26):6147–6164, 2001.

[126] E. C. Marcoulaki and A. C. Kokossis. Scoping and screening complex reaction networks using stochastic optimization. *AIChE Journal*, 45(9):1977–1991, 1999.

[127] M. Martin and I. E. Grossmann. Process optimization of FT-diesel production from lignocellulosic switchgrass. *Industrial & Engineering Chemistry Research*, 50(23):13485–13499, 2011.

[128] M. Martin and I. E. Grossmann. Energy optimization of bioethanol production via hydrolysis of switchgrass. *AIChE Journal*, 58(5):1538–1549, 2012.

[129] M. Martin and I. E. Grossmann. Simultaneous optimization and heat integration for biodiesel production from cooking oil and algae. *Industrial & Engineering Chemistry Research*, 51(23):7998–8014, 2012.

[130] J. C. Meerman, A. P. C. Faaij, and W. C. Turkenburg. Flexible integrated gasification co-generation facilities: A technical and energy analysis. *Energy Procedia*, 1(1):4241–4248, 2009.

[131] J. C. Meerman, A. Ramirez, W. C. Turkenburg, and A. P. C. Faaij. Assessing the economic feasibility of flexible integrated gasification co-generation facilities. *Energy Procedia*, 4:1973–1980, 2011.

[132] J. C. Meerman, A. Ramirez, W. C. Turkenburg, and A. P. C. Faaij. Performance of simulated flexible integrated gasification polygeneration facilities. Part A: A technical-energetic assessment. *Renewable & Sustainable Energy Reviews*, 15(6):2563–2587, 2011.

[133] C. A. Meyer and C. A. Floudas. Global optimization of a combinatorially complex generalized pooling problem. *AIChE Journal*, 52(3):1027–1037, 2006.

[134] P. Michelon and N. Maculan. Lagrangean decomposition for integer nonlinear-programming with linear constraints. *Mathematical Programming*, 52(2):303–313, 1991.

[135] A. Mitsos. *Man-Portable Power Generation Devices: Product Design and Supporting Algorithms.* PhD thesis, Massachusetts Institute of Technology, June 2006.

[136] R. Monaghan. Task 2: Dynamic reduced order modeling of entrained flow gasifiers. In *BP-MIT Advanced Conversion Research Program Technical Review Meeting*, London, UK, 2010.

[137] I. M. Mujtaba and S. Macchietto. Optimal operation of multicomponent batch distillation multiperiod formulation and solution. *Computers & Chemical Engineering*, 17(12):1191–1207, 1993.

[138] S. M. S. Neiro and J. M. Pinto. A general modeling framework for the operational planning of petroleum supply chains. *Computers & Chemical Engineering*, 28(6-7):871–896, 2004.

[139] S. M. S. Neiro and J. M. Pinto. Multiperiod optimization for production planning of petroleum refineries. *Chemical Engineering Communications*, 192(1):62–88, 2005.

[140] K. S. Ng and J. Sadhukhan. Process integration and economic analysis of bio-oil platform for the production of methanol and combined heat and power. *Biomass & Bioenergy*, 35(3):1153–1169, 2011.

[141] K. S. Ng and J. Sadhukhan. Techno-economic performance analysis of bio-oil based Fischer-Tropsch and CHP synthesis platform. *Biomass & Bioenergy*, 35(7):3218–3234, 2011.

[142] K. S. Ng, N. Zhang, and J. Sadhukhan. Decarbonised coal energy system advancement through CO_2 utilisation and polygeneration. *Clean Technologies and Environmental Policy*, 14(3):443–451, 2012.

[143] M. P. Nowak and W. Romisch. Stochastic Lagrangian relaxation applied to power scheduling in a hydro-thermal system under uncertainty. *Annals of Operations Research*, 100:251–272, 2000.

[144] S. D. Oh, H. J. Lee, J. Y. Jung, and H. Y. Kwak. Optimal planning and economic evaluation of cogeneration system. *Energy*, 32(5):760–771, 2007.

[145] A. Pertsinidis, I. E. Grossmann, and G. J. McRae. Parametric optimization of MILP programs and a framework for the parametric optimization of MINLPs. *Computers & Chemical Engineering*, 22(S):S205–S212, 1998.

[146] A. Piacentino and F. Cardona. An original multi-objective criterion for the design of small-scale polygeneration systems based on realistic operating conditions. *Applied Thermal Engineering*, 28(17-18):2391–2404, 2008.

[147] Z. N. Pintaric and Z. Kravanja. A strategy for MINLP synthesis of flexible and operable processes. *Computers & Chemical Engineering*, 28(6-7):1105–1119, 2004.

[148] A. Pongsakdi, P. Rangsunvigit, K. Siemanond, and M. J. Bagajewicz. Financial risk management in the planning of refinery operations. *International Journal of Production Economics*, 103(1):64–86, 2006.

[149] J. A. Quintero and CA Cardona. Process simulation of fuel ethanol production from lignocellulosics using Aspen Plus. *Industrial & Engineering Chemistry Research*, 50(10):6205–6212, 2011.

[150] J. B. Rosen and P. M. Pardalos. Global minimization of large-scale constrained concave quadratic problems by separable programming. *Mathematical Programming*, 34(2):163–174, 1986.

[151] A. Ruszczynski. On convergence of an augmented Lagrangian decomposition method for sparse convex-optimization. *Mathematics of Operations Research*, 20(3):634–656, 1995.

[152] H. S. Ryoo and N. V. Sahinidis. A branch-and-reduce approach to global optimization. *Journal of Global Optimization*, 8(2):107138, 1996.

[153] N. Sahinidis and M. Tawarmalani. *Baron Users Mannual.* Available at: http://www.gams.com/docs/document/baron.pdf (2008).

[154] N. V. Sahinidis. BARON: A general purpose global optimization software package. *Journal of Global Optimization*, 8(2):201–205, 1996.

[155] M. Sakawa, K. Kato, and S. Ushiro. Operational planning of district heating and cooling plants through genetic algorithms for mixed 0-1 linear programming. *European Journal of Operational Research*, 137(3):677–687, 2002.

[156] T. Santoso, S S. Ahmed, M. Goetschalckx, and A. Shapiro. A stochastic programming approach for supply chain network design under uncertainty. *European Journal of Operational Research*, 167(1):96–115, 2005.

[157] J. K. Scott. *Reachability Analysis and Deterministic Global Optimization of Differential-Algebraic Systems.* PhD thesis, Massachusetts Institute of Technology, June 2012.

[158] W. D. Seider, J. D. Seader, D. R. Lewin, and S. Widagdo. *Product and Process Design Principles: Synthesis, Analysis, and Evaluation.* John Wiley & Sons, Hoboken, NJ, 2009.

[159] Z. G. Shang and A. Kokossis. A transhipment model for the optimisation of steam levels of total site utility system for multiperiod operation. *Computers & Chemical Engineering*, 28(9):1673–1688, 2004.

[160] R. M. V. Slyke and R. Wets. L-shaped linear programs with applications to optimal control and stochastic programming. *SIAM Journal on Applied Mathematics*, 17(4):638663, 1969.

[161] L. V. Snyder. Facility location under uncertainty: A review. *IIE Transactions*, 38(7):537–554, 2006.

[162] F. Starfelt, E. Thorin, E. Dotzauer, and J. Yan. Performance evaluation of adding ethanol production into an existing combined heat and power plant. *Bioresource Technology*, 101(2):613–618, 2010.

[163] J. Stöcker, M. Whysall, and G. Q. Miller. 30 years of PSA technology for hydrogen purification. Technical report, UOP, Antwerp, Belgium, and Des Plains, IL, 1998.

[164] R. A. Stubbs and S. Mehrotra. A branch-and-cut method for 0-1 mixed convex programming. *Mathematical Programming*, 86(3):515–532, 1999.

[165] Y. H. Sun, W. W. G. Yeh, N. S. Hsu, and P. W. F. Louie. Generalized network algorithm for water-supply-system optimization. *Journal of Water Resources Planning and Management*, 121(5):392–398, 1995.

[166] B. Tarhan, I. E. Grossmann, and V. Goel. Stochastic programming approach for the planning of offshore oil or gas field infrastructure under decision-dependent uncertainty. *Industrial & Engineering Chemistry Research*, 48(6):3078–3097, 2009.

[167] T. J. Tarka, J. G. Wimer, P. C. Balash, T. J. Skone, K. C. Kern, M. C. Vargas, B. D. Morreale, C. W. White III, and D. Gray. Affordable, low-carbon diesel fuel from domestic coal and biomass. Technical Report DOE/NETL-2009/1349, National Energy Technology Laboratory, Pittsburgh, PA, 2009.

[168] M. Tawarmalani and N. Sahinidis. *Convexification and global optimization in continuous and mixed-integer nonlinear programming.* Kluwer Academic Publishers, Dordrecht, the Netherlands, 2002.

[169] M. Tawarmalani and N. V. Sahinidis. Global optimization of mixed-integer nonlinear programs: A theoretical and computational study. *Mathematical Programming*, 99(3):563–591, 2004.

[170] M. Tawarmalani and N. V. Sahinidis. A polyhedral branch-and-cut approach to global optimization. *Mathematical Programming*, 103(2):225249, 2005.

[171] M. Theis, B. J. Skrifvars, M. Zevenhoven, M. Hupa, and H. Tran. Fouling tendency of ash resulting from burning mixtures of biofuels. Part 2: Deposit chemistry. *Fuel*, 85(14-15):1992–2001, 2006.

[172] A. Tuohy, P. Meibom, E. Denny, and M. O'Malley. Unit commitment for systems with significant wind penetration. *IEEE Transactions on Power Systems*, 24(2):592–601, 2009.

[173] L. van Bibber, E. Shuster, J. Haslbeck, M. Rutkowski, S. Olson, and S. Kramer. Baseline technical and economic assessment of a commercial scale Fischer-Tropsch liquids facility. Technical Report DOE/NETL-2007/1260, National Energy Technology Laboratory, Pittsburgh, PA, 2007.

[174] L. van Bibber, E. Shuster, J. Haslbeck, M. Rutkowski, S. Olson, and S. Kramer. Technical and economic assessment of small-scale Fischer-Tropsch liquids facilities. Technical Report DOE/NETL-2007/1253, National Energy Technology Laboratory, Pittsburgh, PA, 2007.

[175] S. A. van den Heever and I. E. Grossmann. An iterative aggregation/disaggregation approach for the solution of a mixed-integer nonlinear oilfield infrastructure planning model. *Industrial & Engineering Chemistry Research*, 39(6):1955–1971, 2000.

[176] D. K. Varvarezos, I. E. Grossmann, and L. T. Biegler. An outer-approximation method for multiperiod design optimization. *Industrial & Engineering Chemistry Research*, 31(6):1466–1477, 1992.

[177] J. P. Vin and M. G. Ierapetritou. Robust short-term scheduling of multiproduct batch plants under demand uncertainty. *Industrial & Engineering Chemistry Research*, 40(21):4543–4554, 2001.

[178] J. Viswanathan and I. E. Grossmann. A combined penalty-function and outer-approximation method for MINLP optimization. *Computers & Chemical Engineering*, 14(7):769–782, 1990.

[179] X. Wang, Y. Xiao, S. Xu, and Z. Guo. Predicting the performance of system for the co-production of Fischer-Tropsch synthetic liquid and power from coal. *Journal of Engineering for Gas Turbines and Power-Transactions of the ASME*, 130(1), 2008. DOI: 10.1115/1.2747644.

[180] C. Weber, F. Marechal, D. Favrat, and S. Kraines. Optimization of an SOFC-based decentralized polygeneration system for providing energy services in an office-building in Tokyo. *Applied Thermal Engineering*, 26(13):1409–1419, 2006.

[181] D. S. Wicaksono and I. Karimi. Piecewise MILP under- and overestimators for global optimization of bilinear programs. *AIChE Journal*, 54(4):991–1008, 2008.

[182] M. C. Woods, P. J. Capicotto, J. L. Haslbeck, N. J. Kuehn, M. Matuszewski, L. L. Pinkerton, M. D. Rutkowski, R. L. Schoff, and V. Vaysman. Cost and performance baseline for fossil energy plants. Volume 1: Bituminous coal and natural gas to electricity. Technical Report DOE/NETL-2007/1281, National Energy Technology Laboratory, Pittsburgh, PA, 2007.

[183] K. Yamashita and L. Barreto. Energyplexes for the 21st century: Coal gasification for co-producing hydrogen, electricity and liquid fuels. *Energy*, 30(13):2453–2473, 2005.

[184] G. Yi and G. V. Reklaitis. Optimal design of multiperiod batch-storage network including transportation processes. *AIChE Journal*, 57(10):2821–2840, 2011.

[185] Q. Yi, J. Feng, and W. Y. Li. Optimization and efficiency analysis of polygeneration system with coke-oven gas and coal gasified gas by Aspen Plus. *Fuel*, 96(1):131–140, 2012.

[186] Q. Yi, B. Lu, J. Feng, Y. Wu, and W. Li. Evaluation of newly designed polygeneration system with CO_2 recycle. *Energy & Fuels*, 26(2):1459–1469, 2012.

[187] G. W. Yu, Y. Y. Xu, X. Hao, Y. W. Li, and G. Q. Liu. Process analysis for polygeneration of Fischer-Tropsch liquids and power with CO_2 capture based on coal gasification. *Fuel*, 89(5):1070–1076, 2010.

[188] M. Yunt. *Nonsmooth Dynamic Optimization of Systems with Varying Structure.* PhD thesis, Massachusetts Institute of Technology, Feburary 2011.

[189] M. Yunt, B. Chachuat, A. Mitsos, and P. I. Barton. Designing man-portable power generation systems for varying power demand. *AIChE Journal*, 54(5):1254–1269, 2008.

[190] N. Zhang. Comparative study of two low CO_2 emission cycle options with natural gas reforming. In *Proceedings of The ASME Turbo Expo*, volume 3, pages 81–94, Montreal, Canada, 2007.

[191] Y. Zhang, D. Monder, and J. F. Forbes. Real-time optimization under parametric uncertainty: A probability constrained approach. *Journal of Process Control*, 12(3):373–389, 2002.

[192] Z. Zhong and F. You. Oil spill response planning with consideration of physicochemical evolution of the oil slick: A multiobjective optimization approach. *Computers & Chemical Engineering*, 35(8):1614–1630, 2011.